論文 / 著書情報
Article / Book Information

題目(和文)	
Title(English)	A centrifuge model study on behavior of ground movement and pile group response to tunneling in sand
著者(和文)	BoonsiriIttichai
Author(English)	Ittichai Boonsiri
出典(和文)	学位:博士（学術）, 学位授与機関:東京工業大学, 報告番号:甲第9897号, 授与年月日:2015年3月26日, 学位の種別:課程博士, 審査員:竹村　次朗,北詰　昌樹,岩波　光保,高橋　章浩,佐々木　栄一
Citation(English)	Degree:, Conferring organization: Tokyo Institute of Technology, Report number:甲第9897号, Conferred date:2015/3/26, Degree Type:Course doctor, Examiner:,,,,
学位種別(和文)	博士論文
Type(English)	Doctoral Thesis

A centrifuge model study on behavior of ground movement and pile group response to tunneling in sand

Ittichai Boonsiri

March 2015

A Dissertation Submitted to

Faculty of Graduate School of Science and Engineering at

Tokyo Institute of Technology

For the degree of Doctor of Philosophy

Department of Civil Engineering

ABSTRACT

In developing urban areas, there are unavoidable interactions between existing structures and new construction such as tunneling through pre-existing pile foundations. An accurate prediction of the ground deformation due to tunneling is necessary to prevent damage to those existing structures. In the past, due to the complexity of the interaction, the ground movement was estimated without the presence of pile foundations or assumed green-field condition. This assumption tends to overestimate the damage in the adjacent building and the shape of the settlement trough may not correspond to the realistic settlement.

Many researchers have investigated this complex mechanism of pile-soil-tunnel interactions using various method such as empirical equations, numerical and physical modeling. However, the proposed numerical studies have provided valuable results but there are still some uncertainties and the validation of the proposed parameters and construction methods are required. In numerical analysis, it is difficult to include all the influential effects such as change of stress due to tunneling, types of soil, types of piles (single or group), tunnel characteristic, relative pile positions, and alternation of pile bearing capacity etc. Therefore, the development of physical modeling using centrifuge technique becomes popular to study these complex mechanisms because it can reproduce ground stress of a full-scale prototype of a small scale model. Although, many researchers have provided useful results from the centrifuges, but the performance of tunnel model and the interaction of pile group with various positions have not well addressed.

Therefore, in this study, a series of centrifuge model tests has been carried out to investigate the effects of tunnel-induced soil movements on the adjacent pile group with four piles in sand. The tunneling process was simulated by reducing the diameter of the model tunnel in 100g centrifugal acceleration. The tunneling machine is a mechanical type which can reduce the diameter in co-axial direction to create a clear boundary condition from small to large ground loss values. Effects of horizontal distance between the pile and tunnel center (X_p), relative pile end position to the tunnel center (Z_{pe}), vertical loads on the pile groups (Q_d), and cover depth ratio (C/D) were investigated. Zones of influence which are defined by the soil movements were applied to explain the typical response of the pile group such as displacement of pile cap and deformation of piles. For small ground loss ratio ($\Delta V/V_0$), the pile group movements increased almost proportionally to $\Delta V/V_0$. While for the large $\Delta V/V_0$ over 3%, the pile movement increment gradually decreased with $\Delta V/V_0$, except for the pile group with the front pile resting in the large displacement zone, of which movement still proportionally increased with $\Delta V/V_0$. The effect of X_p and Z_{pe} on the pile cap movement could be reasonably combined with the relative depth from the boundary of less movement zone to the pile length. Relative pile depth in the less displacement zone to the pile length and the horizontal pile position are the critical controlling factors to the pile bending moment and axial force.

ADKNOWLEDGEMENT

I would like to say my deepest gratitude to my academic advisor, Jiro Takemura sensei for many supports, suggestions, guidelines and encouragement since I have stayed here. He taught many things about the research woks and life style that I could not be successful without his opinions. If the problems are occurred during the analysis, he is the one who gave me many reasons and methods to solve those difficult problems. Apart from the research work, Takemura sensei is very kind. He is always treating us and his wife is very good at cooking when we joined his annual New Year home party.

I could not graduate without the help from our technician of soil laboratory, Sakae Seki san that helped me prepared many instruments and control the process of all experiment cases. He is always treating me a beverage during rest period of experiment.

In addition, I am thankful to Osamu Kusakabe sensei who help me plan the theme of my research and provided a budget for the instrumented piles.

I am really appreciating the kind suggestions from Masaki Kitazume, Akihiro Takahashi and Thirapong Pipatpongsa sensei. They always gave me valuable comments during a lab seminar and also gave me many important points to improve my master and doctoral thesis.

I am thankful to Satoshi Sasaki and Mitsuyasu Iwanami sensei. They also gave me many kinds advice as committees of my doctoral thesis.

I also would like to thank all my dear friends to help me passed through many difficult situations such as Ke Lin, my late mate, who helped and encouraged me since the first day I came to the soil laboratory, Yashushi Gungi, my tutor, who help me manage many documents and teach me how to use the experimental equipment, Cocjin Micheal, Ippei Yoshimura, Takeshi Fujita, my lab and class mate, who taught and shared many stories to me. I also thank to all my Thai friends and other friends that I could not mention in this limited space. They made me feel that Japan is my second home.

I acknowledge the Monbusho scholarship to support and gave me a chance to live and study in Japan.

The last persons that I would like to thank are my family, my dad, mom, brother and my girlfriend. They always stayed by my side and encourage me from the beginning through the end.

Content

LISTS OF FIGURES

Chapter 1

Chapter 2

Chapter 3

Chapter 4

Chapter 5

Chapter 6

LISTS OF TABLES

Chapter 2

Chapter 3

Chapter 6

Notations

g is a centrifugal acceleration

X_p is the horizontal distance between the centers of the nearest pile and the tunnel

Z_{pe} is relative vertical distance between pile tip and center of tunnel

Q_d is the vertical load on the pile cap

C is soil cover depth

D is tunnel diameter

ΔV is volume of tunnel contraction

V_0 is the initial volume of the tunnel

PIV is Particle Image Velocity (GeoPIV)

PTM is potentiometer

CCTV is closed-circuit television

LVDT is Linear Variable Differential Transformers

PVC is Polyvinyl chloride

JLE is Jubilee Line Extension of tunnel construction

Z_o is depth of tunnel center

Z is depth of soil

R is the radius of the tunnel

δ_1 is maximum soil settlement at the surface

δ_2 is maximum soil settlement at the subsurface

$S(x)$ is settlement at a horizontal location x from tunnel axis

S_{max} is maximum settlement at the tunnel center line, x=0

x is the horizontal distance from the tunnel axis

x_i is the horizontal distance from the tunnel centerline to the inflection point

$x_i(Z)$ is the horizontal location of the inflection point of the subsurface settlement profile at depth Z

V_s is the volume of the settlement trough per unit length

K is trough width parameter

TRTS is the construction of Taipei Rapid Transit System

EPB is earth pressure balancing tunnel machine

m is empirical values depend on the type of the surrounding soil (m=0.4 and 0.8 for sand and clay respectively) by **Moh et al., 1996**

S_v is soil vertical settlement

S_x is soil horizontal displacement

K^* is K parameters of published data based on the fit of a Gaussian curve **Marshall et al., (2012)**

V_l is ground loss in **Marshall et al., (2012)**

$CTRL$ is the new Channel Tunnel Rail Link

TBM is tunnel boring machine

Q_u is the load capacity of the pile

Q_s is the shaft friction load of pile

Q_e is an axial force at the pile end position by strain gauges

Q_h is an axial force measuring by load cell (at pile head)

S_h is vertical settlement at pile head level

S_e is vertical settlement at pile end level

$Q_{(z=0)}$ is the load of the structure

Q_1 is the end bearing load which is not fully mobilized

Q_2 is the shaft friction which is not fully mobilized

$f(z)$ is the average unit skin friction

$\Delta Q_{(z)}$ is the difference of measured axial force between two points in the pile model

Δz is distance between two points of axial force measurement

s is perimeter of pile cross section

q_n is negative skin friction

σ'_v is effective overburden stress

M is the ratio of wall friction

K_s is earth pressure coefficient in the soil

FAB is finite and boundary element method

l is length dimension

A is area

V is the volume

σ is a vertical stress

γ is soil unit weight

E is Young's modulus

$Ø$ is pile model diameter

L is pile embedment length

t is pile thickness

I is an area moment of inertia

N is model linear scale

ρ_d is dry density

D_r is a relative density of sand

$Ø'$ is internal friction angle

σ'_1 is principal stress

σ'_3 is confining stress

σ'_c is consolidation pressure

ε is strain

ε_a is axial strain

ε_m is the moment strain

ΔR is change of resistance of strain gauge (ohm)

R is the resistance of strain gauge

K' is gauge factor of strain gauge (depend on the material of strain gauge)

e is the output voltage

E is the input voltage

ξ is Poisson ratio

PMG is potentiometer on the ground

PMP is potentiometer on the pile cap

ΔR is decrement of model tunnel radius

S_p is soil surface settlements of cases with pile groups

S_{np} is soil surface settlements of cases without pile groups

$S_{np,max}$ is maximum soil surface settlements of cases without pile groups

δz is vertical settlement of pile cap

δx is the horizontal movement of pile cap

δx_{pe} is the horizontal movement of pile end

θ is inclination of pile cap

θ_p is angle of pile deflection

L' is a total length of pile

Z_{da} is the average value of pile end depth from the boundary of Zone C and D

Z_{df} is pile end depth from zone C and D of the front pile

Z_{dr} is pile end depth from zone C and D of the rear pile

Chapter 1

Introduction

1.1 Background and problem statements

In general, the foundations consist of shallow foundations and deep foundations and the main function of the foundations is to transfer the load of the superstructure to the soil surface (shallow foundations) or to the deeper depth (deep foundations). In the shallow foundations, the design load should not exceed the bearing resistance of the soil. Overstressing the soil can lead to a large settlement or shear failure of the soil and causes the damage to the foundation, which eventually leads the deterioration of the functions of the superstructures. The bearing capacity of shallow foundation can be increased by increasing the size of spread footing. However, there are some difficulties in constructing the shallow foundations, such as a limited space of the foundation, presence of weak soil at shallow depth, and very strict requirement for the foundation, e.g., small allowable differential settlement. Therefore, in the urban area, deep or pile foundation is the most common type of building construction because the pile is able to transmit large loads to the deep soil with a smaller size of foundation or footing than the shallow foundation and it can secure the differential settlement smaller than the shallow foundation.

In the development of the urban area, tunnels have been constructed because of the increasing demands of transportation capacity and underground lifeline facilities. Nevertheless, the tunnel engineers have been forced to construct the tunnel with limited public area due to the high density of development. Sometimes, it is unavoidable to construct the tunnel close to the existing pile foundations. The tunneling tends to cause adverse effects on the adjacent pile foundation such as stress reduction around the pile, negative skin friction caused by relative settlement of soil and piles, and extra bending moment and axial force (**Loganathan et al., 2000;**

Tol, 2006; Lee and Chiang, 2007). The engineers have to find the methods to mitigate or prevent those adverse effects by reducing the tunnel induced ground movement and/or reinforcing the soil or foundation. Controlling ground loss in the tunneling work is one of the best way for reducing the movement and if there is an unavoidable risk of the damage even in the well-controlled tunneling process, the additional countermeasures should be implemented, as such, ground improvement and underpinning of the foundation.

The prediction of soil movement caused by tunneling is one of the most important aspects to minimize the damage to nearby structures. Many researchers have investigated the characteristic of soil movement from field observations and physical and numerical modeling. The proposed empirical equations to predict the soil movement show relatively good agreement under green-field condition (soil movements without the presence of pile foundations). However, the soil movement becomes complicated by the presence of pile elements. If the zone of influence (zone with induced large pile settlement by tunnel induced soil movement) can be justified by presence of single and group piles, the preliminary assessment of existing structures within the zone could be conducted prior to the excavation. There is some research on the response of pile foundation subjected to the tunneling but the level of impact to the pile, and the assessment of structural safety have not been well understood. The load transfer between individual piles within the pile group is needed for further clarification. In addition, the evaluation of pile performance against the large ground loss due to large over excavation and even collapse of the tunnel has not been also well studied.

Therefore, for fulfilling the gap in previous researchers, the development of sophisticated physical modeling on pile-soil-tunnel interaction is essential. The finding from such physical models will contribute to the rational planning and designing of tunnels, and minimizing the adverse effects on existing pile foundations.

1.2 Objectives and scope of the study

The important of safe tunnel construction nearby pile foundations has been focused since a few decades ago. In the past, the field observation of the pile response and characteristic of soil movement had been limited (for example, **Lee et al., 1994, Kaalberg et al., 2005**) under well-known conditions. It is quite difficult to install the measured instruments (i.e. strain gauge, extensometer, and inclinometer) especially for the existing piles before starting the excavation.

Therefore, in order to clarify the complexities of interaction between pile-soil-tunnel, the physical modelings using geotechnical centrifuge have been developed. Centrifuge modeling has become a powerful tool in geotechnical engineering for studying the pile-soil-tunnel system at a stress level similar to real conditions. In addition, it can investigate the behavior of various parameters (i.e. the relative position between pile and soil, various range of ground loss value) under controlled initial and boundary conditions. The developments of tunnel model which can reduce the tunnel diameter size by extracting the liquid or reducing air pressure from a flexible bag were first done. However, even rigid tunnel model is installed in the bag; displacement of the tunnel perimeter from the initial condition to the final condition (the inner tunnel) cannot be controlled and is very difficult to measure as illustrated in **Fig. 1.1(a)**. This remains uncertainties in an important boundary condition of the tunnel during the tunneling process. In addition, few researchers have discussed the problem of tunnel excavation adjacent to pile groups with various relative positions between tunnel and pile.

Therefore, the primary objective of this research can be categorized into three points:

(1) To develop centrifuge model with clear boundary (**Fig. 1.1(b)**) for clarifying soil movements caused by tunneling from small to large ground loss ratio.

(2) To illustrate the tunnel-ground-pile group interactions with variation of the key parameters (see **Fig.1.2**) such as horizontal distance between front pile and tunnel centerline (X_p), relative depth between pile end and tunnel (Z_{pe}), cover depth of sand (C), and vertical load on the pile cap (Q_d).

(3) To introduce zone of influence and propose simple evaluation methods for the assessment of pile foundation subjected to tunnel induced soil movements.

1.3 Dissertation structures

This dissertation consists of 7 chapters as the following:

- Chapter 1 explains about the background and state the problem in this study. The proposed objectives to fill the gap of previous researchers are described.

- Chapter 2 reveals the literature reviews which are related to the study of pile-soil-tunnel interaction. The development of physical modeling on tunneling with some ambiguous

feather is discussed along with proposed mechanical tunnel equipment used in this study. Published results from field measurements and physical modelings about the behavior of soil movement and pile response to tunneling are also reviewed. Theory of large soil movement area and the method of measured soil movement are defined. The fundamentals of pile foundation, such as, types, load transfer mechanism and negative skin friction are also explained.

- Chapter 3 illustrates the centrifuge apparatus and introduces the principle of centrifuge modeling. Calibration techniques for each instrument and how to improve accuracy are suggested in this chapter. The procedures and results of the vertical loading tests of the single and the pile group used in this study are also depicted, in which the basic mechanical characteristics are clarified, such as bearing behavior and vertical bearing capacity of the model piles.

- Chapter 4 provides the results of ground movements with and without pile foundation. Settlements of the soil surface and subsurface movements are discussed. The accuracy of Particle Image Velocimetry (PIV) is confirmed by comparing with results from potentiometer (PTM). Performance of tunnel model is justified by comparison with the real field data. Zones of influence are defined from the literature and also observed subsurface displacements.

- Chapter 5 focuses on the mechanical response of pile group due to tunneling by applying the theory of zone of influence to explain the induced behavior. The relative positions of pile from the tunnel, which could cause large adverse effects on the pile are explained.

- Chapter 6 proposes a preliminary and simple assess the stability of nearby structures using the relative position of the pile group to the zones of influence. If the existing piles resting on the proposed zone of influence, tunnel construction should carefully control the ground loss values.

- Chapter 7 describes the conclusion from the study and suggests the recommendation for future study.

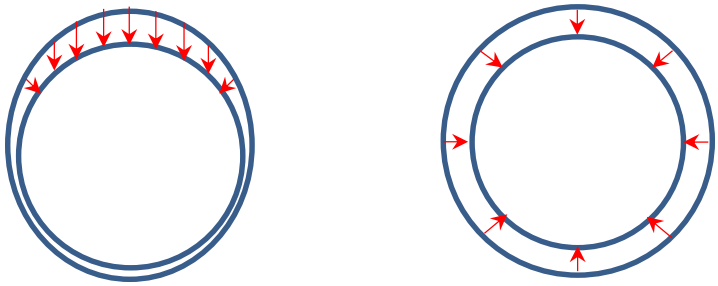

(a) (b)

Figure 1.1 Shapes of radius reduction of tunnel model:
(a) Liquid or air pressure type; (b) Mechanical type (co-axial radius reduction)

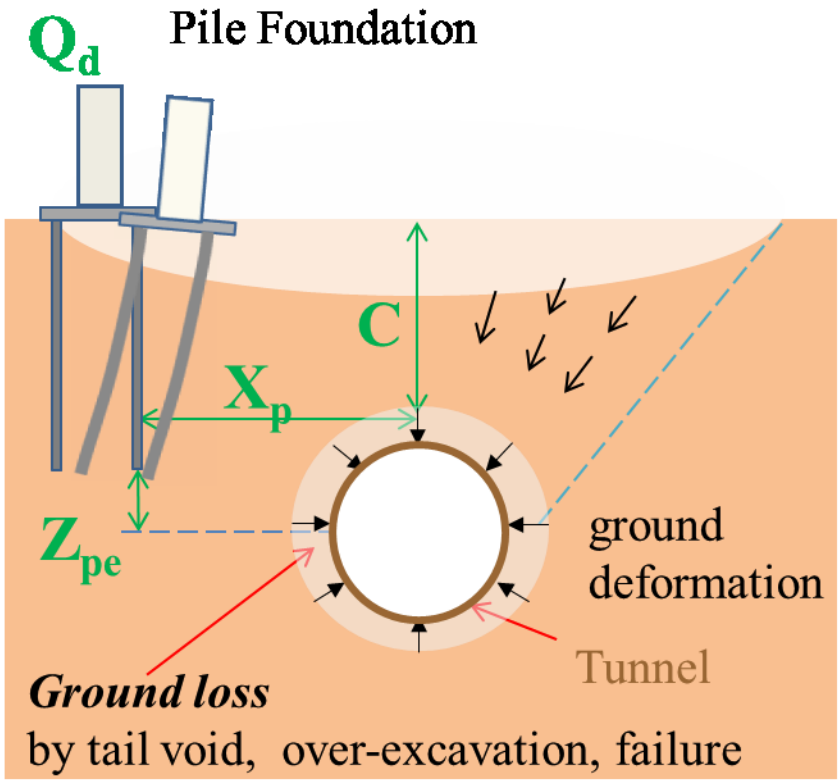

Figure 1.2 Tunnel-ground-pile group interactions with variation of the key parameters

Chapter 2

Literature review

2.1 Introduction

Development of urban with limited space is inevitably required the underground facilities in both small scales (i.e. waste treatment system) and large scale (i.e. transportation system, tunnel). The effects of newly construction of tunnels through the existing structures especially, pile foundation, have been focused since a few decades ago. Normally, when the soils are excavated for tunneling, it triggers the ground loss around the tunnel lining caused by the tail void, over excavation and poor grouting. The soil movements could lead adverse effects to the adjacent pile foundations such as extra bending moment and axial force, differential settlement and lateral deflection along the piles. The estimations of soil movement due to tunneling have been analyzed by many methods such as empirical assessment (**Peck, 1969; Clough and Schmidt, 1981; O'Reilly and New, 1982; Mair, 1993**), numerical assessment (**Gunn, 1993; Chen et al., 1999; Mroueh and Shahrour, 1999; Loganathan et al., 2001; Lee and Ng, 2005**). However, there are some drawbacks to those methods due to the change of stress level and validity of input data. In addition, those methods could not include the effect of present adjacent structures. The soil movement tends to use greenfield condition (soil movement without structures) for the input parameter.

It is difficult to place the instrumented piles for monitoring prior to tunneling work in the real site condition. Physical models especially centrifuge model become more popular to study in this complex interaction because it can create clear conditions and gives precise results of soil-pile-tunnel interaction by using a small model in the laboratory. However, researches on the pile group adjacent to tunneling by centrifuge are relatively scarce. In this chapter, the literature review will firstly focus on the development of tunnel model and soil movement caused by tunneling. Then, it will focus on the pile response caused by the soil movement within the zone of influence.

2.2 Tunneling

2.2.1 Development of physical modeling on tunneling

The study of tunnel-soil-pile interaction by centrifuge has become a common method to investigate this complex mechanism. Fundamentals to simulate the tunneling process is to create the void between tunnel model and surrounding soil by reducing the size of the tunnel diameter. The stress around the tunnel perimeter is reduced, and the soil will move to fill the open cavity. The soil movement will propagate from the subsurface to the soil surface. There are many techniques in order to reduce the diameter of model tunnel. From the previous studies, the types of model tunnel could be grouped into three categories:

2.2.1.1) Air pressure type

A latex rubber membrane filled with compressed air was introduced by **Grant and Taylor (1996)**. The membrane was inserted into the cylindrical cavity, and the air pressure was reduced to simulate the tunneling process. CCTV and LVDTs were applied to investigate the ground movements on both subsurface and soil surface respectively.

Lee and Chiang (2007) developed the air-pressure method for the tunnel model. The air-pressure model was adapted from **Mair (1979**). The stress states around the tunnel could be more realistic if the tunnel can maintain its shape during the preparation and prior to reduction of the diameter. The rubber bag was reinforced by wide filament tape pasting on the rubber surface. This process will enhance the extension stiffness and slightly increase the compression stiffness. Inside the tunnel model, there is no installation of rigid liner. If the net air pressure (internal pressure minus external pressure) is less than the certain value, the diameter will be reduced.

Mahmoud and Magued (2011) adopted the transparent soil which represented saturated sand. The internal soil deformation induced by tunneling could be observed by this particular technique. The model tunnel was established by the PVC tube with latex membrane at the end of PVC to represent the tunnel face. The air pressure was filled inside the tunnel and was assumed to be constant over the tunnel face. On the model ground, rubber tire was placed on the soil surface to provide the surcharge pressure.

The air pressure inside the tunnel face was reduced to simulate the tunneling process. However, it should be noted that the model might not precisely duplicate the construction process in the real condition due to stress in 1g condition. The surface settlement can be correlated with

the normal probability curve proposed by **Peck (1969)** but the maximum settlement and inflection point appear to be different prediction

2.2.1.2) Fluid type

Loganathan et al., (2000) described a centrifuge testing device by equivalent ground loss values. The model tunnel was made by aluminum inner core and was covered by the rubber membrane (**Fig. 2.1**). The surface of the membrane was overlapped with PVC spring to enhance the tunnel stiffness. The most outer layer of the tunnel was then covered with the rubber membrane. The layer between inner core and rubber membrane was filled with silicone oil. The tunnel diameter was reduced by draining the silicon oil through a hole at the end of the inner core.

Jacobsz (2004) investigated the zone of influence by installing the single pile with various relative positions from the tunnel. The brass pipe was used to create the core of the tunnel model. The pipe was covered with a latex membrane and a thick annulus filled with water was inserted between the pipe and latex layers. The balance pressure between the tunnel and overburden pressure was controlled by the standpipe of constant water. The tunneling process was conducted by slowly extracting water from the annulus.

Marshall et al., (2012) conducted the centrifuge tunnel in dry sand to investigate the effect of size, depth and ground loss caused by tunneling. The tunnel model was made by brass cylinder covered with latex membrane. The annulus between latex and brass was filled with the water as illustrated by **Fig.2.2.** Sand model was automatically poured to achieve the relative density of 90%. The soil movements were captured by three cameras and GeoPIV (White and Take, 2002) technique was used to analyze the displaced vectors.

2.2.1.3) Mechanical type

Bezuijen and Schrier (1994) proposed the model tunnel which can reduce the outer diameter as shown in **Fig. 2.3**. The tunnel consisted of 4 synthetic tunnel elements. Those elements were placed on the aluminum core. When the core was moved, the outer diameter of tunnel elements could be changed. The two displacement transducers were mounted on the tunnel elements to measure the tunnel diameter. The soil model consisted of sand overlain by clay layer. The position of the tunnel was varied by two depth levels inside the sand layer. 6 piles with 75% of ultimate bearing capacity were placed at different distances from the model tunnel. The results indicated that the distances between the pile and the tunnel had an effect on the load settlement

behavior. In addition, the type of soil material around the tunnel also had an effect on the pile models.

2.3 Researches on soil movement by tunneling

There are many factors related to the settlement caused by tunnel construction such as volume loss, the depth of the tunnel and trough width parameter. The volume loss has to be precisely predicted to assess the stability of nearby structures. The induced volume loss depends on many parameters. Even the ground loss magnitude is well predicted during design phase, there are still some uncertainties which could occur during construction of the tunnel. Therefore, influence factors which induced higher ground loss than the expectation have been reported by many previous studies. For example, **Standing and Burland (2006)** investigated the measured ground loss from the construction site at Jubilee Line Extension (JLE), London project. From the results, the main influence factors to vary the volume loss magnitudes were related to the tunneling construction method, the layer of clay cover and the variation of characteristics of London clay which is strongly related to permeability. The permeability becomes the most important parameter for the clay layer. The clay with high mass permeability tends to show loosening and softening behavior. In the tunnel construction, the increase in face support played an important role in a significant reduction of volume loss. The length of unsupported tunnel face had to be controlled to provide an adequate degree of support.

2.3.1 Behavior of soil movement by tunneling

The tunneling process is associated with surface settlements and subsurface movement. The effect on structures depends on the width of the subsurface settlement profile and on the magnitude of settlement (**Mair et al., 1993**). The example of single tunnel settlement trough above and ahead of the advancing heading is shown in **Fig. 2.4** (**Attewell et al., 1986**). In the figure, it shows that a tunnel at depth Z_o below ground level causes the propagation of surface settlement trough as the excavation of the tunnel. The shapes of the settlement trough between surface and subsurface are similar (**Fig. 2.5**). In the ground surface, the settlement trough develops giving a maximum settlement (δ_1) over the tunnel center line. At a deeper elevation, at a distance (Z_o-Z) above the tunnel axis, the maximum subsurface settlement (δ_2) is developed in the tunnel center line (**Mair et al., 1993**). In general, trough width is narrowed by the depth layers and the maximum settlement of subsurface (δ_2) is larger than the maximum settlement of the soil surface (δ_1).

The soil movements caused by tunnel construction need to be evaluated for the safety issue of adjacent structures. From the considerable amount of field measurement data (e.g. **Martos, 1958**; **Schmidt, 1969; Peck, 1969; Clough & Schmidt, 1980; Rankin, 1988; Mair et al., 1993**), the behavior of soil settlement could be approximated as a Gaussian normal distribution curve as illustrate by **Fig. 2.5**. The equation of soil settlement is defined as:

$$S(x) = S_{max}\exp(\frac{-x^2}{2x_i^2}) \tag{2.1}$$

where S(x) = settlement at a horizontal location x from tunnel axis

S_{max} = maximum settlement at the tunnel center line, x = 0 (δ_1 in **Fig. 2.5**)

x_i = transverse distance from the tunnel centerline to the inflection point of the curve (trough width parameter)

Main features of the normally distributed curve and the parameters are shown in **Fig. 2.5**. Settlement at inflection point is about $0.606S_{max}$ and half width of the settlement trough is approximately about 2.5 times x_i. From the previous observation, **O'Reilly and New (1982)** showed that the trough width parameter (x_i) can be approximately linear function of tunnel depth (Z_o) as

$$x_i = KZ_o \tag{2.2}$$

where K = empirical constant, called trough width parameter, that can be taken as average value of 0.4 for stiff clay to 0.7 for soft and silty clay (see **Fig. 2.6**), and 0.2 to 0.3 for granular material, regardless of tunnel size and tunneling method.

Z_o = depth of tunnel axis

Mair et al. (1993) proposed the constant K value of 0.3 (for sand) and0.5 (for clay) for prediction of trough width settlements. However, the K values may vary by the depth of the ground. **Grant and Taylor (1996)** suggested that the K value of clay may depend on the movements of the clay layer. As a result, the K value was larger than the prediction of constant K value. The design of the tunnel should be paid more attention to get the realistic prediction of tunnel induced soil movements.

For subsurface settlements at depth Z, it is also assumed that the shapes of subsurface settlement profiles can be represented by a Gaussian distribution curve, the same as equation (2.1). However, Z_o in equation (2.2) is replaced by (Z_o-Z) and K value varies with the depth. It has been found that troughs in the subsurface is narrower and steeper than that of the surface (**Attewell and Farmer, 1974; Barratt and Tyler, 1976; Glossop, 1978; Mair, 1979**). From the observed subsurface settlement records, **Mair et al (1993)** found the relation given in equation (2.3).

$$\frac{x_i}{Z_o} = 0.175 + 0.325\left(1 - \frac{Z}{Z_o}\right) \tag{2.3}$$

Replacing Z_o in equation (2.2) by (Z_o-Z) and substituting equation (2.3) gives the relation between trough width parameter (K) and depth of the trough (Z) into the equation

$$K = \frac{0.175 + 0.325\left(1 - \frac{Z}{Z_o}\right)}{1 - \frac{Z}{Z_o}} \tag{2.4}$$

Therefore, many researchers have tried to develop the empirical equation to predict the soil movement caused by the tunnel excavation. The trough width parameter (K) is an important parameter which is used to define the shape of the settlement trough along the depth layers. The results of field measurements and experiments are summarized in the following:

2.3.1.1) Field measurement

Because the equation (2.2) tends to underestimate the trough width along the depth, **Moh et. al., (1996)** developed the correlation equation based on equation (2.2) by observing the construction of Taipei Rapid Transit System (TRTS)**.** The excavation was done by the earth pressure balancing machine (EPB) with the outer diameter of 6m. The observed data can generate the following equation

$$x_i = \left(\frac{D}{2}\right)\left(\frac{Z_o}{D}\right)^{0.8}\left(\frac{Z_o - Z}{Z_o}\right)^m \tag{2.5}$$

where D = diameter of the tunnel

m = empirical values depend on the type of the surrounding soil. In **Fig. 2.7**, the data from ground loss settlements from TRTS excavation were plotted against the depth. The fitted values for sand and clay equal to 0.4 and 0.8 respectively.

This empirical equation will use for computing the subsurface settlement in the latter chapter.

The measurement of large ground loss value (around 20%) and the result of variation of K parameters along the depth were reported by **Dyer et. al., (1996).** The excavation was conducted to construction the Sudden Valley Sewer in Rochdale. The sewer with 1.43m diameter was rested in the loose to moderately dense sand (around 10m). Using the equation (2.1), the trough width parameter (x_i) was back calculated by measured subsurface settlements (**Fig. 2.8**) and the values were in the range of 2.5 to 3.0. As a result, the K parameter was approximated to 0.32 by equation (2.2). The K value was consistent with the granular range proposed by **O'Reilly and New (1982).** A variation of K parameters at large ground loss value along the subsurface was plotted in the **Fig. 2.9**. **Dyer et. al., (1996)** also concluded that the zone of influence was extended above and below from the tunnel roughly 3 times of the tunnel diameter.

2.3.1.2) Physical modeling test

Multi-layered grounds for the variation of K parameters have been studied by the centrifuge modeling (**Grant and Taylor, 1996**). The data of soil surface settlement with many types of layers has not been focused in the past. Therefore, the two layers of clay overlain by sand were prepared for the centrifuge experiment. The rubber latex filled with air-pressure for the model tunnel was inserted into the clay layer. The variation of trough width (x_i) at the intersect surface by the ground loss is illustrated in **Fig. 2.10**. In the figure, the trough widths (x_i) are scattered at the low ground loss value (< 4%) and become constant at the large ground loss ratio. A predicted subsurface movement by equation (2.2) underestimated the zone of influence as shown in **Fig. 2.11**. The measurement values were wider than the suggested value (K = 0.5 for clay and K = 0.3 for sand). However, in the sand layer, the suggested value was similar to the measurement. The measured values displayed large magnitude because the induced wide trough width from the clay layer. Therefore, the trough width parameters should be separately predicted for each type of soil to the depth.

The soil movement patterns with various cover and depth ratio (C/D = 1 to 4.5) has been reported by **Mahmoud and Magued (2011)**. The tests were conducted under 1g condition with artificial transparent sand. The air pressure supported the tunnel face for simulating tunneling process. The air pressure gradually reduced and the soil movements were captured by CCD

camera for each decrement. Subsurface settlements with different tunnel elevations are shown in **Fig.2.12.** In the figure, Z_o is the tunnel axis depth; S_v is the soil settlement, and D is the tunnel diameter. From the figure, trough width (x_i) increases, and maximum settlement at the center line decrease as the tunnel depth increase. The increment of trough width (x_i) with the cover and depth ratio is consistent with the result proposed by **Sugiyama et al., (1999).**

In addition, the magnitude of settlements between the surface and subsurface depth are varied by the tunnel depth. In shallow tunneling ($Z_o \leq$ 3D), the propagation of soil movements was transmitted to the soil surface. However, in deep tunneling ($Z_o >$ 3D), the soil movement showed less propagation to the soil surface as illustrated by **Fig. 2.13**.

The effects of various parameters such as size of the tunnel, tunnel depth, and the ground loss were investigated by **Marshall et al., (2012)**. Three centrifuge tests were conducted in dry sand by the centrifuge to isolate the effect of those parameters. The results indicated that the Gaussian curve does not well represent the soil movements in the sand especially, at the depth near the tunnel and large ground loss ratio. Therefore, the equation for a change of K values (K^{*}) along the depth was proposed based on the centrifuge results. The proposed equation included the effects of ground loss and cover and depth ratio as shown in the following

$$K^* = \frac{K_S^* - 0.436(\frac{Z}{Z_o})}{1 - \frac{Z}{Z_o}} \tag{2.6}$$

$$K_S^* = 0.440 + 0.055(\frac{C}{D}) - 0.041(V_l) \tag{2.7}$$

where K* = K parameter of published data based on the fit of a Gaussian curve

C = cover depth

D = tunnel diameter

V_l = ground loss

The different of contour settlement with two depth of the tunnel model (C/D=1.3; C/D=4.4) showed the different soil propagation to the soil surface (**Sugiyama et al., 1999; Mahmoud and Magued, 2011)** (**Fig. 2.14**). In addition, the characteristic of soil movements can be illustrated as chimney shape mechanism. In the figure, ground settlement (S_v) is normalized by the maximum soil settlement above the tunnel crown and plotted against normalized depth and normalized horizontal distance from the tunnel center line.

2.3.2 Large soil movement area (zone of influence)

The areas that caused large piles settlement due to tunnel excavation have been studied by many researchers. **Kaalberg et al., (1999, 2006)** investigated the full-scale study of Heinenoord 8.3m twin tunnel excavation near Rotterdam. The bunch of timber and concrete piles with various locations from the tunnel were monitored during the excavation. The piles were rested in the multi-layers of soft clay, peat and dense sand. If the distance effect was confirmed, the depth of tunnel construction could be reduced, and the cost of tunnel construction could be substantial minimized. The settlements of the existing pile can be induced by two causes: the settlement of the soil layer around the pile and the diminution of stress around the pile end.

By the settlements of those piles, the zone of influence could be categorized into three zones depend on the relative location of pile ends and the tunnel (**Fig. 2.15**). When the pile ends are rested in zone A, piles are settled larger than the surrounding soil but the piles show smaller settlement than the surrounding soil as the pile ends are rested in zone C and equally settlement for the piles in Zone B.

Similar zone of influence was observed in new Channel Tunnel Rail Link (CTRL) by **Selemetas (2006).** The twin 8m tunnel was constructed by Earth pressure balance shield with the grouting through the London clay. The settlements and end bearing loads of reinforced concrete piles with various offset from the tunnel were monitored. The kentledge reaction platforms were applied on the piles top to give the 50% of ultimate bearing capacity. The heave due to grouting pressure by TBM could be observed in the friction pile where the pile end was located above the TBM and had pile end-tunnel crown distance of 1.9m but the bearing pile displayed slightly settlement with the same relative position and had the distance of 6.4m. For both of friction and end bearing piles at $X_p/R=3.0$, piles experienced no differential settlement between the pile head and the ground surface settlement and had an increase of end bearing loads slightly. In contrast, for the friction and end bearing piles above the tunnel ($X_p/R=0$), the piles suffered large differential settlement and a large reduction of end bearing load. As a result, by the pile and soil settlements, zones of influence could be drawn as illustrated by **Fig. 2.16.** Piles in zone A showed larger settlement than the soil surface with reduction of end bearing load. In zone B and C, pile settlements are equal to and smaller than the soil surface respectively without the reduction of end bearing loads.

The zone of influence was also defined by the centrifuge test series by **Jacobsz (2002)** and **Jacobsz et al., (2004)**. The single pile made from aluminum alloy was placed in dry sand at a relative density of 75%. Extracting water from the brass pipe of tunnel was made for simulating the tunneling process. The soil surface and pile settlements were recorded by Linear Variable Differential Transformers (LVDTs). The pile with 50% of resistance load was installed at various relative locations from the tunnel as shown in **Fig.2.17**. In the figure, pile ends positions are shown as circular solid (large pile settlement) and open (small pile settlement) shapes. When the piles are settled larger than 20mm (prototype scale) at 1.5 % ground loss, the piles are defined as a large settlement. Line *a* and *b* are drawn at 90° and 45° + half magnitude of soil internal friction respectively from the tunnel spring line. Line *d* is tangent at 45° from the tunnel toe and line c is drawn based on the experimental observation from the joint of $2x_i$ points at the surface to line *d*. In zone A and B, pile suffered large settlement with reduction of the end bearing load. In zone D, pile showed small settlement due to less effect from the tunneling. The transition of pile settlement between zone A, B and zone D could be found in zone C. In addition, the behavior of pile groups is unclear, if the front and rear piles are rested in different magnitude of soil movements.

The pile settlements and volume loss are plotted in the **Fig. 2.18**. In the figure, the numbers indicate the locations of piles correspond to the pile ends positions in **Fig 2.17**. In position 1, 2 and 3, piles underwent large pile settlement since small ground loss ratio (<1.5%). The pile in position 4 showed large development of settlement and the settlement increment became small as the ground loss increases. The tunneling effect is negligible in the area outside influence zone (position 5). In addition, the piles resting in zone A and B developed the reduction of end bearing as indicated in **Fig.2.19**.

2.3.3 Particle Image Velocimetry (PIV)

The measurements of soil movement at the model tests have been developed since 1960s. Many researchers tried to trace the soil displacement by various techniques such as X-ray method (**Roscoe et al., 1963**), stereo photogrammetric method (**Andrawes and Buttefield, 1973**) and close-range photogrammetry method (**Taylor et al., 1998**). These methods have to provide the reference points such as markers or artificial bead within the model for tracing the soil particles movement. The presence of those reference points could interfere with the magnitudes and directions of soil particles movement due to friction or stiffness (**White et al., 2003**). In addition,

the reference points are difficult to prepare for some model tests and it is a time-consuming process.

In the conventional methods (X-ray and stereo-photogrammetric), the object-space coordinates were scaled directly from the image-space measurements. Those methods assumed that the convert ratio between image-space to object-space was constant across the measurement area. It could be inaccurate for the real displacement of soil particles. Therefore, the development of close-range photogrammetry (**Fig. 2.20**), become popular nowadays because the technique shows flexible and accurate convert ratio magnitudes. **White et al., (2003)** introduced the Particle Image Velocimetry (PIV) technique by applying the inexpensive digital camera to capture the sequence of soil movement images. The technique does not require the colored mark or the reference points to trace the soil particles movement. Natural soil has its own color and texture which are used for finding the vectors of soil movement.

Particle Image Velocimetry (PIV) has developed from the measurement of seed flow in the fluid experiments. In PIV, the consecutive images are captured during the geotechnical experiment. The analysis areas within the images are divided into a grid of test patches. The test patch of the first image will be traced the displacement vector within the defined search zone of the second image. Individual soil texture is utilized for the most correlation between each pair of the test patches as shown in **Fig. 2.21**. The correlation offset is equal to the displacement vector (**White et al., 2003**). The displacement vectors could be traced from the first picture to the third picture or from the second picture to the third picture which depends on the input route of analysis process. The accuracy of PIV could be reduced by the poor image qualities such as poor brightness, shaking of the camera and distortion by uneven planes between lens and model screen etc. Those factors will lead to the random or noise vectors.

The calibration of the test setup (e.g. camera, soil and the model container) need to be carried out to find the approximate calibration factors and increase the precision of the results. For example, **White (2002)** and **Take (2002)** conducted the defined increment of soil translation with a fixed camera. The displacement vectors obtained by PIV should be identical for over the area of analysis. Some error of displacement vectors was related to the precision of the test set up. The summation of influence factors for PIV are listed in **Table 1 (White and Take; 2002).**

2.4 Pile foundations

Foundation is the lowest part of the structure for supporting the load from the superstructure. There are two types of foundation: shallow foundation and deep foundation. The first type transfers the load to the soil on which it is attaching. The second type transfers the load to the underground stronger layer than the surface. The deep or pile foundation was used in the building of concern about structural safety such as structure with sensitive to differential settlement, structure subjecting to the lateral force and worse soil condition at shallow depth (high swelling, very high water table, soil erosion). Pile cap is defined as the connection between the superstructure and the pile element. The top of the pile which is connected to the pile cap is called the pile head, and the end of the pile is called the pile toe (pile end). Pile shaft is the element lie between the pile head and the pile toe.

Pile was made by many types of materials such as timber, steel and concrete and many shapes of cross-section. The selection of pile types depends on the characteristic of site construction and the method of installation. In general, piles are used as a group with the same pile cap. The behavior of single pile is different from the individual pile in the pile group because of the group effect. For example, when the pile group subjects to the lateral force at one side, the piles will resist the push and pull force for the opposite and the same side respectively.

2.4.1 Point bearing pile and friction pile

The load capacity of the pile (Q_u) consists of end bearing load (Q_e) and shaft friction load (Q_s) as written in equation (2.8). If the pile is installed to the bedrock which can resist the load of the structure and the load capacity rely entirely on the end bearing load, the pile will be categorized as point bearing pile (equation (2.9)) (see **Fig.2.22 (a)**). On the contrary, if the pile could not penetrate to the strong layer and the resistant at the pile end is very small, the pile is considered as friction pile (equation (2.10)) (see **Fig.2.22 (b)**).

$$Q_u = Q_e + Q_s \tag{2.8}$$

$$Q_u \approx Q_e \tag{2.9}$$

$$Q_u \approx Q_s \tag{2.10}$$

2.4.2 Load transfer Mechanism

Normally, the resisting load of pile comes from the end bearing load (Q_2) and the shaft friction (Q_1) as shown in **Fig. 2.23 (a)**. If the load of the structure ($Q_{z=0}$) is increased to a certain value (i.e. Q_u), the pile will settle creating the mobilized of skin friction. When the skin friction is fully mobilized, the shaft friction of Q_1 will become Q_s as shown in **Fig. 2.23 (b).** At the same time, the pile end will be settled, and the end bearing will be mobilized to Q_e. In general, the mobilization of pile end requires larger settlement than the mobilization of shaft friction. Therefore, the load transfer mechanism could be represented in **Fig 2.23**. In addition, the average of unit skin friction along the pile can be calculated by the following equation.

$$f_{(z)} = \frac{\Delta Q_{(z)}}{(s)(\Delta z)} \tag{2.11}$$

where $\Delta Q_{(z)}$ = difference of measured axial force between two points along the pile model

Δz = distance between two points of axial force measurement

s = perimeter of pile cross section

2.4.3 Negative skin friction

Shear stress along the interface of pile is mobilized by a relative movement between pile and surrounding soil. The relative movement causes by many mechanisms such as a pile is pushed to the ground, a pile is pulled up from the ground, and soil along the pile is consolidated or swelled. Positive skin friction or positive shaft friction is caused by pile is settled larger than surrounding soil. On the contrary, if the soil is settled larger than the pile, negative skin friction is developed.

In general, negative skin friction relates to drag load acting along on the pile. Drag load can become the extra load which reduces the allowable load on the pile (**Johannessen and Bjerrun, 1965; Bozozuk, 1972).** In addition, drag load can only be induced by the reconsolidation caused by the pile installation (**Fellenius, 1972**). The small relative movement without slip behavior is enough to cause reverse shear load along the pile (**Walker and Darvall, 1973; Fellenius, 1984**). **Bozozuk (1972)** proposed the relation of negative skin friction in the following equation.

$$q_n = \beta\sigma'_v = MK_s \tan \quad (2.12)$$

where β = beta-coefficient (constant value)

σ'_v= effective overburden stress

M = ratio of the wall friction

K_s = earth pressure coefficient in the soil

The modes of relative movements between pile and surrounding soil are summarized in the **Fig. 2.24** **(Fellenius, 1984)**. In mode A, the pile is pushed into the ground causing the settlement of soil and positive skin friction. The pile will be compressed, and thus the earth pressure coefficient (K_s) is increased. The effective overburden is also increased due to induced positive skin friction. In mode B, the pile is pulled out from the ground causing the upward movement of ground and negative skin friction. The pile is elongated thus the lateral pressure is reduced. However, the pull load test in mode B could not simulate the drag load effect on pile due to the reduction of effective overburden stress. In general, the normal dragl oad will occur as shown in mode C. The pull load test should be arranged in mode D where the pull load is also applied at the pile end. The soil expansion effect is illustrated in mode F and the soil expansion test could be arranged in mode E.

When the pile is subjected to the drag load, there is a point that the summation between the working load and drag load equal to the end bearing load and shaft friction. That point is called a neutral plane as indicated in **Figure 2.25** **(Fellenius, 1984)**. There is no relative displacement between pile and soil at the neutral plane. By load transfer mechanism, if the pile end resistance is increased or presence of bedrock at the pile end, the neutral plane will move deeper into the soil. On the contrary, if the working load of the superstructure increases, the neutral plane will move up toward the soil surface.

Negative skin friction can be mitigated by reducing the friction between pile interface and soil such as coat the surface with bitumen (**Bjerrun et al., 1969**).

2.5 Research on the pile foundation responding to tunneling

2.5.1 Field measurement

Jacobsz (2006) has observed the behavior of relatively deep long pile groups supporting bridge (Renwick Road Bridge) and flyover (Ripple road flyover) subjected to the Channel Tunnel Rail Link (CTRL) construction. The monitor was conducted to investigate that the mitigation work should be conducted or not. The pile ends of both bridge and flyover were rested inside the zone of influence (**Jacobsz et al., 2004**) with the significant reduction of end bearing could be occurred. When the pile end bearing was reduced, the shaft friction of the pile would be mobilized to compensate the loss of end bearing load. If the fully mobilized shaft friction is smaller than the reduction of end bearing, the pile will suffer significant magnitude of settlements.

In small ground loss ratio, the magnitudes of settlements for those pile bases were approximately equal to the green-field settlement. From the monitoring data, due to small ground loss values, the reduction of end bearing could be compensated by mobilized shaft friction. Consequently, those piles produced negligible settlements, and there was no requirement for the mitigation work.

Kwast (2006) described the interaction between newly tunneling to existing tunnel of the project of Pannerdensch Canal tunnel (PC). The distance between two tunnels were varied from 0.3 D to 0.5D (tunnel diameter, D = 9.5m). Both tunnels were mostly embedded in the filled sand which had uniform layers. The information of the sand layer was well provided due to intended backfill operation. From the first tunnel (existing tunnel), the measured results

The induced maximum increase of lateral ground stresses and water pressure could occur during the passage of the shield tunnel. In addition, the ovalisation of the existing tunnel should be monitored during construction of the second tunnel. From the field measurement, the effect of the second tunneling to the first tunnel at the distance 0.3D-0.5D was negligible due to well-compacted sand layer. However, the awareness of adverse effect should be focused when the tunnel is constructed in soft soil condition with small distance between the tunnels.

Pang (2006) conducted the response of full-scale working piles at MRT North East Line project in Singapore. Twelve piles were attached to various positions of strain gauges to measure axial forces and bending moments during the excavation. The relative horizontal distance from the center of the tunnel and the nearest pile (X_p/R) was 1.5. The piles were installed prior to

excavation, and most of the soil layer was residual soil type. The soil surface settlement shapes behaved like Gaussian distribution curve, and trough width parameters (K) were consistent with value of 0.5. The volume loss caused by face loss, shield loss, and the tail void was calculated by the volume of surface settlement. In axial force profiles, drag loads which were mobilized from negative skin friction were developed along the pile and the induced axial forces were triggered when the excavation became close to the piles (< 7.5R). The maximum of transverse bending moment was occurred at the tunnel spring line. The front pile revealed larger magnitude of axial force and bending moment than the rear pile due to pile-soil-pile interaction and the shadowing effect (distance effect) from the front pile. Both axial force and bending moment were increased as the volume loss increased. It should be noted that the induced bending moments were small even the piles located very close to the tunnel. As a result, the induced bending moment at small ground loss is negligible.

2.5.2 Analytical study

Lee and Ng (2006) investigated the three-dimensional elasto-plastic coupled consolidation numerical simulation of tunneling effect. The soil material was modeled by elastic-perfectly-plastic soil model and tunnel lining, and concrete pile were analyzed by linear elastic material. From the results, the zone of influence could be observed as the tunnel face passed through the range of one tunnel diameter ahead and behind the position of the pile model. By using the additional pile head settlement and load settlement curve, the reduction of soil resistance factor of safety could be determined. As the pile was located near the tunnel crown, the pile was settled larger than the soil surface which is consistent with the observation by **Jacobsz et al. (2002)**

During the tunnel excavation, soil movements in the transverse direction were larger than the longitudinal direction. Induced bending moments and axial forces were significant small magnitude when compared to the yield moment and bearing capacity of the pile respectively. Therefore, the tunnel had slightly adverse effects on the induced axial force and bending moment. However, a comparison with the centrifuge results showed that the numerical method underestimated the maximum surface settlement due to exclusion of soil stiffness reduction.

Surjadinata et al. (2006) proposed the method of analysis single piles subjected to tunneling by two sequences of the finite and boundary elements (FAB). The first sequence was dealt with the prediction of free-field soil movement by finite element method. Then, the second sequence was the analysis of single pile response to those soil movements by boundary element

method. The reliability of FAB was proved by comparing with the lateral movement of the real field (**Deane & Bassett (1995)**). A comparison showed that the FAB method underestimates the horizontal movement at the shallow depth and overestimates the maximum horizontal movement near the tunnel elevation. However, in the case of stiff clay and small ground loss ratio (less than 2%), the FAB method predicted the consistent results. The proposed method can simulate quite reasonable outcome and inexpensive with less time consuming than the 3D conventional method. The separate concepts have showed some light of numerical analysis, but there are still lacks of the results such as pile group interaction, soil-plastic yielding and varied soil stiffness by strain levels.

P. Kittiyodom (2006) developed the three-dimensional simplified analytical method to investigate the tunnel induced soil movement for preliminary design of tunnel construction. The method was provided for pile raft type of foundation subjected to the tunneling and showed good consistent with boundary element method (**Loganathan et al., 2001; Xu and Poulos, 2001**) and FLAC3D program (**Itasca, 2002**). The raft, piles, and soil components were modeled as thin plates, elastic beams, and interactive springs respectively. The features of the method utilized the relative deformation between nodes of each types of element (i.e. pile, soil and raft) to calculate the response on the pile raft (i.e. pile movement, pile rotation, axial for and bending moment profiles). Consequently, the proposed method could be applied to the preliminary design tool with less time consuming than the conventional three-dimensional analytical method.

I. Chissolucombe (2006) investigated the influence of soil movement on the building (fuel station) by finite elements method (SIGMA/W by **Geo-Slope, 1998**; POS-3D by **PUC-RJ**). Ground displacement pattern is altered by the presence of the building due to the stiffness of those structures. The soil displacements tended to show flat shape of the settlement trough with reduction of the magnitude. The sequences of tunnel construction are modeled by the stages through the group of piles. Tunneling process is simulated by removing the soil elements and activating the structure elements. The large longitudinal angular distortions became critical parameter due to exceeding the allowed limit.

2.5.3 Physical modeling study

J.R.Standing (2006) introduced the method to investigate the effect of piling to the existing tunnel by photo-elastic technique. The single pile and tunnel are made from perspex material surrounding the pyrex particles which act as the soil layer. The soil was saturated with the paraffin. All of the models had the same refractive index which gave transparent properties to those models. The light and bright could be observed when the elements were stressed. The images were taken during the piling process to investigate the relative positions which provided the most stress region between the pile and the tunnel. The triangular shape zone of influence could be traced by varied the horizontal distances between pile and tunnel. When the pile was penetrated within the range of one pile diameter, the curve column of light due to high stress was connected between pile end and the tunnel. This zone of influence was similar to the zone of large pile settlement proposed by **Jacob et al., 2003**. The unique stress pattern which moved from the pile end toward the adjacent tunnel was related to the high stiffness of solid inclusion tunnel. The results of the study provided the minimum distance (one-time diameter) between the existing tunnel and new pile construction.

Pile responses subjected to tunneling induced soil movements have been studied by centrifuge models. Using 2D mechanical tunnel simulator, **Bezuijen and Schrier (1994)** investigated the behaviour of single piles loaded with 75% of vertical ultimate capacity for two subsoil conditions, namely, uniform sand and sand overlaid by clay. The distance of pile from the tunnel was also a parameter tested for the study. The width of the settlement trough was smaller for the case of tunnel in the uniform sand than that for the sand overlaid by clay. On the other hand, the influence distance of pile from the tunnel was larger for the uniform sand layer than the two layers. The test results also showed the effect of mobilized bearing forces, including shaft friction before tunneling on the pile response during tunneling. **Loganathan et al. (2000)** conducted centrifuge tests on a single pile and pile groups with 4 piles in clay in which two-dimensional tunneling was simulated using very precise rubber bag technique. The length of pile and distance of pile from the tunnel center was fixed by one tunnel diameter, and relative depth of the pile was varied changing the tunnel cover depth. They suggested the applicability of elastic analysis for predicting the behavior.

Caporaletti and Burghignoli (2006) conducted the centrifuge modeling to study the interaction between the tunnel movement and pre-existing structures with multiple layer types and subjected to large ground loss ratio. The rubber bag filled with air-pressure was utilized as a tunnel model. The tunnel was embedded in the kaolin clay layer overlain by the sand. The pre-existing structure was a concrete wall. The image of soil movement was applied to observe to settlement trough. The results showed that the width of the settlement trough (x_i) was constant during the tunneling. Therefore, the shapes of the settlement trough remained constant regardless of the ground loss ratio values. However, this assumption of **Caporaletti and Burghignoli (2006)** is different from the result of the author study. In this study, the shapes of the settlement trough become steep in the larger ground loss ratio. In addition, the case with the presence of the concrete wall tended to reduce the magnitude of surface settlement at the tunnel centerline.

2.6 Conclusions

In the past, the measurement data from the real site construction are relatively limited. The developments of numerical and physical modeling have been introduced to study the interaction behavior. Recently, physical model has been justified validity to investigate this complicated interaction because it can similitude the stress level in prototype scale with model scale in the laboratory and can simulate the change of stress caused by the excavation.

The many types of tunnel model have been developed to simulate the tunneling process. Tunnel filled with liquid or air pressure could not control the radial reduction along the perimeter while lowering the pressure. Those types of tunnel can cause some uncertainty of boundary condition especially at large ground loss ratio. However, in this study, mechanical tunnel model which can reduce the diameter in co-axial direction (reduction in the same magnitude for all radial directions) has been applied. This tunnel is also able to imitate the grouting process during the excavation. The results of new tunnel model could be justified by comparing with the field measurement data from working load condition (low ground loss value) to collapse the state of the tunnel (high ground loss value).

The zone of influence (**Jacobsz et al., 2004**) which uses various positions of single pile in dry sand will be utilized with pile groups in this study. There is some probability to induced larger uneven settlement because the piles are rested within and outside the zone of influence at the same time. The relation of pile group and zone of influence does not address in the previous study.

The development of visual aid (i.e. camera, video recorder) and computer performance provide the high image quality to capture the soil movement during the experiment. The Particle Image Velocimetry (PIV) technique utilizes the soil texture to trace the displacement vectors without the colored mark along the soil. The displaced vectors and trough width parameter (x_i) along the depth are need for clarification the zone of influence in the study.

The above-mentioned researches provided important information about the mechanical of piles subjected to tunneling-induced soil movements. However, the effect of existing structures for soil movements had a very few case records, especially in the pile groups foundations. Few researchers have addressed the modeling technique of pile group and tunneling. There remains a room for improving the modeling technique to obtain the results more reliable. The shape of profile settlements may have been altered caused by surrounding buildings. Therefore, in this study, a series of centrifuge model tests were carried out to scrutinize the tunneling induced soil movement and the effects of pile group on the soil movement.

Table 2.1 The effect parameters of particle image velocimetry (PIV) (**White and Take; 2002**)

Parameter	Setting	Result
Search zone	Too small	- PIV could not get the properly displaced vectors due to search zone is smaller than the largest displacement vectors
	Too large	- Time-consuming
Frame rate	Too low	- The correct peak correlation could not be obtained due to many noise peak correlation
	Too fast	- PIV could not track the initial failure plane
Patch size	Too large	- The important strain field may lose by cover in those strain field
	Too small	- The patches contain less information and sensitive to error caused by poor image and distortion
Leapfrog	Too low	- Precision is reduced due to no displacement update between group of images
	Too high	- Create the wild vector due to the summation of error displacement
Image quality	Window scratch	- Displacement vectors are stuck at the scratch line
	Insufficient texture	- The vectors could not trace precisely creating wild vectors

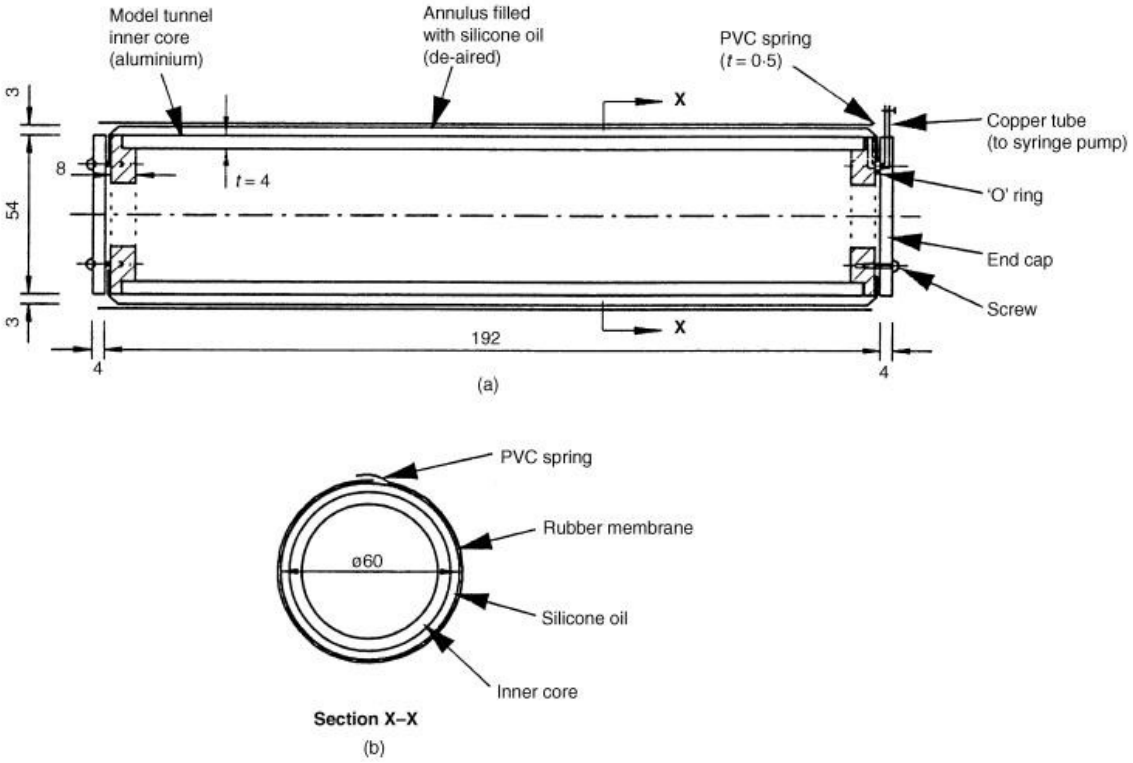

Figure 2.1 Aluminum core tunnel (dimension in mm) by **Loganathan et al. (2000):**
(a) longitudinal section; (b) section x-x

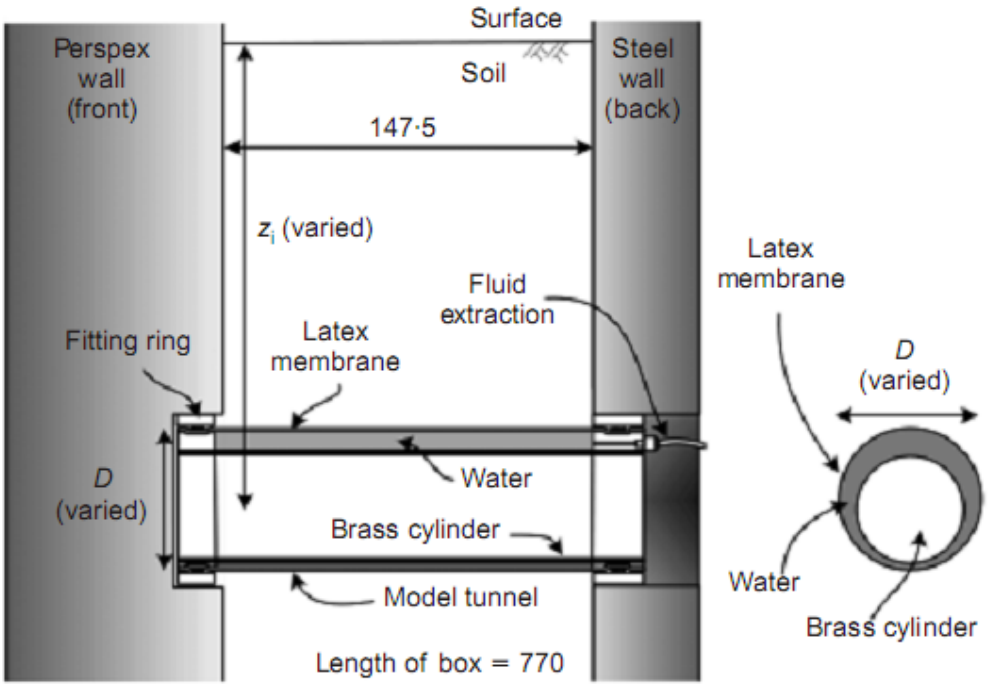

Figure 2.2 The layout of tunnel machine and cross section of the model (**Marshall et al., 2012**)

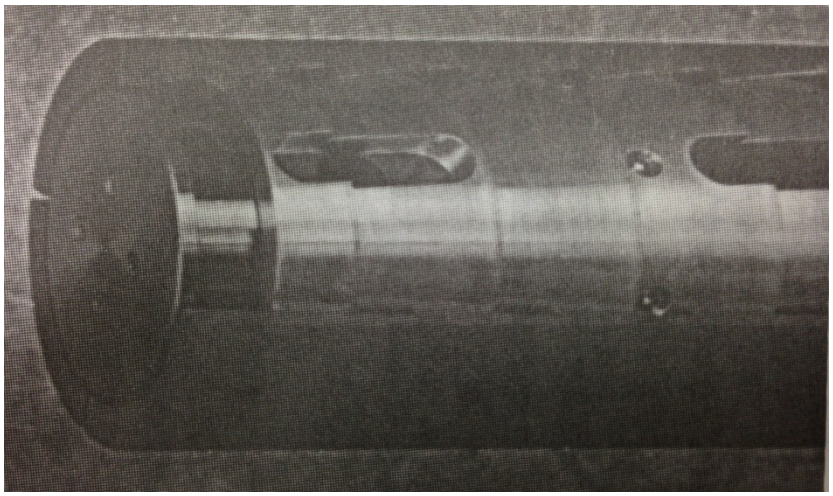

Figure 2.3 Mechanical model tunnel by **Bezuijen and Schrier (1994)**

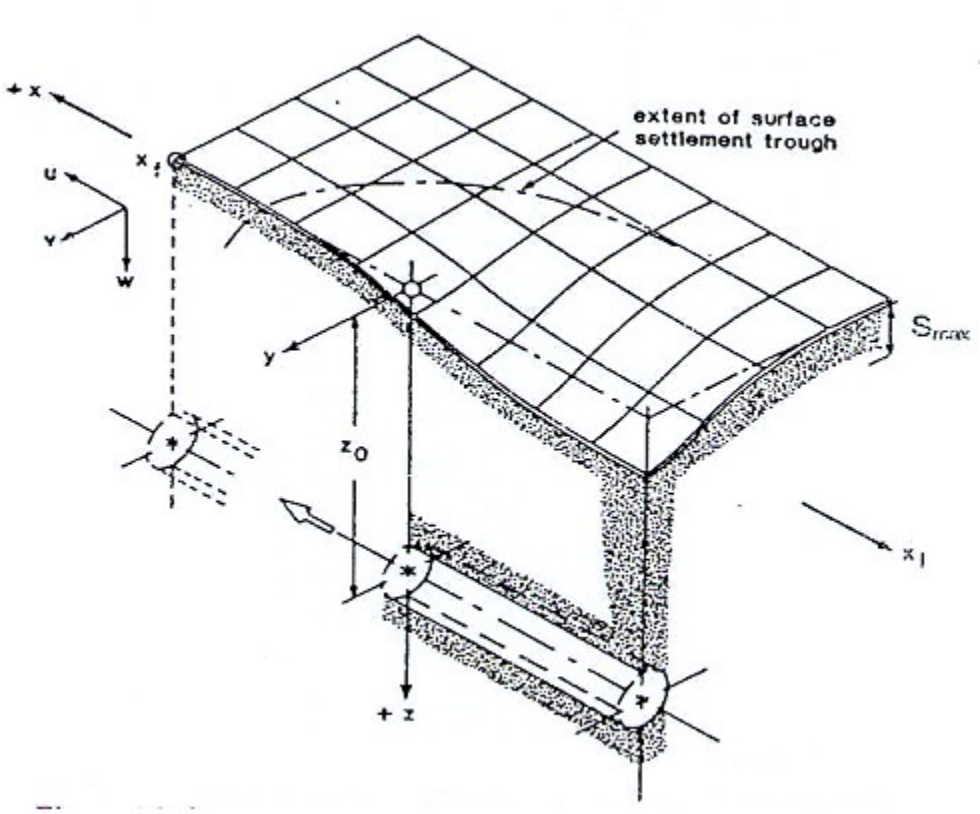

Figure 2.4 Characteristic of soil settlement above advancing tunnel heading (**Attewell et al., 1986**)

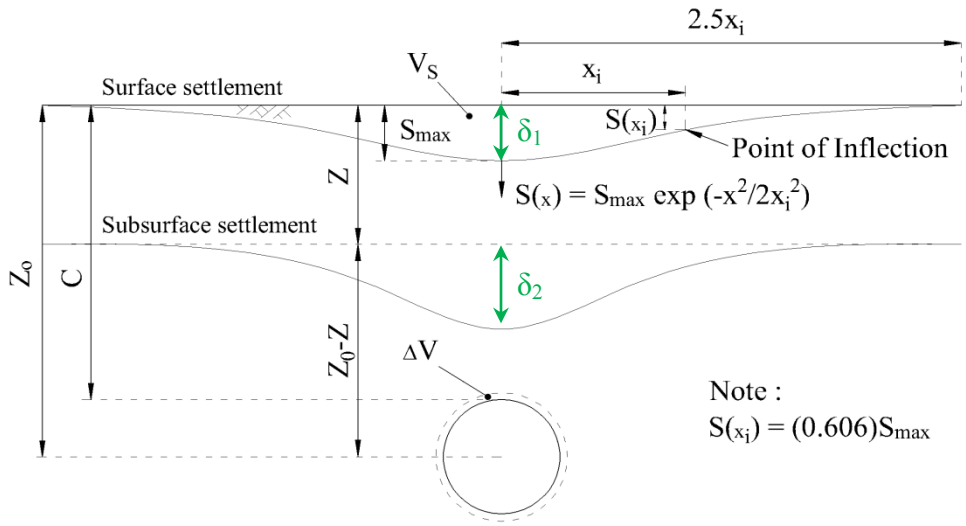

Figure 2.5 Parameters and settlement profile described by normal distribution curve

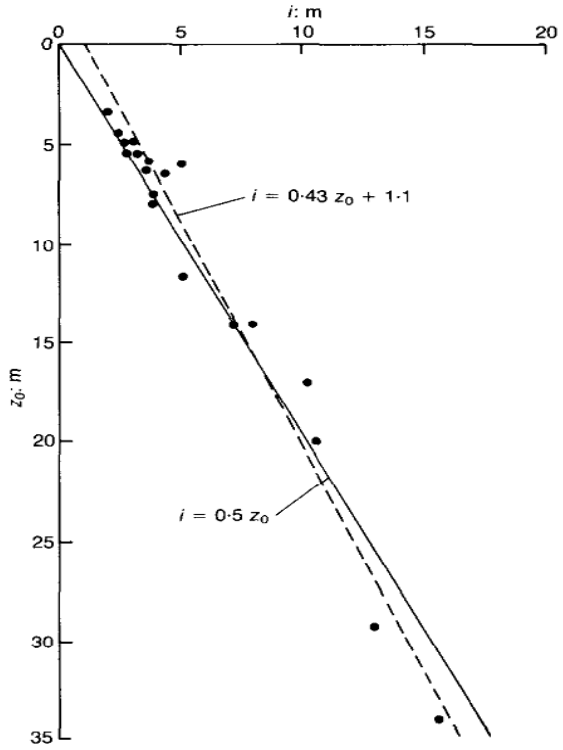

Figure 2.6 The measurement of trough width parameter with various tunnel depths in clay (**O' Reilly, New, 1982**)

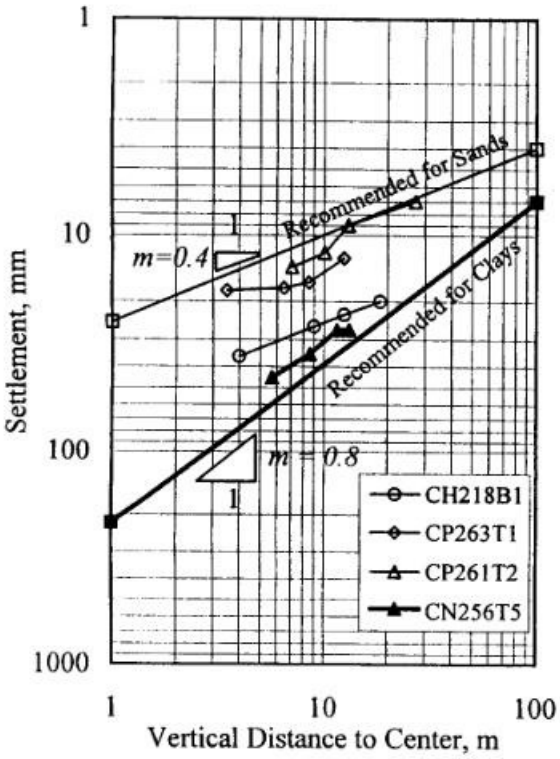

Figure 2.7 Determination of parameter m (**Moh et al., 1996**)

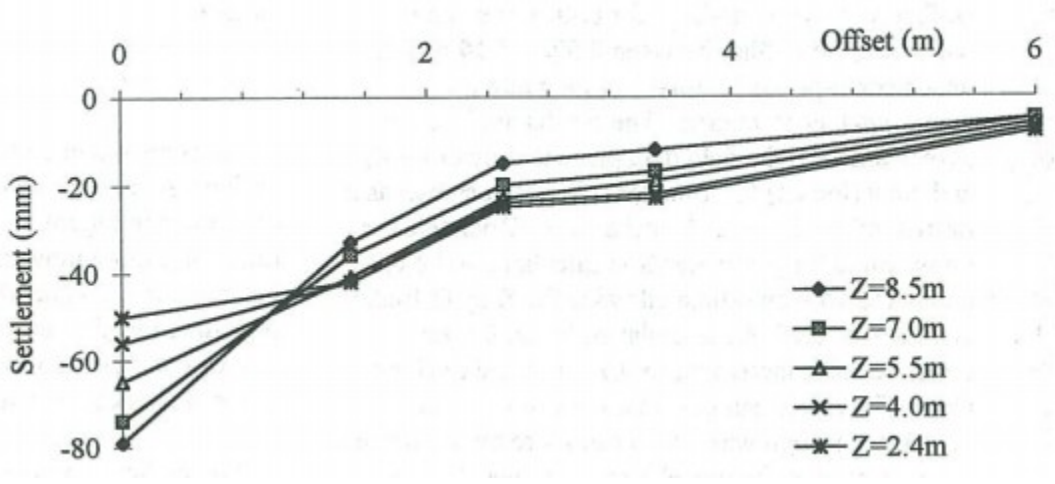

Figure 2.8 Subsurface settlement profile (**Dyer et al., 1996**)

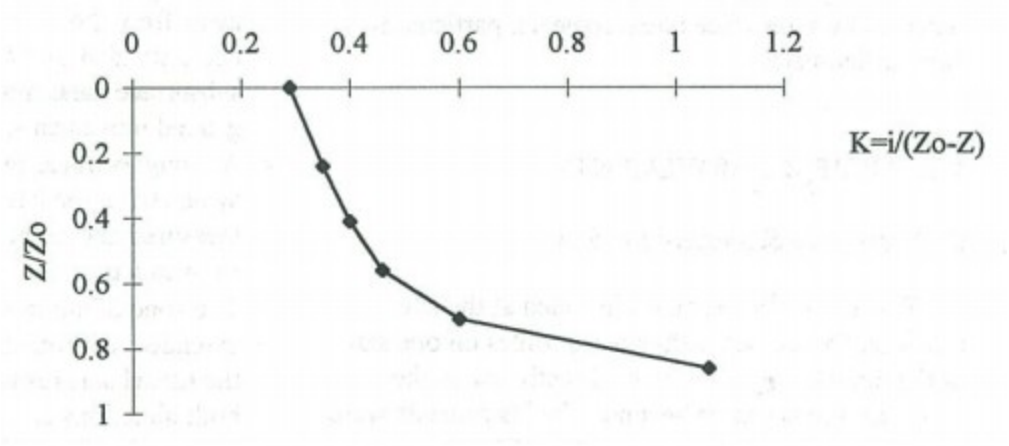

Figure 2.9 An approximate of K values along the depth from subsurface settlement (**Dyer et al., 1996**)

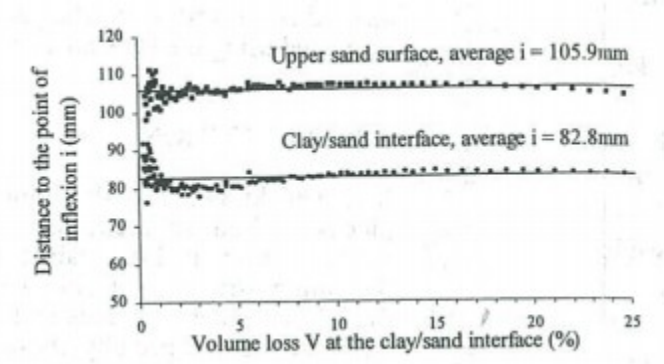

Figure 2.10 Variation of inflection point by volume loss (**Grant and Taylor, 1996**)

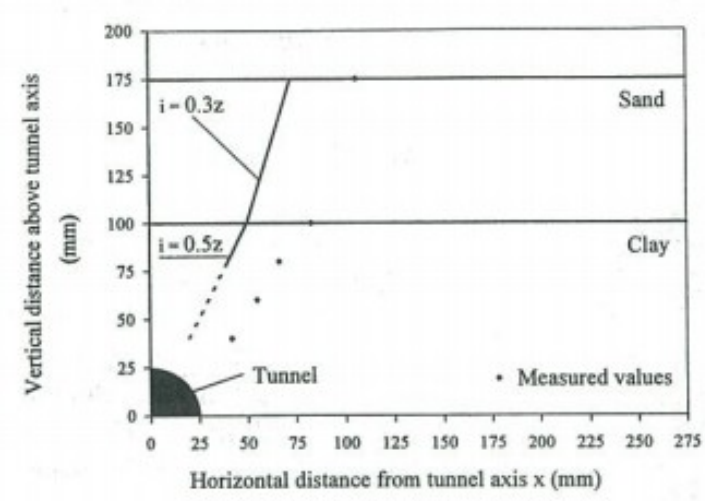

Figure 2.11 Distribution of i with depth from measured and suggested values (**Grant and Taylor, 1996**)

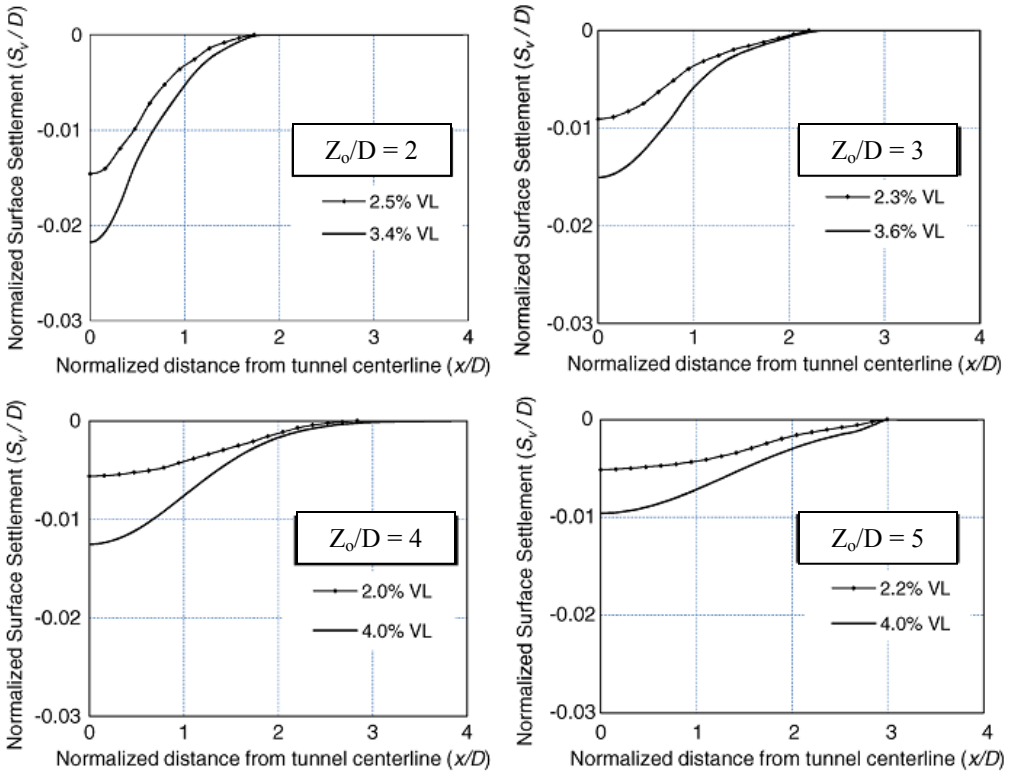

Figure 2.12 Subsurface settlement with ground loss for various tunnel elevations

(Mahmoud and Magued, 2011)

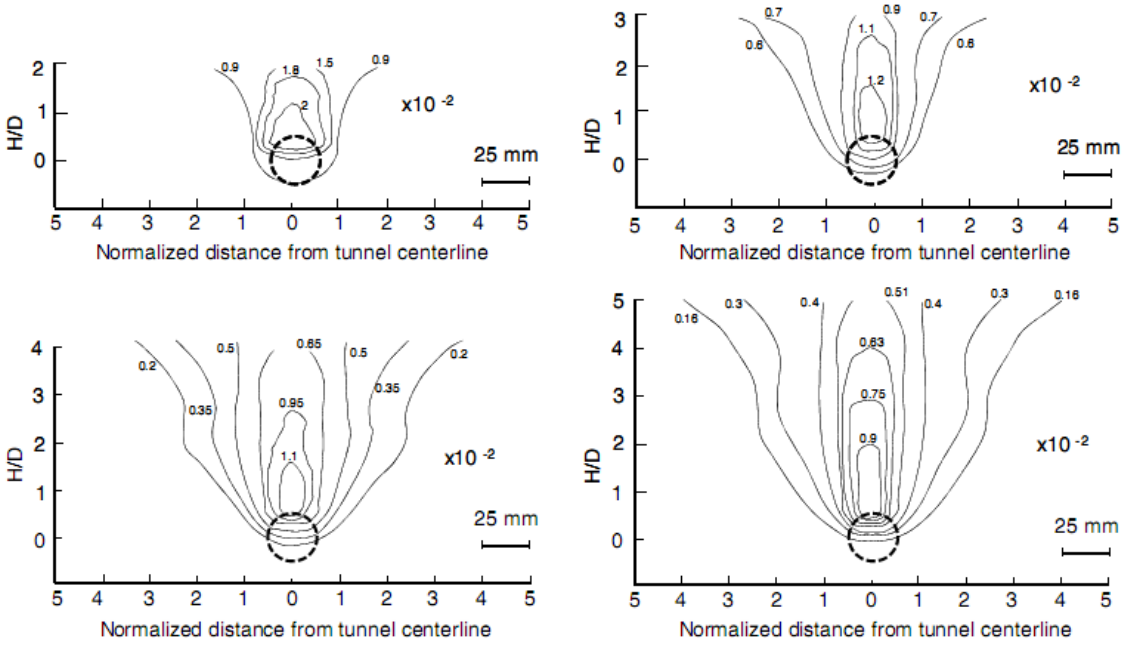

Figure 2.13 Contour of vertical soil settlements at ground loss 2-2.5 %

(**Mahmoud and Magued, 2011)**

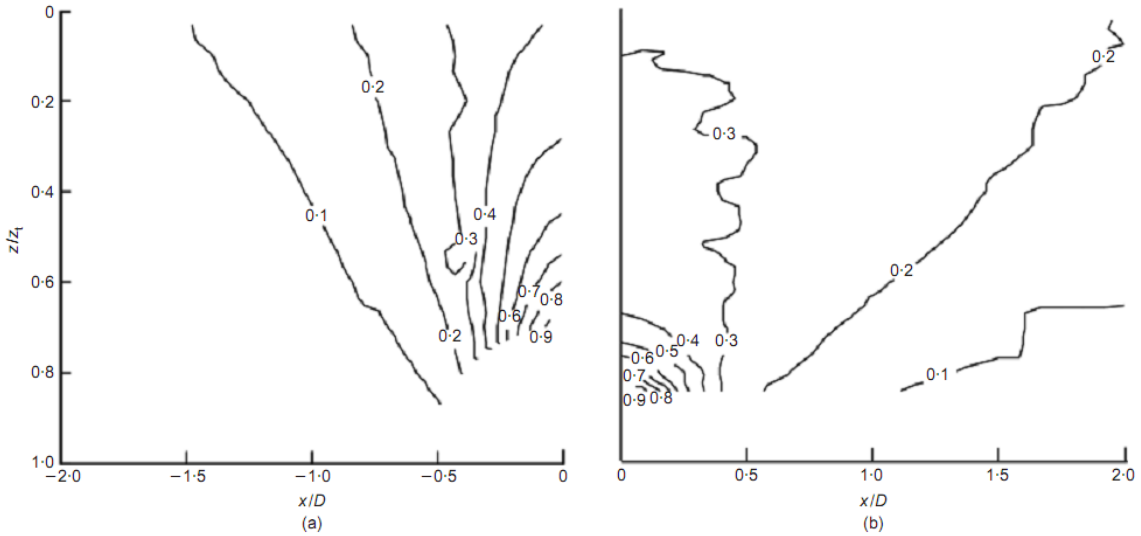

Figure 2.14 Contour of normalized vertical ground settlement at 5% of ground loss: (a) case with C/D=1.3; (b) case with C/D=4.4 (**Marshall et al., 2012**)

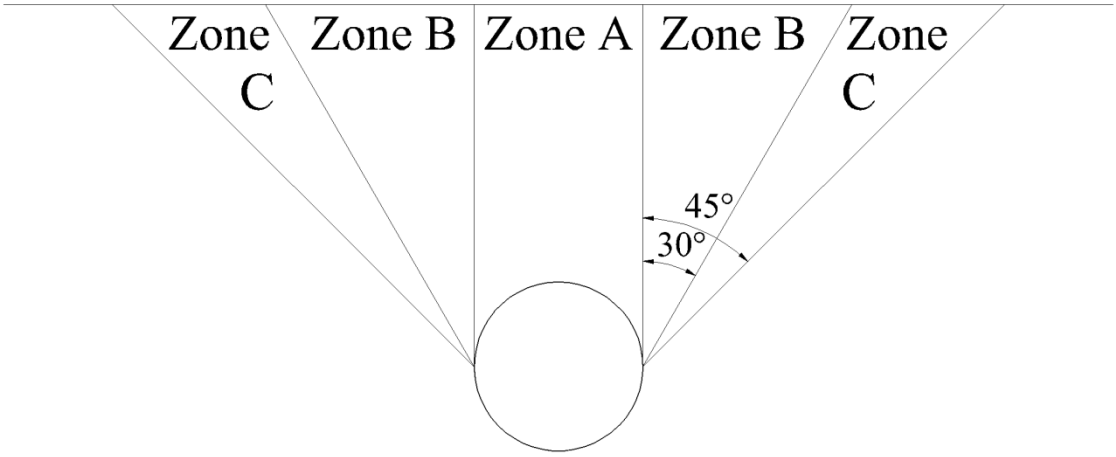

Figure 2.15 Zones of influence between tunnel and pile toes positions of Heinenoord full-scale excavation proposed by **Kaalberg et al., 1999**

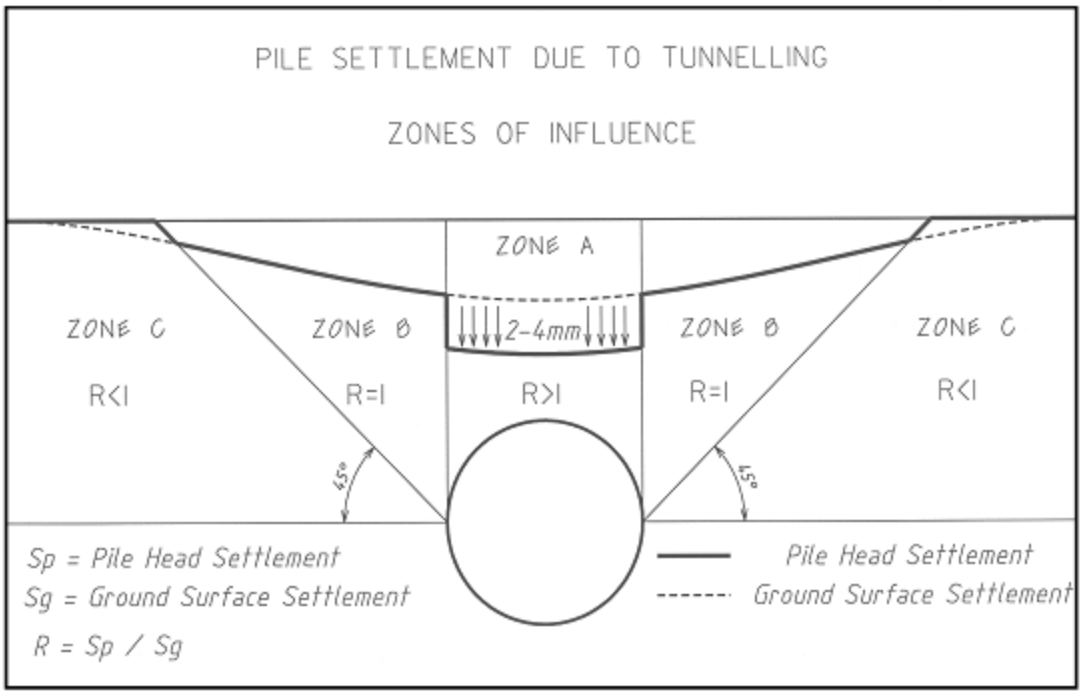

Figure 2.16 Zones of influence between tunnel and pile toes positions of new Channel Tunnel Rail Link (CTRL) full-scale excavation proposed by **Selemetas et al., 2006**

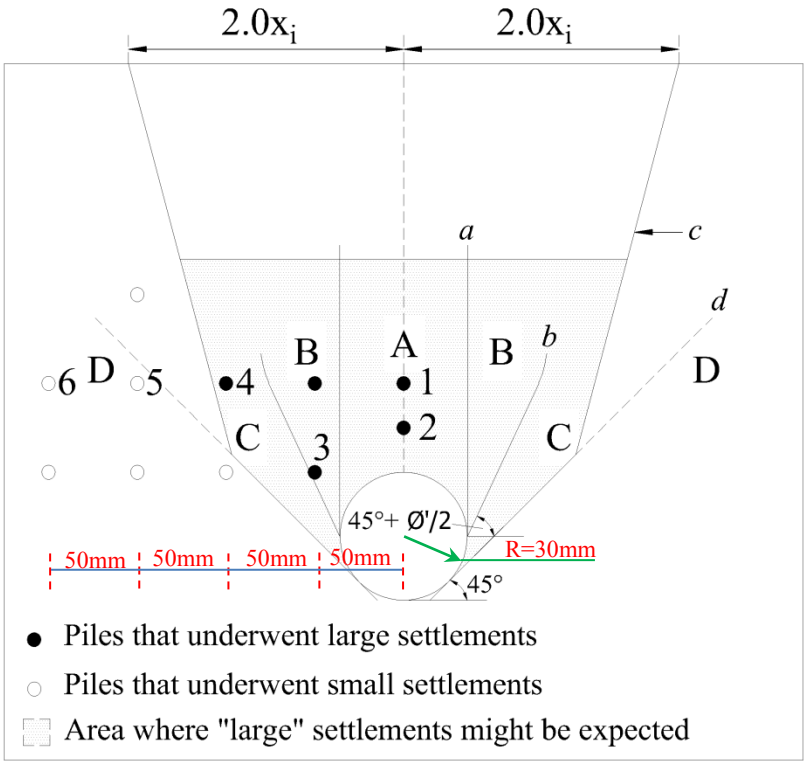

Figure 2.17 Zone of influence by **Jacobsz et al., (2004)**

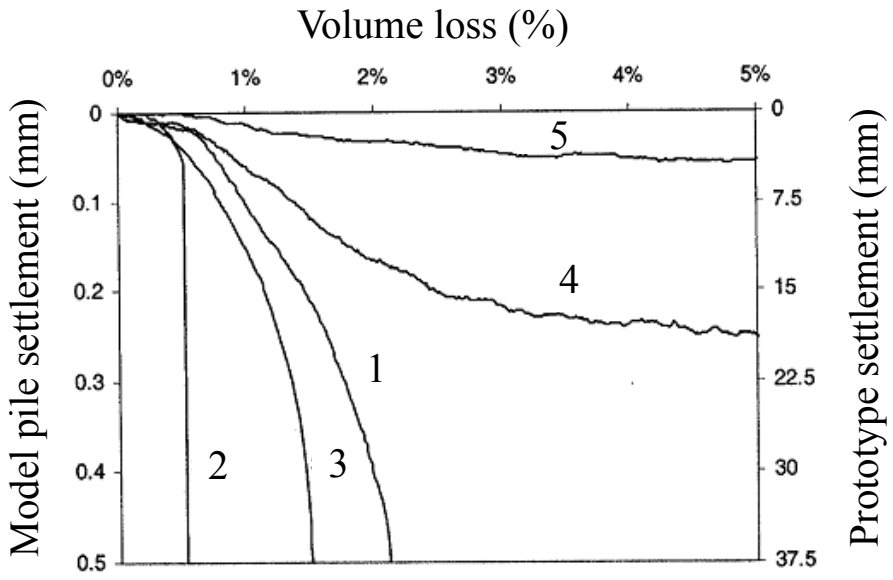

Figure 2.18 Pile settlements against ground loss ratio regarding the zone of influence **(Jacobsz et al., 2004)**

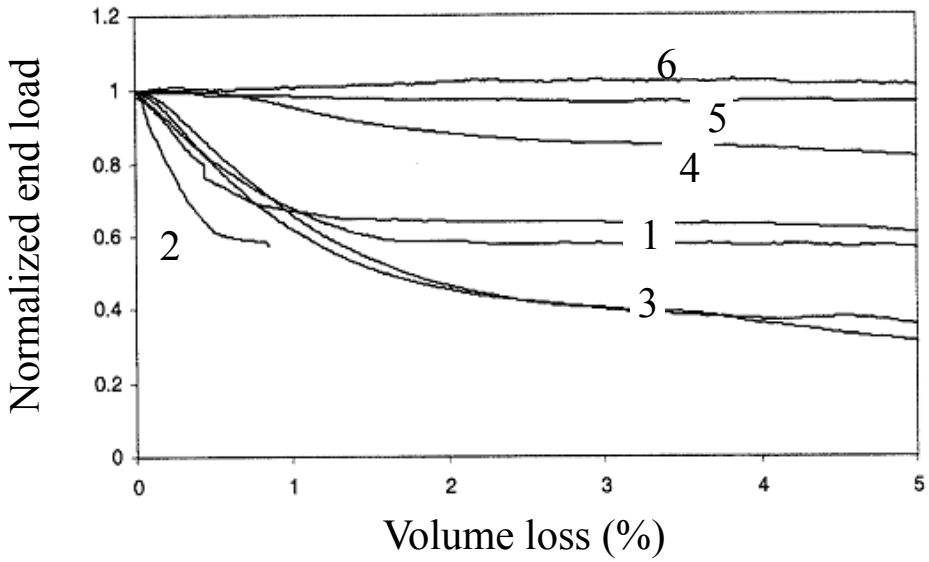

Figure 2.19 Normalized end bearing load against ground loss ratio regarding the zone of influence **(Jacobsz et al., 2004)**

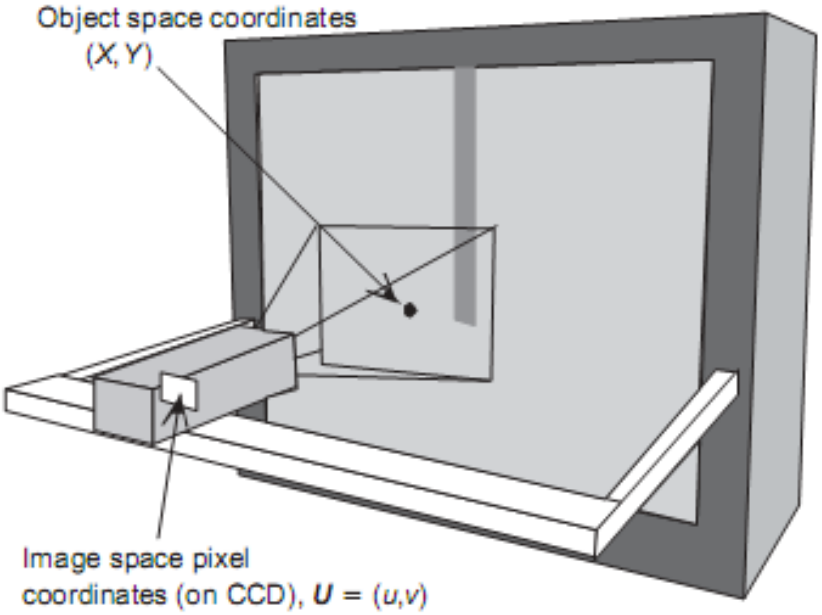

Figure 2.20 The transformation of image-space and object space system
(**White ei al., 2003**)

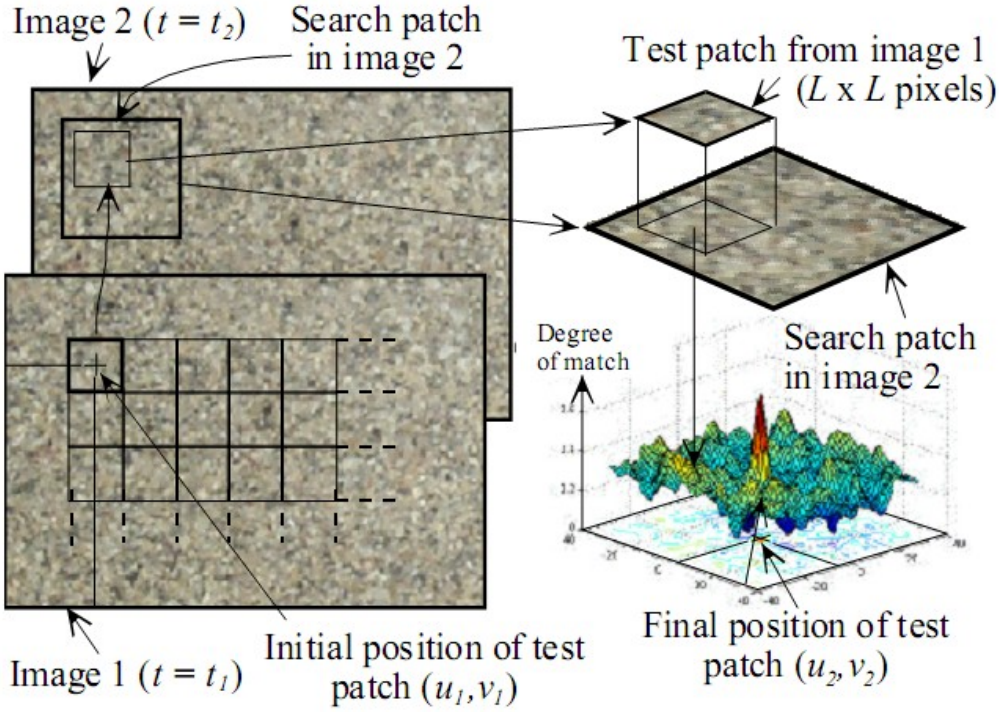

Figure 2.21 Principle of Particle Image Velocimetry (PIV) technique
(**White and Take, 2002**)

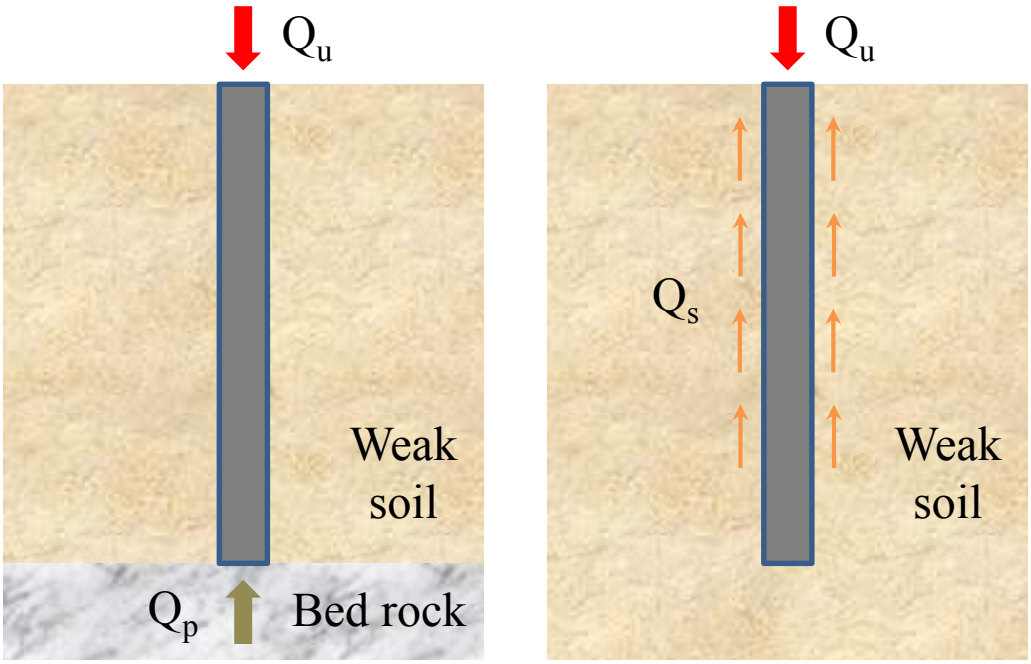

(a) (b)

Figure 2.22 Types of piles by load transfer (a) Point bearing pile; (b) friction pile

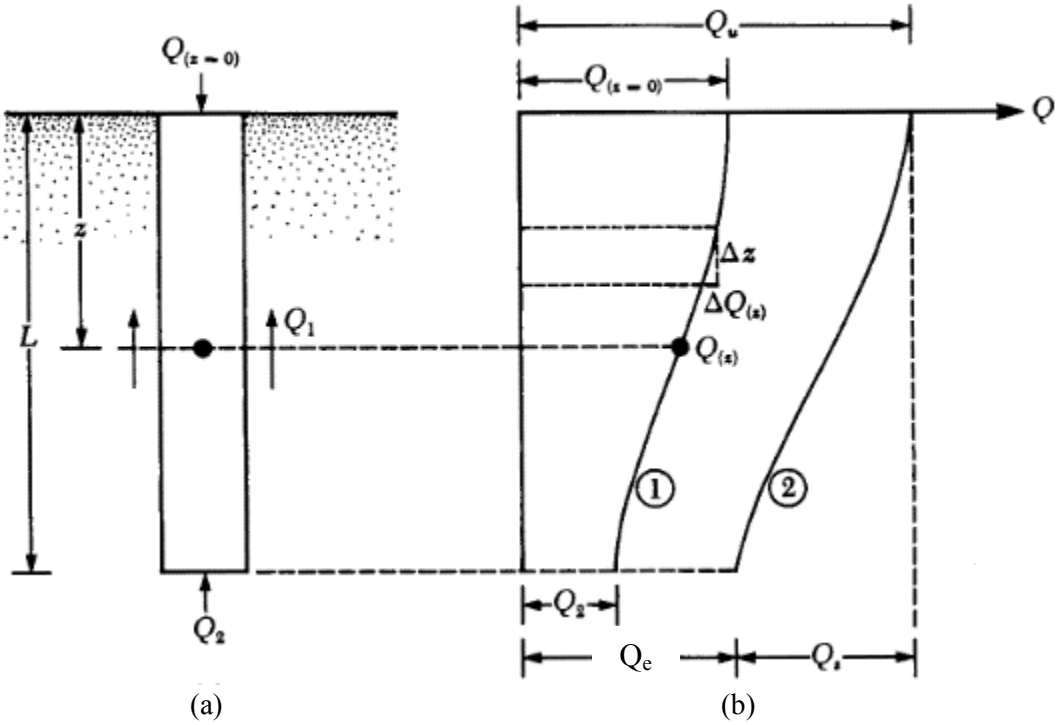

(a) (b)

Figure 2.23 Load transfer mechanism (a) resisting load component (b) transfer load at fully mobilization at pile end and shaft (**Braja, 2000**)

Q_s

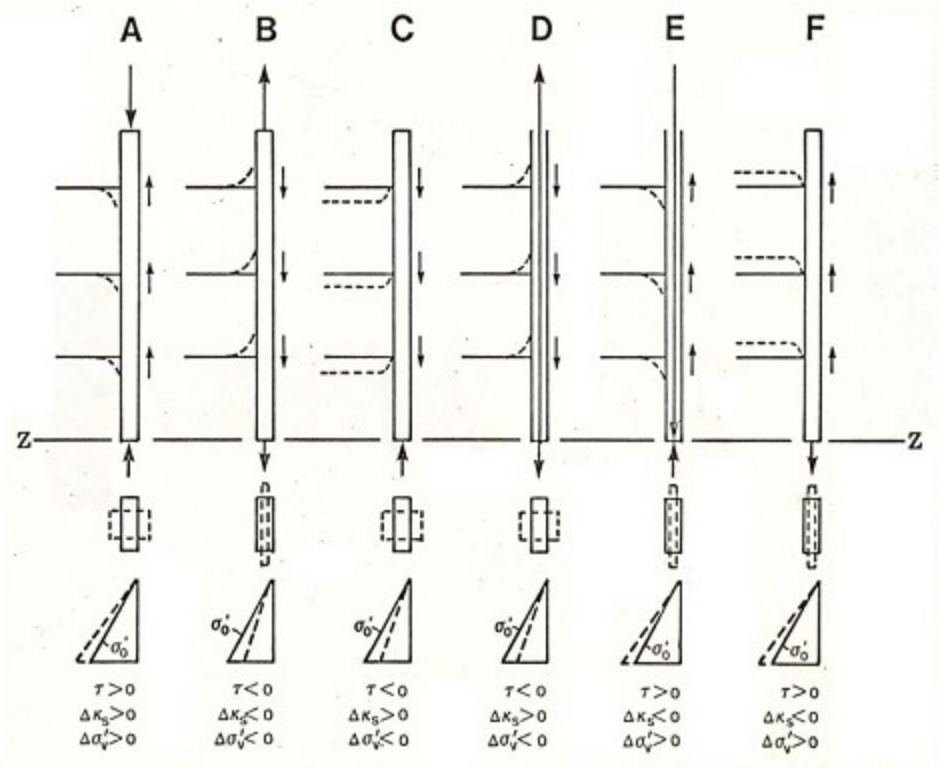

Figure 2.24 Summarized modes of relative movements between pile and surrounding soil with different loading conditions **(Fellenius, 1984)**.

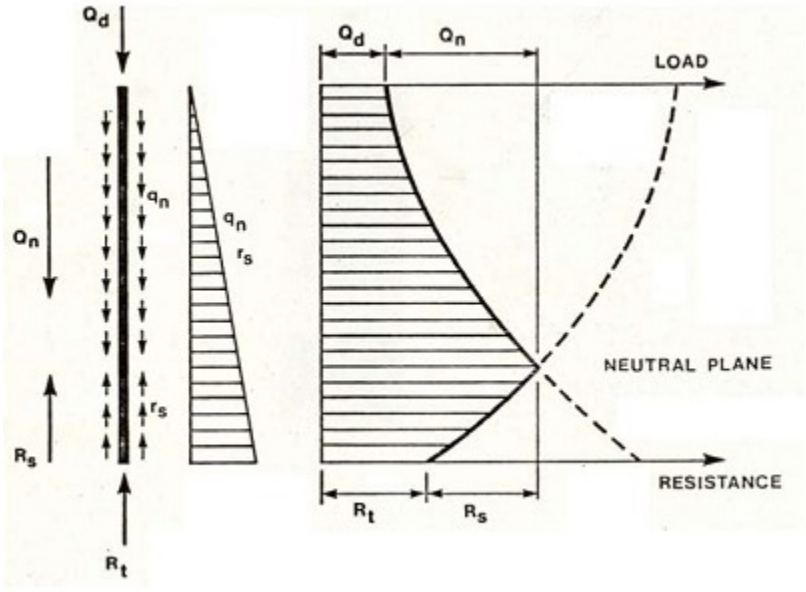

Figure 2.25 The position of a neutral plane along the pile **(Fellenius, 1984)**.

Chapter 3

Development of centrifuge modeling on tunneling-pile interaction

3.1 Introduction

In geotechnical work, data from the field are scarce and sometimes imperfect. Many researchers have tried to generate the data from the physical model tests in a laboratory, and usually in 1g environment. Although this approach may supplement the lack of available data in the field, the results could be misleading due to low stress of the soil at the acceleration of 1g environment (**Taylor, 1995**).

This limitation has been addressed, and more reliable physical modeling has been developed by using geotechnical centrifuge. A major advancement in machine configurations, system control, computers and model design has enhanced the testing in various types of geotechnical problems such as slope and tunnel stability, shallow and depth foundation, etc. (**Craig, 1998; Caicedo, 2000; Madabhushi and Take, 2002**). Therefore, Centrifuge technique is a powerful method to the study of geotechnical engineering.

3.2 Principle of centrifuge

The Scaling relationships between prototypes and models were mentioned by **Phillips (1869)**. By applying appropriate scaling laws, the size in the prototype scale can be scaled down to the small size of the model. In addition, the magnitude of stress which increases with depth could be replicated in the model. This result comes from that all the material properties remain the same regardless of gravity in the centrifuge, except for the self-weight (**Schofield, 1998**). From this property

When the model is placed on the designed gravity acceleration, prototype dimension can correspond to model dimension by N times of gravity. For example, if the model is accelerated at N time of gravity, the length dimension of the model (l_m) will be equal to the prototype (l_p) where $l_p = N(l_m)$.

The model and prototype scale are shown in subscription of m and p respectively. In general, the model and prototype will have the relationships as the following.

$$l_p = N(l_m) \tag{3.1}$$

$$A_p = N(A_m) \tag{3.2}$$

$$V_p = N(V_m) \tag{3.3}$$

Where l = length dimension

A = area

V = volume

It should be noted that the vertical stress between the prototype and the model are identical as can be seen in the following equation.

$$\sigma_p = \gamma_p Z_p = (1/N)(\gamma_m)N(Z_m) = \gamma_m Z_m = \sigma_m \tag{3.4}$$

Where σ = vertical stress

γ = soil unit weight

Z = depth

The scaling law of various parameters can be summarized as listed in **Table 3.1**.

3.3 Tokyo Tech MARK III centrifuge

The centrifuge and test system operated in the test is Tokyo Tech Mark III beam type centrifuge. The centrifuge has a pair of parallel arms which are mounted the testing model and a weight for counterbalance in each side of the arm as indicated in **Fig. 3.1.** The height of the operation room is 2m and the length from rotating the shaft to the platform base is 2.45m. During the centrifuge, the plane of swinging platform of model testing (**Fig. 3.2 (a)**) and counterweight (**Fig. 3.2 (b)**) are normal to the resultant of gravity acceleration. The detail of specifications was demonstrated by **Takemura et. al. (1999)** and the main features are summarized in **Table 3.2**.

When the centrifuge is operated, the data is acquired by using two methods. In classical electrical slip rings process, the equipment is directly connected to the slip rings, and the signals are transmitted through junction box to a computer in the control room. In optical rotary process, the analog signals are transferred and amplified through conditioners and then are converted to digital impulse by converters. The digital impulses are transmitted to the computer in which the user can adjust the gain, voltage and other conditions of those signal. The control box for transferring the record data to the control room is shown in **Fig.3.3**.

3.4 Description of centrifuge apparatus

3.4.1 Centrifuge equipment

A series of physical modeling were conducted to investigate the interaction between pile group, surrounding the soil and adjacent tunnel. All the experiments were conducted under the centrifuge acceleration of 100 g. As a result, dimensions of the model were scaled by a factor of 100 as explained in the previous section. The pile groups were installed in the designed positions along with the row of potentiometers and laser displacement transducers. **Fig. 3.4** illustrates model setup in term of model scale. 70 mm diameter model tunnel was located at the center of the container with 200 mm vertical distance from the container bottom to the tunnel center. Pile groups with 220 mm and 150 mm embedment lengths were placed respectively at the both sides of the model tunnel.

The tunnel cover and diameter ratios (C/D) tested were 1.5 and 2.5. Horizontal distance between the front pile center and the tunnel center (X_p), and relative pile tip depth from the tunnel center (Z_{pe}) are the parameters in the tests, which are normalized by tunnel radius(R). Four horizontal distances of X_p/R= 1.5, 2.0, 2.5 and 3.0 were employed. The relative pile tip depth

takes negative value when the pile tip position is shallower than the tunnel center and positive when the pile tip position is deeper than the center, which was varied with Z_{pe}/R from -1.72 to 2.28.

The model was mounted on the swinging platform, and the weights were calculated for the counterbalance. A digital camera was placed in front of the container at the screen side to capture the images during tunneling.

3.4.2 Tunnel machine

In this study, a two-dimensional mechanical type shield tunneling machine (**Katoh et.al. 1998**) (**Fig. 3.5**) was employed, which can impose a clear boundary condition at tunnel perimeter, namely, the co-axial tunnel diameter reduction from small to large ground loss ratio. Tunnel model can maintain steadily reduction of contraction from the beginning to the end of tunneling.

In this boundary condition, it could be relevant to the small volume loss which is caused by the tail void of shield tunneling works in soft soils. But it should, however, be noted that for the large volume loss condition, which corresponds to a critical condition, such as collapse of tunnel face or segment, relevant boundary conditions might be different from the one in this model.

This mechanical type tunnel machine is composed of a steel ring and a wedge-shaped shaft as shown in **Fig. 3.6**. The ring was divided longitudinally into six parts and covered with a steel sleeve and a rubber membrane as illustrated by section A-A in **Fig. 3.5**. Thickness of steel sleeve and rubber membrane are 0.5mm and 0.2mm respectively. The steel sleeve was also divided and attached to each steel ring parts. At the same positions of front and back walls of the model the container were made circular holes into which the shield tunnel model was inserted (see **Fig. 3.7**). The assembly of tunnel machine before inserting through the container is displayed in **Fig. 3.8.**

The gaps between the tunnel model and the circular holes were filled with silicone material to prevent leakage of the sand. The wedge-shaped shafts were connected to a screw jack behind the container (**Fig. 3.9**), which can move horizontally inward and outward. This process will change the position of the ring in the radial direction. Consequently, this model tunnel covered with a rubber membrane (**Fig. 3.8** and **Fig. 3.10**) can expand or contract its diameter. . A simplify tunneling mechanism is shown in **Fig. 3.11**. The diametrical velocity of expansion and

contraction is controlled in the operation room during the tunneling. The motor speed capacity of the tunnel machine is varied from 0.1mm/sec to 1.3mm/sec. The rubber was used for a consistent circular shape transformation of the tunnel when it reduced or increased the diameter. Moreover, this rubber membrane also prevented sand intrusion inside the model tunnel. One potentiometer (PTM) was installed on the shaft which was connected to the screw jack to measure the diameter change of model tunnel during the in-flight excavation as shown in **Fig 3.5** and **Fig. 3.9**.

As the tunnel model contracted uniformly in the radial direction, the soil in the model displaced two-dimensionally for the case without piles.

3.4.3 Model pile group

Model piles were designed to replicate a circular concrete pile (**Table 3.3**). An acrylic hollow cylinder with Young's modulus (E) of 3.2 GPa was selected to make model piles of 10 mm diameter (Ø) and 1 mm (t) thickness with total length of 185 mm and 255 mm as described in **Fig. 3.12(b)**. By using the relation of flexural rigidity of prototype (E_pI_p) equal to N^4 times the model (E_mI_m), where N is the model linear scale (N=100 in these tests) or the centrifuge acceleration ratio, E is Young's modulus, I is the area moment of inertia, and the subscripts m and p denote prototype and model respectively. The coefficient of friction between dry sand and acrylic materials is approximately around 0.25-0.30. The coefficient of friction of cement concrete on sand is around 0.4-0.5, and the coefficient of friction of steel sheet pile on the sand is around 0.30-0.35 (NAVFAC, 2014). The model setups give small value of friction compare to the prototype material. In addition, the bending and axial rigidity are also smaller than the concrete and steel in prototype scale. However, the acrylic is quite flexible and contains high yield strain. The tests were designed to make large ground loss ratio which cause high strain in the pile models. The pile models are certainly reused in the tests. To make sure the linear behavior during the test, acrylic material was selected for pile materials. Furthermore, in the field condition, there are a few cases report that tunneling can cause the failure of the building structure. The differential settlement is the main concern in this type of problem (Jacobsz, 2006; Kwast, 2006; Pang 2006).

Brass materials were plugged at the end of model piles. There are two types of the model pile: strain gauge pile and dummy pile. Considering the symmetry arrangement of pile group model, one pile group consists of two strain gauged piles in the first row and two dummy piles in the second row as described in **Fig. 3.4.**

The four pile heads are connected with the pile cap and tightened the screws. The pile caps were made from 20 mm thick stainless steel plate and were connected rigidly to the vertical piles positioned at a center-to-center spacing of 50 mm. The specification of pile cap is shown in the **Fig. 3.13**. Complete assembly of short and long pile groups are illustrated in the **Fig. 3.14.**

Two 2x2 pile groups with embedment depths (L) of 150 mm and 220 mm for shorter and longer piles are installed on either side of the tunnel in the dry sand (**Fig. 3.4**). The coefficient of friction between dry sand and acrylic materials is approximately around 0.25-0.30. Inside the hollow acrylic pile, strain gauges were placed to measure axial and bending strain. The reasons to place the strain gauges inside the model pile are: (1) to maintain the size of the diameter of the pile; (2) to reduce disturbance of soil particles and temperature. The arrangements of the types of the strain gauge are displayed in **Fig. 3.12(a)**. For positions of bending and axial strain gauge, the strain gauges are attached at the right and left sides of individual pile. The induced strain can be individually measured from both sides. As a result, in that position, axial force and bending moment can be estimated at the same time.

3.4.4 Model superstructures

Acrylic or aluminum made plate was fixed on top of the pile cap to add an extra weight on the pile group. The types and combination of superstructure are displayed in **Fig. 3.15**.

Total masses of 760 g and 1040 g were put in the short pile group. As a result, one pile model was carried distributed load equal to 1900 KN and 2600 KN at the prototype scale respectively. While 1040 g and 2030 g masses were added to the long pile group to have distributed load equal to 2600 KN and 5070 KN at the prototype scale per one pile respectively. Block of stainless and acrylics were connected with the pile cap by four screw jacks as shown in **Fig.3.15 (d)**. For the case without the block of stainless steel and acrylic (**Fig. 3.15(a)**), small acrylic plate was attached to the two measurement points of laser displacement transducer (LVDT). The blocks of weight not only provide the vertical load on the pile caps but also serve as measurement points for two laser displacement transducer (LVDT) as illustrated in **Fig.3.4**. Summary of carrying load per pile is shown in **Table 3.4**.

3.4.5 Soil model

Dry Toyoura sand was employed in the study. The sand has uniform gradation curve as shown in **Fig. 3.16**. In the figure, the soil mostly has particle size from 0.15 to 0.30 mm. Soil model was prepared by air pluviation method using sand hopper with constant falling height to achieve relative density at 80%. The dry density (ρ_d) equals to 1.550-1.565 g/cm^3 at 80 %. The summary of Toyoura sand properties is listed in **Table 3.5**. In addition, the results of this study are based on the ground conditions of dry sand with relative density of 80%. The relation between standard penetration resistance (N-values) and relative density is provided in the table (Meyerhoff 1956). From the table, the results could be approximately applied in the soil with N-values in the range of 30-50 as shown in **Table 3.6**. The main concern in this study is the relative position of pile group and tunnel. Therefore, to simplify the test condition, the relative density of 80% is controlled for all the test cases.

In the test using container box, it is necessary to know the relation of internal friction (Ø') at low stress because it can be used to analyze abruptly failure of sand slope. **Fukushima and Tatsuoka (1984)** conducted a series of drained triaxial compression tests at low pressure with Toyoura sand. The results of principal stress ratio and axial strain with relatively dense sand (80%-88%) are illustrated in are illustrated in **Fig 3.17.** The internal friction can be derived from the equation (5).

$$Ø' = \boldsymbol{arcsin}\frac{(\sigma'_1-\sigma'_3)}{(\sigma'_1+\sigma'_3)_{\boldsymbol{max}}} \qquad (3.5)$$

Where Ø' = internal friction angle

σ'_1 = principal stress

σ'_3 = confining stress

In addition, this internal friction showed varied values with the void ratio of the sand specimen covered with latex membrane as shown in **Fig. 3.18**. In the figure, principal stress ratio and axial strain increase as consolidation pressure (σ'_c) decrease. Then, the selected values of void ratio at 0.7 (D_r=80%) and 0.85 (D_r=34 %) were plotted against effective minor principal stress as indicated in **Fig. 3.19**.

Tatsuoka et al., (1986) presented the development of internal friction with various void ratio and consolidation pressure as shown in **Fig.3.20**. The trends of the results are similar to the

results proposed by **Fukushima and Tatsuoka (1984)** in **Fig. 3.16**. In addition, **Tatsuoka et al., (1986)** also summarized the results of development of internal friction angle with effective minor principal stress of dense and loose soils including the results from **Fukushima and Tatsuoka (1984) (**see **Fig. 3.21).** Because the stress condition in this study is similar to the triaxial test, the internal friction angle is approximately 40 degrees according to dense sand condition in **Fig. 3.21**.

3.4.6 Equipment and apparatus

a) Plain strain container

The container which has internal plan area of 150mm width, 550mm length and an internal height of 600mm was provided by Toyo Corporation as illustrated by **Fig. 3.22**. Front wall of the container is made of acrylic plate, through which the ground movement can be observed. The container is made of aluminum. The front and the back sides of the container provide a hole for inserting the tunnel machine. Both container and tunnel machine are mounted on the steel base.

b) Camera and LED light

A digital camera (Canon power-shot G7) was fixed at the front of the box to capture the images of soil movements through the front window as shown in **Fig. 3.23.** This camera can be operated and monitored via wireless connection into the control room during the centrifuge operation. The highest speed of the camera to automatically captures the images equal to 20 seconds per one picture. The brightness and spatial variation of the ground model texture affect the result of displacement (**White et al., 2003**). Rows of LED lights (**Fig. 3.24**) were installed in the upper and lower position of the front window to enhance image quality.

c) Potentiometers (PTM)

A set of potentiometers (**Fig. 3.25**) were attached to an aluminum frame (instrument mounting unit) which can adjust the potentiometer position for each different horizontal distance cases to measure the surface settlement trough (**Fig. 3.26**). In addition, other pairs of potentiometers were mounted on the top of pile cap to measure the pile cap settlement. The data of pile model response with tunneling process were recorded at all time during the testing. One of potentiometer is installed on the back side of the container to measure the reduction and expansion of the tunnel size (see also **Fig. 3.5**).

d) Long-range linear variable differential transformers (LVDTs)

One set of two LVDTs which have a spacing of 40 mm in the vertical direction (**Fig. 3.28**) was installed on one side of each pile group as shown in **Fig. 3.4**. The point of measurement from LVDTs was rested on the weight plate (blocks of stainless steel or acrylic). It should be noted that the surface of the weight plate needs to be attached with the opaque tape for LVDT measurement. LVDT could not measure the transparent or high glittery surface. The data of pile model horizontal movement and pile model inclination were recorded during the tunneling process. When the pile model was induced by ground movement, the LVDTs could provide an output proportional to the footing displacement and rotation.

Inclination and horizontal movement at the center of the pile cap were calculated using the ratio of the difference in horizontal displacement output to the distance between the fix two LVDTs.

e) Load cell (one-way type)

Load cell with load capacity of 5kN (see **Fig. 3.29**) was used in the pile load test to measure the pile load settlement curve. The load cell was applied on both single dummy pile and the pile group.

f) Large and small size of sand hopper

Air pluviation method (see **Fig. 3.30**) using sand hopper was applied to prepare the ground model. The large hopper was utilized to prepare the base of the sand layer (under the tunnel's invert elevation). The small hopper with long slender tube was used to fill the ground model above the invert elevation, especially at the narrow space between the piles. The long tube of small hopper was inserted through the holes of pile cap (**Fig. 3.13**) to fill the sand under the pile cap. It should be noted that the falling height and direction may not constant in the very narrow space area (i.e. case with the smallest distance between pile group and a tunnel). The preparation process was carefully conducted to reduce the inconsistent of sand density as much as possible.

3.5 Calibration technique

3.5.1 Tunnel calibration

Tunnel need to be changed the rubber membrane before testing because the flexible of rubber is deteriorated by the time as illustrated in **Fig.3.31**. The tunnel is reassembled to check the tightness of the contact surface between steel rings and the new membrane (**Fig.3.32**). In 1g condition, tunnel machine is forced to reduce gradually and increase the size of the diameter. The change of tunnel's size measured by vernier is compared with the potentiometer (PTM) at the back side of the container for checking the accuracy of PTM.

The sand was poured into the container with air pluviation method with relative density at 80% as the same as in normal test condition. Then, the filled container (without the presence of piles) was accelerated to 100g and started to reduce the tunnel size. The optimal rate of tunnel's reduction is carried out in this process. As a result, in 100g condition, the tunnel diameter can be reduced from 70 mm to 60 mm within 180 seconds.

3.5.2 Camera and Particle Image Velocimetry (PIV) calibration

The accuracy of displaced vectors from PIV depends on the quality of images. In the testing, camera was needed to be rigid while taking the ground movement's images. The movement of the camera is caused the wild vectors in PIV analysis as shown in **Fig. 3.33**.

The movements of the images were checked by Photoshop (version CS5). If the result from PIV shows the wild vectors caused by shifting of images, those set of images were modified by Photoshop program. In the program, by the reference points (see also **Fig. 3.22**) marked at the front screen, the shifts of images are solved by cutting and moving corresponding to the reference points. This process is repeated until wild vectors are minimal.

3.5.3 Potentiometer (PTM), laser displacement transducer (LVDT), and sand hopper calibration

Potentiometers (PTM) are calibrated by micrometer, and the setup is shown in **Fig. 3.34(a).** The potentiometers were held at one side and connected to the block. By rotating the micrometer, the screw jack was lengthened and pushed the block to the potentiometers direction. The movement of the block was measured by the micrometer's scale. The increments of the movement were plotted to calculate the calibration factor.

Laser displacement transducers (LVDT) (**Fig. 3.34(b)**) were also calibrated using the same method by replacing the PTM by LVDT. The increments of block's movement are defined the calibration factor of LVDT. In addition, the LVDT could not measure the transparent object. Opaque tape should be pasted in the area of measurement.

Sand hopper was calibrated in a new container without presence of tunnel machine. The heights of long tube and soil surface were varied to find the target relative density. In addition, the effect of inclination between the perpendicular line and plain of the soil surface was also calibrated. The container with fully sand was weighted and calculated relative density.

3.5.4 Pile calibration

3.5.4.1) Principle of strain gauges

Knowing the induced stress is one of the key parameters for designing the structures. In general, measured stress is indirectly obtained by the measurement of induce strain. Therefore, the development of strain gauge with appropriate system plays an important role in the engineering society including geotechnical engineering.

By using the Hooke's law, the induced stress (σ) is proportional to the induced strain (ε) in the elastic limit of those materials. The constant proportional property is called Young's modulus (E) as shown in equation (6).

$$E = \frac{\sigma}{\varepsilon} \tag{3.6}$$

Therefore, if the Young's modulus of material's strain gauge is known, stress could be calculated by the relation in equation (1). In addition, the ratio between strain in lateral (orthogonal) direction and longitudinal direction is called Poisson's ratio, and the value is approximately around 0.3.

In general, strain gauge is made from metallic resistive foil cover with laminate and plastic film. Then, the strain gauge is attached to the measurement surface area. When the structure is subjected to the force, the strain gauge will contract or elongate along with the element's structure and undergo alter in electric resistance. The strain value will be measured by change in resistance as describe in equation (7).

$$\frac{\Delta R}{R} = K'\varepsilon \tag{3.7}$$

Where ΔR = change of resistance of strain gauge (ohm)

R = resistance of strain gauge

K' = gauge factor of strain gauge (depend on the material of strain gauge)

ε = Induced strain

However, the change of resistance is very less value. Thus, the development of new circuit which is called Wheatstone bridge has been introduced to amplify the measured value. Wheatstone bridge (**Fig. 3.35**) is very useful to detect minor change of strain, especially in the model testing condition. The Wheatstone bridge's circuit has the relation in the following equation:

$$e = \frac{1}{4}\frac{\Delta R}{R}E = \frac{1}{4}K\varepsilon E \tag{3.8}$$

Where e = output voltage

E = input voltage

Therefore, in this study, the induced strain in each strain gauge type can be obtained by the following relation:

For strain gauges with axial force and bending moment measurements $\varepsilon = \frac{4}{(1+\xi)}\frac{e}{KE}$ (3.9)

For strain gauges with measurement only axial force or bending moment $\varepsilon = \frac{2}{(1+\xi)}\frac{e}{KE}$ (3.10)

In balance condition, the output voltage is zero, and when the condition is unbalanced, the resistance change is measured by the variation of the e values.

In **Fig. 3.12(a)**, at the elevations that can measure axial force and bending moment, the individual strain gauge (ε_1, ε_2) can be used to define the axial strain (ε_a) and bending strain (ε_m) in the following equation:

$$\varepsilon_a = \frac{\varepsilon_1+\varepsilon_2}{2} \tag{3.11}$$

$$\varepsilon_m = \frac{\varepsilon_1-\varepsilon_2}{2} \tag{3.12}$$

3.5.4.2) Calibration methods

Axial force and bending strain gauges were calibrated by fixing the head of a pile model and hanging the weight at the end of another side as illustrated in **Fig. 3.36(a)**. The weights were gradually put at the pile end side. The induced strains along the pile model were used to calculate the calibration factor.

The axial strain gauges at the pile end were calibrated by applying the vertical weight at the pile end as shown in **Fig. 3.36(b)**. The development of end bearing load was used to define the calibration factor.

3.6 Pile load tests

Vertical load tests were conducted to measure the bearing capacity of the model piles which were prepared in a container without tunnel model with the same relative density of the sand for the tunneling model (D_r = 80%). In one set of preparation, with the same piles length, the pile group was installed at the center of the container and two dummy piles were installed separately on the right and left of the pile group as shown in **Fig. 3.37.** The container was brought to the centrifuge platform, and the one-direction of load cell was mounted on the top of the container (see also **Fig. 3.38**). At 100g condition, the piles were pushed by the load cell, and the load settlement curves were plotted to investigate the pile bearing capacity. **Terzaghi (1942)** proposed that the ultimate bearing capacity of the pile can be acquired from pile-load settlements curve at 10% of pile diameter settlements.

3.6.1 Single pile

For single (dummy) piles, the load cell was gradually pushed those piles to the ground. The loads and settlements were measured by the load cell and the potentiometer respectively as illustrated by **Fig. 3.39**. The load cell (Q_h) and pile head settlement (S_h) curve in prototype scale for short and long piles can be observed in **Fig. 3.40**. The results of test 1 and 2 of single short piles show identical development of load-pile head settlement (S_h) in the beginning and slightly difference at the large bearing load. However, for the single long piles, the load settlement curves tend to show slightly different since the small pile head settlement. It could be due to by the slight difference of relative density of two piles but the difference is not significant (less than 10% of load cell (Q_h) at the same pile head settlement (S_h)). Therefore, the load settlement could be used as the fundamental property to find the bearing capacity. It should be noted that the acrylic pile is

quite flexible, so the pile head settlement measured by potentiometer may not show the real settlement due to the pile compression.

3.6.2 Pile group

As mention above, the pile compression should be clarified by the strain gauges pile of the pile group. Short and long pile groups which were gradually loaded by mechanical jack and pile cap settlements were measured by a load cell and potentiometers as illustrated by **Fig. 3.41**. Vertical settlements of pile at prototype scale which were measured at the pile head (S_h) and pile end (S_e) were plotted against axial force measuring by the load cell (Q_h) and the strain gauges at the pile end position (Q_e) as shown in **Fig. 3.42**. However, as mention above, acrylic pile behaved flexible property due to its relatively low stiffness. Therefore, vertical settlement of pile end was estimated by subtracting the pile compression from the pile head settlement. Considering the compression of the pile, the pile bearing capacity can be determined by the pile head load at 10% pile diameter settlements at the pile end position as shown in **Fig. 3.42**. Pile bearing capacity can be approximately around 3600 KN and 8000 KN for short and long pile model respectively.

3.7 Test procedure

3.7.1 Test series

The test cases can be categorized into two groups; with and without the installation of pile. For the cases without the pile group or cases with greenfield condition, the tunneling was conducted to inspect the fundamental of ground movement. For the cases with the pile groups, the interactions between pile foundation and tunnel with various conditions were observed. In addition, those results between the cases with and without the pile groups are compared to indicate the influence of existing pile groups for the movement of soil caused by tunneling. Method of preparation and the test process between the tests with and without the pile groups are identical.

In total, four series of model tests were conducted. Test conditions are shown in **Table 3.4.** In test series A (**Fig. 3.43**), tunneling processes were studied without pile installation for the models of tunnel cover and diameter ratio (C/D) equal to 1.5 and 2.5, where C is the distance between the ground surface and the tunnel crown, and D is the initial tunnel diameter (70 mm). These test results will be used as a basic behavior of induced ground movements in contrast to those with existing piles. One of the purposes of the tests is to check the symmetrical movement

of the tunnel machine. The symmetrical trough settlement should be justified by further analysis of complex pile-soil-tunnel interaction. The potentiometers position and cover and depth are shown in **Fig. 3.44**. In the Figure, PMG notation means the potentiometer on the ground as illustrated in **Fig. 3.45**.

In test series B, both short and long piles were embedded with C/D = 2.5. The horizontal distance between pile and tunnel was varied (X_p = 1.5R, 2.0R, 2.5R, and 3R). In test series B(1), the distributed loads per pile from the weight and the pile cap were 2600 KN and 5070 KN for short and long pile groups respectively in the prototype scale. In test series B(2), the distributed loads were reduced to 1900 KN and 2600 KN for both short and long pile groups respectively.

In test series C, the distributed loads were the same as test series B(2) except the tunnel cover and diameter ratio (C/D = 1.5). The relative pile tip depth to the tunnel (Z_{pe}) was varied with different C/Ds and pile embedment lengths. Positive and negative sign conventions of Z_{pe} depend on the positions of the pile tips and the tunnel model. Positive sign means the pile tips are deeper than the tunnel model and negative sign when the pile tips are shallower than the tunnel model.

In **Table 3.4**, test conditions of thirteen tests are given by normalized values, C/D, X_p/R and Z_{pe}/R. In the case X_p/R = 3.0, the distance of container side wall and the rear side piles was minimum of 120 mm (twelve times pile diameters) that is considered adequately enough to minimize the boundary effects (**Lee and Chiang, 2007**).

3.7.2) Sand preparation

The soil model was made by pluviation method (**Fig. 3.30**) using small hopper with a long and small tube for a nozzle. The dry Toyoura sand was fully filled inside the hopper, and the sand was poured by layers in 20 mm thickness each until it reached the designed depth. In the elevation of the invert of the tunnel, large hopper was used to make a ground layer (5 cm from the bottom of the container). Then, small sand hopper was used to fill the rest of the ground model. One advantage of small size hopper is the slender tube can insert through the pile cap to fill the sand under the pile group.

The sand was poured by Internal friction angle (Ø') of dry Toyoura sand was assumed to 40° using the correlation between Ø' and effective minor principal stress (σ'_3) at relative density

of 80% with drained triaxial compression test proposed by **Fukushima and Tatsuoka (1984) and Tatsuoka et al.,(1986) (**see also **Fig.3.21.)**

3.7.3) Pile group installation

After the ground layer was made until the invert elevation, two assembled pile groups were suspended on either side of the tunnel at the predetermined vertical and horizontal locations at equal horizontal distances from the tunnel axis for each case as shown in **Fig. 3.46**. Dry Toyoura sand (**Table 3.5**) was then pluviated by a small hopper with a constant falling height and flow rate. **Fig. 3.47** shows the preparation of sand model at the mid-height of designed ground level. The miniature hopper was connected with small long tube to make certain that the sand can fill a small space area. The aluminum girder was removed, and the vacuum with flat nozzle was utilized to level the ground surface. At this process, the foundation models are supported by their own piles as shown in **Fig. 3.48**.

3.7.4) Checking the relative density

After finish the sand preparation, the model container was brought on the weighing machine for checking weight. The relative density of sand should equal to 80%. The ground model needs to reproduce if the relative density is larger or smaller than 2% of target relative density.

3.7.5) Centrifuge platform and camera setup

The model container with acceptable relative density was mounted on the centrifuge platform. The base of the container was securely attached to the swinging platform. The camera (canon power shot G7) was installed in front of the container at the window side as shown in **Fig. 3.49.** The camera was attached to the steel girder and the position. The height of the camera position could be adjusted by increasing the acrylic blocks under the camera's base. The camera base made from the steel girder and was connected with the acrylic block and centrifuge platform through the screws. Relative positions of camera and container are illustrated in **Fig. 3.23**. The picture was taken to check the soil area and image's quality. The position can be adjusted by add or remove the stack of steel blocks under the steel girder.

3.7.6) Installation of Potentiometers (PTM) and Laser displacement transducer (LVDT)

Pairs of potentiometers on pile cap (PMP) and laser displacement transducers were placed to measure the displacement (horizontal and vertical movements, and inclination) of each pile cap. Potentiometers were also placed on the sand surface (PMG) to measure the surface settlements as shown in **Fig. 3.50**. Strain gauges cables, PTM and LVDT were connected to the channel box which was connected to the slip rings to transform the testing data to the monitor floor.

3.7.7 Centrifuge acceleration

After installation of all equipment, the weight counterbalance was calculated, and the sheets of steel were brought to put on the other side of the centrifuge arm. In the operation room, all channels from the centrifuge were calibrated, and the centrifuge model was accelerated every 10g until it reaches 100g. The images were taken at every step of 10g to check the stability of pile group model.

3.7.8 Tunneling

After confirming the steady condition in all measurements, the tunneling test was started reducing the diameter from 70 mm to 64.5 mm for simulating the tunneling process two-dimensionally. The average time for the tunneling process was about 150 seconds. In the tunneling process, the digital camera captured the image of the front side of the container every 20 seconds. The radius contraction of the tunnel was measured by potentiometer, which is converted to ground loss ratio ($\Delta V/V_0$).

3.8 Conclusions

The principal of centrifuge model and the development of centrifuge modeling of pile foundation are described in this chapter. The centrifuge is a powerful method to simulate the pile-soil-tunnel behavior with prototype stress in model scale. In previous study, the interaction between tunnel and pile groups is not well understood and the tunnel model using liquid, and air pressure may be showed some limitation in large ground loss ratio. However, in this study, tunnel machine with can reduce the diameter size in co-axial direction was applied to simulate tunneling process. With the control of radial reduction, the boundary condition could control from the small

to large ground loss ratio. In addition, the radius reduction with consistent magnitude around the perimeter can be approximate as grouting process in the field excavation. This tunnel machine can provide the large ground loss value to simulate the failure of the tunnel.

Particle Image velocimetry (PIV) is very useful to study the ground movement because this technique uses the texture of soil model to trace the displacement vectors. The reduction of shifting effect caused by shaking of the camera by Photoshop is discussed in this chapter. Set of images is modified according to reference points and redo in the PIV to eliminate the wild vectors. The accuracy of PIV has to be discussed in the next chapter.

Pile model made from acrylic has the property of repeatability for advantage point but the pile models appear to be quite compressible during the pile load testing. The proposed method to find bearing capacity with settlement at the pile end is presented. Therefore, the flexible pile models could be approximated the bearing capacity by proposed method.

Table 3.1 Scaling laws

Parameter	Scale (model : prototype)
Stress	1 : 1
Strain	1 : 1
Density	1 : 1
Length	1 : N
Area	1 : N^2
Force	1 : N^2
Time	1 : N^2
Volume	1 : N^3
Mass	1 : N^3
Unit Weight	1 : 1/N
Gravity	1 : 1/N

Table 3.2 Specifications of Tokyo Tech Mark III centrifuge (**Takemura et al., 1999**)

Platform radius	2.45m
Effect radius	2.0-2.2m
Maximum rotation speed	300rpm
Maximum load capacity	50g*ton
Platform width	0.9m
Platform depth	0.9m
Platform height	0.97m
Electrical slip rings for operation	18 channels
Electrical slip rings for instrumentation	72 channels
Available channels for measurement	62 channels

Table 3.3 Pile properties in model scale and prototype scale

Properties	Model	Prototype	Prototype	Prototype
Material	Acrylic pile	Acrylic pile	Concrete pile	Steel pipe
Diameter : Ø	10mm	1.0m	1.0m	42in (1.05m)
Thickness : t	1mm	0.1m	Solid	0.5in (0.0125m)
Young's Modulus : E	3.2 GPa	3.2 GPa	20-28 GPa	200 GPa
Embedment depth : L	150mm 220mm	15m 22m	15m 22m	15m 22m
Bending rigidity : EI	0.93Nm^2	0.093GNm^2	(0.98-1.37)GNm^2	1.09GNm^2
Axial rigidity : EA	0.09MN	0.9GN	(15.7-21.9)GN	8.15GN

Table 3.4 Test conditions and results

Test Series	Test Code	Dr (%)	C/D	X_p/R @ Front pile	Short pile			Long pile			x_i/R	
					Z_{pe}/R	Loading mass* (kg)	Load per pile** (kN)	Z_{pe}/R	Londing Mass* (kg)	Load per pile** (kN)	$\Delta V/V_0$	
											2%	15%
A	Case0-D	80	2.5	Without pile groups installation							2.6	2.2
	Case0-S		1.5								1.8	1.5
B(1)	Case2.0-DH		2.5	2.0	-1.72	1.04	2600	0.28	2.03	5070	3.3	2.6
	Case2.5-DH		2.5	2.5	-1.72	1.04	2600	0.28	2.03	5070	3.2	2.5
	Case3.0-DH		2.5	3.0	-1.72	1.04	2600	0.28	2.03	5070	2.9	2.2
B(2)	Case1.5-DL		2.5	1.5	-1.72	0.76	1900	0.28	1.04	2600	3.1	2.5
	Case2.0-DL		2.5	2.0	-1.72	0.76	1900	0.28	1.04	2600	3.0	2.4
	Case2.5-DL		2.5	2.5	-1.72	0.76	1900	0.28	1.04	2600	2.9	2.4
	Case3.0-DL		2.5	3.0	-1.72	0.76	1900	0.28	1.04	2600	2.7	2.3
C	Case1.5-SL		1.5	1.5	0.28	0.76	1900	2.28	1.04	2600	2.1	1.7
	Case2.0-SL		1.5	2.0	0.28	0.76	1900	2.28	1.04	2600	2.0	1.7
	Case2.5-SL		1.5	2.5	0.28	0.76	1900	2.28	1.04	2600	1.9	1.6
	Case3.0-SL		1.5	3.0	0.28	0.76	1900	2.28	1.04	2600	1.8	1.6

* : model, ** : prototype for 100g

Table 3.5 Dry Toyoura sand property

Specific gravity, G_s	2.65
Mean particle diameter, D_{50}	0.19
Coefficient of uniformity, Uc	1.62
Maximum void ratio, e_{max}	0.973
Minimum void ratio, e_{min}	0.609
Soil friction angle, Ø’	40°

Table 3.6 Relation between SPT values and soil properties

SPT N3 [Blows/0.3 m – 1 ft]	Soil packing	Relative density [%]	Friction angle [°]
< 4	Very loose	< 20	< 30
4 – 10	Loose	20 – 40	30 – 35
10 – 30	Compact	40 – 60	35 – 40
30 – 50	Dense	60 – 80	40 – 45
> 50	Very dense	> 80	> 45

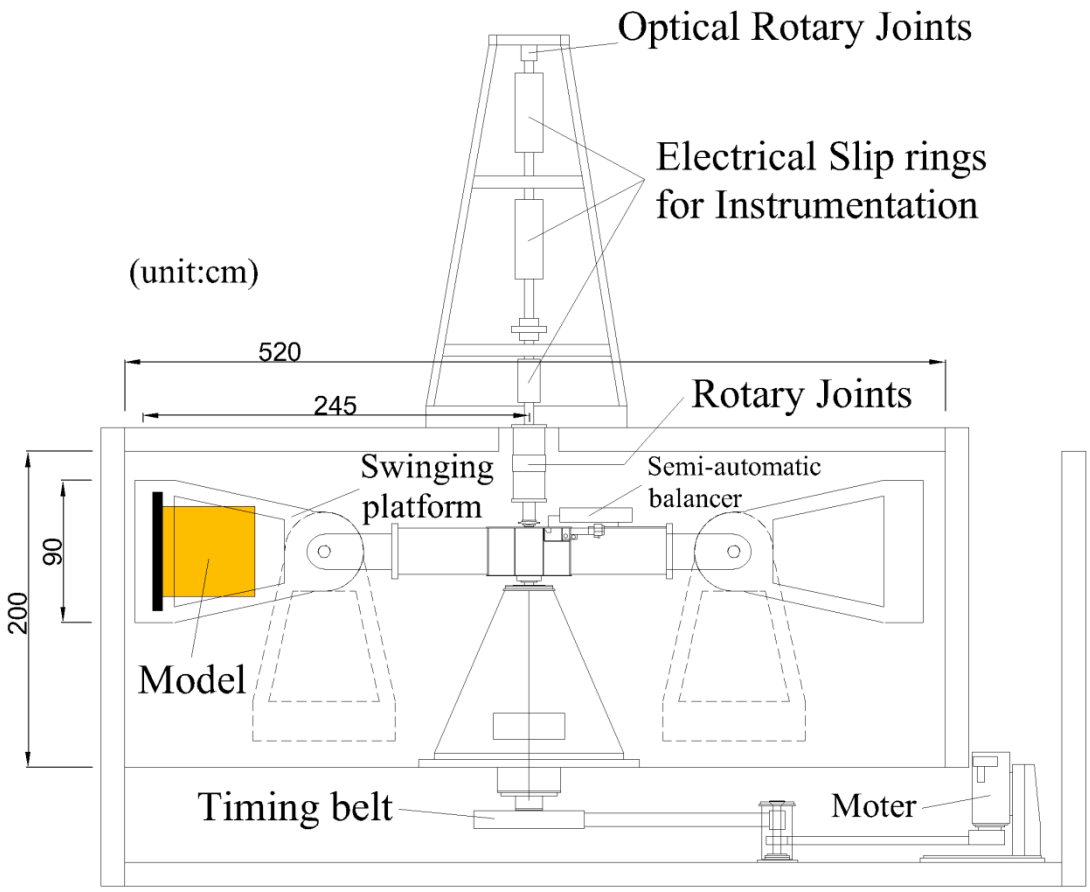

Figure 3.1 Specification of Tokyo Tech MARK III centrifuge

(a)

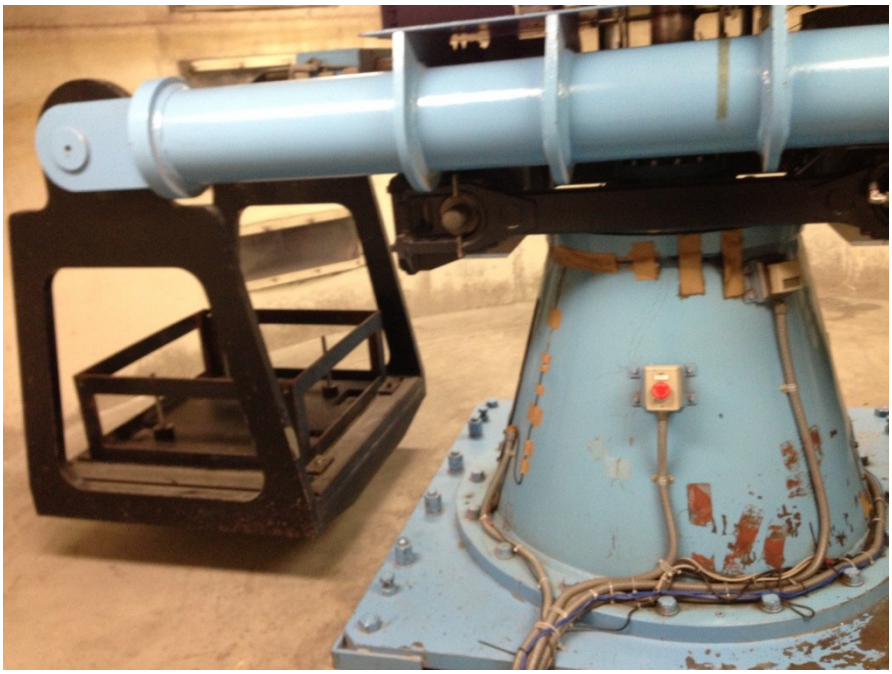

(b)

Figure 3.2 Tokyo Tech MARK III centrifuge swinging platforms: (a) mounting model testing side; (b) counter weight balance side

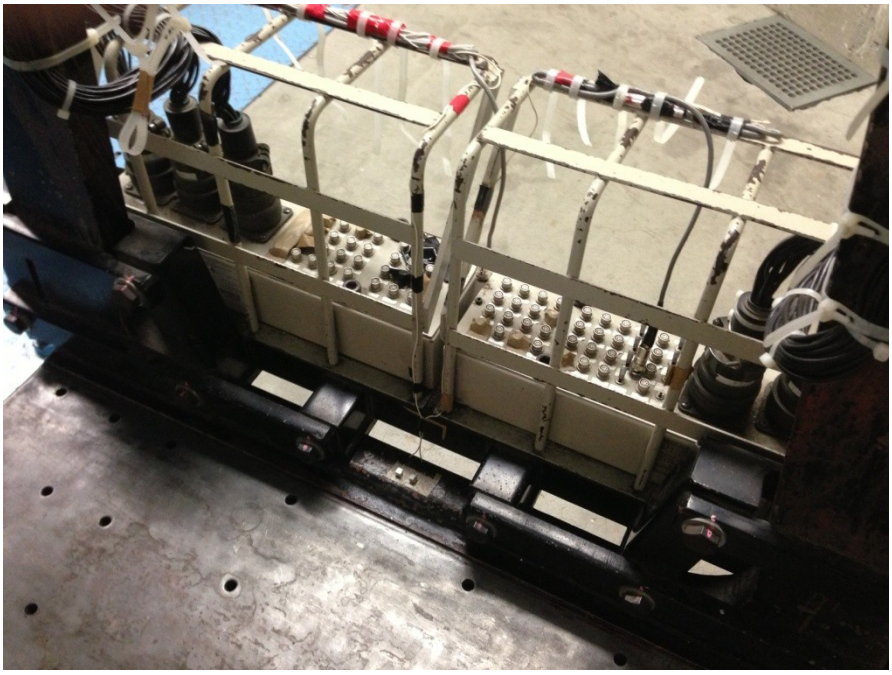

(a)

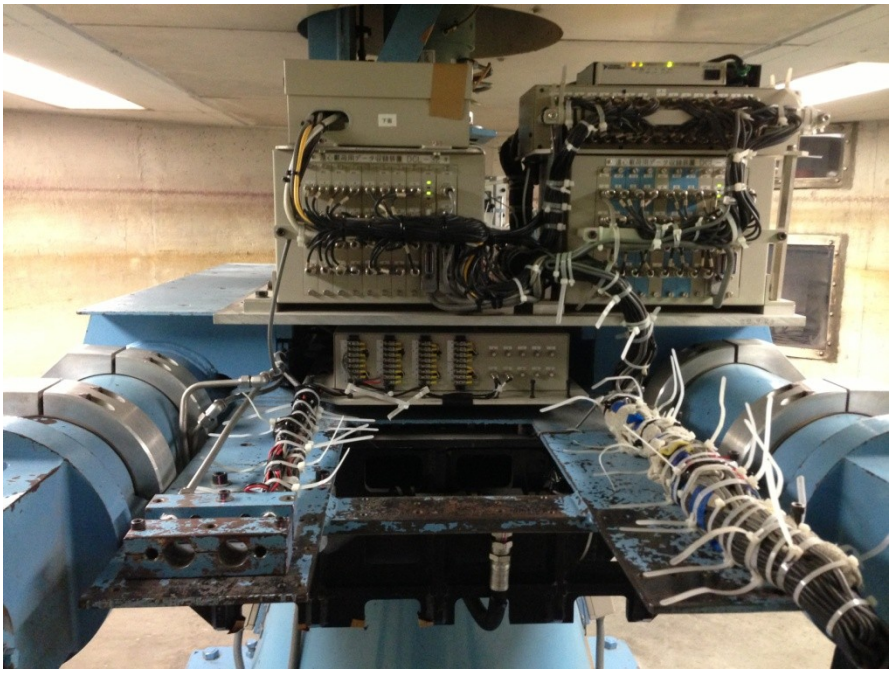

(b)

Figure 3.3 Tokyo Tech MARK III centrifuge control box: (a) junction box for the apparatus; (b) control box for transferring the record data

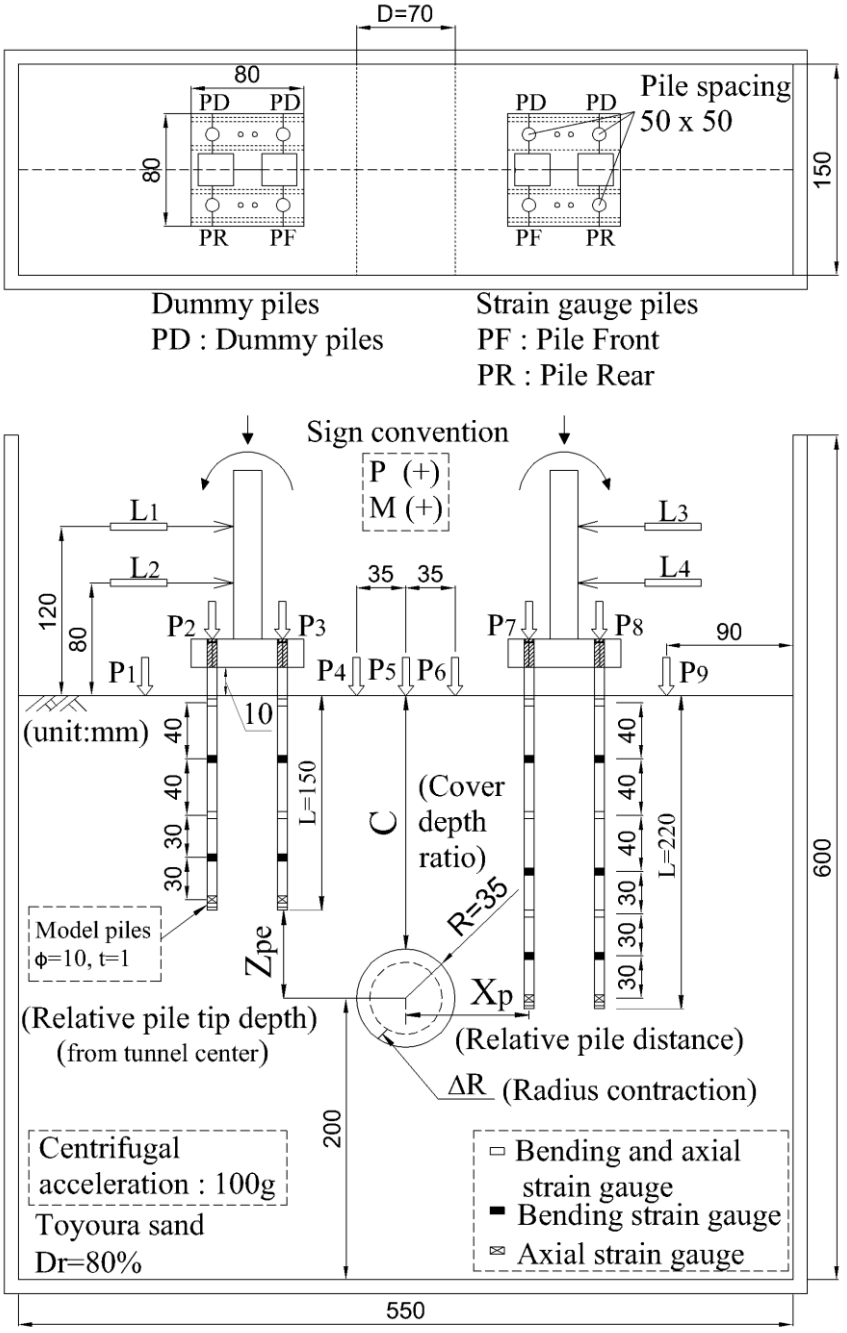

Figure 3.4 Test setup and instrumentation

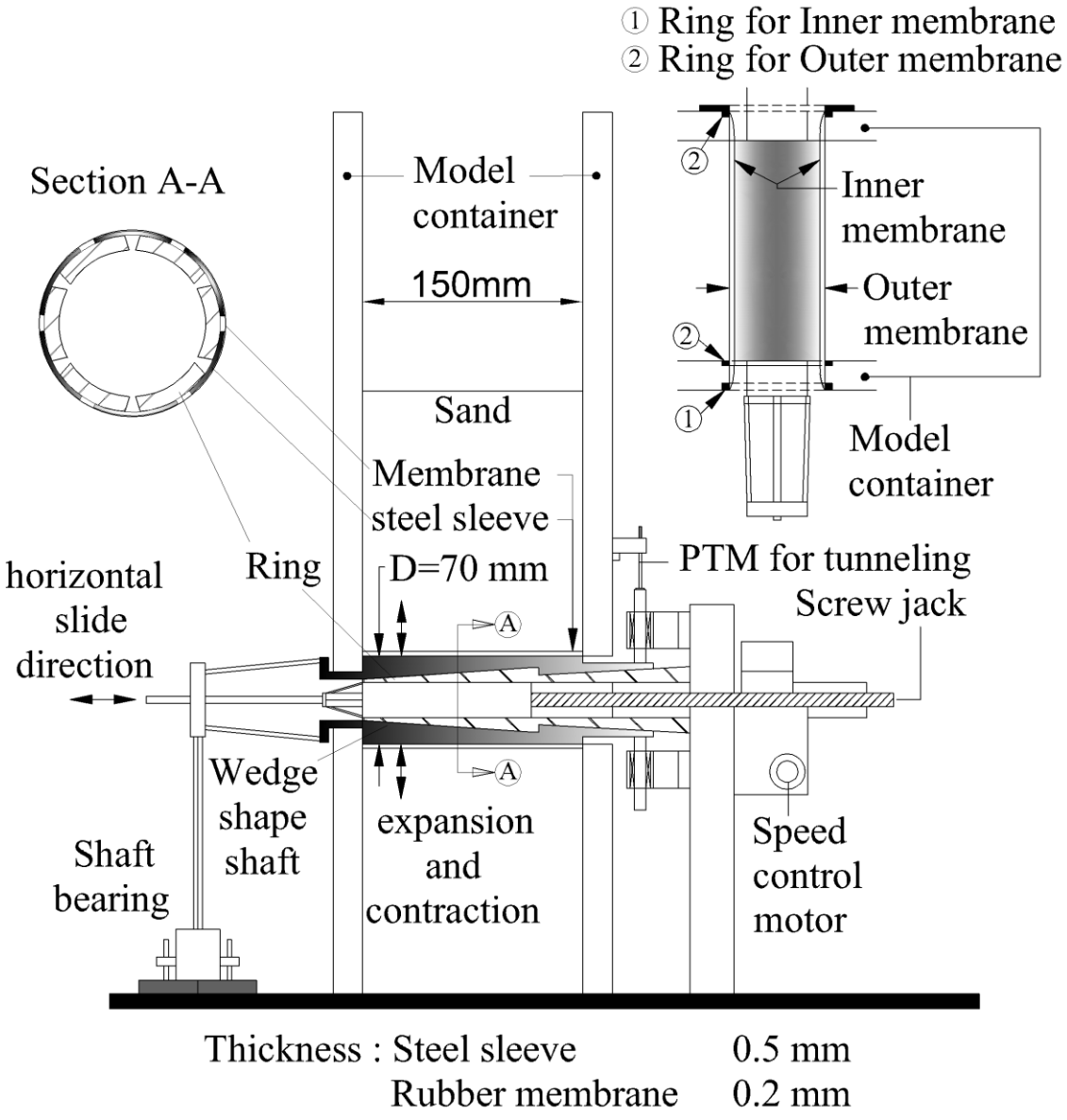

Figure 3.5 Tunnel machine

Figure 3.6 Divided steel rings and wedge-shaped shaft of tunnel machine

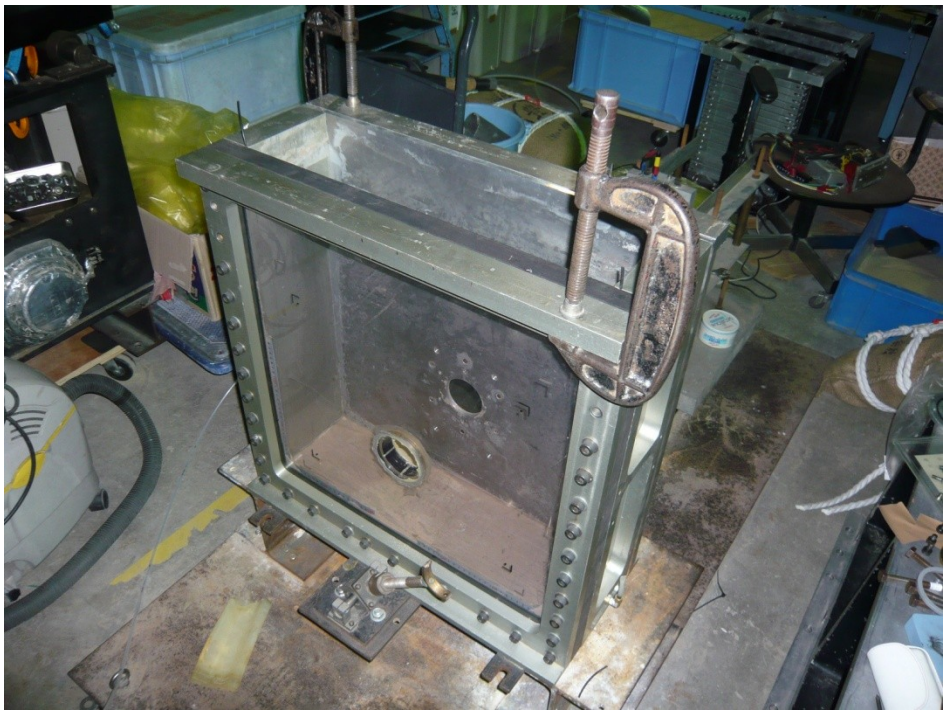

Figure 3.7 Container with two holes at the front and back screens

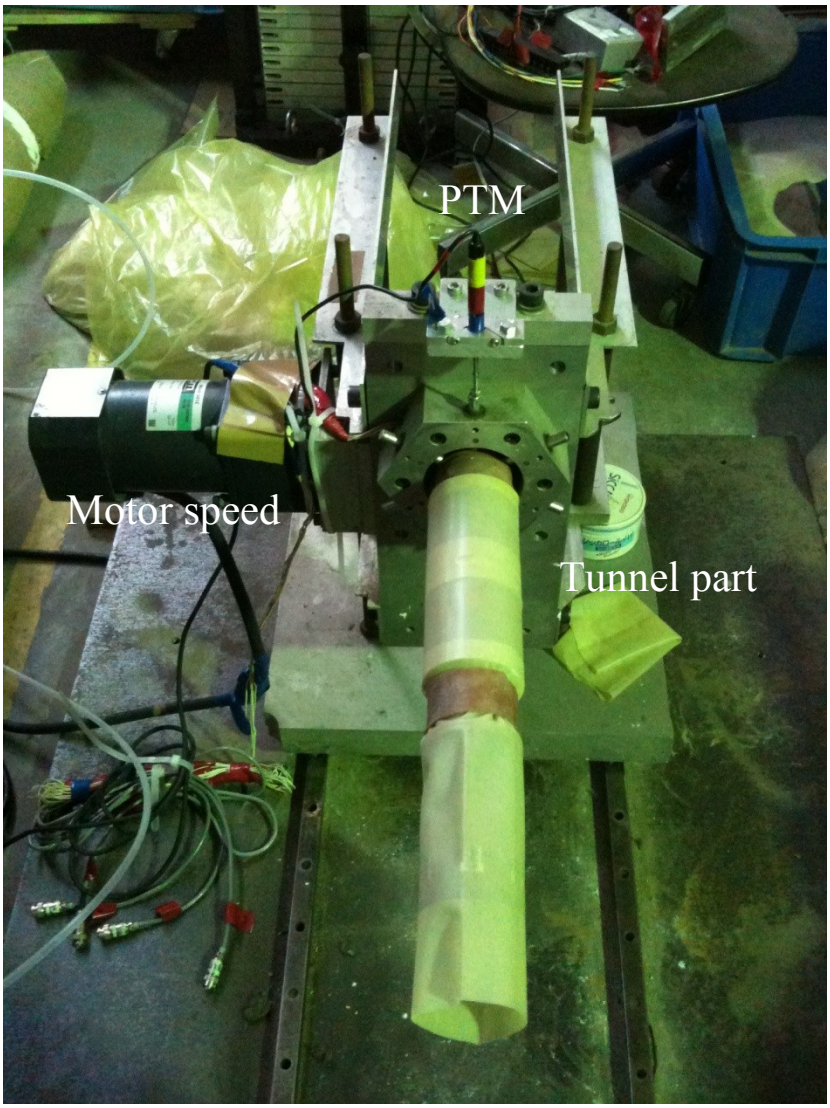

Figure 3.8 Assembly of tunnel machine

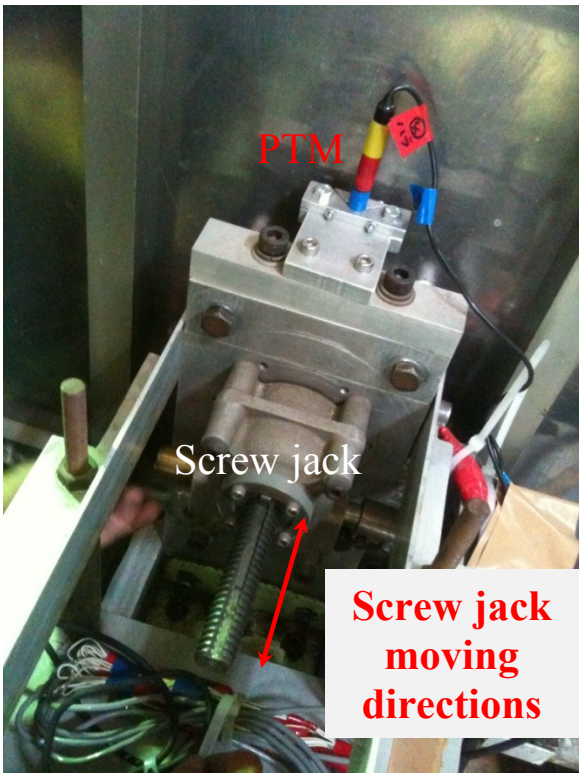

Figure 3.9 Screw jack connected with wedge shaft at the back side of the container

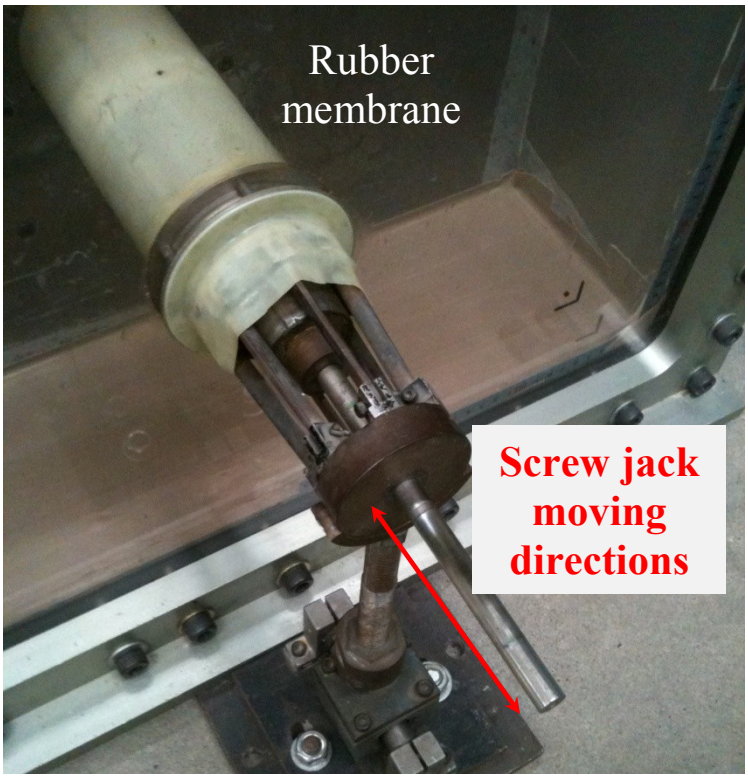

Figure 3.10 Tunnel model cover with a rubber membrane at front screen of container

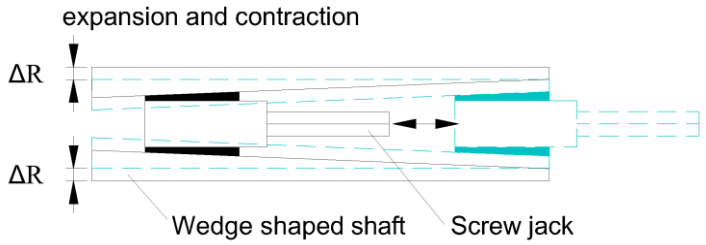

Figure 3.11 Simplified mechanism of tunnel deformation

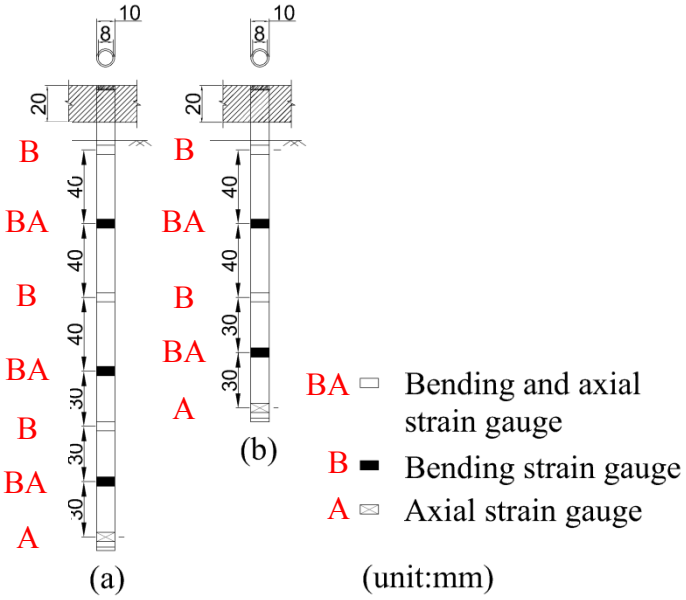

(a)

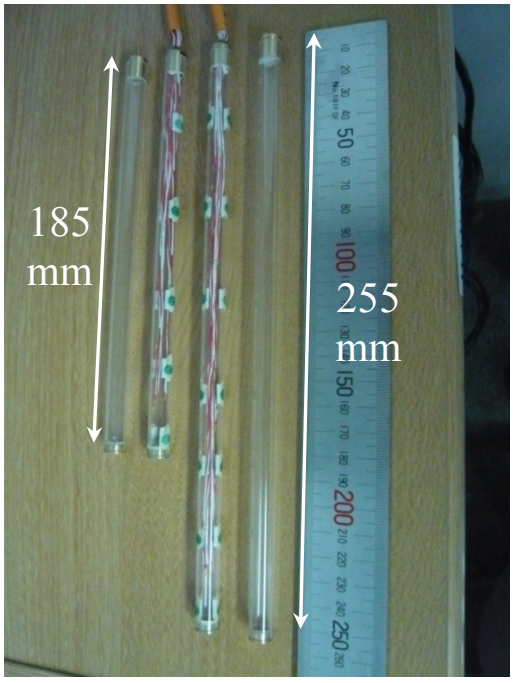

(b)

Figure 3.12 Specification of model piles: (a) Type and position of strain gauges (b) Dummy and strain pile of short and long piles

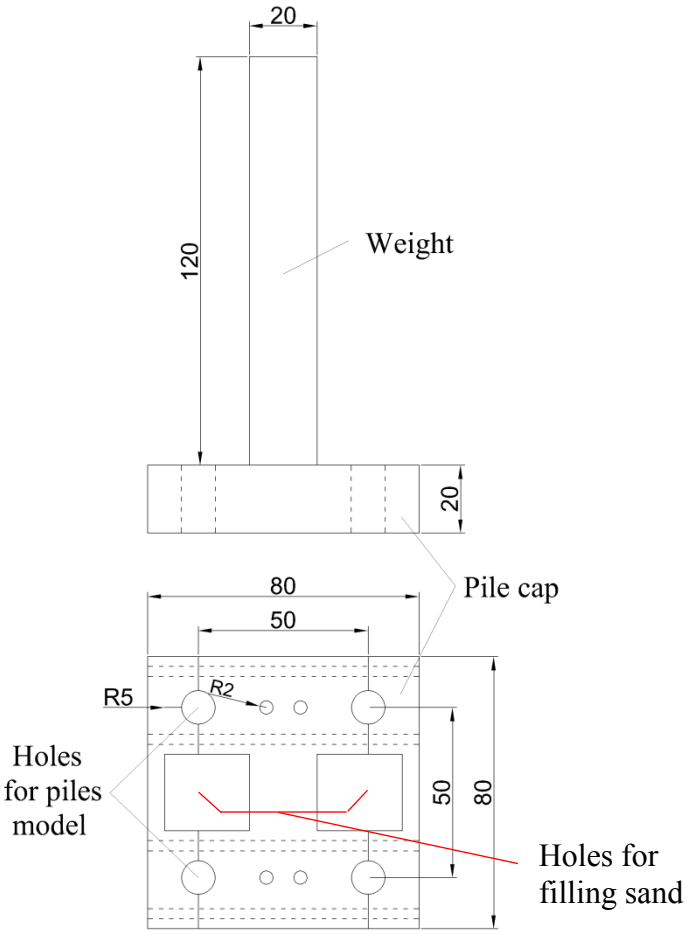

Figure 3.13 Specification of pile cap

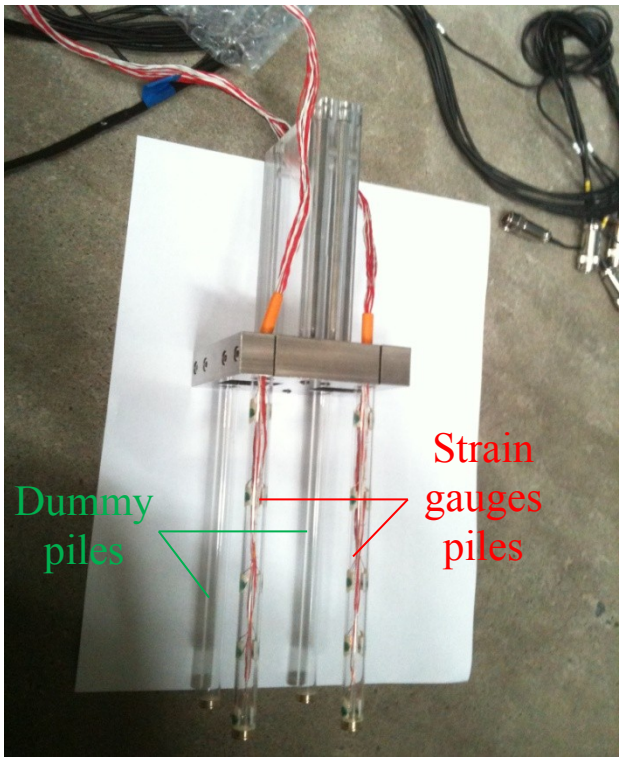

(a)

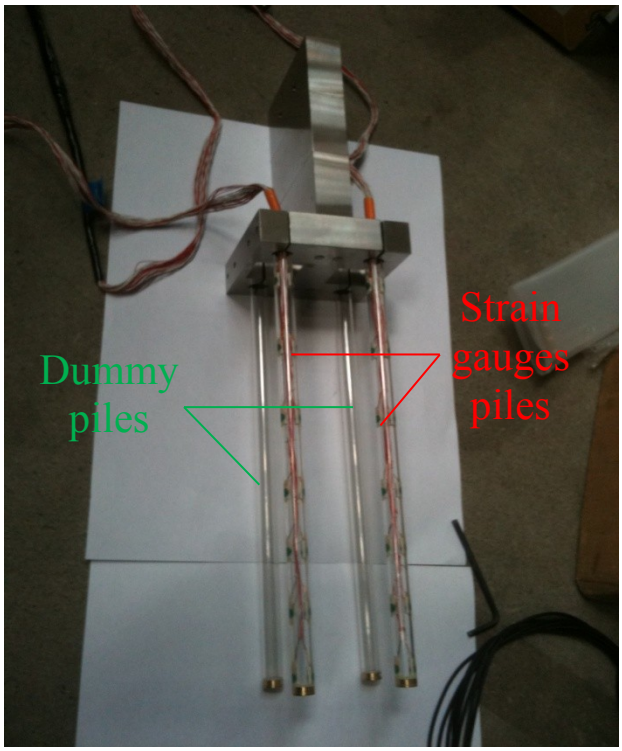

(b)

Figure 3.14 Assembly of model pile groups: (a) short pile group; (b) long pile group

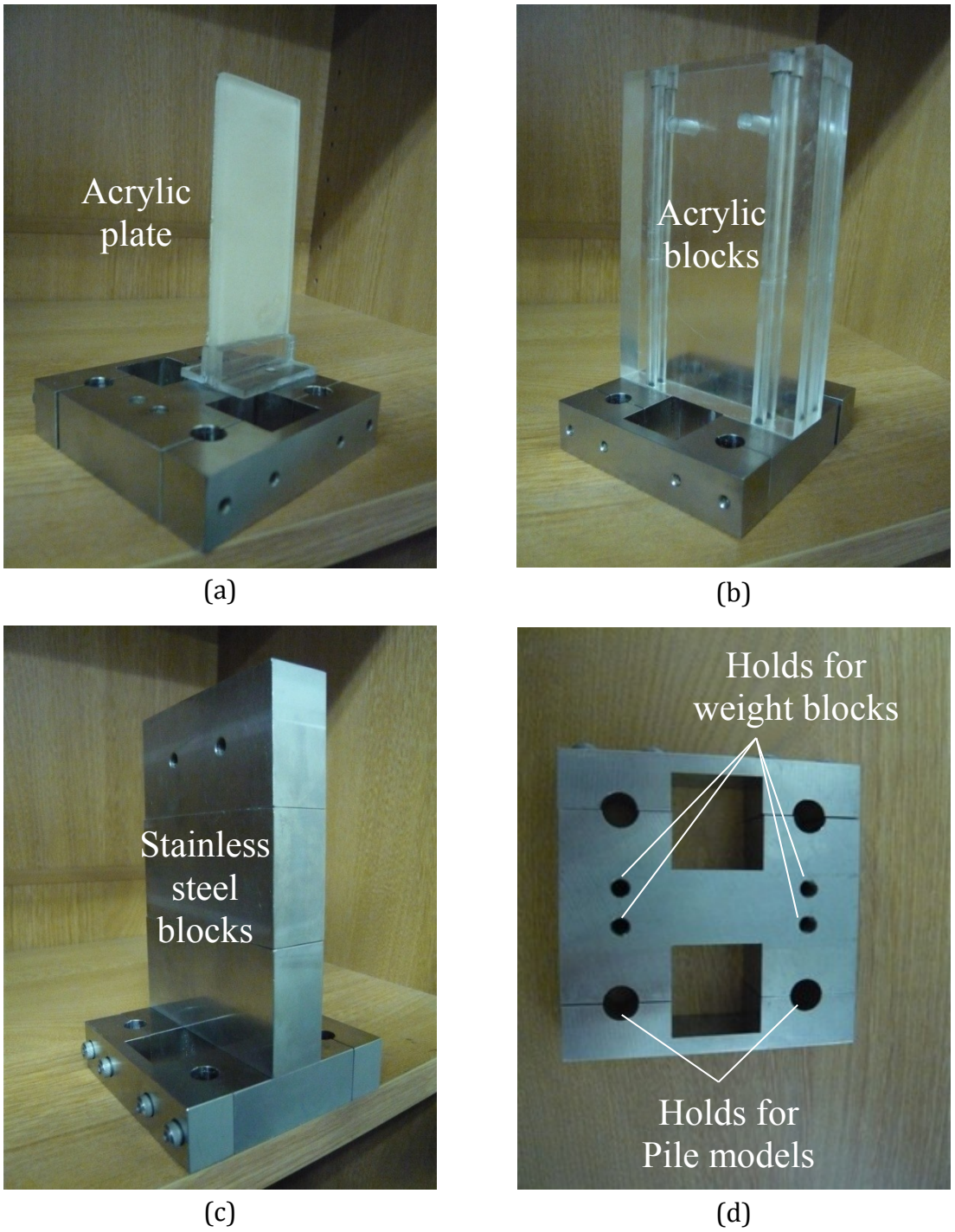

Figure 3.15 Fabrication of weight and pile cap: (a) pile cap without block of stainless steels or acrylics; (b) pile cap with acrylic plate; (c) pile cap with stainless steel plate; (d) stainless steel pile cap

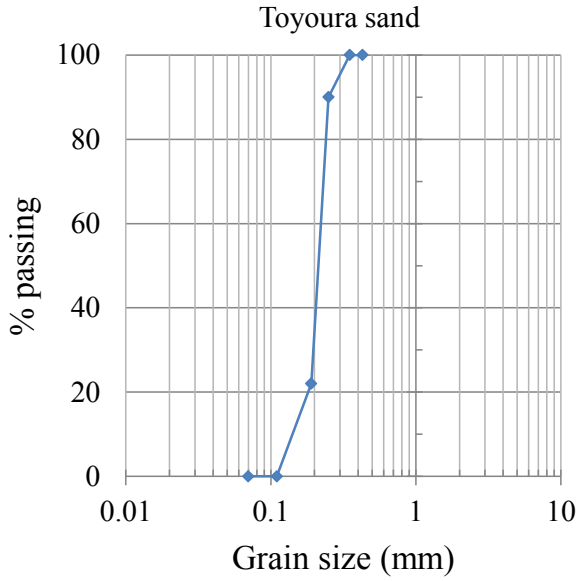

Fig. 3.16 Gradation curve of Toyoura sand

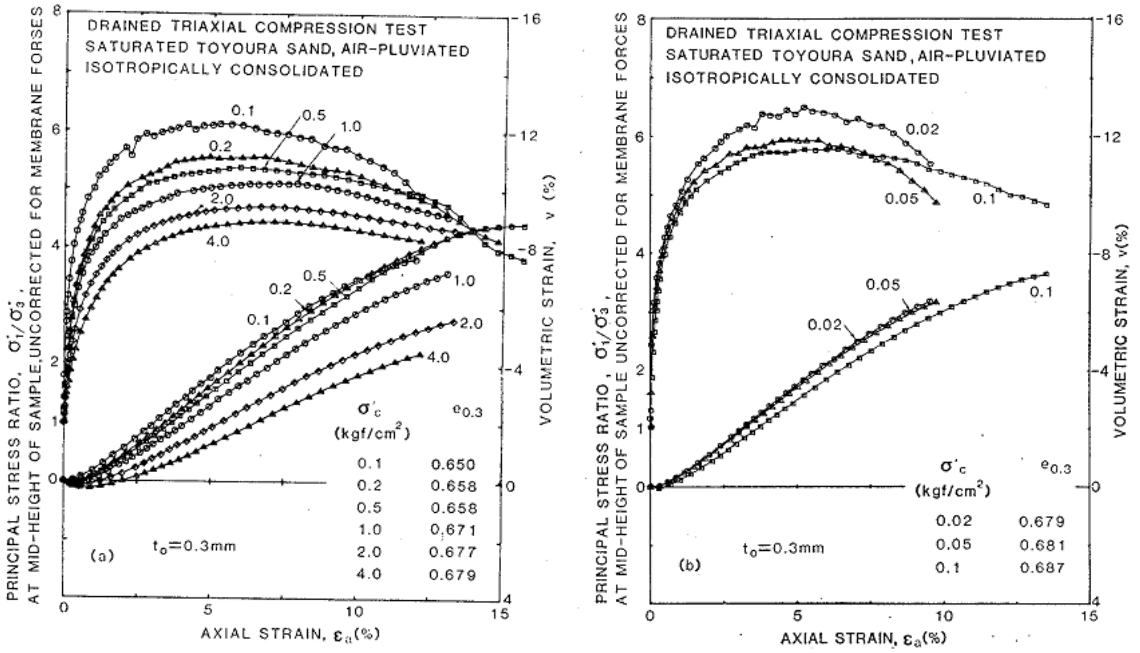

(a) (b)

Fig. 3.17 Relations of principal stress ratio at the mid-height of sample, axial strain and volumetric strain for a membrane thickness of 0.3 mm: (a) dense sand at σ'_c = 10-400 kgf/cm^2 ; (b) dense sand at σ'_c = 2-10 kgf/cm^2 (**Fukushima and Tatsuoka (1984)**)

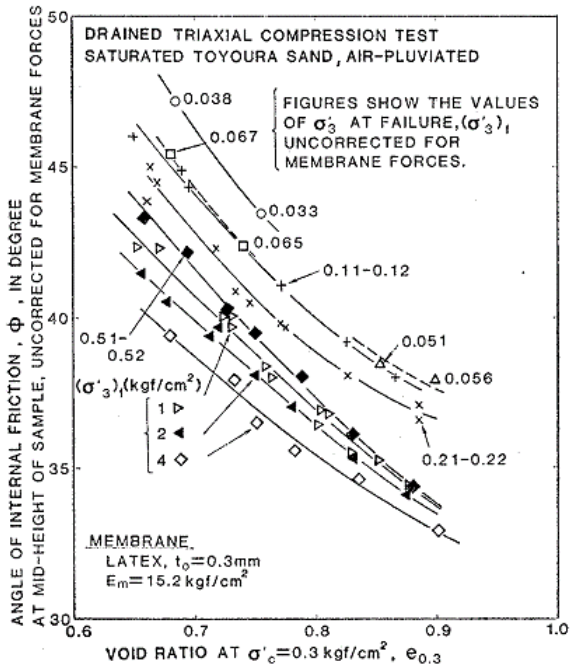

Fig. 3.18 Variation of angle of internal friction against the various void ratio (**Fukushima and Tatsuoka (1984)**)

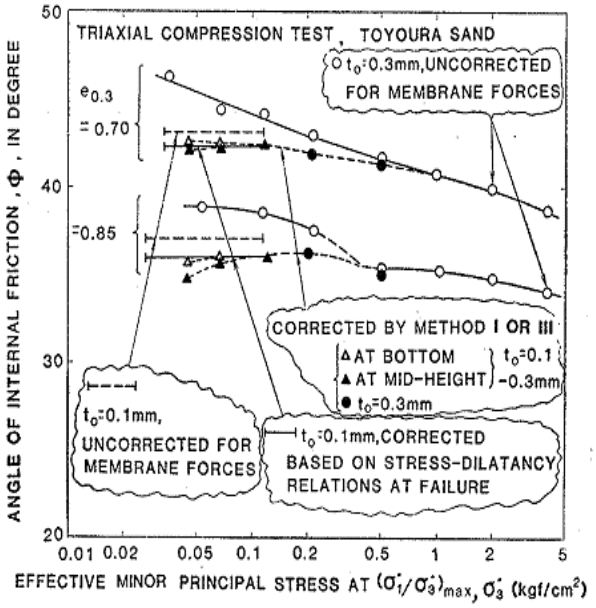

Fig. 3.19 Variation of angle of internal friction against the effective minor principal stress by various methods of testing (**Fukushima and Tatsuoka (1984)**)

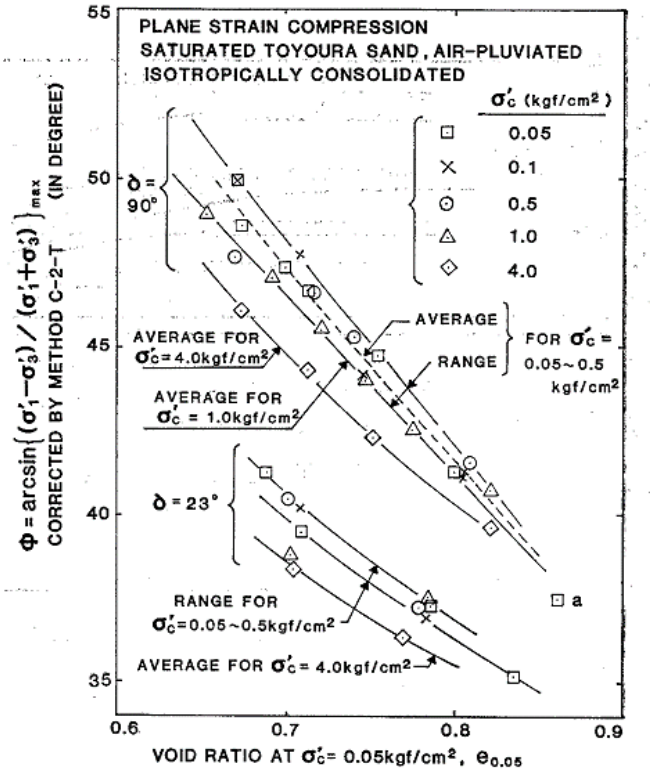

Fig. 3.20 Variation of angle of internal friction against the various void ratio and consolidation pressure (**Tatsuoka et al., 1986**)

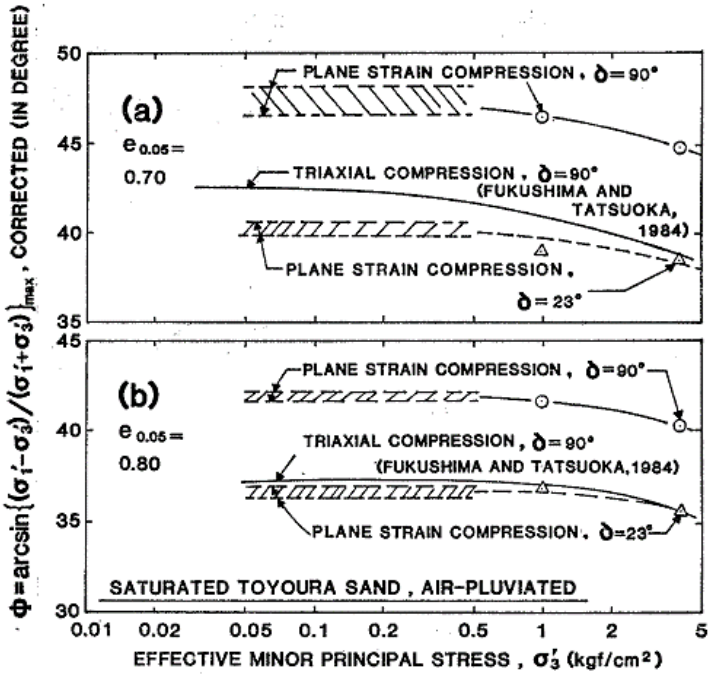

Fig. 3.21 Variation of angle of internal friction against the effective minor principal stress by triaxial and plane strain compression tests: (a) dense sand; (b) loose sand (**Tatsuoka et al., 1986**)

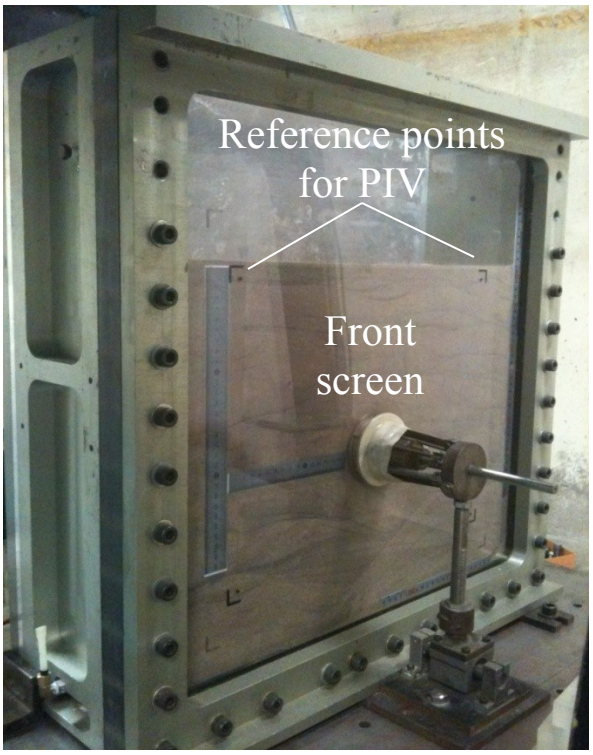

Figure 3.22 Plain strain rigid container

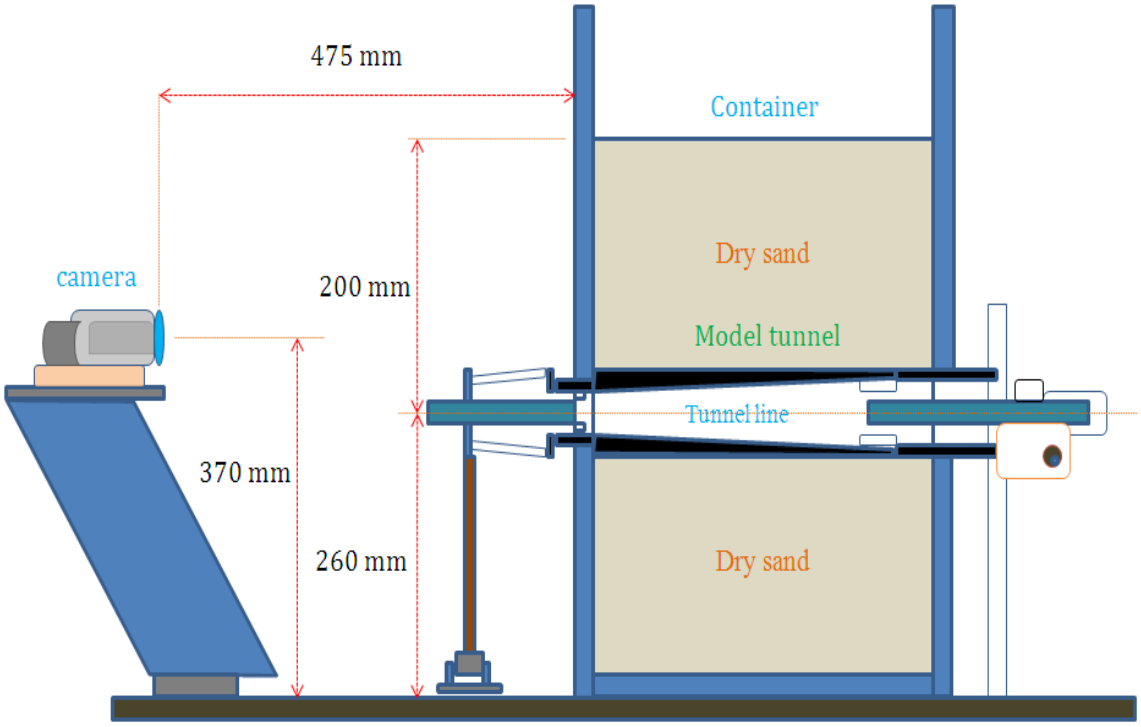

Figure 3.23 PIV setting configuration

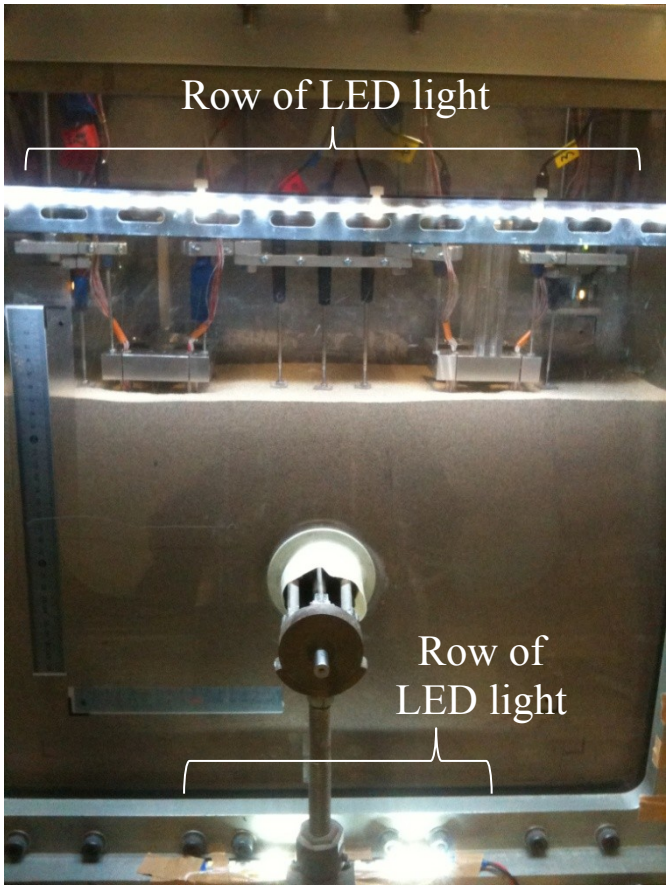

Figure 3.24 Rows of LED light for PIV

Figure 3.25 PTM with aluminum holding plate

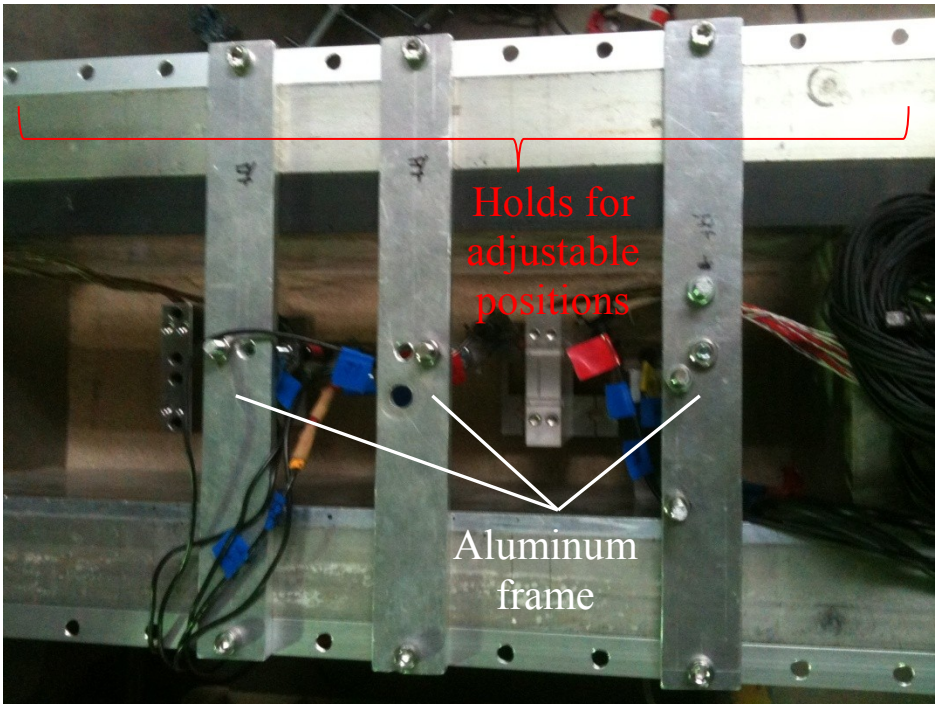

Figure 3.26 Aluminum frame of measured equipment which can adjust the positions

Figure 3.27 PTM on the pile cap and on the soil model

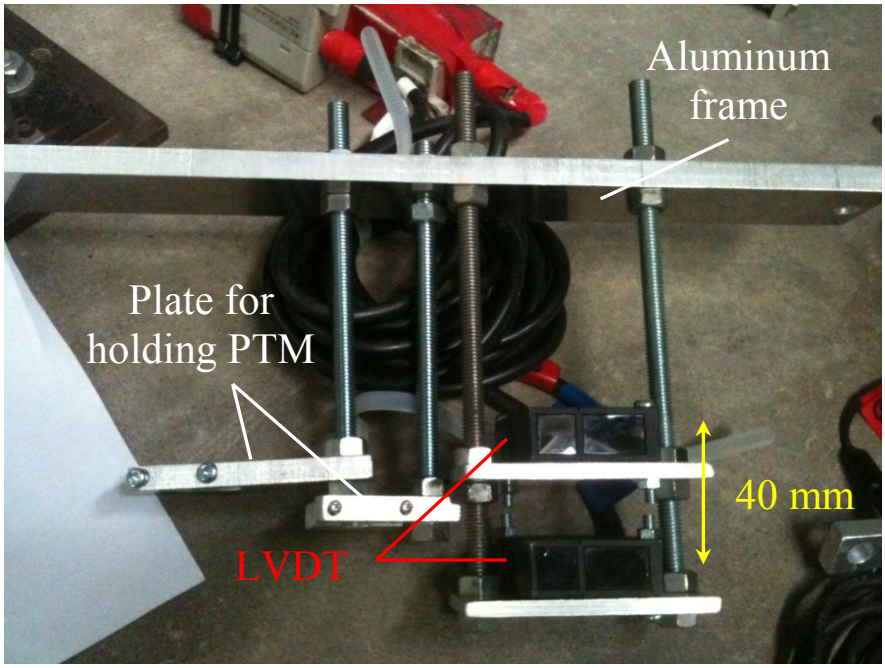

Figure 3.28 Two LVDT with adjustable height of screws and aluminum frame

Figure 3.29 Load cell for pile load test

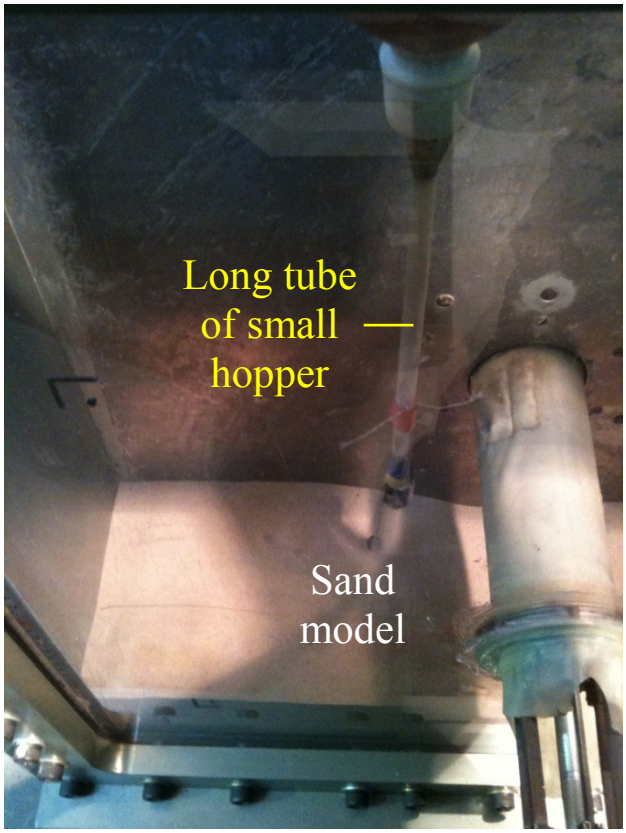

Figure 3.30 Air pluviation method by small hopper with long slender tube

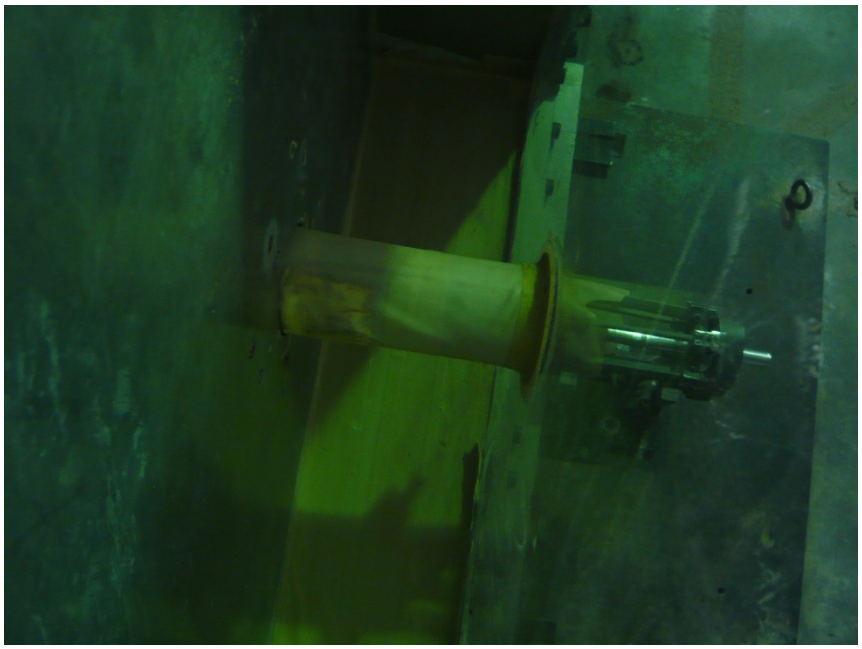

Figure 3.31 Old rubber membranes with inconsistent rubber surface

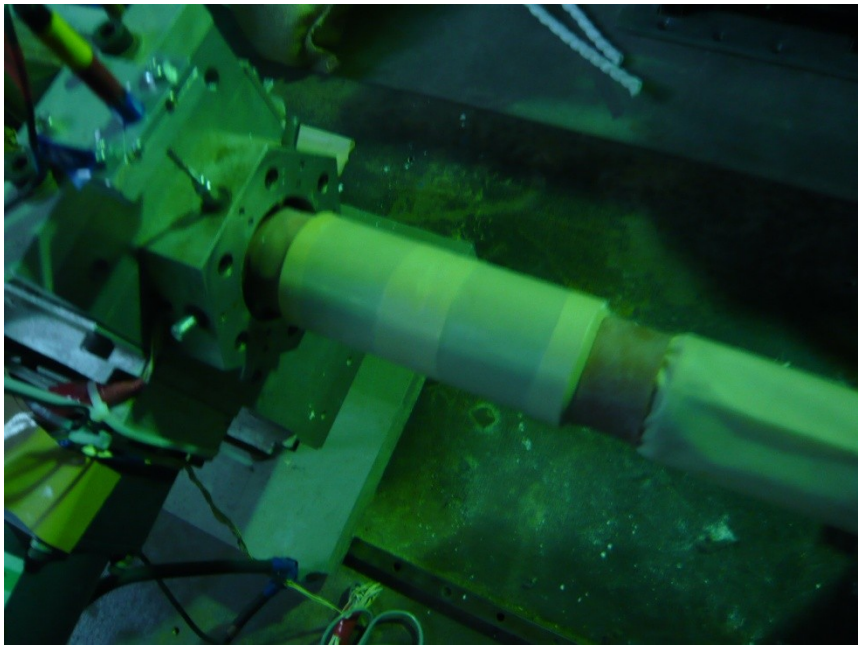

Figure 3.32 New rubber with consistent surface and fitting in well with tunnel machine

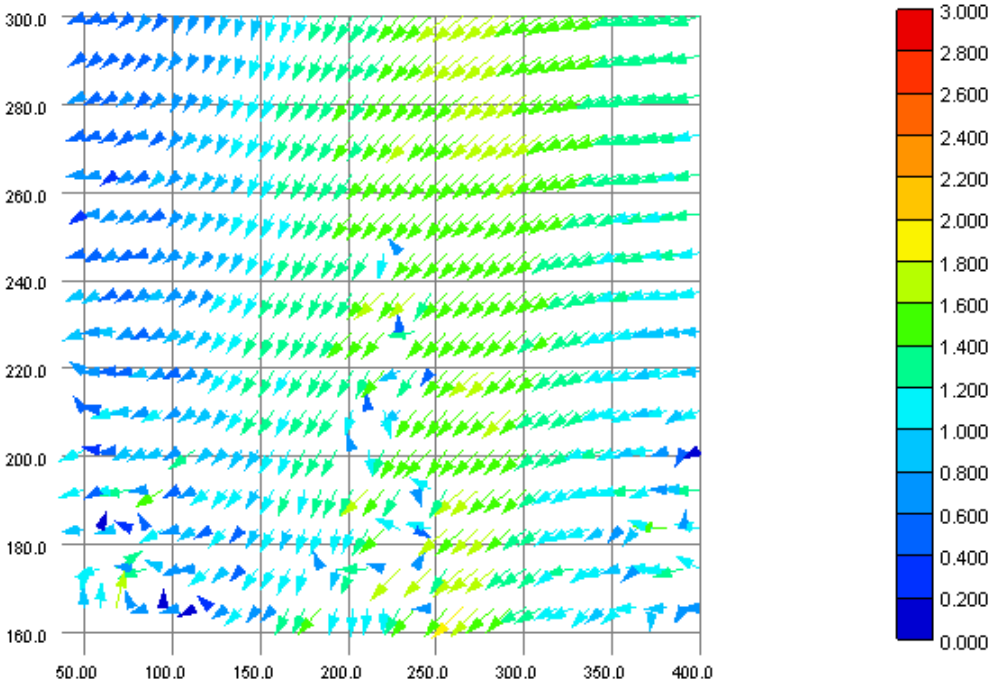

Figure 3.33 Wild vectors due to shifting of interval images

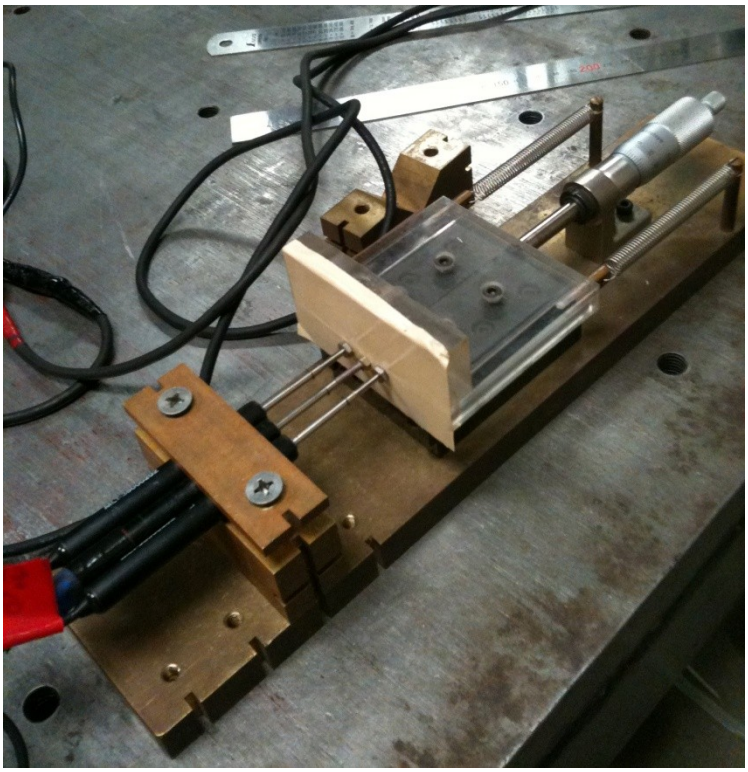

(a)

(b)

Figure 3.34 Calibration method with micrometer: (a) PTM; (b) LVDT

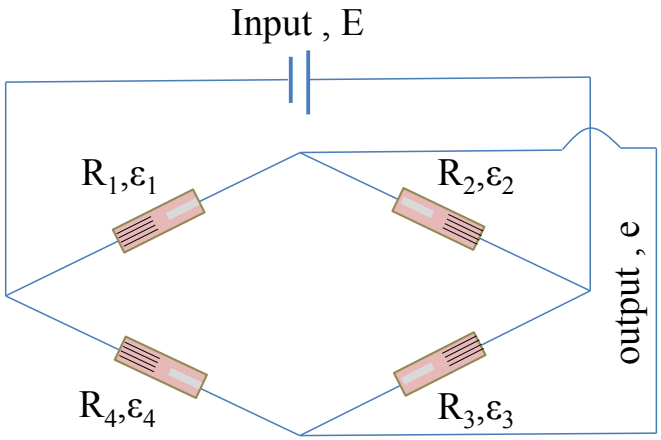

Figure 3.35 Wheatstone bridge circuit

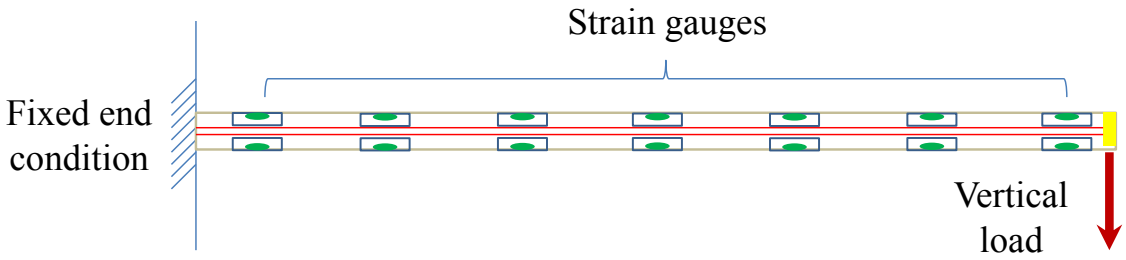

(a)

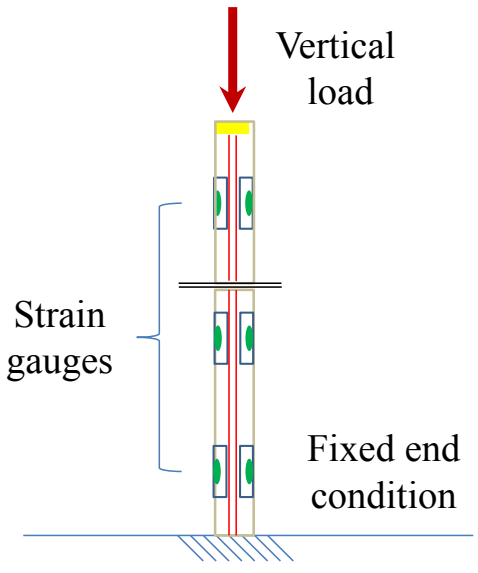

(b)

Figure 3.36 Strain gauges calibration: (a) hanging weight; (b) apply load in a vertical direction

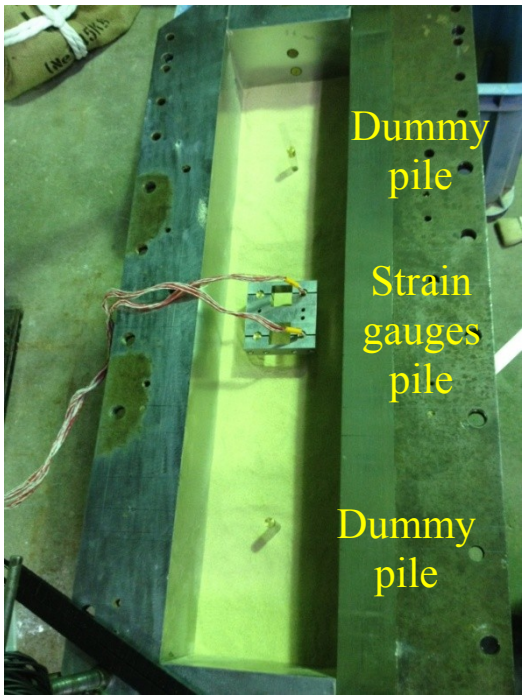

Figure 3.37 Preparation for pile load test (single dummy piles and strain gauges pile groups)

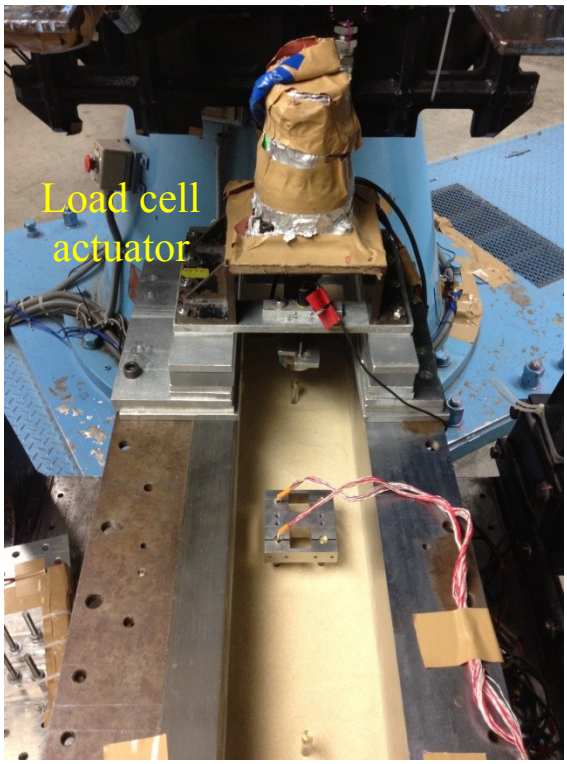

Figure 3.38 Installation of load cell actuator above the test pile

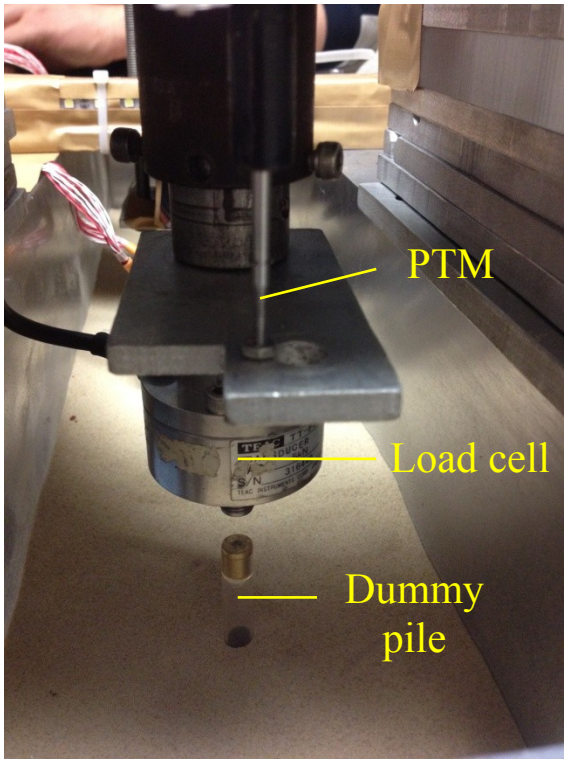

Figure 3.39 Setup of load cell and single dummy pile prior to pushing

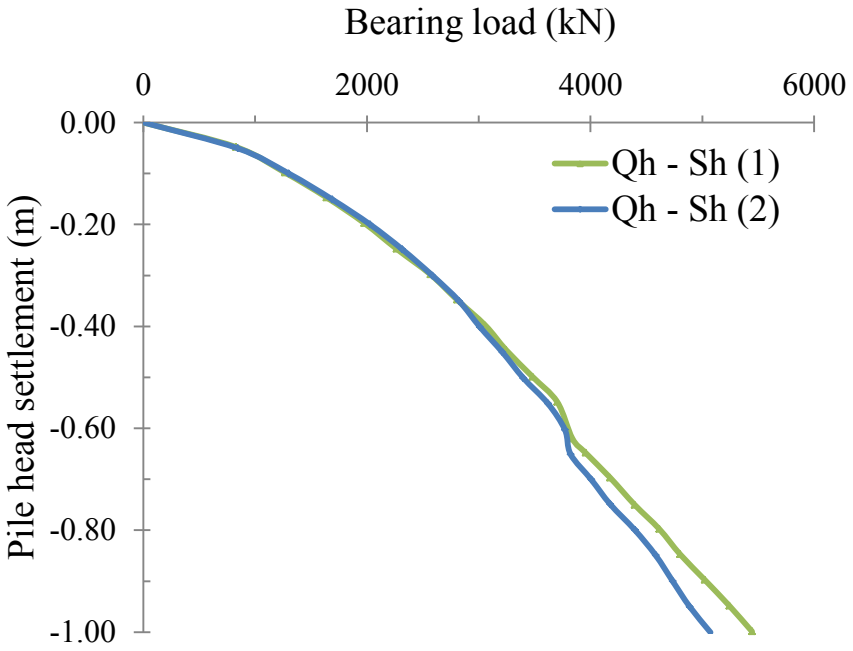

(a) Short single pile

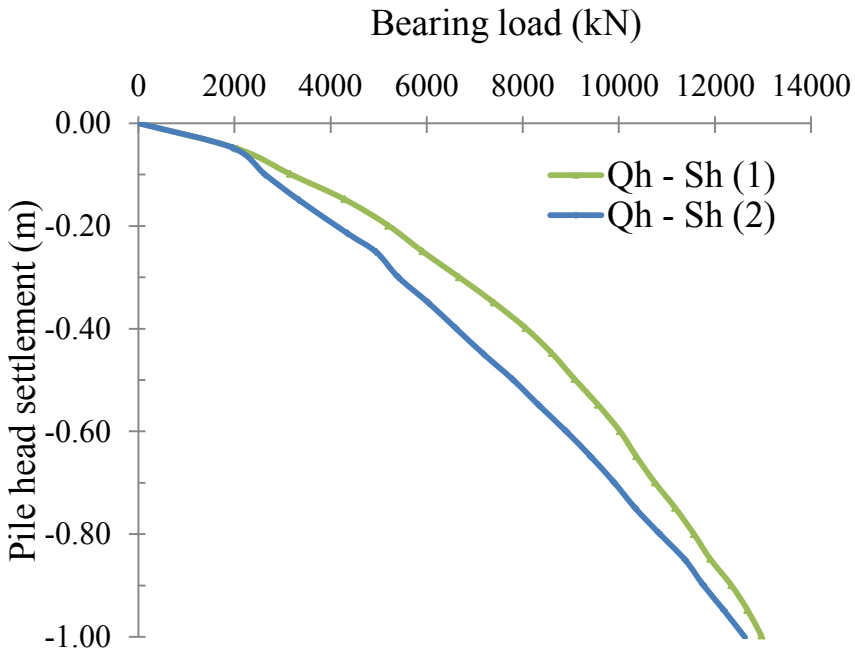

(b) Long single pile

Figure 3.40 Load settlement curve of a single dummy pile:
(a) Short single pile; (b) Long single pile

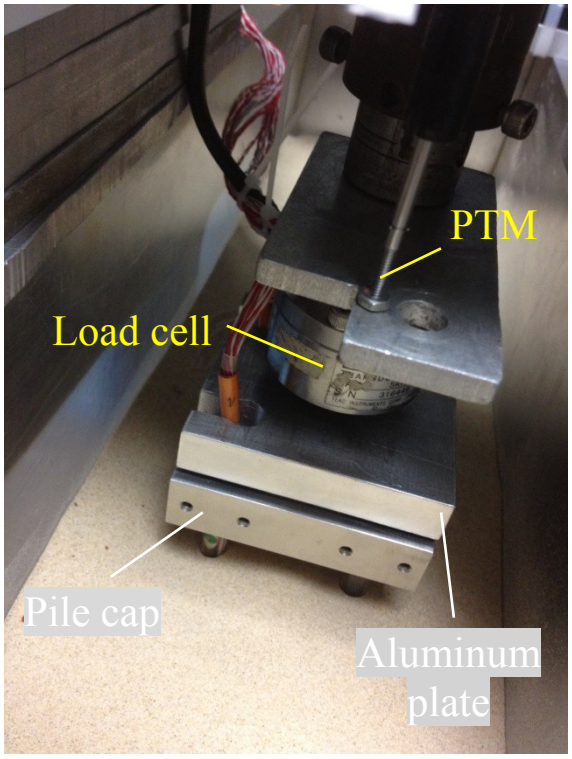

Figure 3.41 Setup of load cell and strain gauges pile group prior to pushing

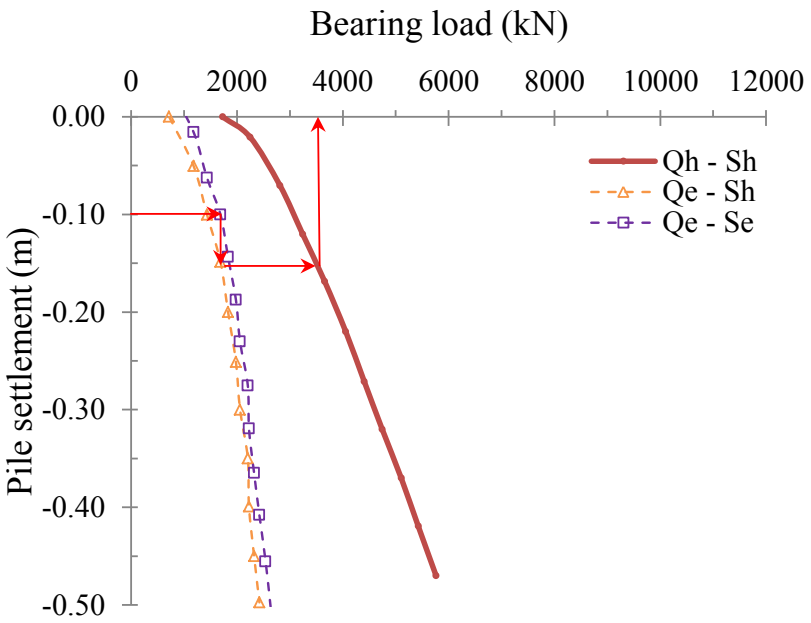

(a) Short pile group

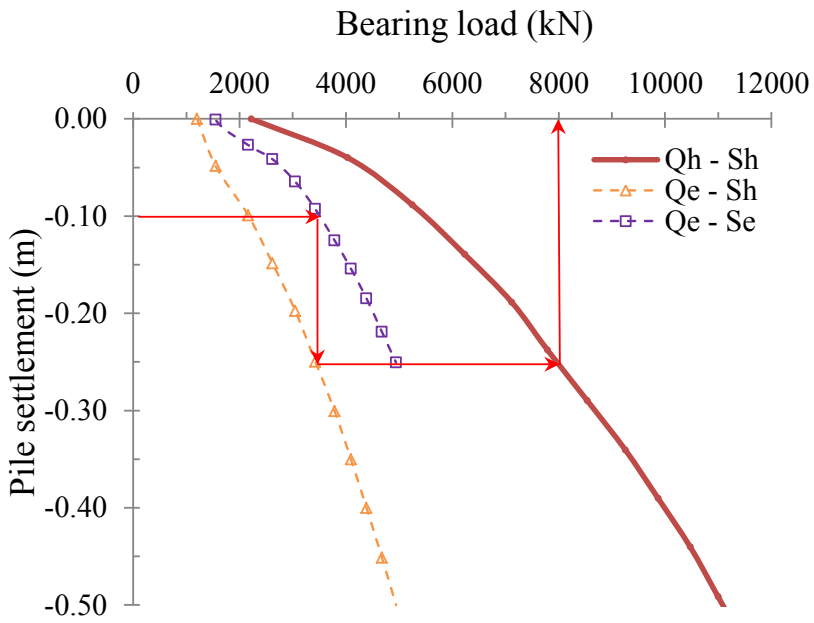

(b) Long pile group

Figure 3.42 Determination of end bearing load

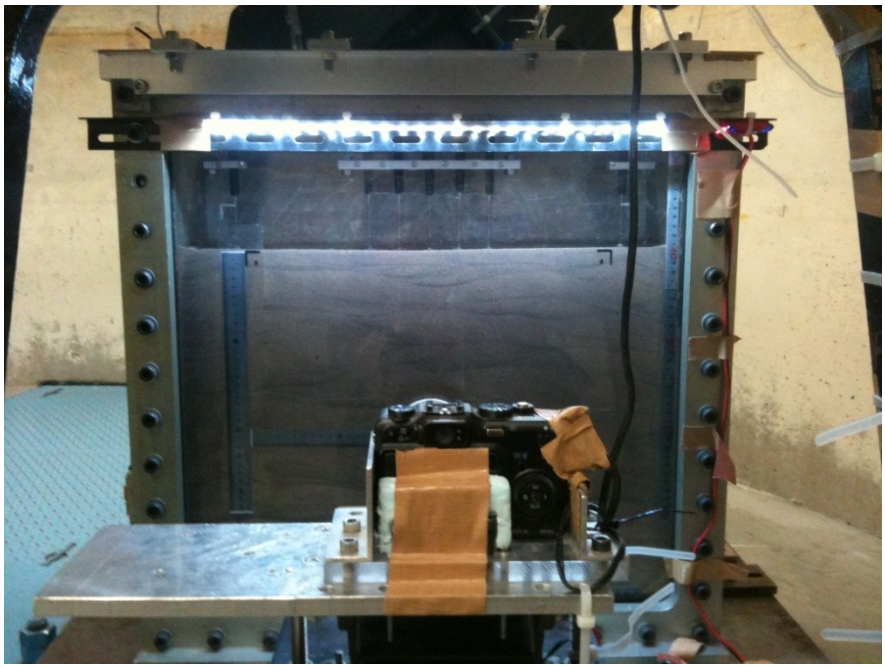

Figure 3.43 Test setup for ground movement without pile foundation

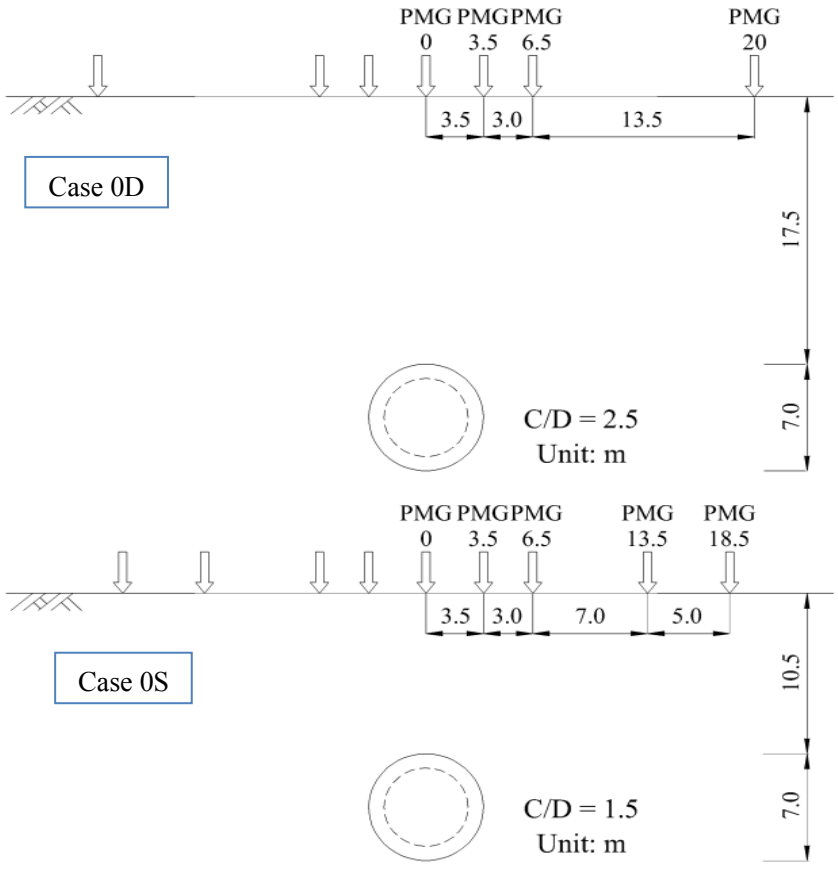

Figure 3.44 PTM positions of Case 0D and Case 0S

Figure 3.45 Potentiometer on ground (PMG)

Figure 3.46 Installation of pile groups

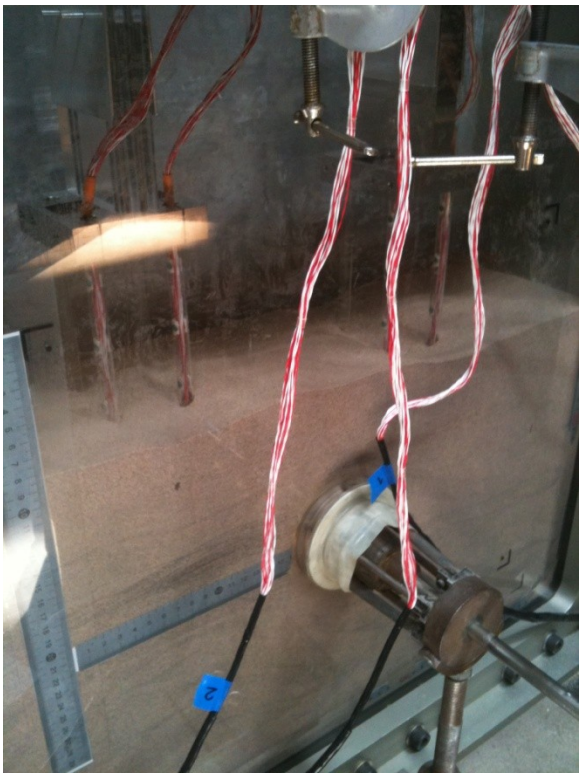

Figure 3.47 Sand preparation at the mid-height of designed ground level

Figure 3.48 Complete preparation of model ground with pile groups

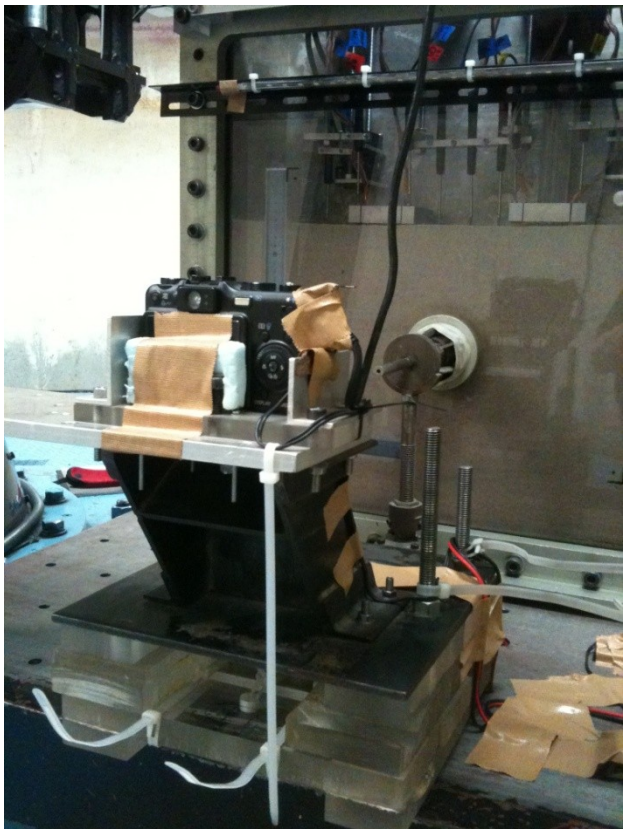

Figure 3.49 Camera setup

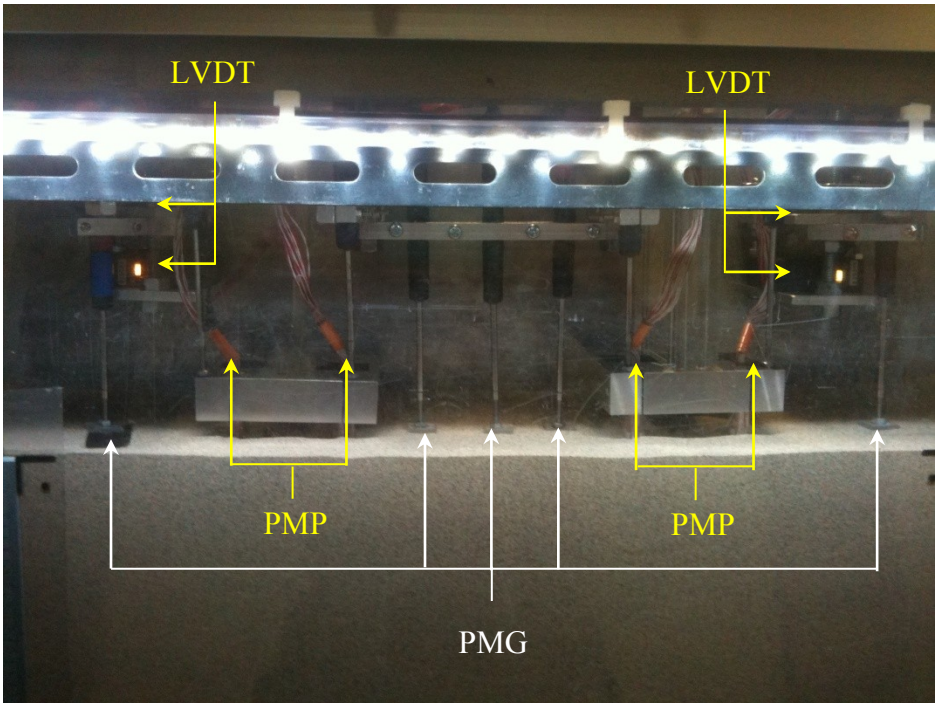

Figure 3.50 PTM and LVDT setup

Chapter 4

Ground movement caused by tunneling with and without pile group

4.1 Introduction

Increasing demand for land use within industrial or urban area has given rise to a growth in the number of excavation projects, especially in tunneling for underground facilities and transportation system. The need for precise prediction of ground movement caused by tunneling for finding appropriate methods to increase the safety of existing structures when designing a tunnel has inspired to growing research attraction. Therefore, the tunneling-induced soil movements have been long studied by many researchers not only ground surface settlement, but also the subsurface settlement (**Peck, 1969**; **Mair et al., 1993**). The potential effects of the ground movement associated with the tunnel construction must be properly considered in the design and construction of tunnel to avoid the adverse effects, i.e. settlement of the road above tunnel, and damages of the adjacent structures, such as pile foundations, buildings, buried pipes.

From the enormous research works, such as accumulation of field data, numerical and analytical simulations, prediction of ground movement by tunneling could have been made reasonably well, which makes it possible to assess the risk of building damage (**Mair et al., 1996**). Although, these numerical studies have produced variable interesting results, there are still some uncertainties and the validation of the proposed construction methods is required, especially

for the effects of many factors, such as, types of soil, types of tunneling and imposed soil movement or ground loss by tunneling, tunnel depth, types of piles (single and group), pile construction methods, depth and location of piles, pile bearing capacity, load supported by piles, and the effects of piles on the soil movements. In addition, the shape of sub soil settlement trough in the green field is a function of depth influenced by magnitude of ground loss ratio ($\Delta V/V_0$) and cover and depth ratio (C/D) (**Marshall et.al, (2012)**).

Physical modeling, especially centrifuge modeling is a useful tool to tackle these problems with its capability of creating the similar stresses in a small scale model to those of the full-scale prototype. This condition is a critical in a model in which most of the stresses and their changes caused by weight of soils, e.g., excavation of soil in the tunneling process. With this advantage, centrifuge modeling has been used for studying tunneling-induced geotechnical problems and various techniques where tunneling simulators have been developed.

However, few researchers have addressed the problem of ground movement behavior with the presence of nearby structures. The shape of the settlement trough could be affected by the stiffness of bunch of piles. Therefore, in this chapter, the results of fundamental of ground movement, the accuracy of measured instruments, performance of tunnel centrifuge machine and the effect of pile group are discussed.

4.2 Ground movements

Ground settlements and movements are inevitably caused by the tunnel construction in soft ground and are the major concern especially in urban areas. In this study, the results of ground movements are divided into two categories; soil surface settlement and the subsurface settlement.

4.2.1 Soil surface settlement

Soil surface settlements were measured by potentiometers resting on the dry Toyoura sand sample. The ground surface settlement is slightly different from the cases. In the figure, PMG means potentiometer on the ground. The values after these abbreviations define a horizontal distance which set as zero from the center line of the model tunnel. The positive and negative values mean the position of potentiometers are on the right-hand side and left-hand side respectively. All the results of the test cases are indicated in **Fig. 4.1-4.4**. In general, the graphs display nonlinearity between the depth and ground loss ratio. Rapidly soil settlement can be

observed at the small ground loss ratio ($\Delta V/V_0 \leq 4$ %) while these rates of settlement are reduced at the significant value of ground loss ratio. Test case conditions are shown in **Table 3.4**.

The test series A (**Fig. 4.1**) show the soil surface settlement between two values of cover and depth ratio without an installation of pile group model. The settlements increase with increases in the ground loss ratio. The settlement concentrated at the middle part of the trough profile and slightly decreased as a position of potentiometers far from the tunnel axis. In addition, at the same horizontal distance from the tunnel center, Case0-D shows larger vertical settlement than the Case0-S and cases with large cover and depth ratio tend to develop wide trough settlement compare to the case with small cover and depth ratio.

The test series B-1 (**Fig. 4.2**) has a heavy load of the superstructure and the horizontal distance between front pile, and center of the tunnel (X_p) was varied between the test cases. A pile tip level of long group pile was approximately at the level of tunnel spring line ($Z_{pe}/R = 0.28$). Therefore, a pile tip level of short pile is resting over the tunnel position ($Z_{pe}/R = -2.28$). Z_{pe} is the distance between pile end, and center of tunnel and R is the radius of the tunnel. In the middle, two of potentiometers (PMG-35, PMG+35) were effect by the change of pile group position while the potentiometer at the center (PMG00) is identical regardless of pile group position. Potentiometers of PMG-35 and PMG+35 tend to settle close to the potentiometer at the center (PMG00) as the relative horizontal distance (X_p/R) is reduced. In addition, the vertical settlements gradually reduce by the distance from the tunnel center line.

The test series B-2 (**Fig. 4.3**) has an arrangement as the same as test series B-1. The only difference in these test series is the weight of the superstructure which was reduced to a small magnitude. The trends of soil settlements between test series B-1 and B-2 are similar. It should be noted that three potentiometers (PMG-35, PMG00, PMG+35) of the case with $X_p/R=1.5$ (Case1.5-DL) induce larger vertical settlements than the other cases with the large ground loss ratio ($\Delta V/V_0 > 12\%$). Case 1.5DL does not show the results of PMG-185, PMG+185 due to lack of centrifuge channels and less effect from tunnel in these areas.

The test series C (**Fig. 4.4**) has the same weight of the superstructure of the test series B-2. The only different is the cover depth ratio was reduced to 1.5. The pile tip level of short pile was changed to the existing tunnel line, and the pile tip level of long pile was also moved to under the tunnel line. A comparison between case without pile group (Case0-S) and test series C indicates that pile group existence induces additional vertical settlements in the area near the pile group

(PMG-35 and PMG+35). In addition, vertical settlement at the tunnel center (PMG00) shows similar settlement regardless of pile group positions, except for the case of $X_p/R=1.5$ (Case1.5-SL). Three of potentiometers of this case display rapid and significant magnitude of settlement since small ground loss ratio ($\Delta V/V_0 > 4\%$).

Therefore, it can confirm the nonlinear behavior of induced soil surface settlement regardless of pile group positions and the cases with pile groups tend to induce more settlement near the center of settlement trough (PMG-35, PMG00, PMG+35), especially for the case small X_p.

4.2.2 Subsurface settlement

4.2.2.1 Displaced vectors by PIV

GeoPIV which uses Particle Image Velocimetry (PIV) in MatLab program (**White and Take, 2003**) was employed to observe the displacement of model ground. The digital images captured during the reduction of the tunnel diameter were used in GeoPIV program. In the images, the soil layers above a tunnel model were divided by the center of patches in GeoPIV software (**Fig. 4.5 (a)**). The resolution of digital camera used, Canon Power-Shot G7, was 180 pixels per 1 inch. Therefore, this range is converted to 0.14 mm/pixels in real object displacement in model scale. The patch size which used in this analysis was 128 pixels or 18 mm. As a result, spacing between displacement vectors are equal to 18 mm on both horizontally and vertically directions. In addition, the search zone length area between sequence images was imposed to 12 pixels. The first subsurface layer was at 12 mm depth from the ground surface, and the deepest layer was at 138 mm depth and 84 mm depth for C/D ratio of 2.5 and 1.5 respectively.

The displaced vector (**Fig. 4.5 (b)**) show a corresponding trend for normal distribution profile where the highest movements are concentrated in the centerline of the tunnel model. The movements decrease when the position is far from the tunnel axis.

4.2.2.2 Vertical settlement by PIV

The settlement troughs (S_v) at different depths of the models with and without pile groups by PIV are compared with surface settlement by PTM for small and large $\Delta V/V_o$ ratios in **Fig. 4.6-4.9**. In the figures, the settlements are normalized by the decrement of tunnel radius (ΔR) and horizontal distance x is normalized by tunnel radius (R). Wedge boundary region have been proposed for largely induced settlement due to tunneling (**Loganathan, 1998**). In the far position of potentiometers, the settlements became smaller magnitude due to outside an area of wedge boundary. The potentiometers within this area will suffer from large vertical settlement.

As the magnitude of ground loss ratio increases, the magnitudes of normalized settlements become reduced for all the depth layers. These reductions of settlement rate are similar to the soil surface settlement by PTM. In surface settlement by PTM (Fig. 4.1-4.4), the rate of settlement is high at small ground loss ratio ($\Delta V/V_0 \leq 4\%$) and the rate is reduced as increase of ground loss ratio. It could be concluded that both surface and subsurface show nonlinear behavior of settlement caused by tunneling.

For case with C/D=1.5, negligible settlement is confirmed at far position of normalized horizontal distance (x/R> 5, x/R< -5) (**Fig. 4.6(b)**, **Fig. 4.9**), while for C/D=2.5, settlement is still observed in those positions as shown in **Fig. 4.6(a)**, **Fig. 4.7**, **Fig. 4.8**. This indicates that the cover and depth ratio has an effect on chimney shape mechanism (**Cording, 1991; Potts, 1976**), where large displacements occur in the area directly above the tunnel. The chimney-like mechanism is more remarkable for the cases with C/D=1.5 than the cases with C/D=2.5.

Deep layers show narrower trough than the shallower layers near the surface level. The results also support that trough width has been found to vary with the depth of interest (**O'Reilly and New, 1982; Hergarden et al., 1996; Mair and Taylor, 1997**). The shapes of the trough were well symmetrical. However, the model grounds with the pile groups tend to increase the width of the trough (x_i) (see also **Fig. 2.3.2**). These results will lead to difference of inflection points of the subsurface settlement troughs for the grounds with and without pile groups. The change of inflection point along the depth and effect from the presence of pile groups will be discussed later. The settlements obtained from PTM show good agreement with the soil surface settlement by PIV ($Z/Z_o = 0$). It could be said that the accuracy of PIV can be confirmed by PTM.

4.2.2.3 Lateral movement by PIV

Fig.4.10 shows the lateral soil displacement (S_x) profile with depth at the horizontal locations (x) from1.0R to 4.5R. The lateral displacement toward the tunnel direction is taken as a positive, and it is normalized by the decrement of tunnel radius (ΔR) in the figure. Lateral displacements are very small magnitude when comparing with a vertical direction (S_v) and the effect of the pile groups is also small in the lateral direction. As a result, Case0-S and Case0-D are used as a representative of induce soil lateral movement for the cases with C/D=1.5 and 2.5 respectively.

Both the cases with C/D=1.5 and 2.5 at the small and large volume loss ratio ($\Delta V/V_0$), large lateral displacement took place near the soil surface, and it decreased with depth. However, the large lateral movements also occurred slightly above the tunnel, which was more distinct at the large volume loss ratio, especially for the case with larger C/D at X_p less than 2.0R. This characteristic of various peak of lateral movement will be applied in the zone of influence in the letter of this section.

4.3 The accuracy of potentiometers and PIV technique

In order to prove the accuracy of PIV measurements, the measured data by PIV were compared with those by potentiometers for the tunnel models without the pile groups (Cases0-D and0-S), in which purely two-dimensional deformation could be assumed.

Ground surface settlements measured by PIV at the same locations of the potentiometers (**Fig. 3.41**) and those measured by potentiometers are plotted against ground loss ratio $\Delta V/V_0$ in **Fig. 4.11**. In the legend of the figure, the digits after PMG and PIV indicate the horizontal coordinate of the measurement points, that is, the distance from the tunnel center line in prototype scale (meter). For small to medium ground loss ratio ($\Delta V/V_0$ < 6-10%), the graphs show symmetrical settlement for each left and right sides of the tunnel. However, they show slightly uneven settlements at large ground loss ratio.

Magnitude of settlements obtain by potentiometers were slightly larger than PIV results especially for the large ground loss ratio in Case 0S (C/D=1.5). This might come from the friction between the sand and the window surface of the container. However, the difference is small and almost negligible for the relatively small ground loss ratio, less than 7-10 %. From this fact, it can be said that the quality of PIV results can be considered to an acceptable level. In addition, it is

also inferred that the displacements measured at the front portion by PIV can be considered as the displacements of the central portion of the model without pile group.

4.4 Trough width parameter (K) value

4.4.1 Field measurement method

Research which provided the result of ground movement along the depth with large ground loss ratio is quite deficient. One of previous case study from Sudden Valley Sewer (**Dyer et al., 1996)** is picked up for comparing with the results in this study as shown in **Fig.4.12**. In the project, the ground movement was caused by a combination of tunneling and pipe jacking with induced large ground loss ($\Delta V/V_o > 20\%$) by the pipe jacking part. The soil profile is multilayers of made ground (0-2.5 m), silty clay (2.5-6.5 m) and loose to moderately sand (6.6 – 18.5 m). The excavation of 1.43 m of outer diameter was conducted in the sand elevation. Inclinometers and extensometers were installed along the depth above the tunnel and various horizontal distances from the tunnel. By using Equation 2.2 and the field measurement results, the variation of K values could be plotted and showed the increment of K values along the depth layers as shown in **Fig.4.12**. In addition, the magnitudes of vertical settlement at the tunnel center line were gradually reduced from the tunnel crown to the surface elevation and area of large ground movement could be approximated 3 times of tunnel diameter above and below from the tunnel..

4.4.2 Empirical method

Moh et al., (1996) developed the empirical equation to predict the ground movement caused by tunnel in soft ground layer because the existing equation by **O'Reilly and New (1982)**, and **Clough and Schmidt (1981)** show underestimate the trough width along the ground depths. The proposed equation was derived from the data observed at construction of Taipei Rapid Transit Systems (TRTS) using a 6m diameter earth pressure balancing shield machine with tunnel cover depth of about 15m in sandy soil. The ground loss caused by excavation was small in the project ($\Delta V/V_o \leq 4\%$). By regression analysis and the field measurement data, equation (2.5) was derived. The distributions of K values along the depth by equation 2.5 (m=0.4 for the sand layer) are plotted in **Fig. 4.12.** The K value also shows increased magnitude along the depths.

Mair et al., (1996) collected the field measurement and centrifuge data of clay material to find the relation of K values along the depth. The existing relation shows that the K values do not constant along the depth, but the values are increased along the depth layer. From the results of subsurface settlement, the proposed equation 2.4 shows consistent with the field measurement

and centrifuge results by **Attewell and Farmer (1974), Barratt and Tyler (1976), Glossop (1978) and Mair (1979)**. The distributions of K values along the depth by equation 2.4 are also plotted in **Fig. 4.12**.

4.4.3 Comparison of trough width parameter (K)

As mention above, many previous researchers proposed equation for predict trough width parameter K as a function of relative depth (Z/Z_0). In this study the parameters were obtained from average horizontal distance between the inflection points (xi) of the trough curve, which were estimated at S(x)=0.606Smax (see also **Fig. 2.5**) at the right and left sides. In **Fig. 4.12**, K values obtained from PIV results are plotted against normalized depth Z/Z_0 for small and large ground loss ratio. In the figure, the normalized relations reported by **Mair et al., (1996); Dyer et al., (1996); Moh et al., (1996)** are also given.

As shown in **Fig. 4.12**, for both tunnel models with C/D = 1.5 and 2.5 displayed similar trend, that is, K values increasing with the depth. Result of Case0-D and Case0-S (C/D= 2.5 and 1.5, without pile groups) for small ground loss ratio ($\Delta V/V_0 < 2.5\%$) showed good agreement with that estimated data from **Moh et.al., (1996)** which was obtained from sandy ground layers for relatively small $\Delta V/V_0$. In addition, in the cases with pile groups (Case2.0-DH, Case3.0-DH, Case2.0-DL and Case3.0-DL for C/D=2.5 and Case1.5-SL and Case3.0-SL for C/D=1.5), K values tended to increase as the pile groups position get close to the tunnel.

Nevertheless, K values shifted to a small magnitude when the ground loss ratio increased ($\Delta V/V_0$ =14.0-14.5%) as shown in **Fig. 4.12(b)** and **Fig. 4.12(d).** The reduction of K values showed that the trends got close to the field measurement of large ground loss ratio measured by **Dyer et al., (1996)**. These results can be summarized that in lathe shape of normalized trough settlements at largeground loss value (**Fig. 4.6-4.9**) becomes steeper at the central portion than the cases with small ground loss value. **Hergarden et al., (1996), Jacobsz (2002), Vorster (2005) and Marshall et al., (2012)** also concluded that trough width reduced with the magnitude of ground loss ratio.

4.5 Effect of pile group positions for pile group settlement and soil surface settlements

4.5.1 Comparison of the soil surface settlement with and without pile group

To investigate the effect of pile groups on the ground movement, soil surface settlements of the case with and without pile groups are compared at the same locations of potentiometers (P4, P5, and P6 in **Fig. 3.4**) as illustrated in **Fig. 4.13-4.15**. The plot without line of PMG is for soil settlement of the cases with pile groups and the plot with a line of PMG is for soil settlement of the cases without pile group. Horizontal movements of the pile cap (δx) are also shown in the figure. The settlement increased with increasing the ground loss ratio but showed nonlinearity with the ground loss ratio. In small ground loss ratio ($\Delta V/V_o \leq 4\%$), the settlement rates to $\Delta V/V_0$ was higher than those in relatively large ground loss ratio. Such behavior was observed in the models without the pile groups (**Fig. 4.1-4.4**). Furthermore, the settlements above the tunnel were relatively larger for the cases with C/D=2.5 than those with C/D=1.5. This difference was more significant for the smaller ground loss ratios, which was also seen in **Fig. 4.6-4.9**.

Compared with the ground surface settlements, the horizontal movements of pile caps are more significantly affected by the test conditions. For the models with pile groups closer to the tunnel (X_p/R=1.5: Case1.5-DL and Case1.5-SL; X_p/R=2.0: Case2.0-DH, Case2.0-DL and Case2.0-SL) the horizontal movements of pile caps are much greater than those for the cases with X_p/R=3.0 (Case 3.0-DH, Case3.0-DL and Case3.0-SL).

For the long piles group with X_p/R =2.0 and Z_{pe}/R =0.28, case with large vertical load (Case2.0-DH) showed large magnitude of horizontal movements when it was compared with Case2.0-DL. However, the effect of vertical load became small as pile groups were far from the tunnel (X_p/R =3.0 and Z_{pe}/R =0.28). In addition, the vertical load on short pile groups with Z_{pe}/R =-1.72 displayed similar effect of induced horizontal movements as the pile group close to the tunnel (Case2.0-DH and Case2.0-DL). The horizontal movements of pile caps with pile tip depth below the tunnel center (Z_{pe}/R=2.28, namely the long piles in Case1.5-SL, Case2.0-SL, Case2.5-SL and Case3.0-SL) were significant reduced. The reduction of pile caps movements may come from the pile groups are outside the zone of influence (**Jacobsz et al., 2004**). Relative positions between zone of influence and pile groups will be introduced in the next chapter.

4.5.2 Difference of ground settlement ratio between case with and without pile group

Ground movements of the model without pile groups can be considered as a reference in the discussion of the effects of piles on the ground movement by tunneling process. The differences in the ground surface settlement between the cases with and without pile groups are compared with the measurements by potentiometers in Figures 4.11-4.13 and by PIV in Figure 4.14-4.16 respectively. In the figures, normalized settlement difference obtained by equation 4.1 was plotted against the ground loss ratio.

$$\frac{S_p - S_{np}}{S_{np,max}} \tag{4.1}$$

where S_p is soil surface settlements of cases with pile groups, S_{np} is soil surface settlements of cases without pile groups, and $S_{np,max}$ is maximum soil surface settlements of cases without pile groups, that is, the settlement at tunnel centerline.

4.5.2.1 Measurement by PTM

As shown in the results of the cases with C/D=2.5 (**Fig. 4.16-4.17**), the PTM measured settlements of cases with pile groups showed small difference from those of case0-D without pile group for relatively small ground loss ratio ($\Delta V/V_0 \leq 4\%$). However, for the large ground loss ratio ($\Delta V/V_0 > 4\%$), Cases with $X_p/R < 2.5$ induced larger vertical settlements than Cases with $X_p/R=3.0$ (Case =3.0-DH and Case3.0-DL) in comparison with Case0-D. The reason might come from the presence of pile groups which induced more settlement in surrounding soil.

In addition, presence of pile groups has more effect on induced ground settlements for the cases with C/D=1.5 (**Fig. 4.18**). Cases with $X_p/R < 2.5$ displayed larger settlements in the central part than the case without pile groups (Case0-S), especially at large ground loss ratio ($\Delta V/V_0 >$ 4% (**Fig. 4.18(a)**, **Fig. 4.18(b)**). Ground settlements on both sides (PMG-35, PMG+35), especially at side of short pile group (PMG-35) showed large magnitude of normalized settlement difference. The influence of pile groups on the surface settlements became less when the pile groups were located far from the tunnel (Case3.0-SL) in **Fig. 4.18(d)**.

4.5.2.2 Measurement by PIV

The trends of the settlement difference between the case with and without the pile group observed by PIV shown in **Fig. 4.19–Fig. 4.21** are similar to those by potentiometers (**Fig. 4.16-Fig. 4.18**). However, the magnitudes of the difference by PIV are smaller than those by potentiometers. A reason may come from the difference of position of measurement between two methods. Pile groups were installed at the center line of container along with a row of potentiometers. On the other hand, the PIV technique measured the ground movements at the container front, which had a distance 5 times pile diameter from the closest piles in the tunnel longitudinal direction as shown in **Fig. 4.22**. From the settlement observations at different relative locations to the pile group, it can be said that the effect of existing pile groups was gradually reduced from a position of pile group. However, there was a certain effect of the pile groups on the ground movement at the location more than five times pile diameter, even for the simple pile groups with four piles.

4.6 Conclusion

In this chapter, the fundamental behavior of ground movement and the alteration caused by presence of pile groups are presented. The shape of the settlement trough and the variation of trough width are also reported. The following conclusions were drawn from the study in the ground movement caused by tunneling with and without pile group.

- From PIV result, it was confirmed that the settlement profiles could be represented by Gaussian distribution curve from small (2%) to large (15%) ground loss ratio ($\Delta V/V_o$). In terms of distance of two deflection points of the curve as a representative value of the settlement trough width, the model grounds with the pile groups tend to increase the width as the pile group position becomes closer to the tunnel. For the large ground loss ratio, the shape of normalized trough settlements becomes steeper at the central portion than the cases with small ground loss ratio

- For cases without pile groups, surface settlements measured by PIV at the front of the model shows good agreement with those measured by the potentiometers at the central cross section line of the model, which verifies the applicability of PIV for measuring the subsurface displacements. For large ground loss ratio, there are some differences in the observed settlements between those two methods due to the effect of the side wall friction.

However, the magnitudes of difference are small (less than 10% of the total settlement).

- Displacements of the pile cap and the soil surface settlements showed nonlinearity to the ground loss ratio, the higher settlement rate for the small ground loss ratio (less than 4%). This behavior was also observed in the model without the pile groups.

- The observed depth variations of settlement trough width parameters (x_i) show good agreement with an empirical relation derived from sandy soils at small ground loss ratio. The xi values decrease with increasing ground loss ratio, implying the validity of tunneling method used in this study.

- Widths of the settlement trough (X_i values) decrease almost linearly with depth.

- The pile group induces large settlement above the tunnel. This trend shows large significant for the cases with small C/D (=1.5) and the cases with large ground loss ratio ($\Delta V/V_o$).

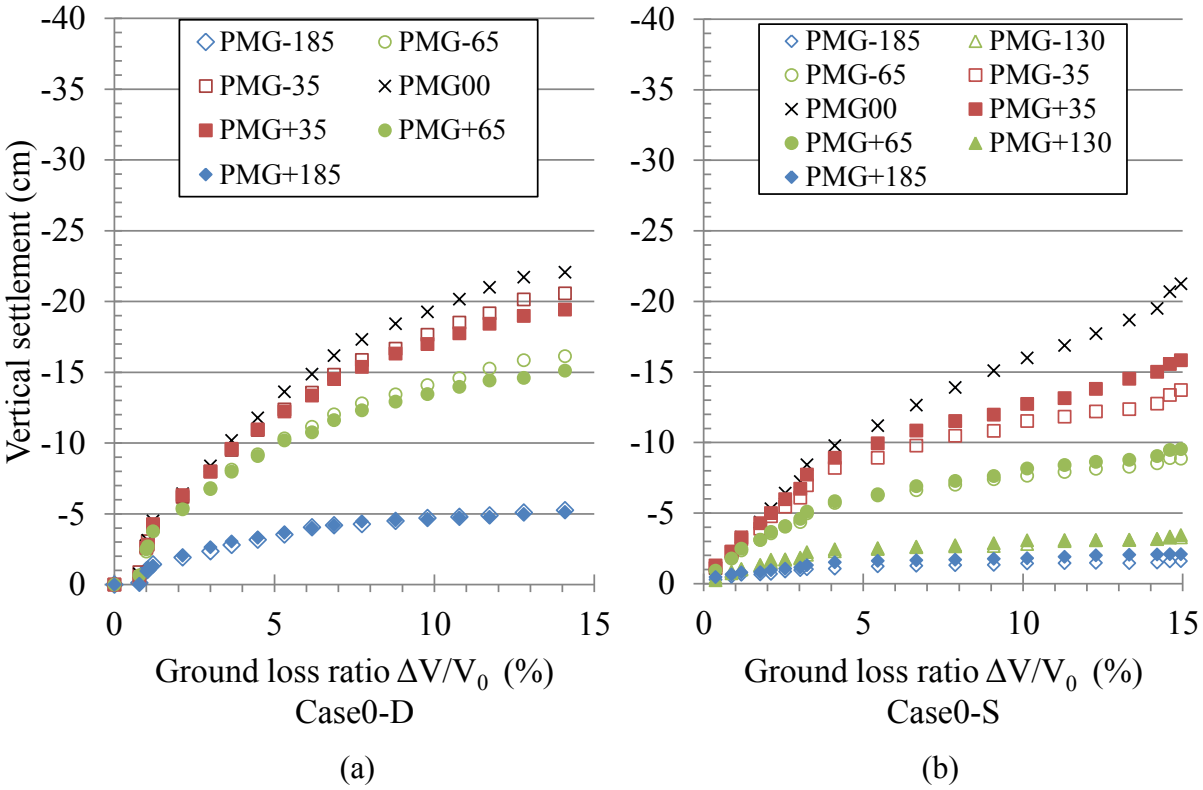

Figure 4.1 Soil surface settlements by PTM for case A series (without pile group):

(a) Case0-D; (b) Case0-S

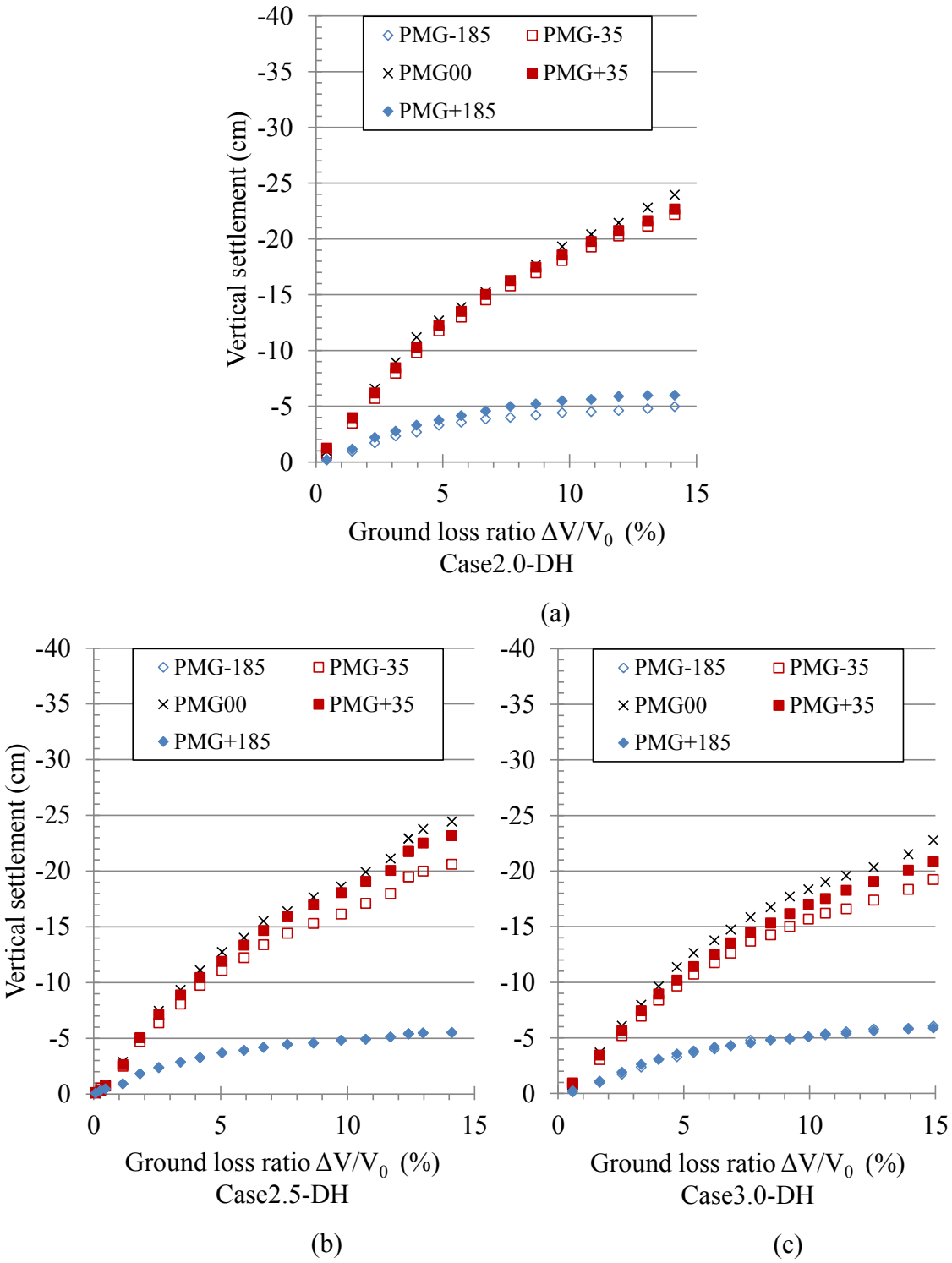

Figure 4.2 Soil surface settlements by PTM for case B-1 series (C/D=2.5, heavy loads): (a) Case2.0-DH; (b) Case2.5-DH; (c) Case 3.0-DH

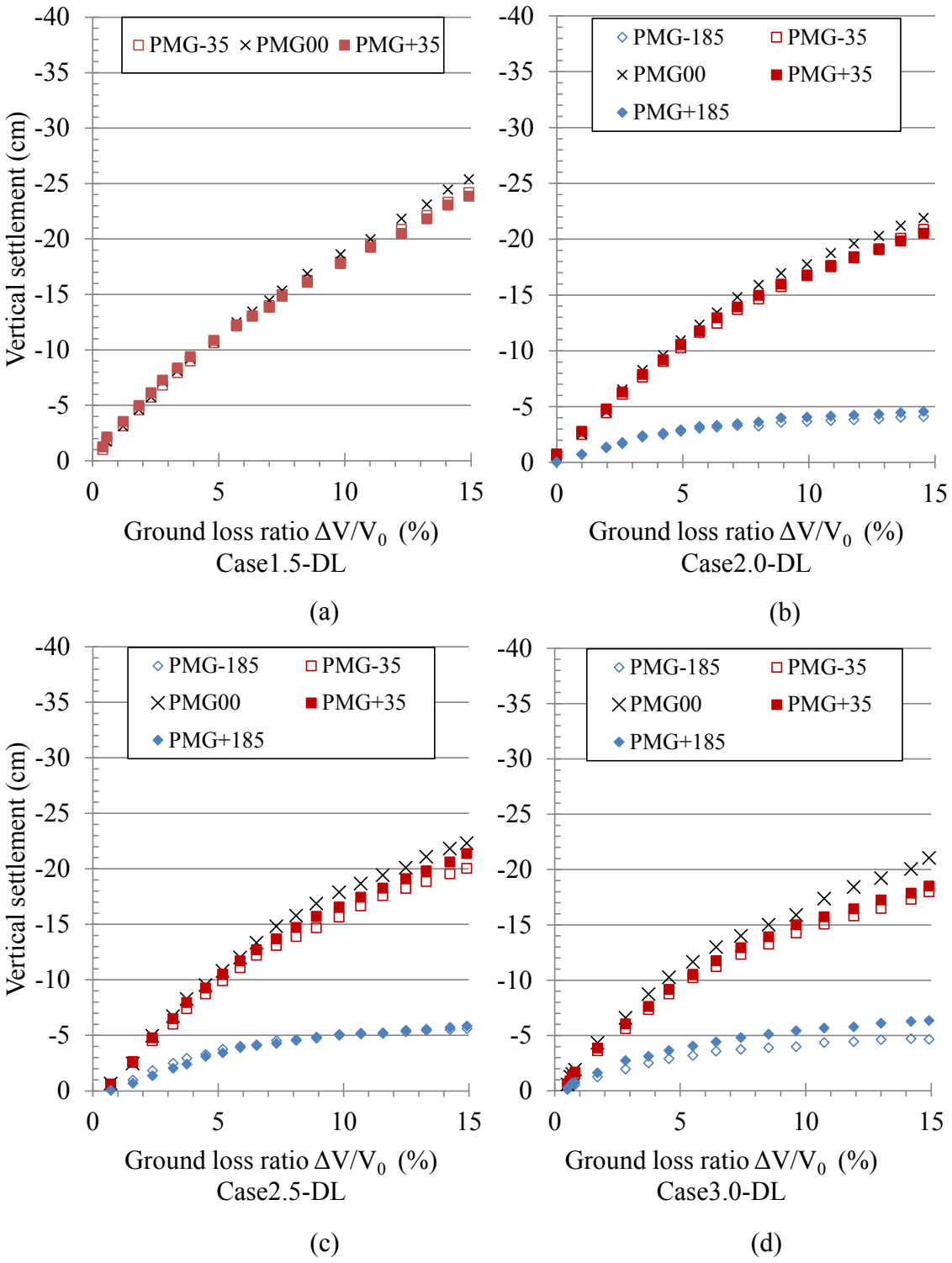

Figure 4.3 Soil surface settlements by PTM for case B-2 series (C/D=2.5, light loads): (a) Case1.5-DL; (b) Case2.0-DL; (c) Case 2.5-DL; (d) Case3.0-DL

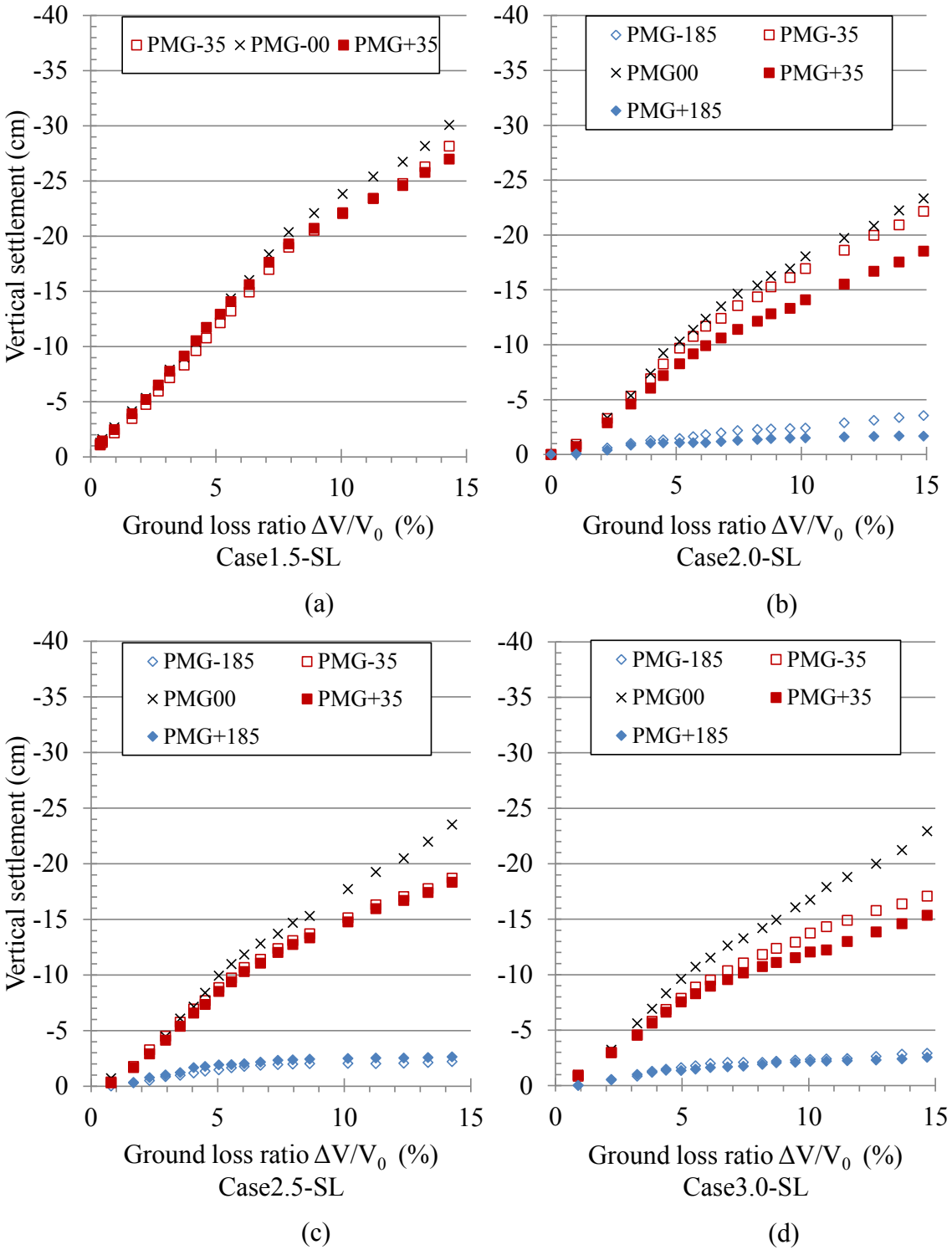

Figure 4.4 Soil surface settlements by PTM for case C series (C/D=1.5, light loads): (a) Case1.5-SL; (b) Case2.0-SL; (c) Case 2.5-SL; (d) Case3.0-SL

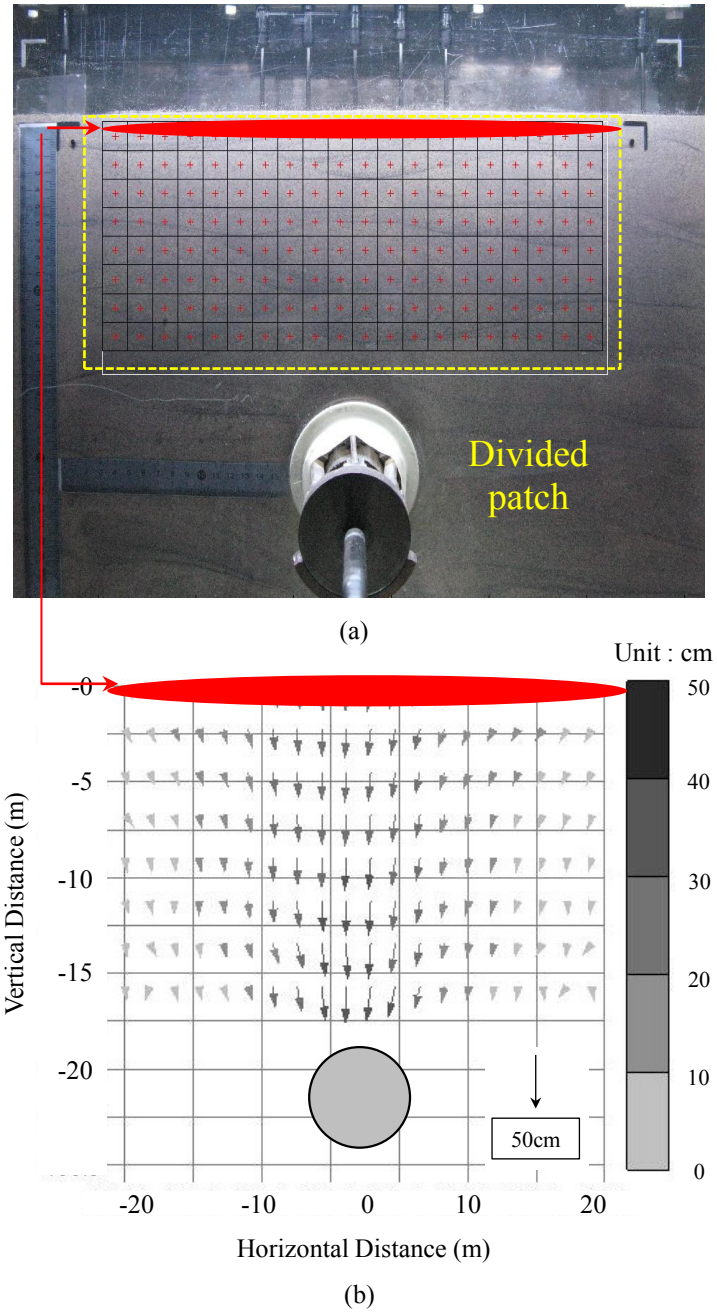

Figure 4.5 Particle Image Velocimetry technique: (a) divided patches for tracing the displaced vectors; (b) displacement vectors along the depth layers.

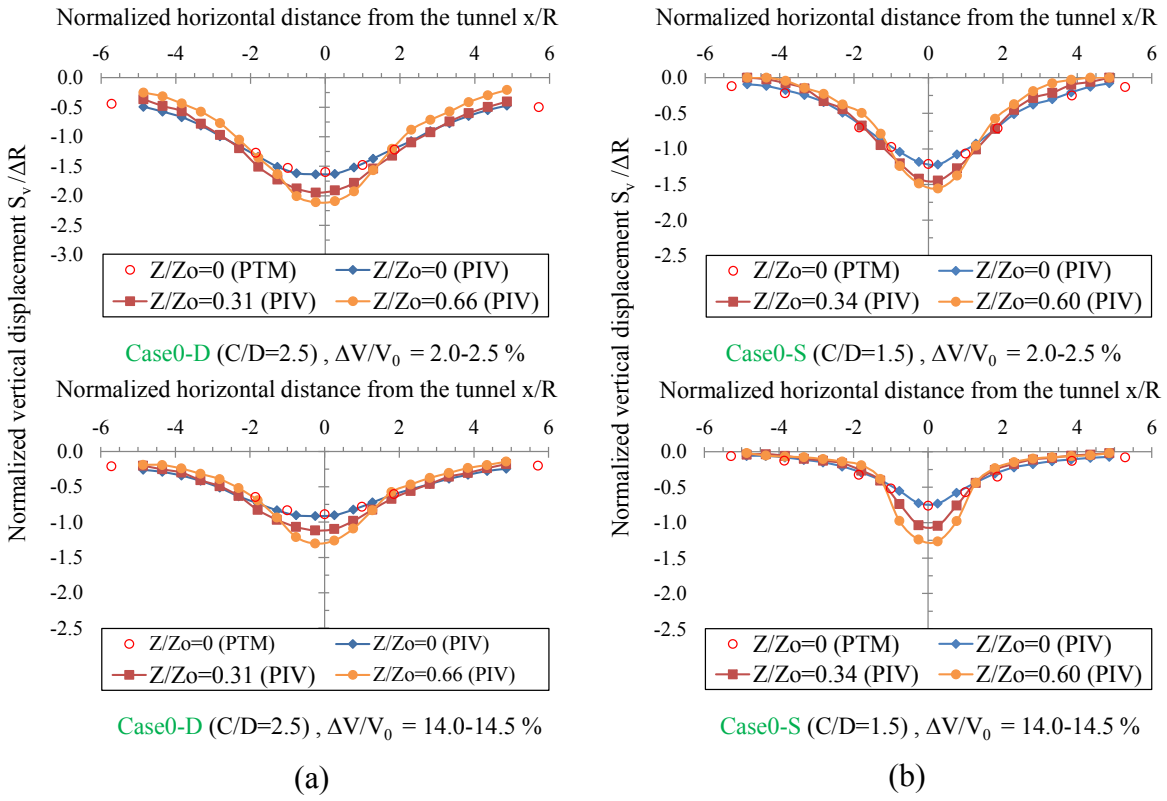

Figure 4.6 Normalized vertical settlements against horizontal distance: (a) Case0-D; (b) Case0-S

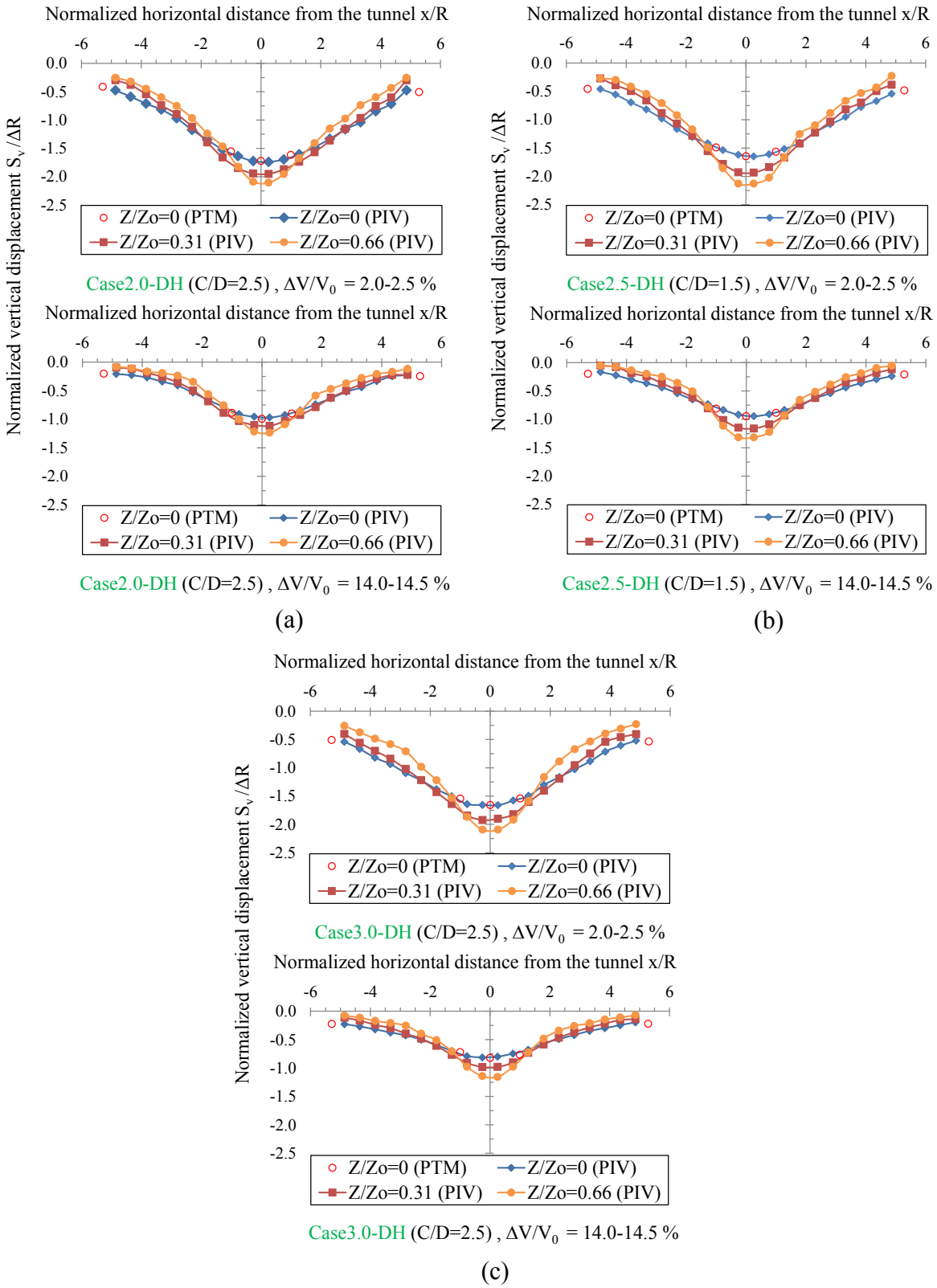

Figure 4.7 Normalized vertical settlements against horizontal distance:

(a) Case2.0-DH; (b) Case2.5-DH; (c) Case3.0-DH

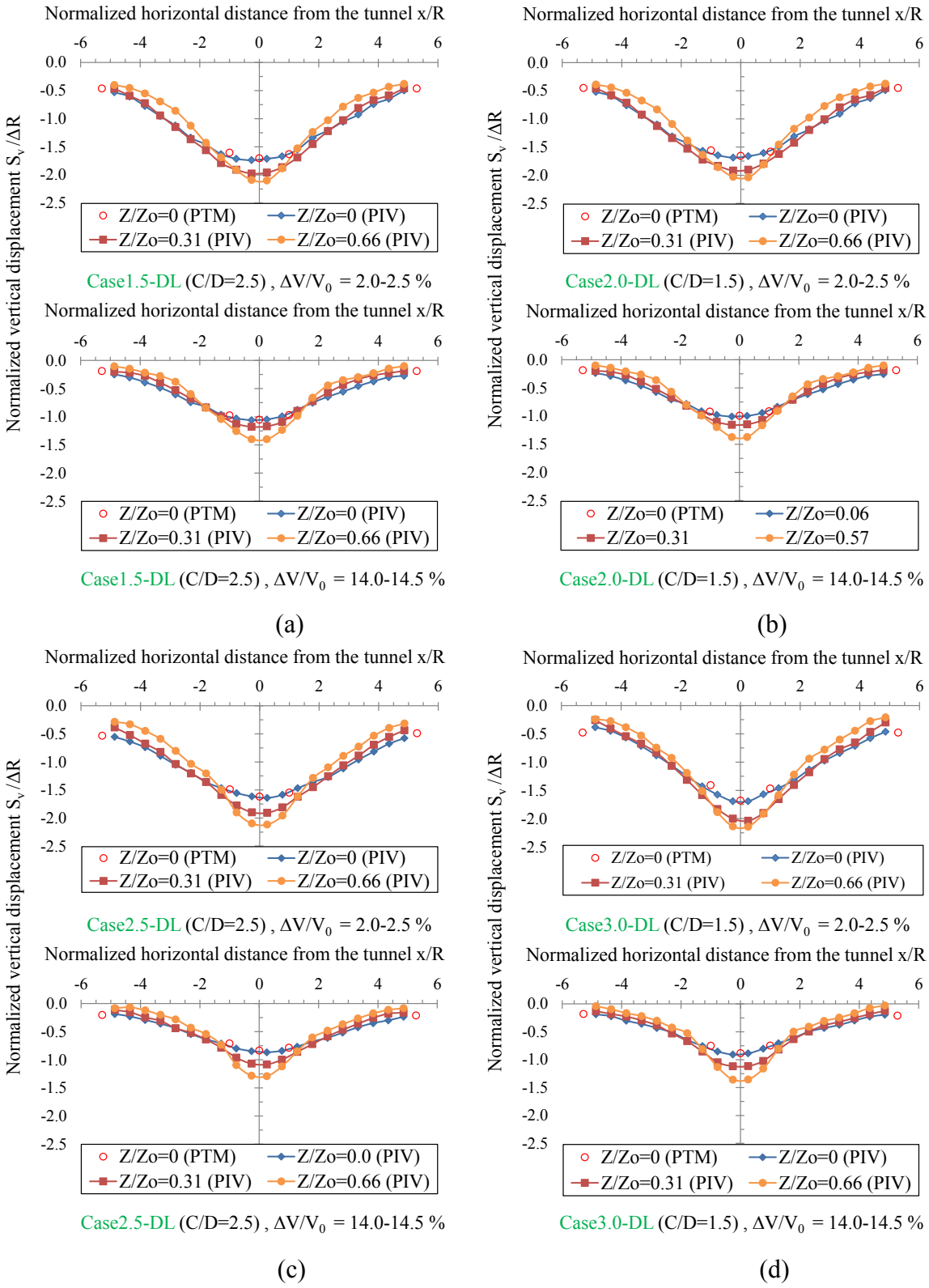

Figure 4.8 Normalized vertical settlements against horizontal distance:

(a) Case1.5-DL; (b) Case2.0-DL; (c) Case2.5-DL; (d) Case3.0-DL

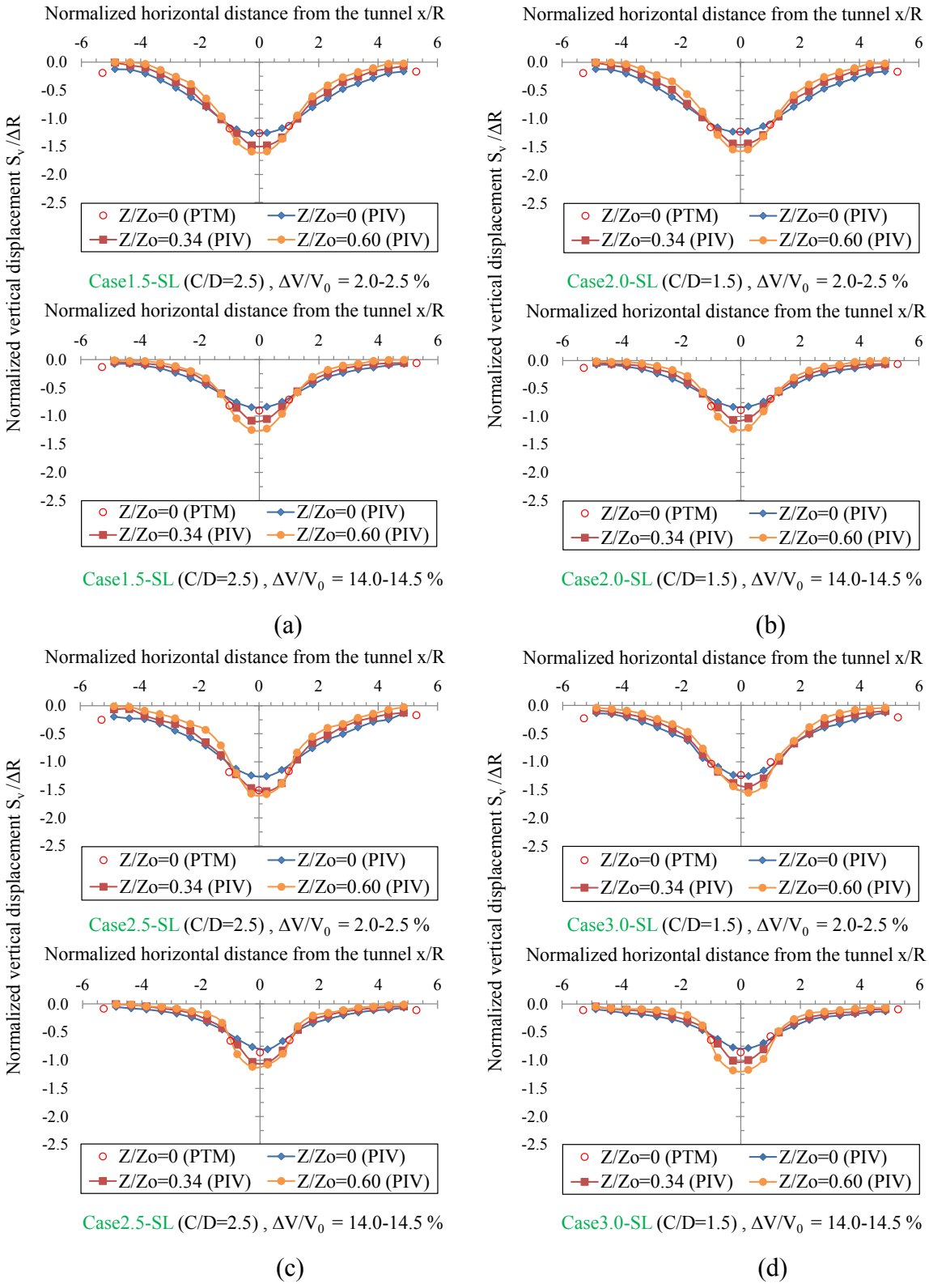

Figure 4.9 Normalized vertical settlements against horizontal distance:
(a) Case1.5-SL; (b) Case2.0-SL; (c) Case2.5-SL; (d) Case3.0-SL

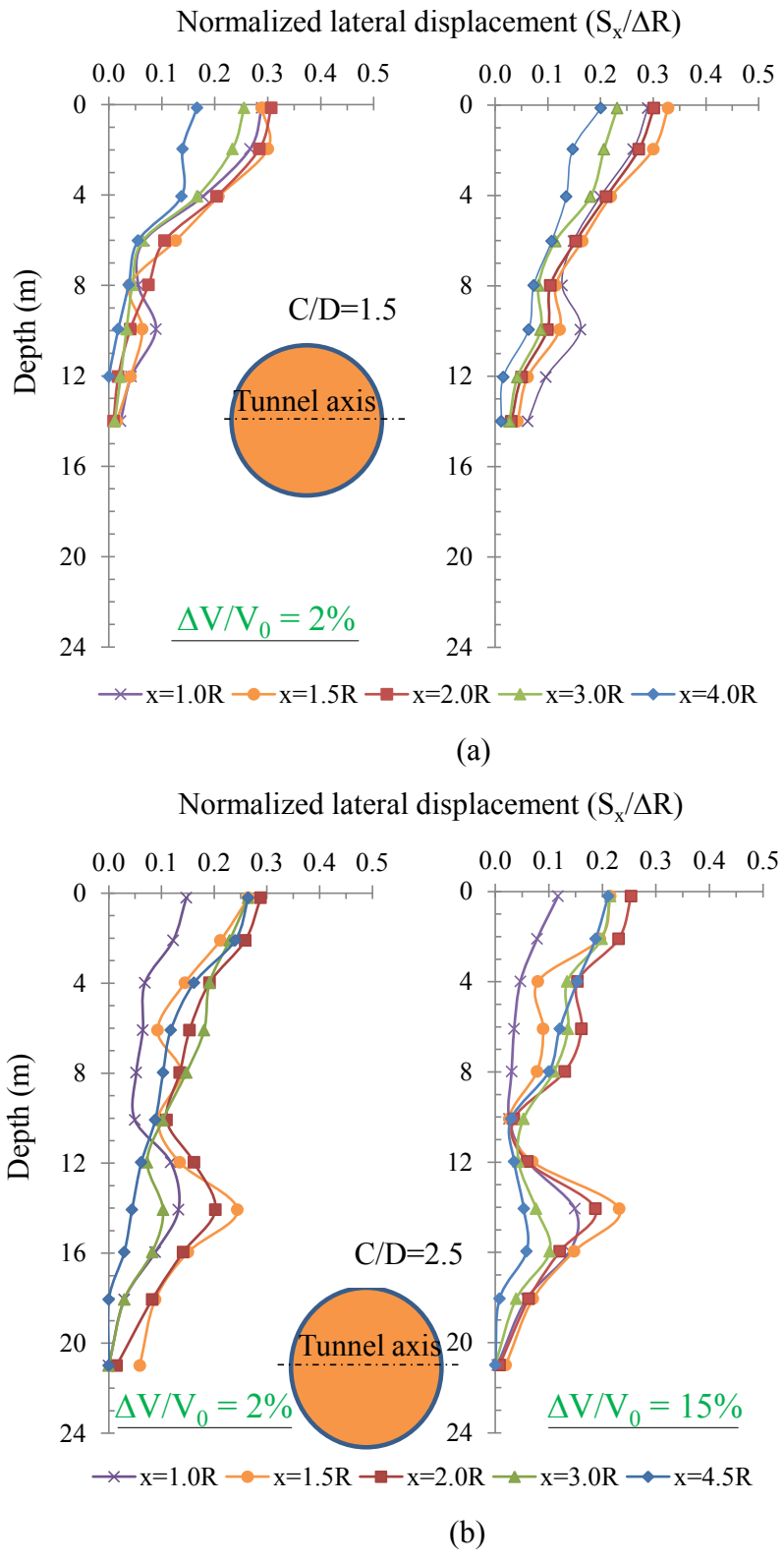

Figure 4.10 Lateral soil displacement profiles along the vertical lines of x=1.0R to 4.5R at the ground loss ratio of 2% and 15%: (a) Case0-S; (b) Case0-D

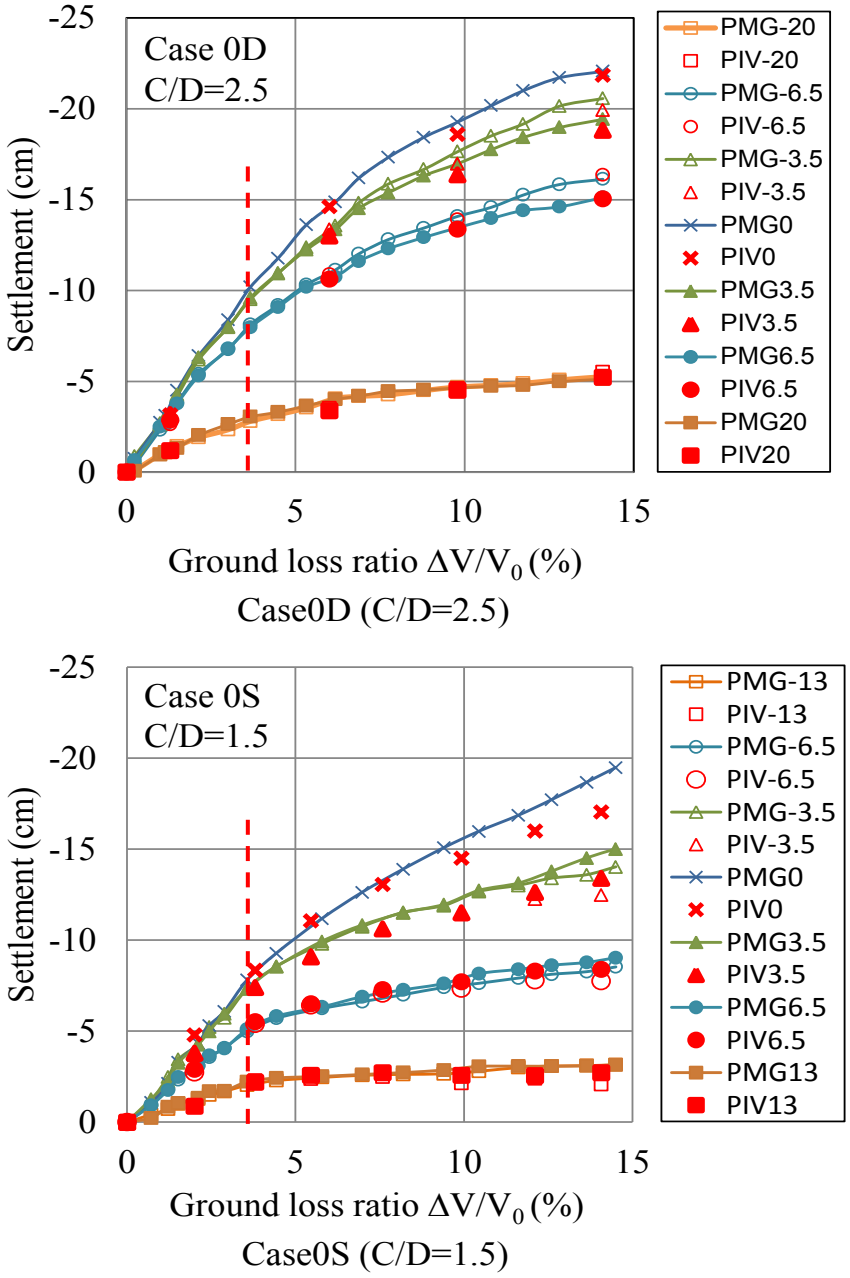

Figure 4.11 Comparisons of surface settlements measured by PTM and PIV of Case0-D and Case0-S

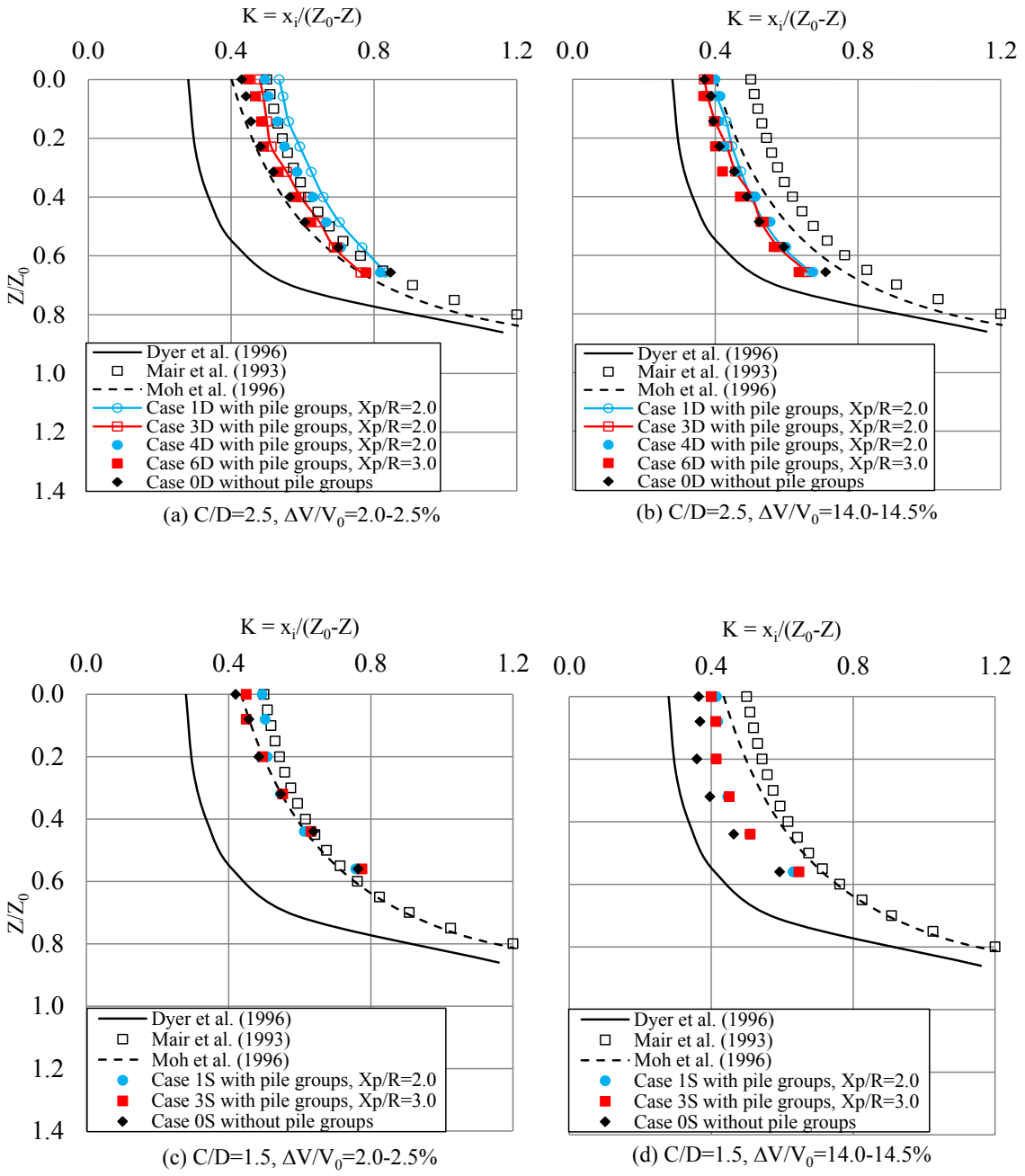

Figure 4.12 Variation of K with depth for subsurface settlement profiles

$$K = \frac{0.175+0.325\,(1-\frac{Z}{Z_o})}{1-\frac{Z}{Z_o}} \quad \text{(Mair (1993))} \qquad K = \frac{(\frac{D}{2})(\frac{Z_o}{D})^{0.8}(\frac{Z_o-Z}{Z_o})^{0.4}}{(Z-Z_o)} \quad \text{(MOH (1996))}$$

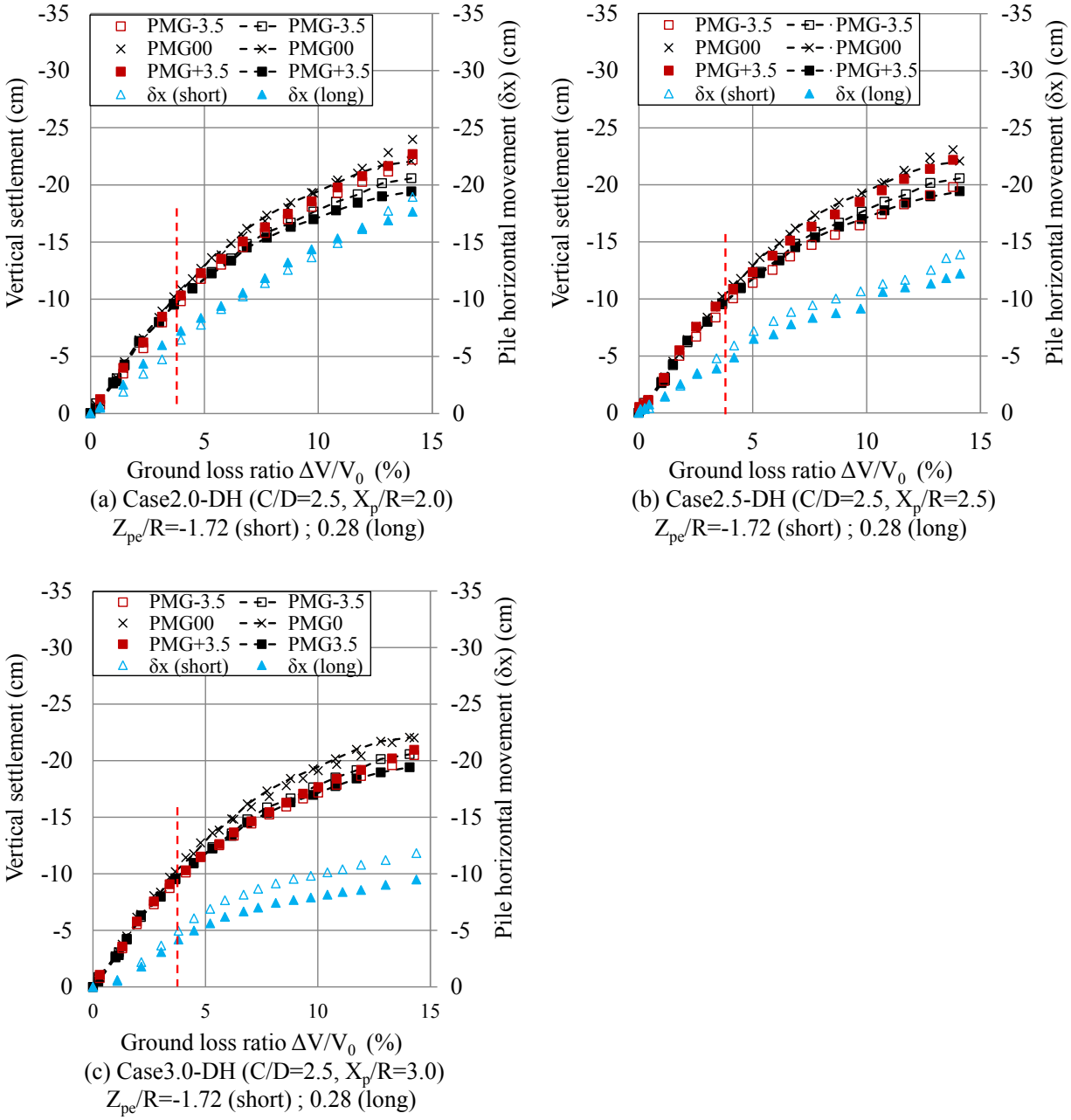

Figure 4.13 Horizontal movement of pile cap by LVDT and soil surface settlement by PTM against ground loss ratio: (a) Case2.0-DH; (b) Case2.5-DH; (c) Case3.0-DH

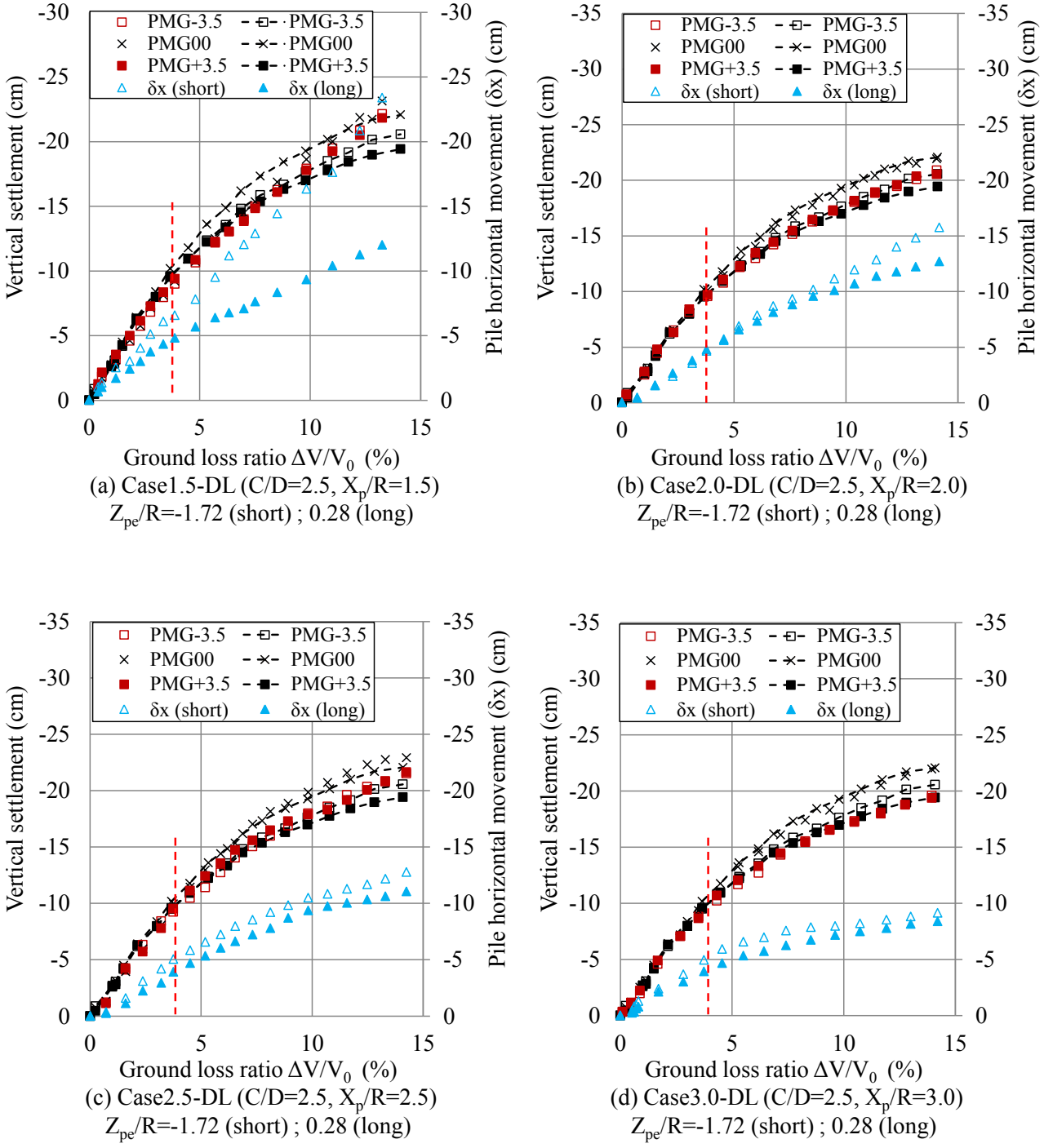

Figure 4.14 Horizontal movement of pile cap by LVDT and soil surface settlement by PTM against ground loss ratio: (a) Case1.5-DL; (b) Case2.0-DL; (c) Case2.5-DL; (d) Case3.0-DL

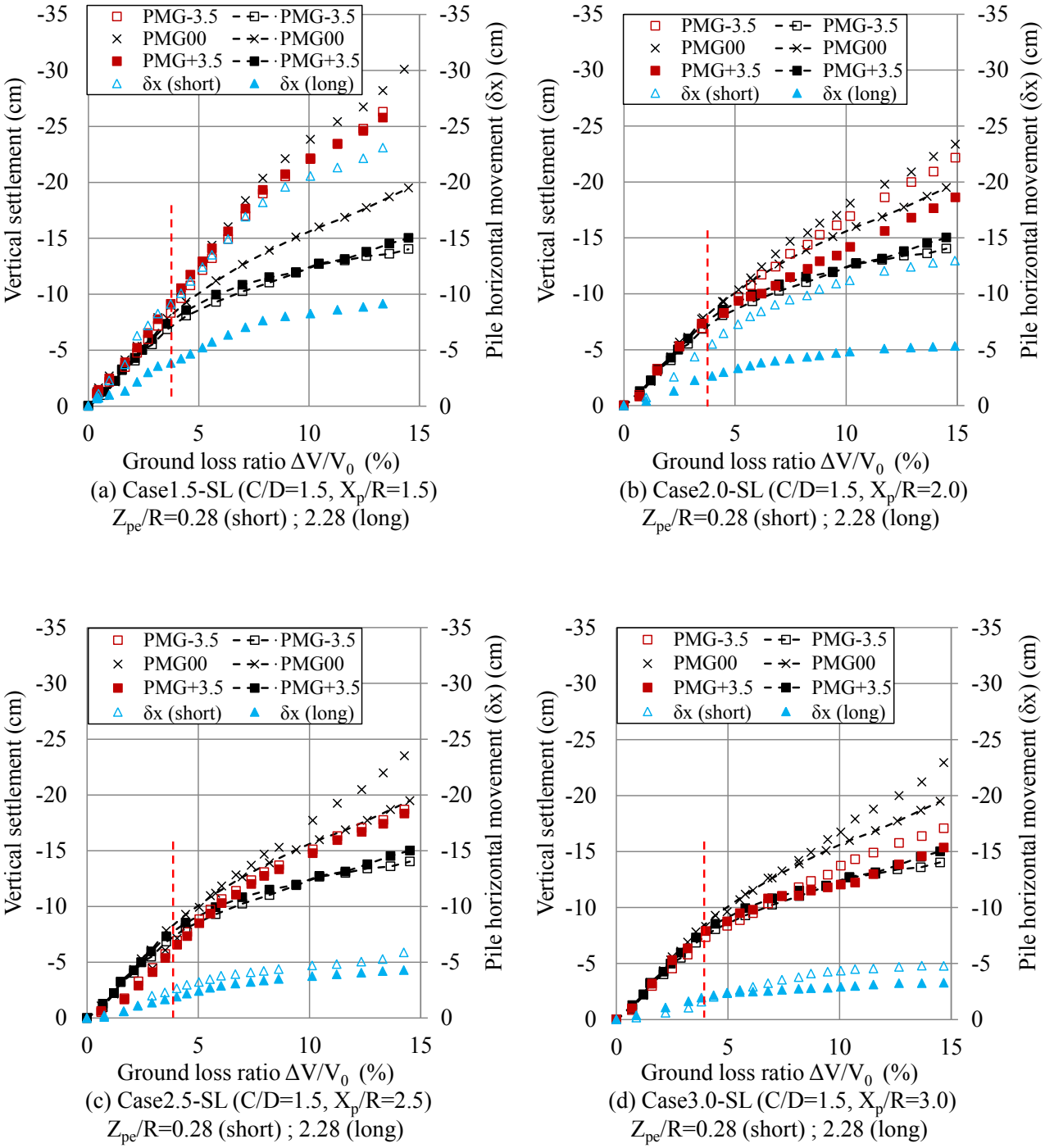

Figure 4.15 Horizontal movement of pile cap by LVDT and soil surface settlement by PTM against ground loss ratio: (a) Case1.5-SL; (b) Case2.0-SL; (c) Case2.5-SL; (d) Case3.0-SL

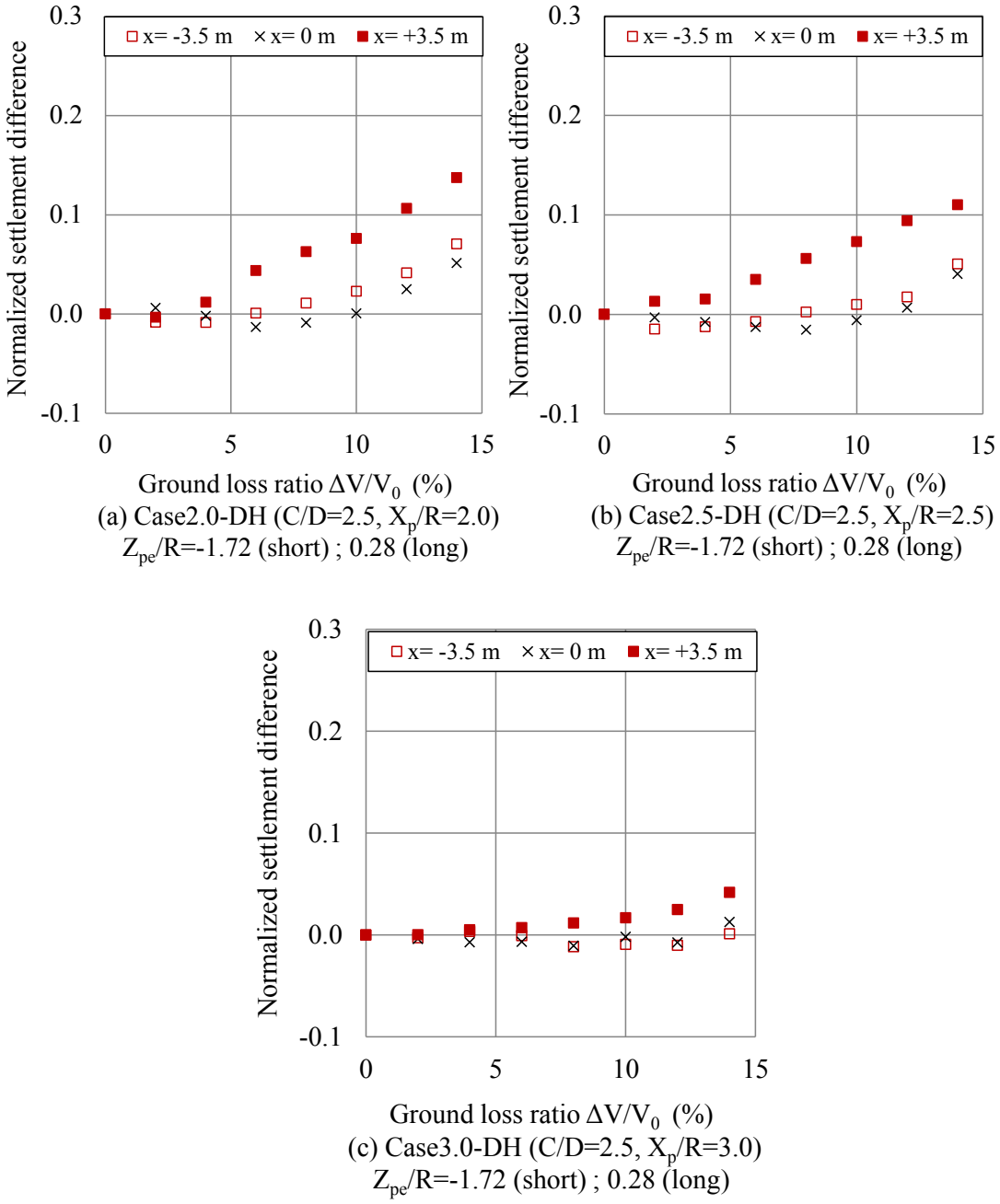

Figure 4.16 Difference between ground surface settlement between the cases with and without pile groups by PTM against ground loss ratio: (a) Case2.0-DH; (b) Case2.5-DH; (c) Case3.0-DH

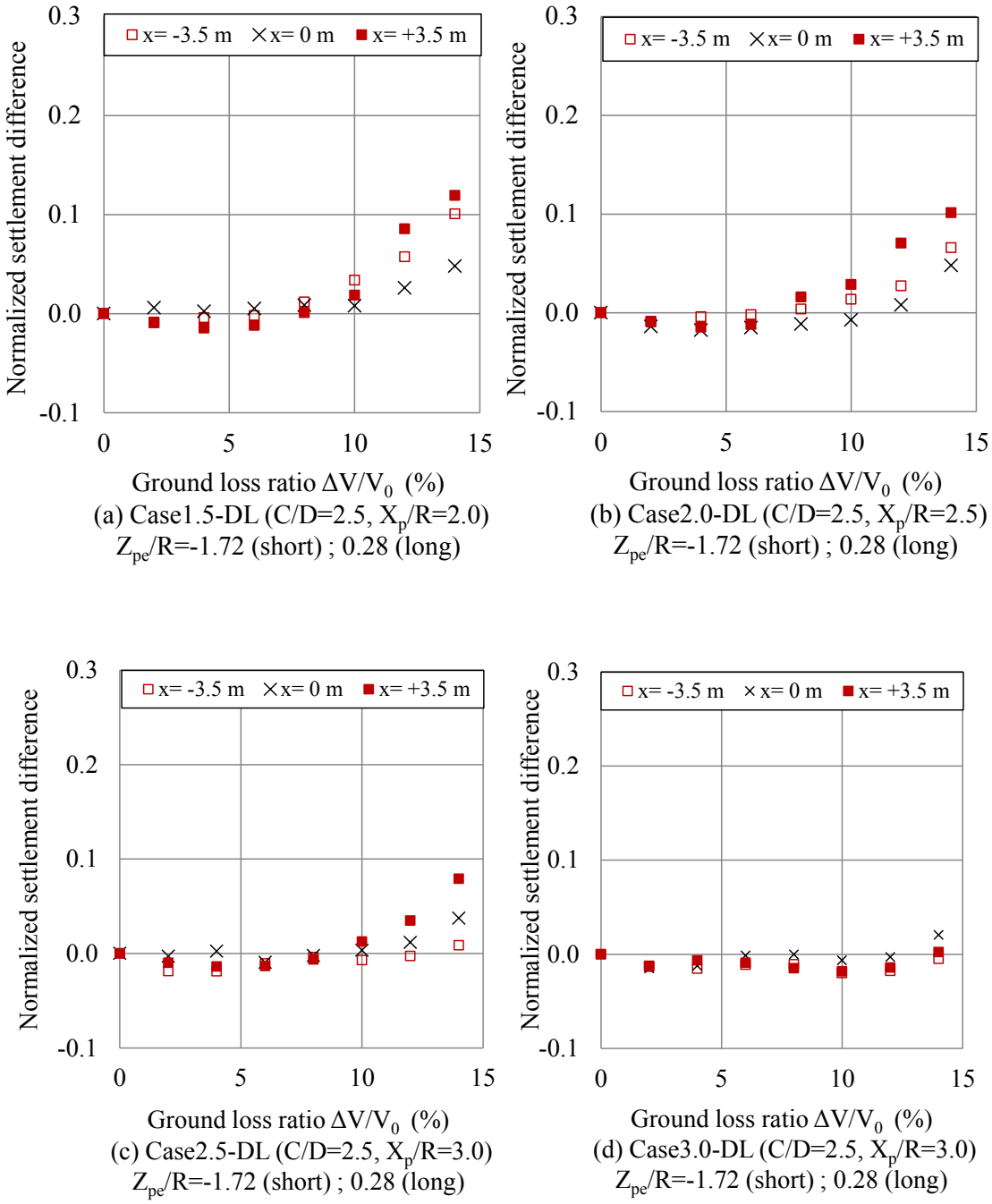

Figure 4.17 Difference between ground surface settlement between the cases with and without pile groups by PTM against ground loss ratio: (a) Case1.5-DL; (b) Case2.0-DL; (c) Case2.5-DL; (d) Case3.0-DL

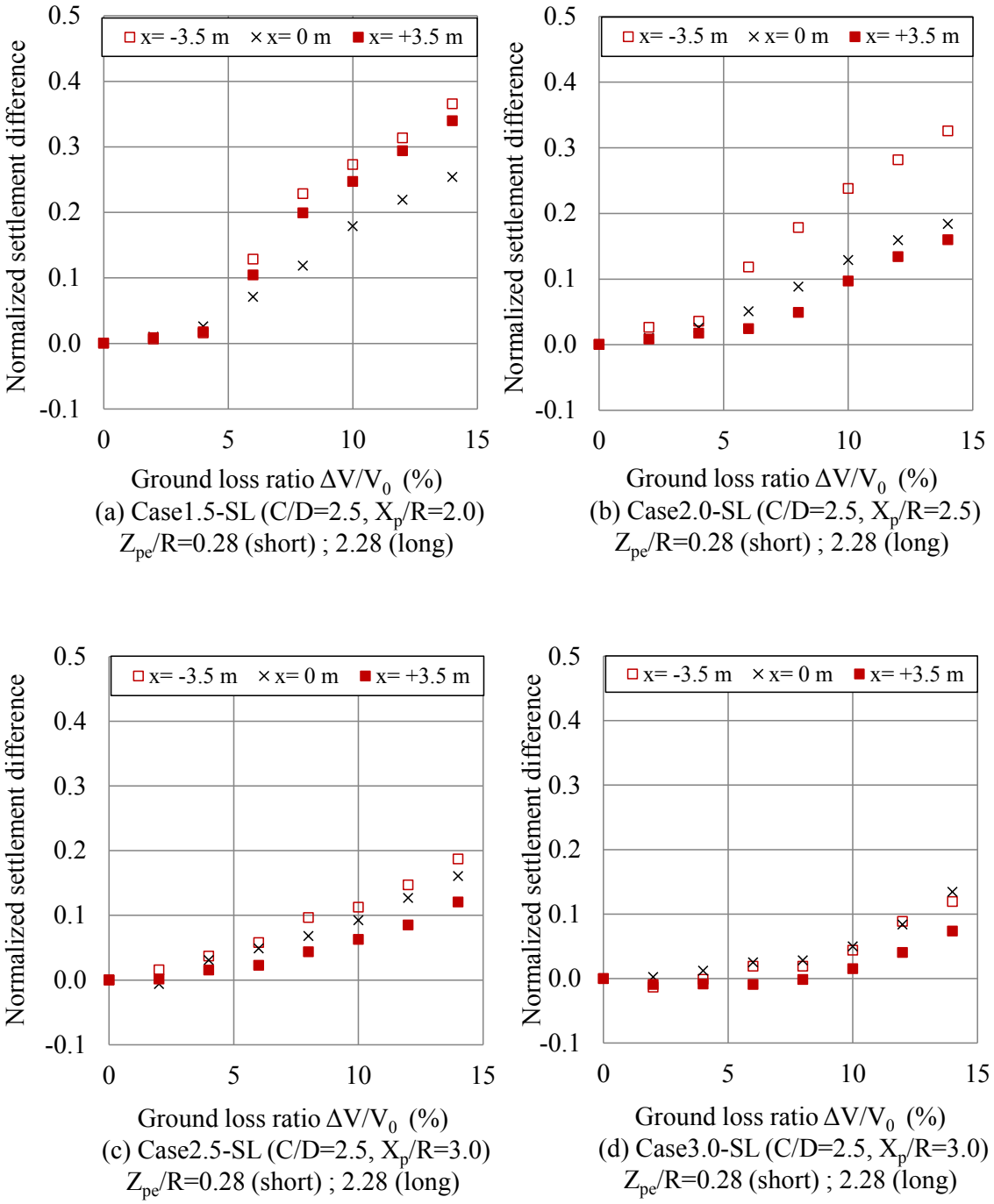

Figure 4.18 Difference between ground surface settlement between the cases with and without pile groups by PTM against ground loss ratio: (a) Case1.5-SL; (b) Case2.0-SL; (c) Case2.5-SL; (d) Case3.0-SL

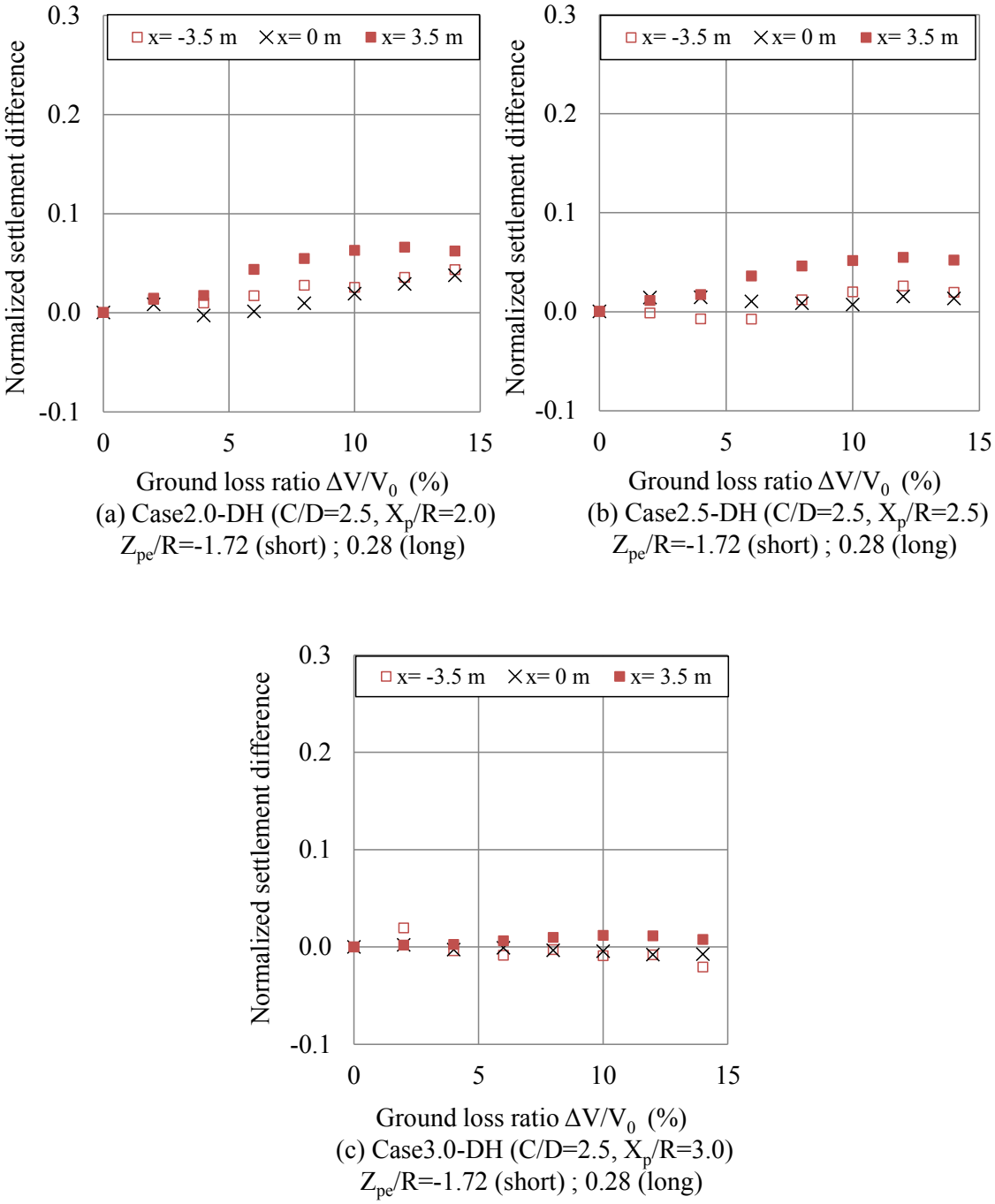

Figure 4.19 Difference between ground surface settlement between the cases with and without pile groups by PIV against ground loss ratio: (a) Case2.0-DH; (b) Case2.5-DH; (c) Case3.0-DH

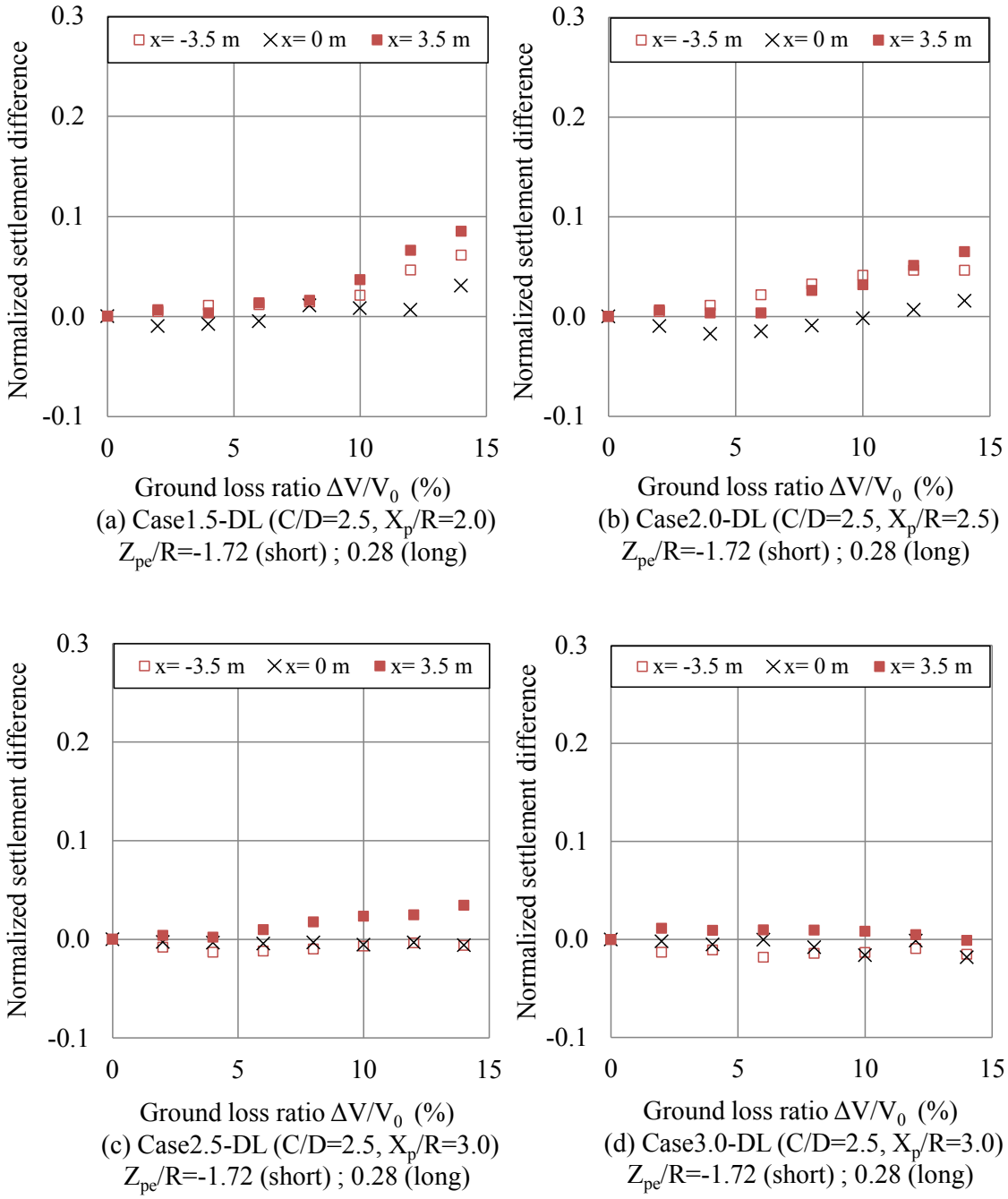

Figure 4.20 Difference between ground surface settlement between the cases with and without pile groups by PIV against ground loss ratio: (a) Case1.5-DL; (b) Case2.0-DL; (c) Case2.5-DL; (d) Case3.0-DL

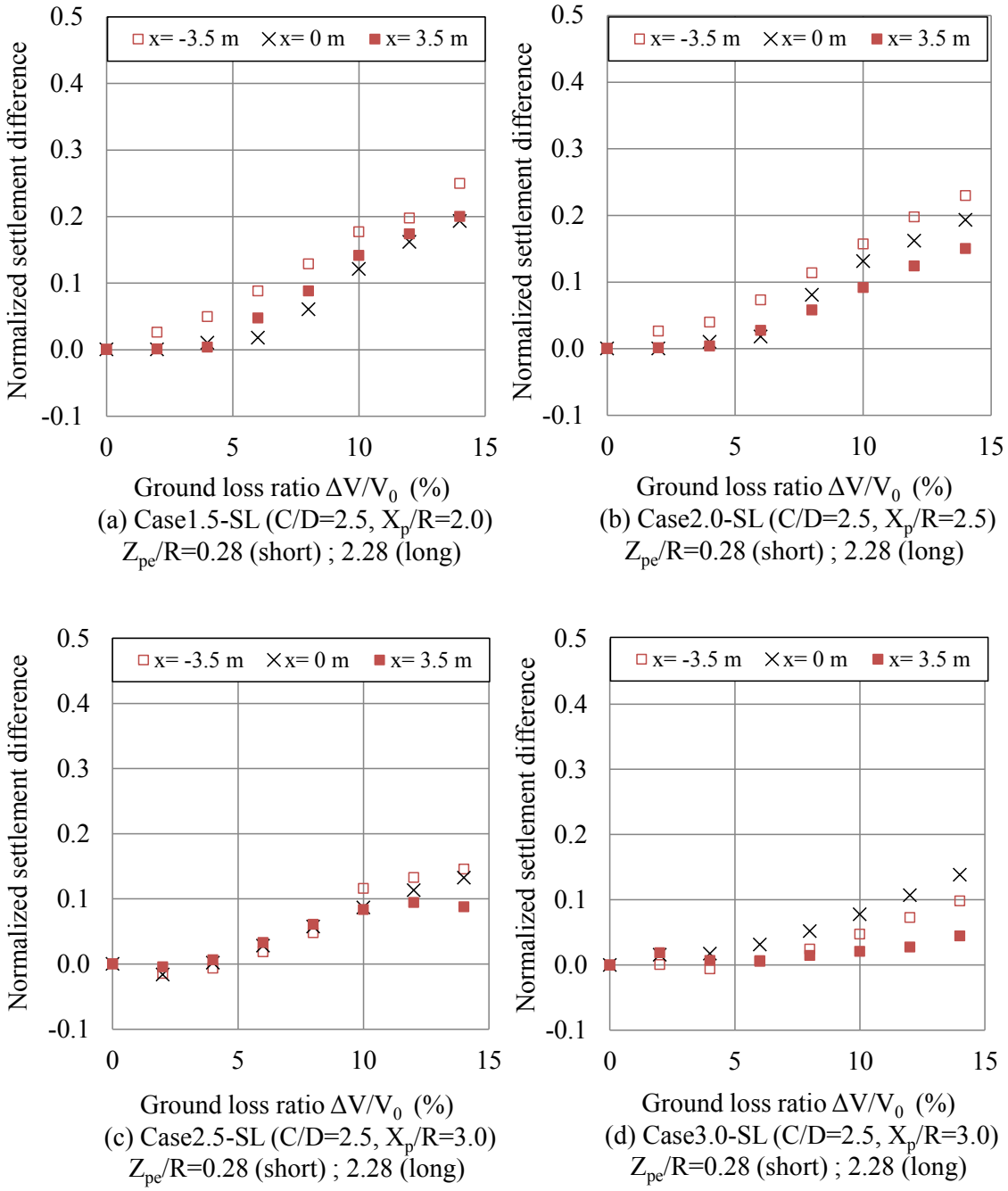

Figure 4.21 Difference between ground surface settlement between the cases with and without pile groups by PIV against ground loss ratio: (a) Case1.5-SL; (b) Case2.0-SL; (c) Case2.5-SL; (d) Case3.0-SL

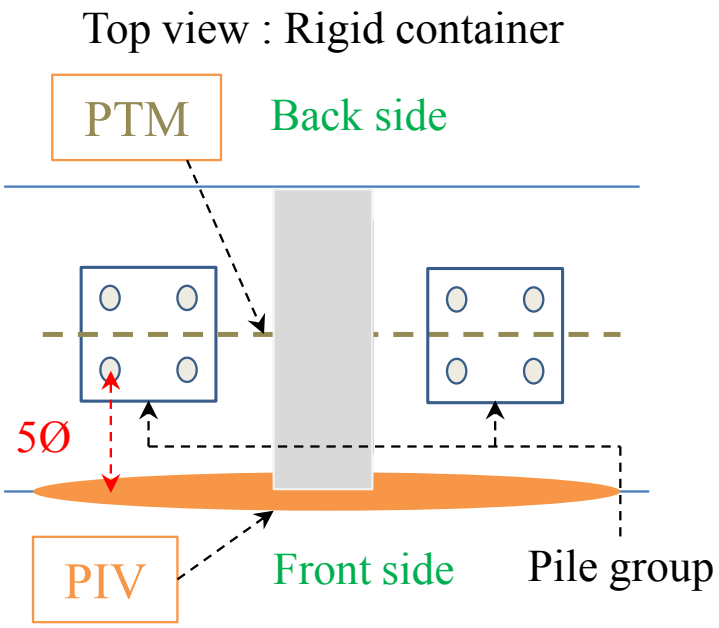

Figure 4.22 Top view of the container to indicate the measurement points of PTM and PIV

Chapter 5

Mechanical response of pile group to tunnel induced ground movement

5.1 Introduction

In an urban area, many new tunnels have been planned to construct in congested underground space. The adverse effects of tunnel construction on the present structures should be minimized, especially pile foundations. During the tunnel boring process, it is difficult to control the volume of soil removal, leading to alters in the stress state and the movement of the soil. The potential effects of the ground movement associated with the tunnel construction must be properly considered in the design and construction of tunnel to avoid the adverse effects, i.e., damages of the adjacent structures, such as pile foundations, buildings, and buried pipes. The study on the effects of these changes on the adjacent pile foundation is essential when a bored tunnel is constructed in an urban area with many pile foundations.

There are few case histories available about the behavior of piles subjected to tunnel excavation (**Lee et. al., (1994); Kaalberg et. al., (2005)**). Several researchers have proposed numerical methods for evaluating the behavior of existing piles and inverse effects of nearby tunneling on them. **Chen et al. (1999)** used two-stage approaches, in which firstly free-field soil movements were estimated by an analytical method, and secondly, these estimated soil movements were imposed on the pile in a simplified boundary element analysis to compute the pile responses. **Lee and Ng (2005)** conducted a three-dimensional, elasto-plastic, coupled-consolidation numerical analysis to investigate the effects of an advancing open face tunnel excavation on an existing pile in clay.

However, compared to the shallow foundations, tunnel, the interaction between soil-pile-tunnel is more complicated to model with numerical calculation such as the corrected input parameter, and soil characteristic due to change of stress, especially in three-dimensional problem (**Bezuijien and Schrier (1994)**). In addition, it is difficult to preinstall the piles and measured equipment prior to excavation in the field construction. It is also practically impossible to investigate the effects of these factors and detail behavior of pile foundation, e.g., vertical and horizontal load transfer mechanism, and resultant deformation of piles and pile cap from the field data, especially for the critical condition when large soil movements take place.

Therefore, physical modeling using centrifuge technology becomes popular to study these kinds of problems because it can reproduce ground stress of a full-scale prototype of a small scale model. The centrifuge model tests have proved to be valuable in studying deformation and collapse of soil model in a laboratory (**Taylor (1995)**).

5.2 Zone of influence

5.2.1 Introduction of zone of influence

Based on the settlement behavior of single pile in dense, dry sand observed from centrifuge tunneling tests, **Jacobsz et al., (2004)** introduced the zone of influence near the tunnel as shown in **Fig. 5.1**. The zone derived from the various relative positions between single pile and tunnel. The area that caused large settlement when the pile end is rested is called the zone of influence.

For the zoning four lines are introduced, lines a and b from the spring line with horizontal angles of 90 degrees and 45+φ'/2 degrees respectively, line-d tangent to the tunnel toe at 45 degree and line-c, which was drawn from the point of $2x_i$ at the ground surface to bound the pile tip location for the large settlement and small settlement of the piles induced by tunneling as shown in **Fig. 5.1**. The effect from zone of influence depends on the distance between tunnel and pile end position. The test set up is focused on the pile behavior resting in the zone of large soil movement (Zone B and C). If the pile is rested in the zone of small soil movement (Zone D) or farther than two times of tunnel diameter from tunnel perimeter, the effect from tunneling is negligible (**Standing (1996); Jacobsz et al., (2004); Loganathan et al., (2000)**).

To simplify the line-c, the points of $2x_i$ are obtained from the cases without pile group (Case0-D and Case0-S) in small ground loss ratio ($\Delta V/V_o$ = 2.0-2.5%). It should be noted that the line-c from small ground loss ratio provides more conservative shape of influence zone (wider) than large ground loss ratio (narrow).

The measured values of x_i along the depth by PIV are listed in **Table 5.1**. The regression curve between x_i and relative depth (Z/Z_o) of Case 0D and Case 0S are shown in **Fig. 5.2**. As a result, the connected points of 2xi of line-c could be approximated as linear relationship which are reduced as the depth increases. From these linear trend lines of connecting points, the distribution of trough width parameters (K) values could be established by the following equation:

$$K = \frac{\left(\frac{x_{io}}{Z_o} - c_s\frac{Z}{Z_o}\right)}{1-\frac{Z}{Z_o}} \tag{5.1}$$

where K = trough width parameter

x_{io} = trough width at soil surface

c_s = slope of line c (0.24 for C/D=2.5, 0.22 for C/D=1.5)

Z = depth of soil

Z_o = depth of the tunnel

From the distributed x_i values along the depth in line-c (**Fig. 5.1**), the slope of line c (c_s) is approximately equal to 0.24 and 0.22 for cases with C/D=2.5 and 1.5 respectively. The value of c_s becomes small by reduction of cover depth (C). The distributions of K values with relative depth from equation 5.1 are compared with the previous study as shown in **Fig. 5.3**. In the figure, the estimated K values from equation 5.1 show identical results with Case0-D, Case0-S and **Moh et al., (1996)**. As a result, line-c could be drawn if trough width from the soil surface and slope of line-c are known. In addition, line-c can be approximated by equation 2.5 proposed by **Moh et al., (1996)**. The variations of x_i along the depth can be back-calculated using equation 2.5 as shown in **Fig. 5.4**. The variation of c_s with cover depths (C) should be investigated to make the proposed equation (5.1) more applicable. Therefore, the variation of c_s is investigated by comparing with equation proposed by **Moh et al., (1996)** (see also **Fig. 5.5**). From the results, it could be indicated that the variation of cover depth (C) are slightly affected by the distribution of c_s values. However, c_s values show some variation when the tunnel diameter is changed.

The large settlement was defined as that larger than 0.022 times pile diameters at a ground loss ratio of 1.5%. From the test results, it was concluded that the behavior of piles settlement depended on their pile end positions. In Zones A and B, the piles settled rapidly from the beginning of tunneling and underwent very large magnitude of settlement. While in Zone C, the settlement rate gradually increased, finally giving relatively large magnitude of settlement. However, in Zone D the effect of tunneling is limited, causing a small pile settlement.

The settlement profiles induced by a tunnel can be approximated as a normal probability (Gaussian) curve as shown in **Fig.2.5** (**Mair (1979)**). In this study, the displaced vectors from PIV of test series A (without pile group) are illustrated in **Fig. 5.6**. In the figure, the methods to draw a zone of influence are adopted from **Jacobsz et al., (2004)** and overall ground displacements are directed toward the tunnel axis. The line *c* was obtained from two times of trough width (x_i) of subsurface vertical displacement (S_v) profiles obtained by the PIV along the depth layers as shown in **Fig. 5.7** for the Case0-D and Case0-S. It can be clearly seen that the trough width (x_i) gradually reduce from shallow to deep layers for both Case0-D and Case0-S. In **Fig. 5.7**, the positions of trough width or inflection point (x_i) are indicated by arrows and the depths of layers are indicated by relative depth (Z) and tunnel elevation (Z_o).

5.2.2 Relative position between strain gauges and zone of influence

In this study, a similar zone of influence is adopted for the model of C/D = 2.5 and 1.5 as shown in **Fig. 5.1**. For the zoning, the lines a, b and d are drawn by the same manner as those by **Jacobsz et al., (2004)**, but the line c was made by connecting the coordinate of ($2x_i(Z)$, Z) ,where $x_i(Z)$ is horizontal location of the inflection point of the subsurface settlement profile at depth Z as mention before. In the figures, the locations of the front and rear pile tips are indicated for short and long piles in the cases with different relative horizontal distance (X_p) as illustrated in **Fig. 5.8**. Only the pile end of short pile group with Z_{pe}/R = -1.72 (Case 2.0DH-3.0DH; Case1.5DL-3.0DL) were rested in the zone B and C. Short and long pile group with Z_{pe}/R = 0.28 (Case1.5SL-3.0SL for short piles and Case2.0DH-3.0DH; Case1.5DL-3.0DL for long piles) were approximately rested in tunnel elevation with very close to line *c* and *d*. The long pile group with Z_{pe}/R = 2.28 (Case1.5SL-3.0SL for long piles) were the farthest distance from the zone of influence. In **Fig.5.8**, the solid and open dots mean the position of front and rear piles respectively and the triangle shape dots mean the position of two times of inflection points along the depth layers ($2x_i(Z)$).

5.3 Pile cap movements

For safety assessment of superstructures, it is important to predict not only the movement of the structure, the vertical settlement (δz), but also the horizontal movement (δx) and inclination (θ). In **Fig. 5.9-5.11**, the three components of pile cap movements are plotted against relatively horizontal distance (X_p/R) at ground loss ratio ($\Delta V/V_0$) of 2% and 15%. These relatively small and large ratios are considered as a possible normal working conditions and a critical condition closed to a failure of tunnel. The effects of applied vertical load to the foundation are investigated by comparing case series B(1) and B(2) and the effects of cover and depth ratio (C/D) are also discussed by case series B(2) and C. The results of vertical settlement of single pile **Lee and Chiang (2007)** with various X_p/R were also shown in the long pile group curves.

5.3.1 Vertical settlement (see Fig. 5.9)

a) Short pile

- Vertical settlement is increased as the pile group gets close to the tunnel (reduction of X_p/R)
- A comparison between test series B(1) and B(2) (Z_{pe}/R = -1.72) shows that the vertical load has an effect on the vertical settlement. In the heavy vertical load (test series B(1)), pile groups are induced larger vertical settlement than the case with light vertical load (test series B(2)).
- The increase of relative piles end depth from Z_{pe}/R=-1.72 to Z_{pe}/R=0.28 indicates that the magnitude of vertical settlement is reduced.
- In the test series B(1) and B(2) (Z_{pe}/R = -1.72), the increments of vertical settlement are gradually increase when the relative pile position is reduced form X_p/R=3.0 to X_p/R=2.0 (test B(2)) and X_p/R=1.5 (test B(1)) . However, for the test series C (Z_{pe}/R = 0.28), the increment of vertical settlement is begun when the relative pile position is reduced from X_p/R = 2.5
- In test series B(2), vertical settlement significant increases as the relative pile distance (X_p/R) is less than 2.0

b) Long pile

- The results of vertical settlement of single pile (**Lee and Chiang (2007)**) with various X_p/R and Z_{pe}/R=4.0 are also shown in the graphs. The single pile also showed a large increase

as the pile is closed to the tunnel. However, the threshold value of X_p (less than 1.5) is smaller than that obtained in this study (X_p less than 2.0) for the piles with Z_{pe}/R=2.28. It could be said that when the pile end is significant deeper than the tunnel, the effect of tunneling is reduced.

- The vertical load effect for the long pile (Z_{pe}/R=0.28) is similar to the short pile (Z_{pe}/R=-1.72) but the load effect is identical for the long pile with X_p/R >2.5.
- There is unlike between the short and long piles with the same relative pile tip distance (Z_{pe}/R=0.28). The vertical settlement of short piles with X_p/R=2.5 and 3.0 is similar while the long piles reveal that the vertical settlement of the case with X_p/R=2.5 is larger than the case with X_p/R=3.0.
- There is no significance increase of vertical settlement for the long pile with Z_{pe}/R=0.28 as the relative horizontal distance (X_p/R) is reduced from 2.0 to 1.5. This behavior could not be explained, but the reason may come from the locally large relative density near the pile end of the case with X_p/R=1.5

5.3.2 Horizontal displacement (see Fig. 5.10)

a) Short pile

- A comparison between test series B(1) and B(2) (Z_{pe}/R = -1.72) also shows that the vertical load has an effect on the horizontal movement. In the heavy vertical load (test series B(1)), pile groups are induced larger horizontal movement than the case with light vertical load (test series B(2)).
- For the short pile with Z_{pe}/R= 0.28, the horizontal movements between the cases with X_p/R= 2.5 is identical to the case with X_p/R= 3.0. But the significant horizontal movements are observed when the relative horizontal distance (X_p/R) is less than 2.5, especially in the large ground loss ratio ($\Delta V/V_0$=15%)
- A comparison between test B(2) (Z_{pe}/R=-1.72) and test C (Z_{pe}/R=0.28) is apparent that the magnitudes of pile cap movements are minimized when the relative pile end (Z_{pe}/R) becomes more positive magnitude. However, the magnitude of horizontal movements between two case become similar when the X_p/R less than 2.0.

b) Long pile

- It is consistent with the result from short pile groups about the vertical load effect. Cases with heavy vertical load (test B(1)) display higher magnitude of horizontal movement than the cases with low vertical load (test B(2)). In test series B(2), it should be noted that the horizontal movements between cases with $X_p/R=2.0$ is identical with $X_p/R=1.5$.
- It could be inferred that the increasing value of Z_{pe}/R (i.e., $Z_{pe}/R=0.28$ of short pile and $Z_{pe}/R=2.28$ of long pile) increase the threshold value on X_p. In other words, the short pile with $Z_{pe}/R=0.28$ starts to develop large horizontal movement when Xp/R is less than 2.5, while the long pile with $Z_{pe}/R=2.28$ starts to develop large horizontal movement when Xp/R is less than 2.0.
- The horizontal movements are identical when the relative horizontal distance was reduced from $X_p/R= 2.0$ to $X_p/R= 1.5$ as the same as in vertical settlement.

5.3.3 Inclination (see Fig. 5.11)

a) Short pile

- The effect of vertical load is insignificant for the inclination of short pile when compare the results between test series B(1) and B(2). This behavior is different from the vertical settlement and horizontal movement directions.
- The cases with $Z_{pe}/R= -1.72$ and 0.28 indicate significant horizontal movement when the relative pile distance (X_p/R) is less than 2.5.
- It could be confirmed that the magnitudes of inclination are reduced when the value of Z_{pe}/R becomes more positive (pile ends are rested deeper than the tunnel).
- The short pile group with pile end simultaneously rested within and outside zone of influence (i.e. test series B(1) and B(2)) show large induced inclination because the large differential settlement between front pile (Zone B and C) and rear pile (Zone D). The inclination magnitude became small as the pile end rested in Zone D as shown in test series C.

b) Long pile

- Comparing test series B(1) and B(2) shows that the vertical load has an insignificant effect on the inclination of long pile. Therefore, only the inclination does not increase the

inclination magnitude at large vertical load but the vertical load induces more pile cap movement in vertical settlement and horizontal movement directions.

- Long pile groups with Z_{pe}/R= 2.28 indicate significant induced inclination when the relative pile distance (X_p/R) is less than 2.0 which is similar to horizontal movement.
- In test series B(2), the inclination increase as the piles become close to the tunnel for X_p/R from 3.0 to 2.0. However, for X_p/R is less than 2.0, the increase of inclination is insignificant which could be observed in the vertical and horizontal movements.
- The long pile group with Z_{pe}/R = 2.28 show very small of inclination magnitude due to no effect of differential settlements between piles inside and outside zone of influence.

5.4 Pile group response

5.4.1 Individual pile settlement

In **Fig. 5.12-5.14**, the settlements of front and rear piles are plotted against ground loss ratio. In the tests with small and large tunnel cover depth ratio (C/D=1.5 and 2.5), the settlements increased by increasing the ground loss ratio and the front piles settled larger than the rear piles for all the case. It means that the both short and long pile groups are tilted toward the tunnel.

Comparing test series B(1) (**Fig. 5.12**) and test series B(2) (see also **Fig. 5.13**), the cases with heavy working loads (Case2.0-DH, Case2.5-DH and Case3.0-DH) showed more settlement than the cases with light working loads (Case2.0-DL, Case2.5-DL and Case3.0-DL) but the trends of settlement were similar. For the small volume loss ratio ($\Delta V/V_0$ < 3%), the settlements increased linearly with $\Delta V/V_0$. While for $\Delta V/V_0$ over 3%, the settlement rates gradually decreased and became very small at the end of the tests ($\Delta V/V_0$ = 15%), except for the short front piles in Case1.5-DL, Case2.0-DL and Case2.0-DH. These piles showed large settlement, which are almost proportional to the ground loss ratio even for $\Delta V/V_0$ over 5%. As indicated in **Fig. 5.8**, the ends of the short front piles in Case1.5-DL located in Zone B and those in Case2.0-DL and Case2.0-DH were closed to Zone B in Zone C. The ends of all other piles, including the short front pile with $X_p/R > 2$, all short rear piles and all long front and rear long piles rested on Zone D or boundary between Zones C and D.

The closer the pile to the tunnel, the larger the settlement took place, except for the long front piles of Case1.5-DL and Case2.0-DL (**Fig. 5.13(b)**), which had large cover depth ratio (C/D=2.5) and the pile end depth close to the tunnel axis (Z_{pe}/R=0.28) . For $\Delta V/V_0$ over 5%, the settlement for the former with X_p/R=1.5 became slightly smaller than the latter with X_p/R=2.0.

This behavior is consistent with the pile cap movement in three components (vertical, horizontal, and inclination) in which the pile cap shows identical movements between $X_p/R = 1.5$ and $X_p/R = 2.0$.

For the short and long front piles of Case1.5-SL and Case2.0-SL with small cover depth ratio (C/D=1.5), the settlement for the former ($X_p/R = 1.5$) was larger than that for the latter ($X_p/R = 2.0$) as shown in **Fig. 5.14.** The differential settlement between front and the rear pile became small for the short pile because both front and rear piles were rested outside the zone of influence. Therefore, the inclination of short pile of Case1.5-SL is significantly small comparing to short pile of Case1.5-DL.

5.4.2 End bearing load of pile group

Fig. 5.15 shows the variation of pile end bearing loads with the volume loss ratio. The loads shown in the figure are normalized by the load prior to starting the tunnel diameter contraction. The variations of the pile end bearing were larger for the front pile than the rear pile. The short front piles in Case1.5-DL, Case2.0-DL, which showed large settlement (**Fig. 5.12(a)** and **Fig. 5.13(a)**), underwent reductions in the end bearing load during the ground loss, especially for that in Case1.5-DL, resting in the Zone B. In contrast, the measured axial force increased with increasing the ground loss ratio for cases with pile resting in the Zone D both for the front and rear piles. The front piles tended to settle larger than the rear piles as illustrated in **Fig. 5.12-5.14**. Thus, the end bearing load of those front piles were developed larger than the rear piles position.

Vertical load effects on development of end bearing loads are shown in **Fig.5.16**. In Case2.0-DH, front and rear short piles developed reduction of pile end bearing loads. Short piles with large vertical load (test series B(1)) showed a reduction of end bearing smaller than the cases with light vertical load (test series B(2)). In test series B(1), long piles developed increment end bearing load larger than cases in test series B(2). However, long front pile with $X_p/R = 2.0$ (Case2.0-DH) showed magnitude of the end bearing slightly smaller than the cases with $X_p/R = 2.5$ and 3.0.

The settlement of the short and long front pile positions was plotted against the normalized end bearing in **Fig. 5.17**. The cases with the decrement of the end bearing load showed large pile settlement, especially for Case1.5-DL with Xp/R=1.5 (**Fig. 5.17(a)**). In

contrast, pile groups with the pile tip resting in the Zone D (i.e. Case3.0-DH, Case3.0-DL and Case 1.5-SL) endured small pile settlement and were competent of conveying more axial force.

5.4.3 Axial load on pile group

Fig. 5.18 displays the profiles of pile axial force increment for various parameters such as the horizontal distances from the tunnel (X_p), the cover and depth ratios (C/D) and the working loads. The profiles at two different ground loss ratios ($\Delta V/V_0$ = 2% and 15%) were shown for comparison between normal working and failure load conditions. In the figure, the individual relative horizontal distance (X_p/R) is indicated in the square brackets for each pile position. Cases with X_p/R = 1.5, 2.0, and 3.0 are selected for comparison about the axial force development.

The reductions of the end bearing were observed in the short front piles of Case2.0-DH, Case2.0-DL, and Case1.5-DL where the piles rested in the Zone B and closed to the boundary between the Zone B and C respectively. Short front pile with X_p/R = 1.5 showed a significant reduction of both end bearing and axial force at the pile head. At the same time, the short rear pile with X_p/R = 2.93 compensated the reduction of axial force at the pile head by increasing the axial force at the pile head. The reduction of axial force at the pile head corresponds to the previous study by **Hergarden et al., (1996).** The reduction of end bearing came from the stress reduction of surrounding soil caused by the soil movement under the pile end.

The shapes of axial force between the front and rear piles were similar when the large pile portions located on the Zone B (e.g.; long pile groups of Case 3.0-DH, Case 3.0-DL and Case 3.0-SL). In addition, the long front pile with X_p/R = 3.0 developed similar shape of axial force as the long rear pile with X_p/R = 2.93 at the upper portion of pile (inside zone of influence) but the shape are different in the lower portion due to the difference in their own settlements. Two of these piles were rested almost at the same position, but relative settlements of pile and surrounding soil were different. The difference between relative settlements is called skin friction, and different skin friction will lead to difference of shape of axial force.

Pile groups with different loads on the pile cap (case B(1) and case B(2) series) developed similar shape of induced axial forces. However, there were differences in the shape and magnitude of the axial force profiles of the piles with different horizontal distance of piles and tunnel (X_p) and cover and depth ratio (C/D). The outcomes may correspond to the relative position between the piles and the zone of influence. The difference came from the development of skin friction, and the behavior will be explained in the next section.

5.4.4 Development of skin friction at pile portions

From equation 2.8, pile bearing capacity (Q_u) is carried by point end bearing (Q_e) and skin friction (shaft friction load, Q_s). In the study, the average unit skin friction $f(z)$ is calculated by the equation 2.11. The difference of measured axial force between two points in the pile model is obtained by the measured axial forces strain gauges. As a result, in **Fig.5.19**, the mobilization of the average unit skin friction along the piles was obtained from the measured axial forces (**Fig. 5.18**). The skin friction is mobilized by the relative displacement between model pile and surrounding soil. It becomes positive (upward) when the vertical pile displacement is larger than that of the surrounding soil and negative (downward) when the pile displacement is less than the surrounding soil. In general, the front and rear piles showed similar shapes of average unit skin friction but the rear piles developed less magnitude than the front piles.

In the figure, the depths of lines *d* and *c* at the location of piles are indicated by arrows. Inside the Zone B and C (above lines *d* or *c*), negative skin friction was developed due to large soil movements as shown in the short and long front piles of all the cases. But some portion of the short front piles showed positive skin friction due to a large pile settlement. At the lower portion of pile, the cases with small X_p/R (the short front pile of Case2.0-DH, Case1.5-DL, and Case2.0-DL) developed a large negative skin friction even for the large magnitude of pile settlement (**Fig. 5.12(a)** and **Fig. 5.13(a)**). However, they developed positive skin friction at the upper portion of the pile. These results could come from the large soil movements near the depth of pile ends. But as the movements were reduced near the soil surface, the skin friction became positive due to the relatively large pile settlement. This reduction of magnitude soil settlement from the tunnel level to the surface is consistent with the displaced vectors from **Fig. 5.6**.

In case B(1) and B(2) series (**Fig. 5.19 (a) and Fig. 5.19 (b)**), almost of the long piles developed negative skin friction along the length except the near pile end for the cases with $X_p/R \geq 3$ (Case3.0-DH and Case3.0-DL). In these piles, the positive skin frictions were generated at the lower portion due to a small magnitude of soil movement in the Zone D (below lines *d* and *c*). In addition, the magnitude of negative skin friction was increased as the pile became close to the tunnel which can be observed in **Fig. 5.19 (b)** of long front pile. Long front pile with X_p/R = 3.0 developed positive skin friction at the lower portion, but the long rear pile with X_p/R = 2.93 which is very close to the former developed negative skin friction. The opposite sign of skin friction come from the difference of individual pile settlements as shown in **Fig. 5.13 (b)**. Furthermore, the shape of skin friction between short front pile with X_p/R = 3.0 and short rear

pile with $X_p/R = 2.93$ was similar due to the identical individual pile settlements as can be seen in **Fig 5.13 (a)**.

In cover and depth ratio equal to 1.5 (**Fig. 5.19 (c)**), the trends of mobilized skin frictions of the short and long piles were similar, which depended on the pile positions in the zones of influence. At the lower portion of the piles, positive skin frictions were generated for the long front pile with $X_p/R \leq 2.0$ because of relatively large pile settlement and small magnitude of soil movement in the deep zone. In this small cover and depth ratio, the reduction of soil settlement could be observed as the same as cases with large cover and depth ratio. At the mid-depth near the tunnel axis, the long front pile with $X_p/R \leq 2.0$ (Case1.5-SL and Case2.0-SL) developed large negative skin friction. This reduction of skin friction could come from the loss of lateral earth pressure around the tunnel combined with large downward movements of the surrounding soil. Short rear pile with $X_p/R = 2.93$ developed similar shape of skin friction as the same as short front pile with $X_p/R = 3.0$ due to similar of pile settlement as illustrated in **Fig. 5.14 (a)**.

Therefore, the signs of skin friction depend on the relative positions of pile and zone of influence. If the pile developed similar settlement with similar relative horizontal distance from the tunnel (X_p), the shapes of their skin friction are identical regardless of front or rear positions.

5.4.5 Bending moments along the pile group

In **Fig. 5.20**, measured pile bending moment increments are shown for various horizontal distances from the tunnel (X_p), cover and depth ratios (C/D) and working loads. The depths of the lines *d* and *c* at the location of each pile are also shown in the figure. The positive and negative signs of the bending moment mean the pile bends away and toward to the tunnel respectively.

From **Figs. 5.20 (a)** and **Fig 5.20 (b)** on the series B(1) and B(2), it can be seen that the working load on the pile groups has slightly influence on the shape of the bending moment profiles, but the lateral position of the pile (X_p/R) has distinct influence on the shape of the bending moment profiles. Furthermore, the effect of cover and depth ratio (C/D) were also significant. The effects of the parameters on the bending moment are similar to previous study **Lee and Chaing (2007)**; **Loganathan et. al., (2000)**.

The trends of bending moment were similar between front and rear piles at shallow depth. The bending moment near the pile top could be controlled by the displacements and rotation for a rigid fixity of the pile to the cap. For example the short pile group with the front pile rested in the Zone B or closed to the Zone B in the Zone C (Case2.0-DH, Case1.5-DL and Case2.0-DL) in the condition of Z_{pe}/R= -1.72, large maximum negative bending moments were developed at the pile top. The larger the horizontal displacement was, the larger the moment. However, due to less confinement at the pile end, the lower portion of those piles showed small induced bending moment.

While for the pile with relatively deep embedment depth to the tunnel and resting in the Zone D, the bending moment profiles are different from those with the front pile resting in or closed the Zone B. There were several peaks in the profile and location and magnitudes of the peak value depended on X_p/R and Z_{pe}/R. The long front piles with Z_{pe}/R=0.28 had a peak moment at the depth slightly above the tunnel crown, but positive peak values for X_p/R less than 2.0 and negative for X_p/R=3.0. The difference in the confinement at the pile end could be a reason for the difference in the sign of the peak moment. It should be noted that very similar moment profiles were observed in the long pile group, both in the front and rear piles between Case1.5DL and Case2.0DL, implying to similar horizontal force loaded for the two pile group. This could be one of possible reasons for the similar pile cap displacements of the two cases (**Fig. 5.9 (b)**, **Fig. 5.10 (b)**, and **Fig. 5.11 (b)**).

For the cases with the small cover and depth ratio (C/D=1.5 in case C series), a peak negative bending moment were generated in the long front piles near the tunnel, due to the large horizontal soil movement at the depth above the tunnel crown and small movement in the Zone D below the line *d* (**Fig. 4.10**). This peak moment became significant for the location of X_p/R less than 2.0. It should be noted that the moment profiles of the front and rear piles with similar lateral position from the tunnel axis (X_p/R=3.0 and X_p/R=2.93 respectively) are similar at the lower depth near the tunnel but a quite different at the shallow depth.

The moment of the pile is mainly caused by the ground movement at the deeper depth, but at the shallow depth or the top it is mostly determined by the pile cap displacements with the rigid fixity of the pile head. The displacements of the pile groups with the front piles at X_p=3.0R (Cases3.0DL and SL) were much smaller than those with the rear piles at X_p=2.93R (Cases1.5DL and SL). The effect of pile confinement in the Zone D is also confirmed at the lower portion of

the short pile in Case 1.5SL. The moments of the rear pile were larger for the rear pile than the front pile of which pile end was close to the line d, the boundary of the Zones C and D.

From the above discussions it can be said that the bending moment profile of the pile group is a resultant of complicated soil pile interaction, which is affected by many factors, such as the volume loss, the cover and depth ratio, the horizontal pile location, the pile depth, and the position (front and rear) of pile. Among the factors, the relative pile depth in the less displacement zone (Zone D) to the pile length (Z_d/L) and the horizontal position (X_p) are the critical controlling factors to the moment. The pile group tends to develop in the large magnitude near the pile top. The results can be used to decide that whether this existing pile portion should be reinforced or not when tunnel is planned to construct.

5.5 Conclusion

A series of centrifuge model tests was conducted to study the behavior of pile group subjected to tunnel induced soil movement. The model pile groups have four piles with square arrangement and 5 times pile diameter spacing. Two-dimensional tunnel induced soil movement was introduced by using a mechanical machine, which can reduce the diameter with a fixed axis. The effects of tunnel cover depth, pile length, lateral position of piles from the tunnel, and vertical load to the pile group on the pile response were discussed. In the discussion, four zones of influence were defined referring a previous study and observed subsoil deformation: the Zones A and B are large soil movement zones above a tunnel, the Zone D is less movement zone, and the Zone C is a transient zone from the Zone B to the Zone D. From the study the following conclusions were drawn.

- For small ground loss ratio ($\Delta V/V_0$), the pile group movements increased almost proportionally to $\Delta V/V_0$. While for the large $\Delta V/V_0$ over 3%, the pile movement increment gradually decreased with $\Delta V/V_0$, except for the pile groups with the front pile resting in the large displacement zone. Those piles showed large increment of movement even the ground loss ratio ($\Delta V/V_0$) exceeded 3%.

- Three component of pile cap movements become small magnitude when the horizontal distance between front pile and tunnel equal to three times tunnel radius ($X_p/R=3.0$). In

addition, the individual pile settlement of front and rear piles are significantly reduced as $X_p/R=3.0$.

- The behavior of pile group could be closely related to the zone of influence where the pile end rests, and also to the relative position of the pile end in the zone. In particular, the pile group experiences large lateral movement and inclination when the front piles rest in or close to Zone B and the rear piles in Zone D.

- The measured axial force increased with increasing the ground loss ratio for the piles resting in the Zone D. While for the pile resting in or close to the Zone B, the end bearing load decreased during tunneling.

- The negative skin frictions were developed in Zone B and C due to large soil movement relative to the pile, but positive skin friction was mobilized in Zone D.

- The bending moment profile of the pile group is a resultant of complicated soil pile interaction, which is affected by many factors, such as the volume loss, the cover and depth ratio, the horizontal pile location, the pile depth, and the position (front and rear) of pile. Among the factors, The relative pile depth in the less displacement zone (Zone D) and the pile cap movement were significantly affected the shape of bending moment profile.

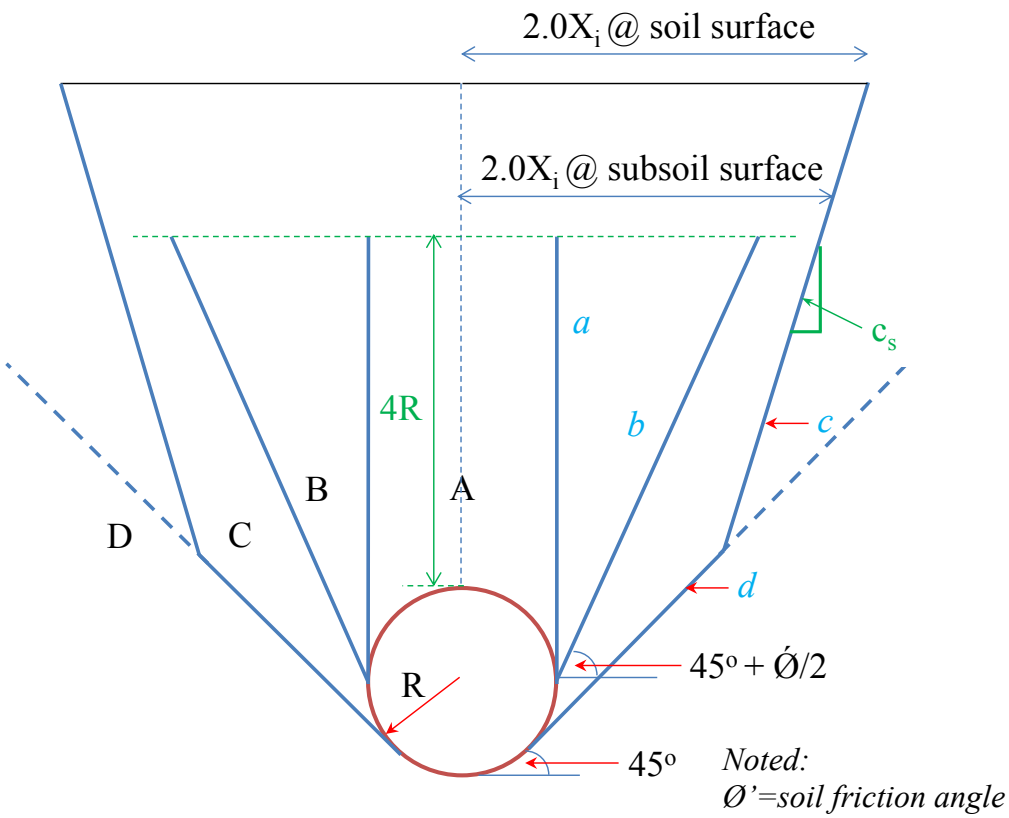

Figure 5.1 Zone of influence in this study after **Jacobz et al., (2004)**

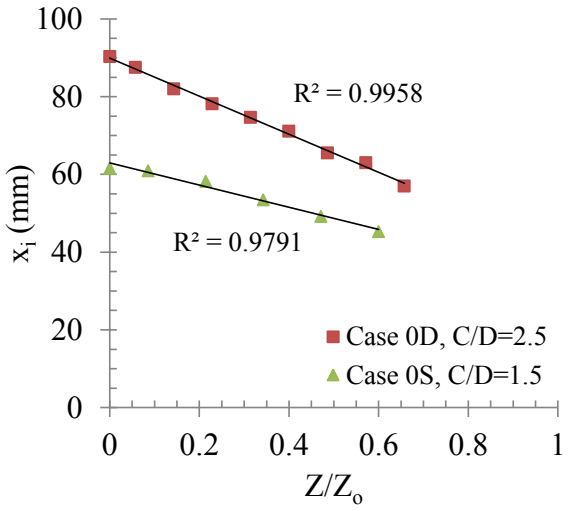

Figure 5.2 Regression curve of distributed x_i with relative depth ($\Delta V/V_o$ = 2.0-2.5%)

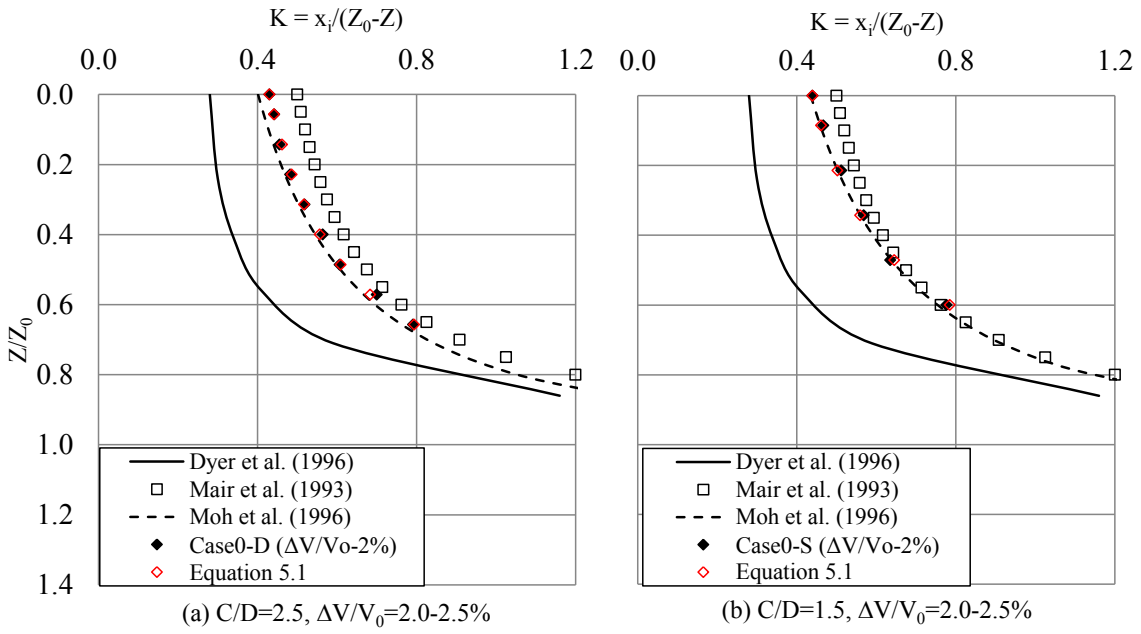

Figure 5.3 Variation of K with depth for subsurface settlement profiles and comparing with equation 5.1

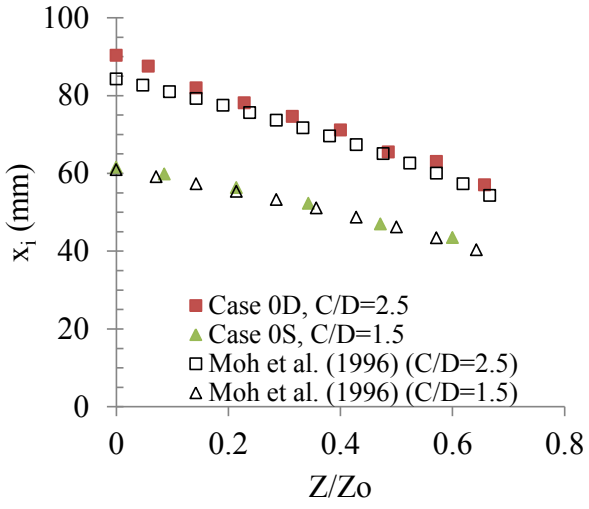

Figure 5.4 Back calculation of x_i along the depth by Moh equation (**Moh et al., (1996)**)

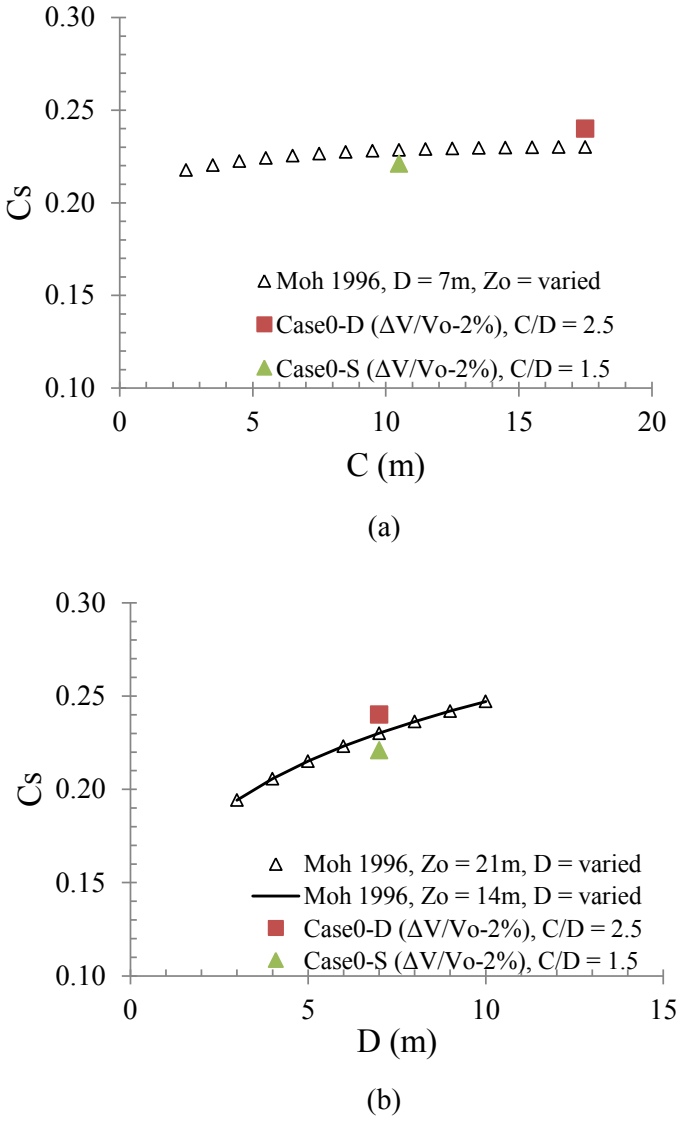

Figure 5.5 Variation of c_s with Case0-S, Case0-D and Moh equation on:
(a) Soil cover depth (C); (b) Tunnel diameter (D)

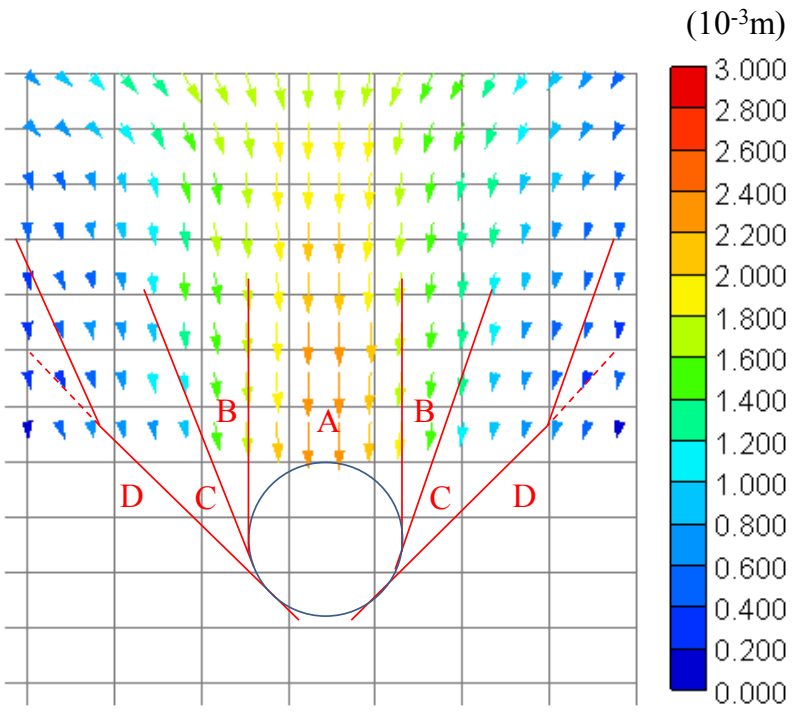

(a)

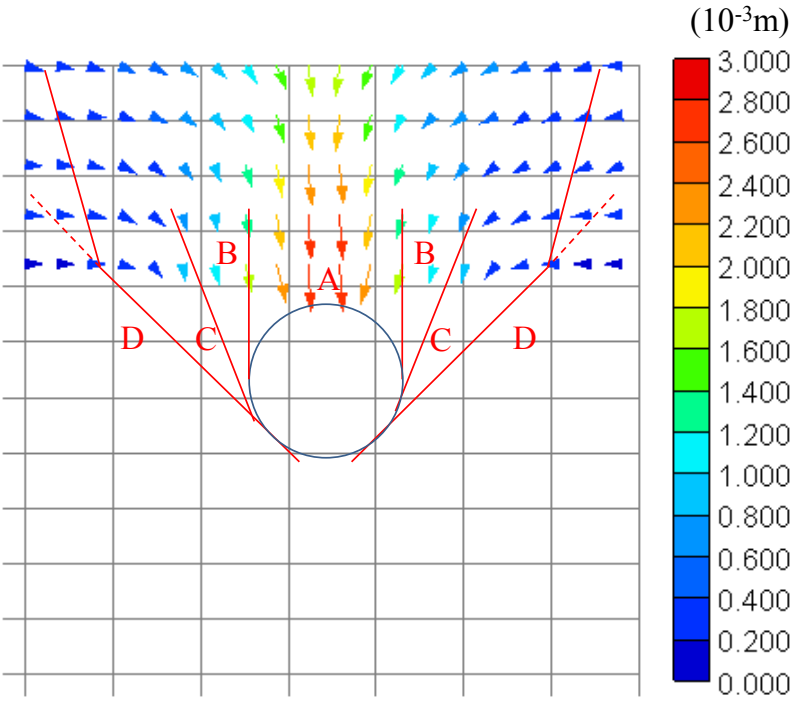

(b)

Figure 5.6 Displacement vectors from PIV at $\Delta V/V_0$=15% with zone of influence : (a) Case0-D; (b) Case0-S

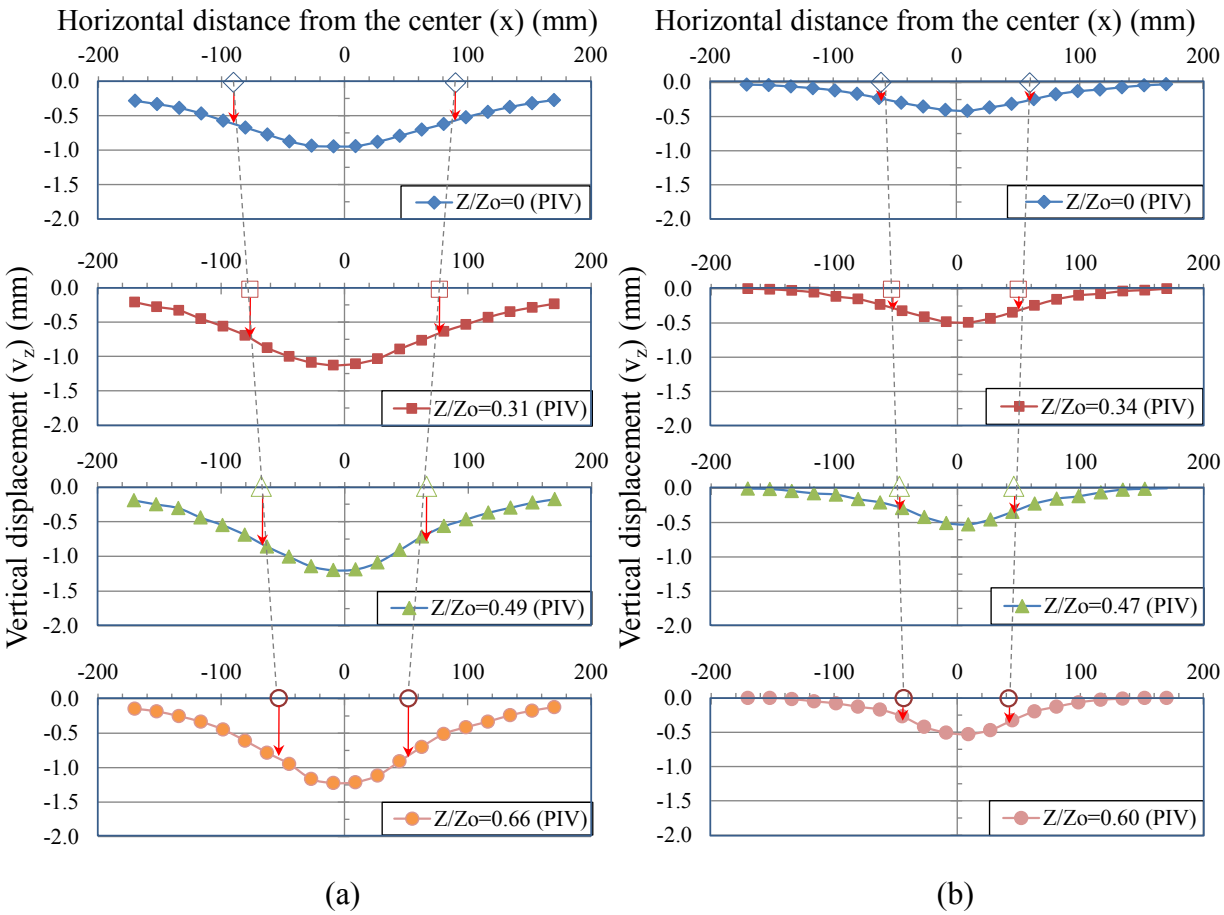

Figure 5.7 Subsurface soil settlement profile with trough width (x_i) position at $\Delta V/V_o$ = 2-2.5%: (a) Case0-D; (b) Case0-S

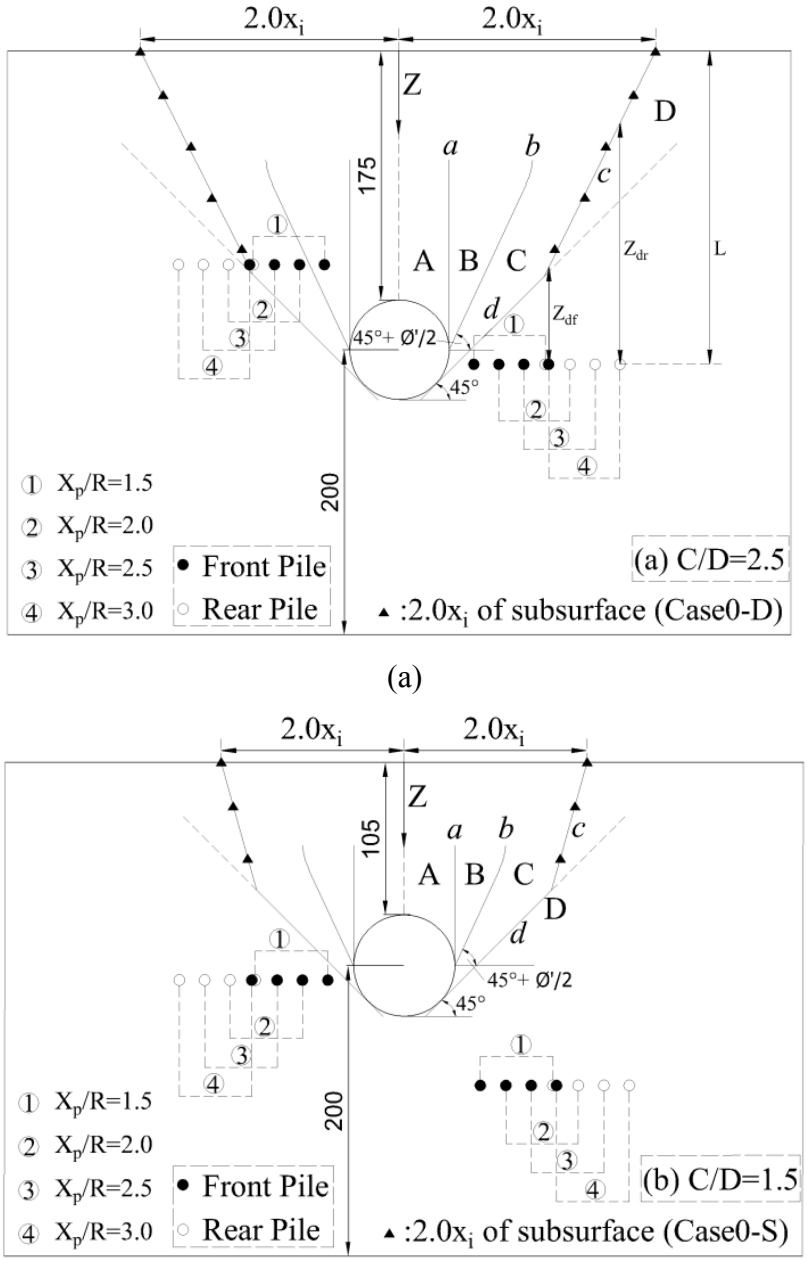

Figure 5.8 Zones of influence defined by this study and the pile base positions for the short and long piles with different horizontal distance from tunnel center (X_p) and cover and depth ratio (C/D) within zone of influence: (a) C/D = 2.5; (b) C/D = 1.5

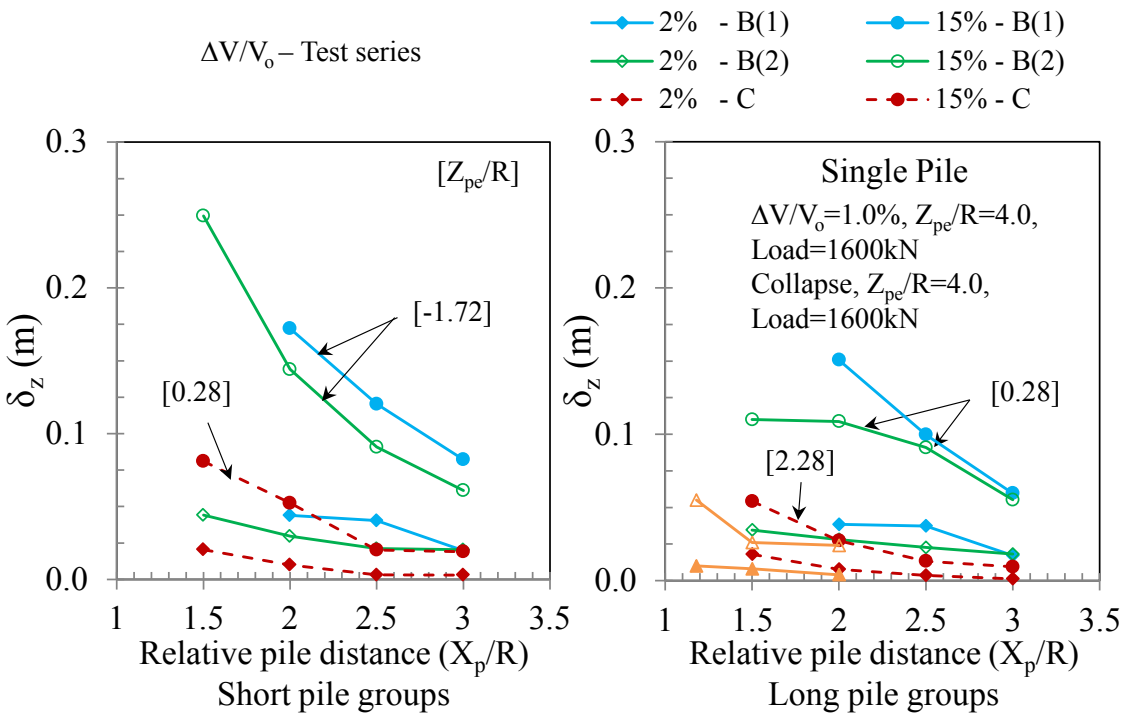

(a)

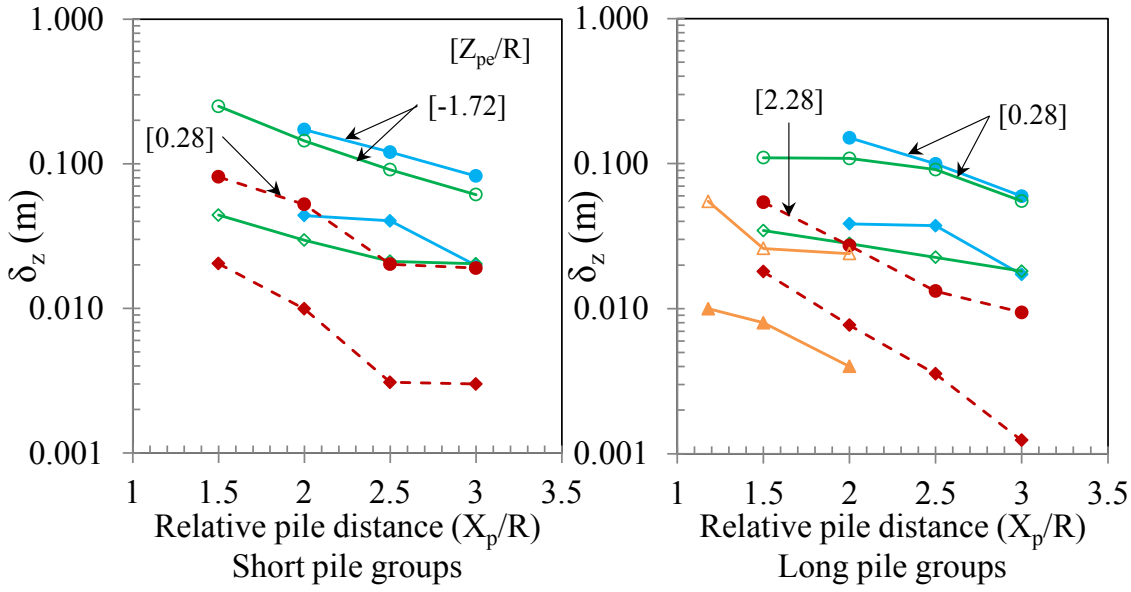

(b)

Figure 5.9 Comparison of vertical settlement of the pile cap at the ground loss ratio of 2% and 15% of relative distance (X_p/R): (a) normal scale; (b) logarithmic scale

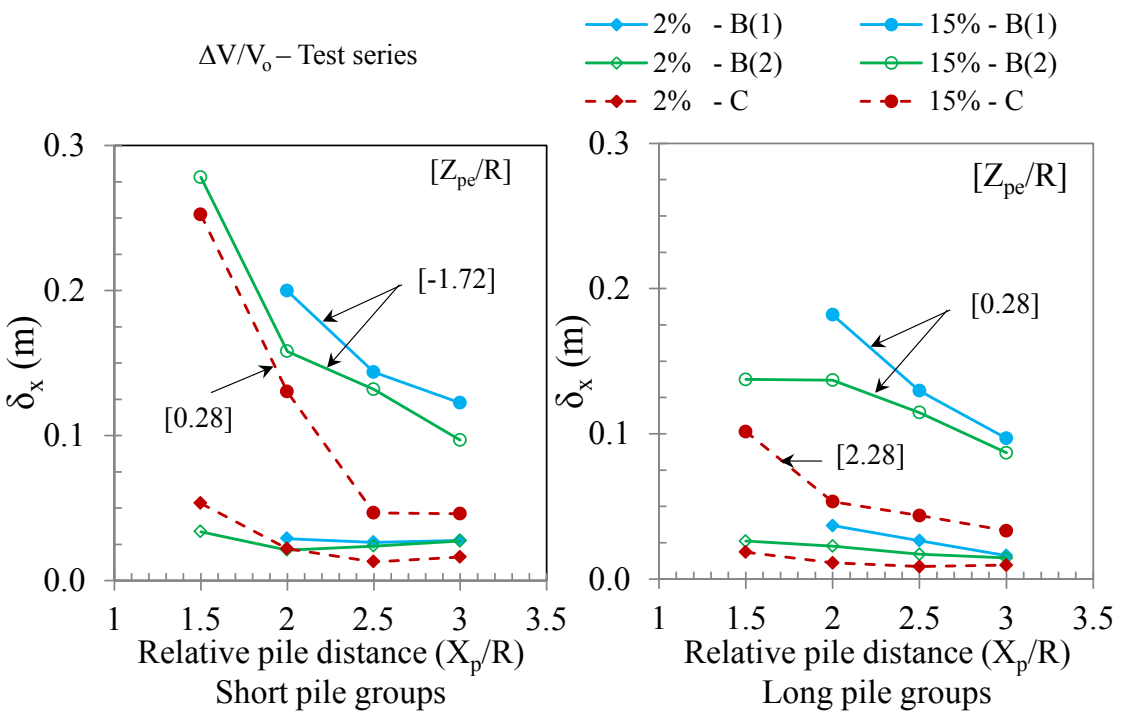

(a)

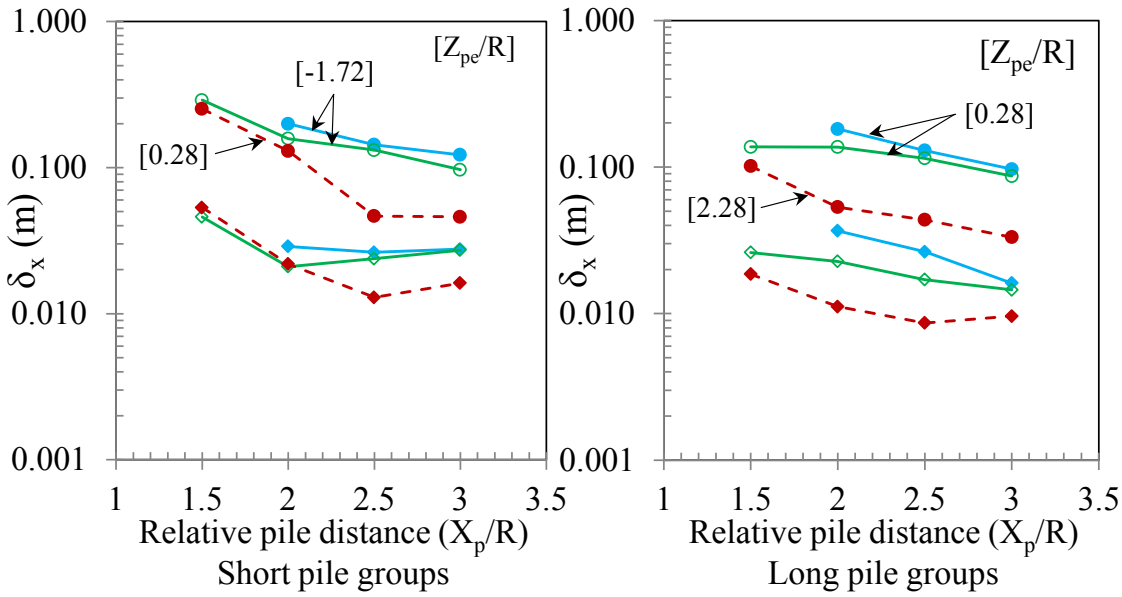

(b)

Figure 5.10 Comparison of horizontal movement of the pile cap at the ground loss ratio of 2% and 15% of relative distance (X_p/R): (a) normal scale; (b) logarithmic scale

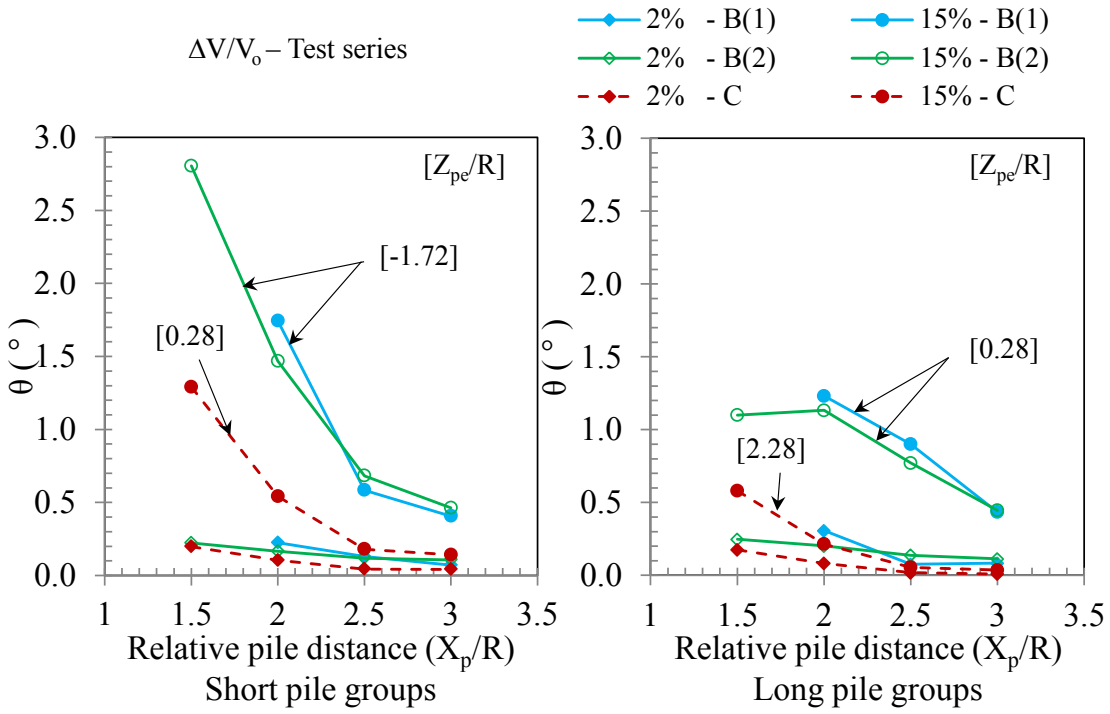

(a)

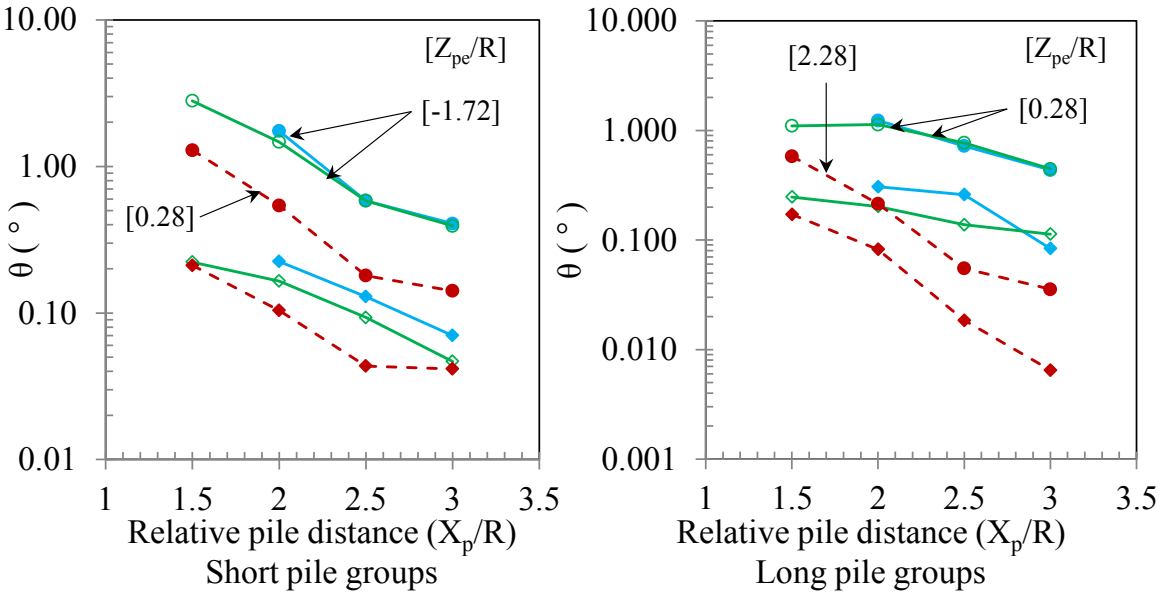

(b)

Figure 5.11 Comparison of inclination of the pile cap at the ground loss ratio of 2% and 15% of relative distance (X_p/R): (a) normal scale; (b) logarithmic scale

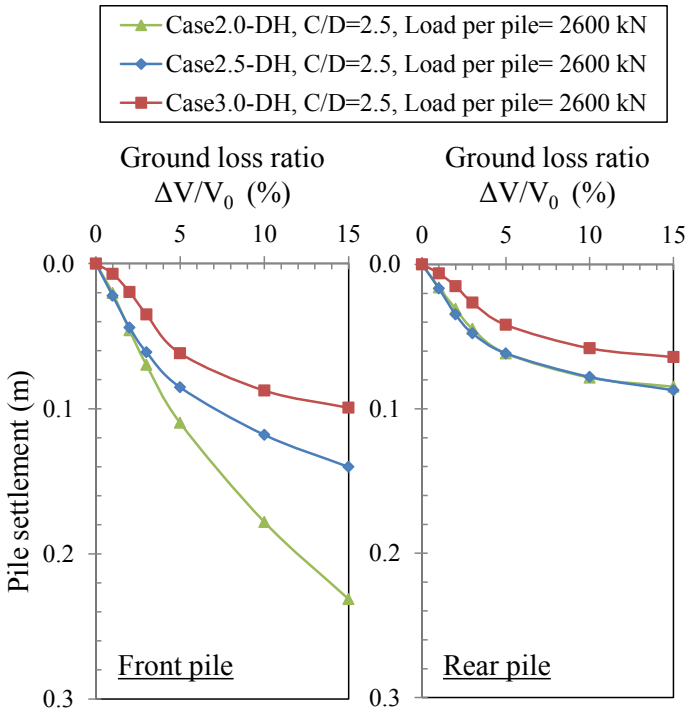

(a) Short pile

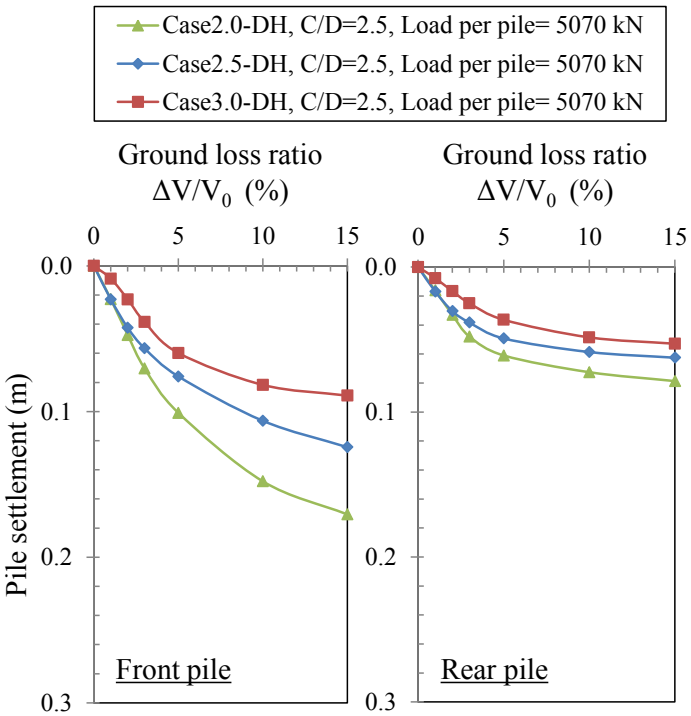

(b) Long pile

Figure 5.12 Settlement of the front and rear piles during tunneling of test series B(1): (a) short pile; (b) long pile

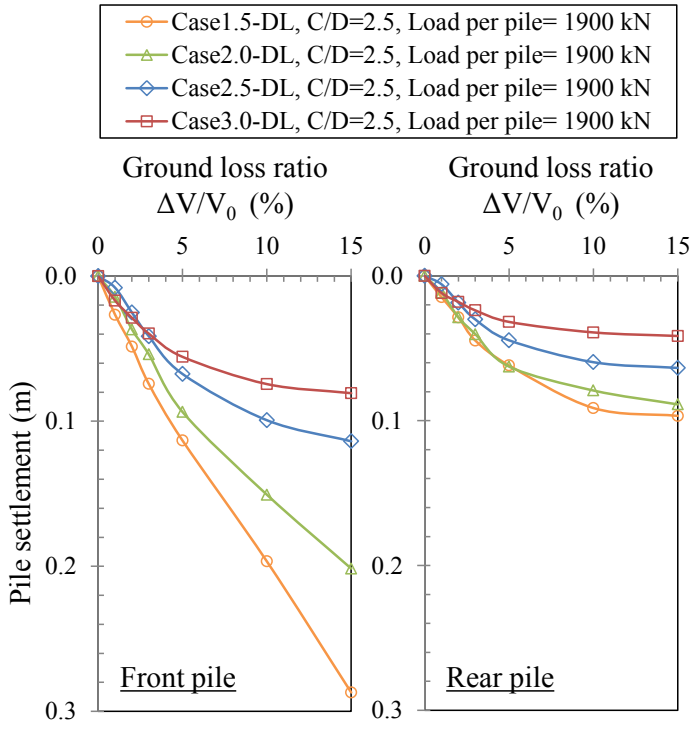

(a) Short pile

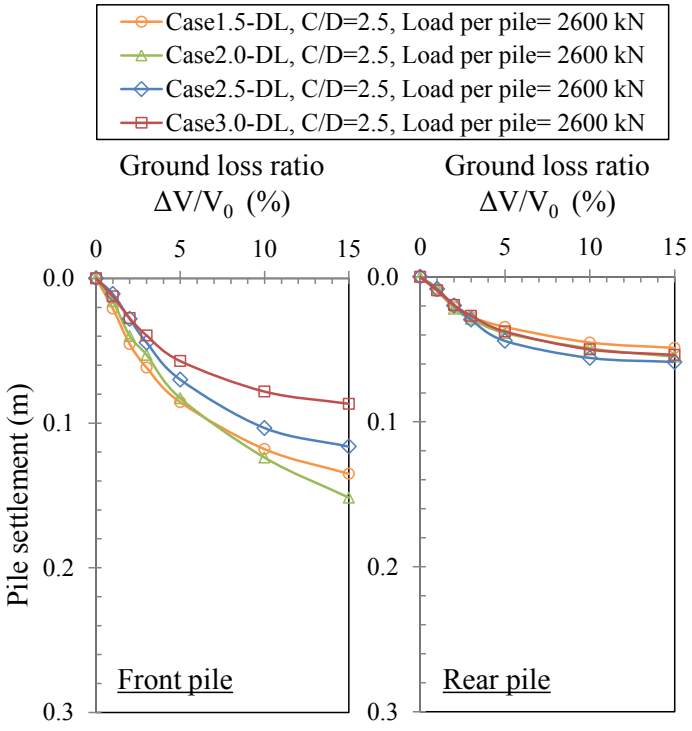

(b) Long pile

Figure 5.13 Settlement of the front and rear piles during tunneling of test series B(2): (a) short pile; (b) long pile

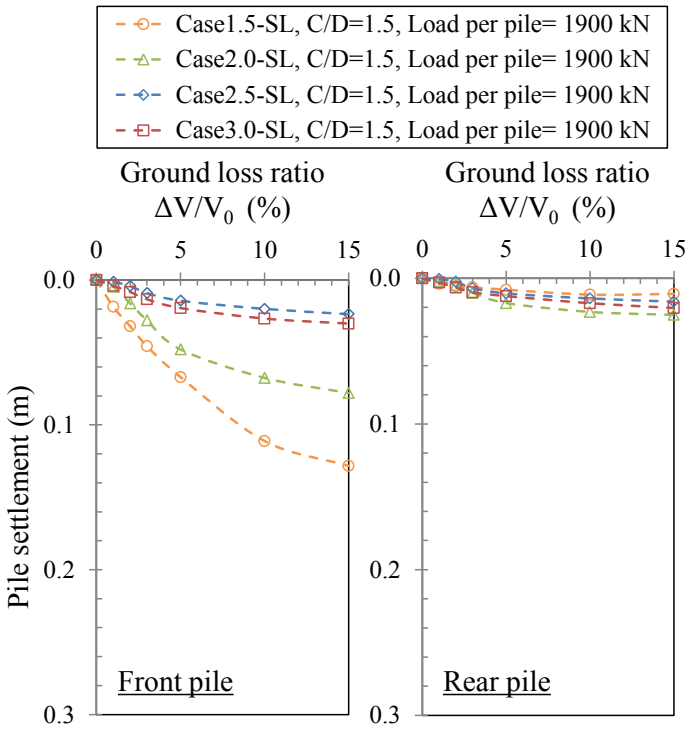

(a) Short pile

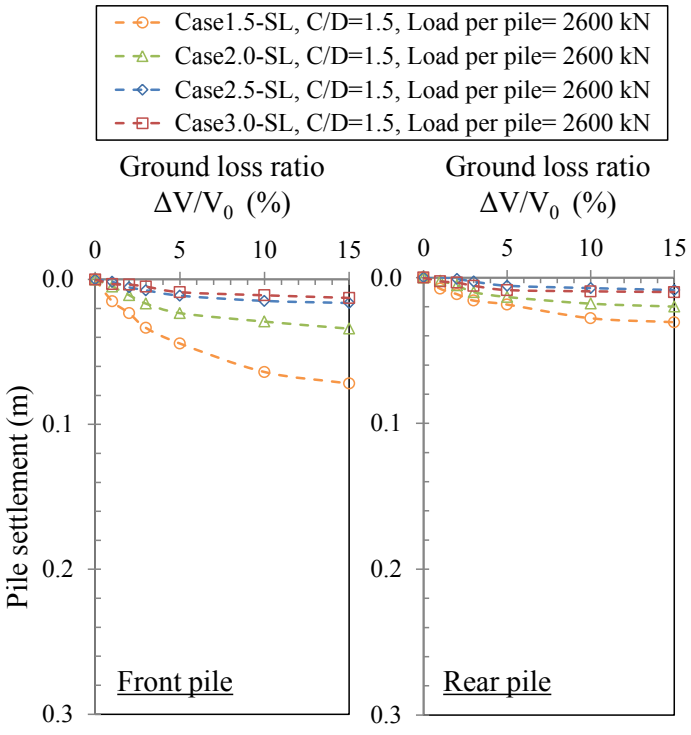

(b) Long pile

Figure 5.14 Settlement of the front and rear piles during tunneling of test series C: (a) short pile; (b) long pile

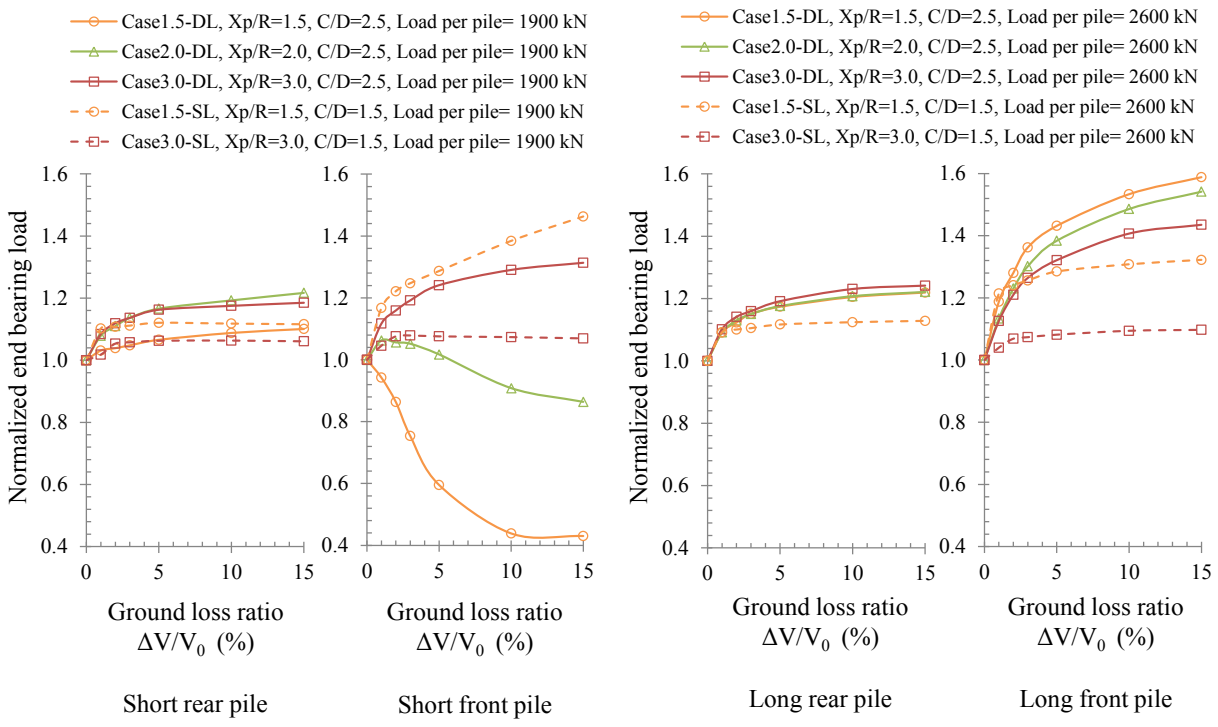

Figure 5.15 Normalized pile end bearing load with ground loss ratio: (a) short; (b) long

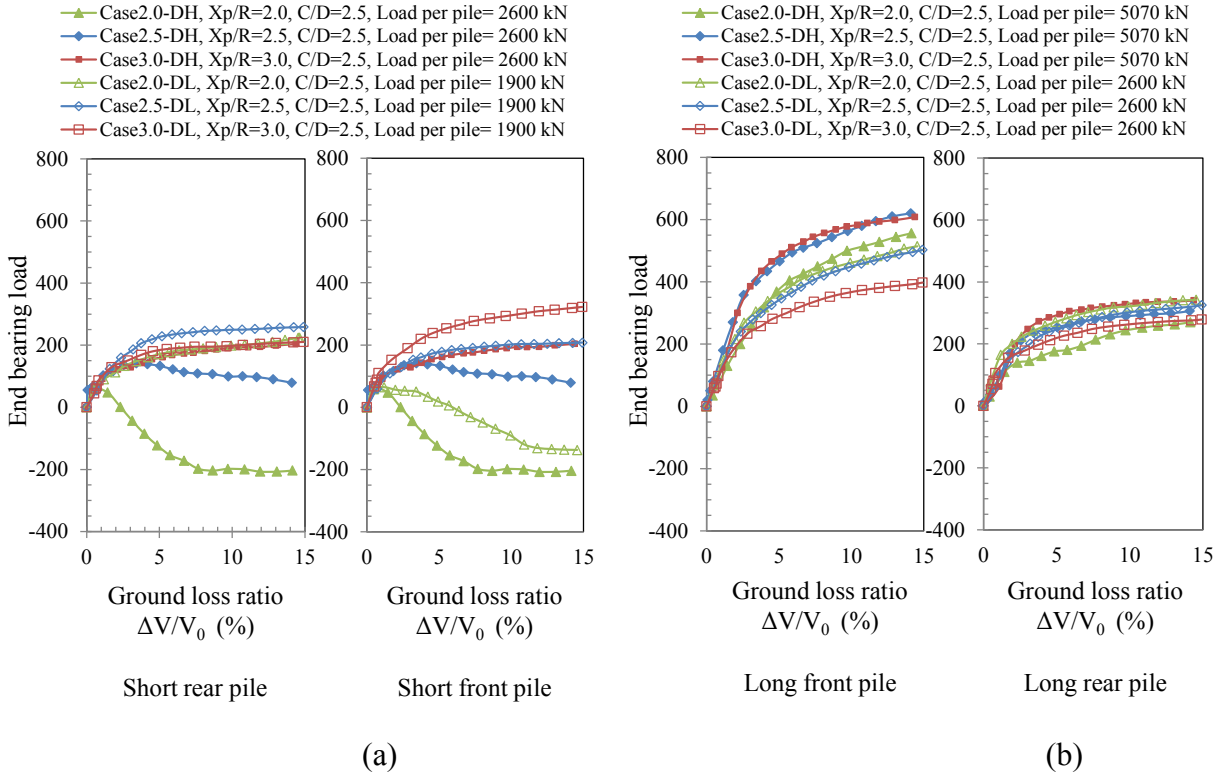

Figure 5.16 Pile end bearing load with ground loss ratio (test B(1), B(2)) :(a) short; (b) long

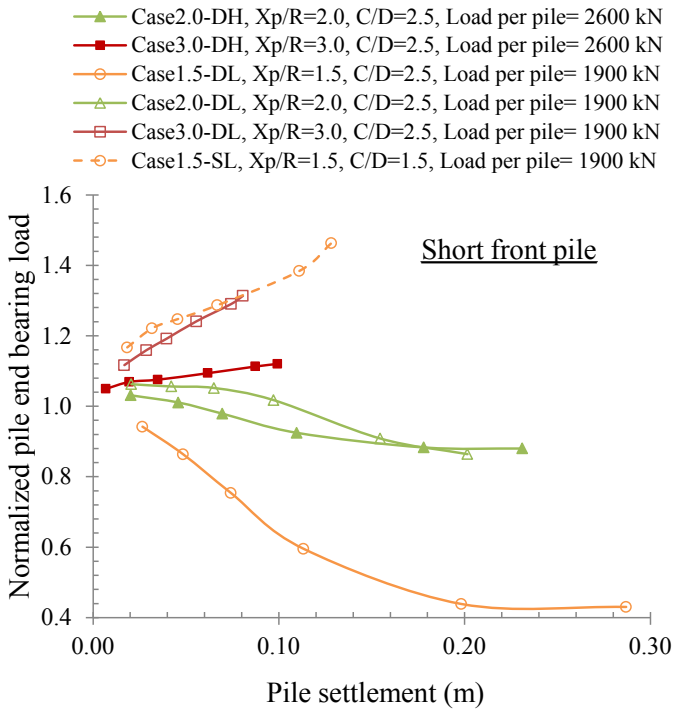

(a) Short front pile

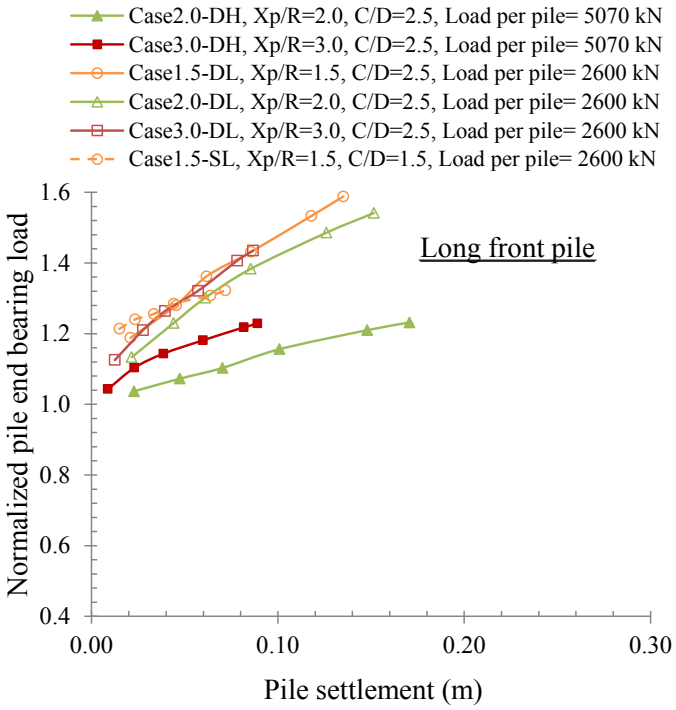

(b) Long front pile

Figure 5.17 Variation of pile end bearing load with pile settlement:
(a) short pile; (b) long pile

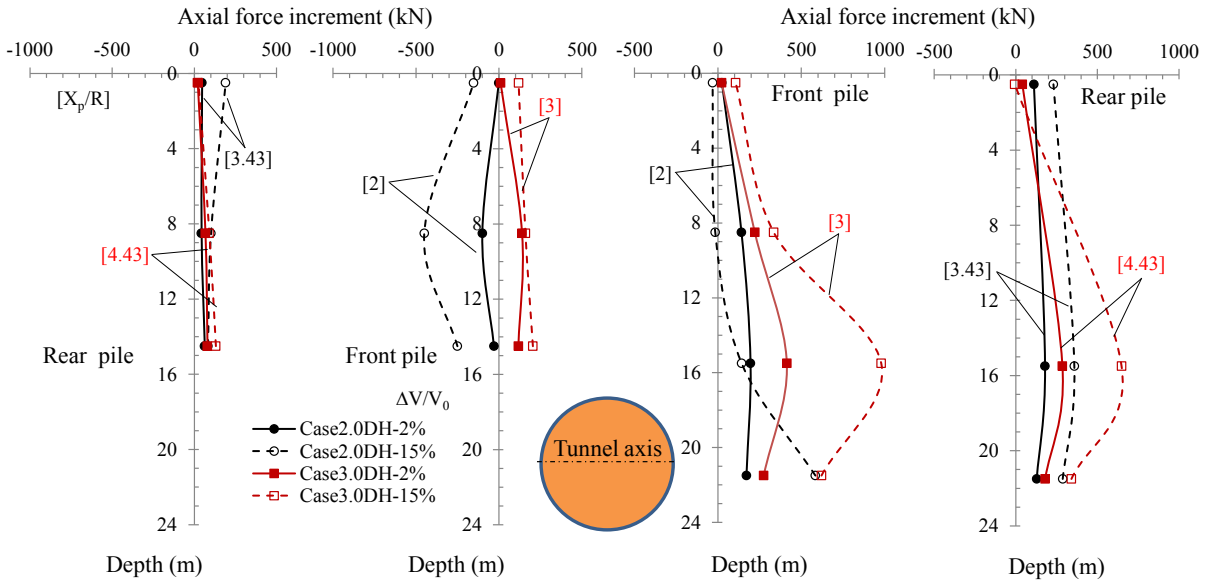

Short pile

Z_{pe}/R=-1.72, Load per pile= 2600kN

Long pile

Z_{pe}/R=0.28, Load per pile= 5070kN

(a)

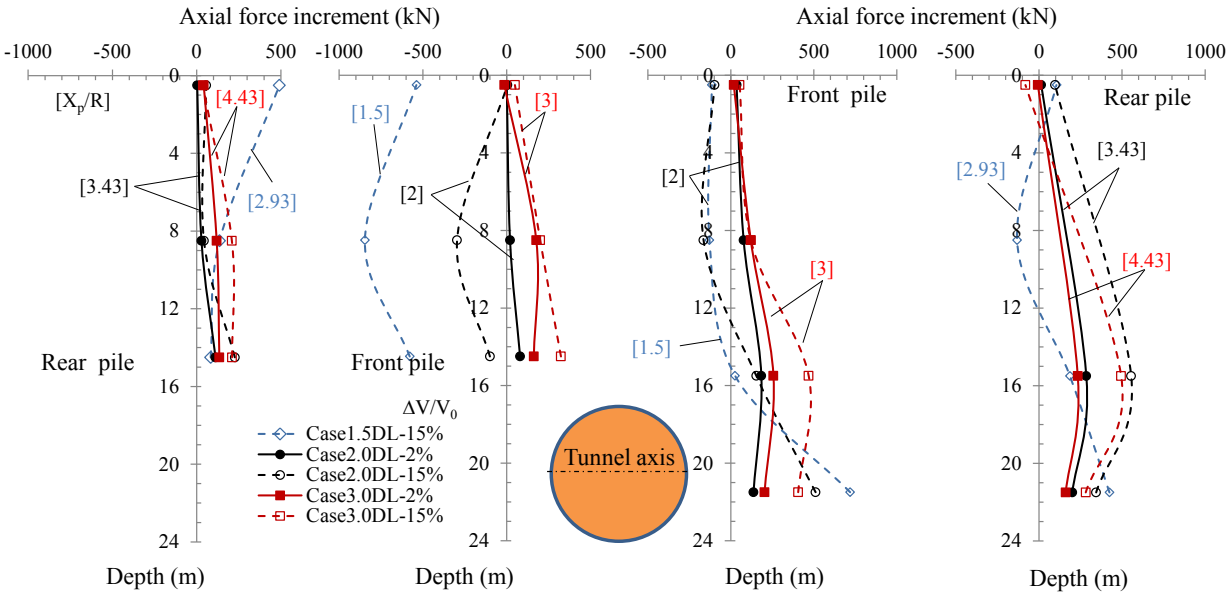

Short pile

Z_{pe}/R=-1.72, Load per pile= 1900kN

Long pile

Z_{pe}/R=0.28, Load per pile= 2600kN

(b)

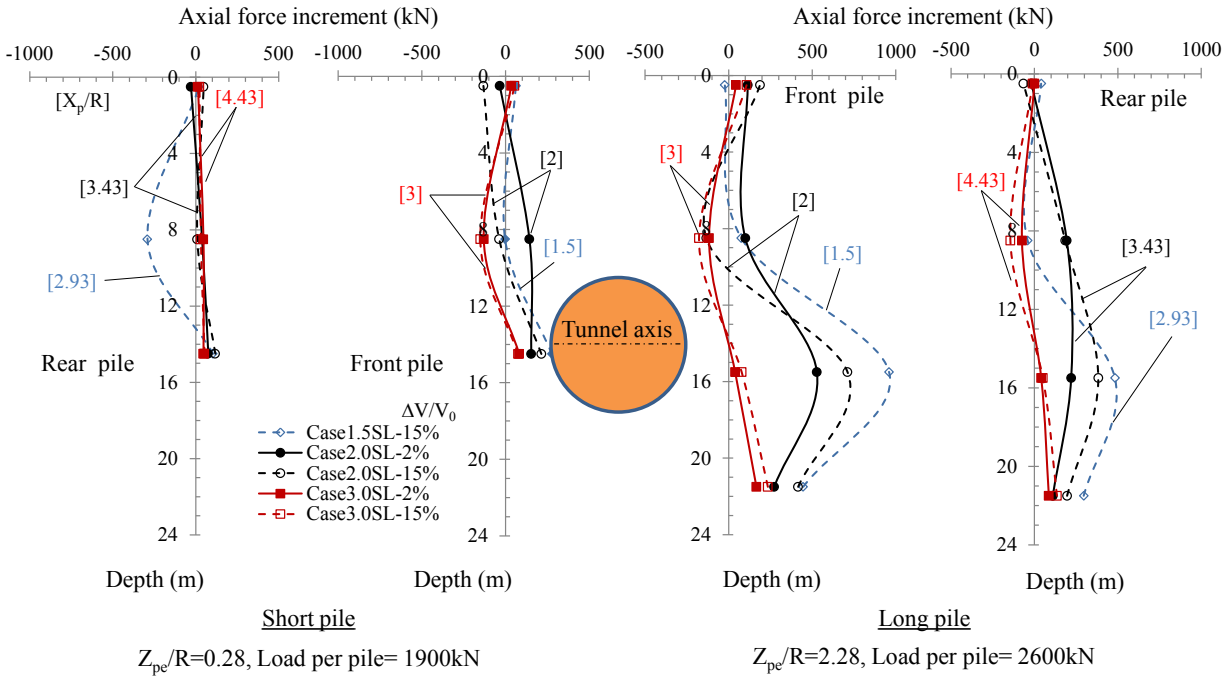

(c)

Figure 5.18 Pile axial force increment profile with depth at ground loss ratio of 2% and 15%: (a) test series B(1); (b) test series B(2); (c) test series C

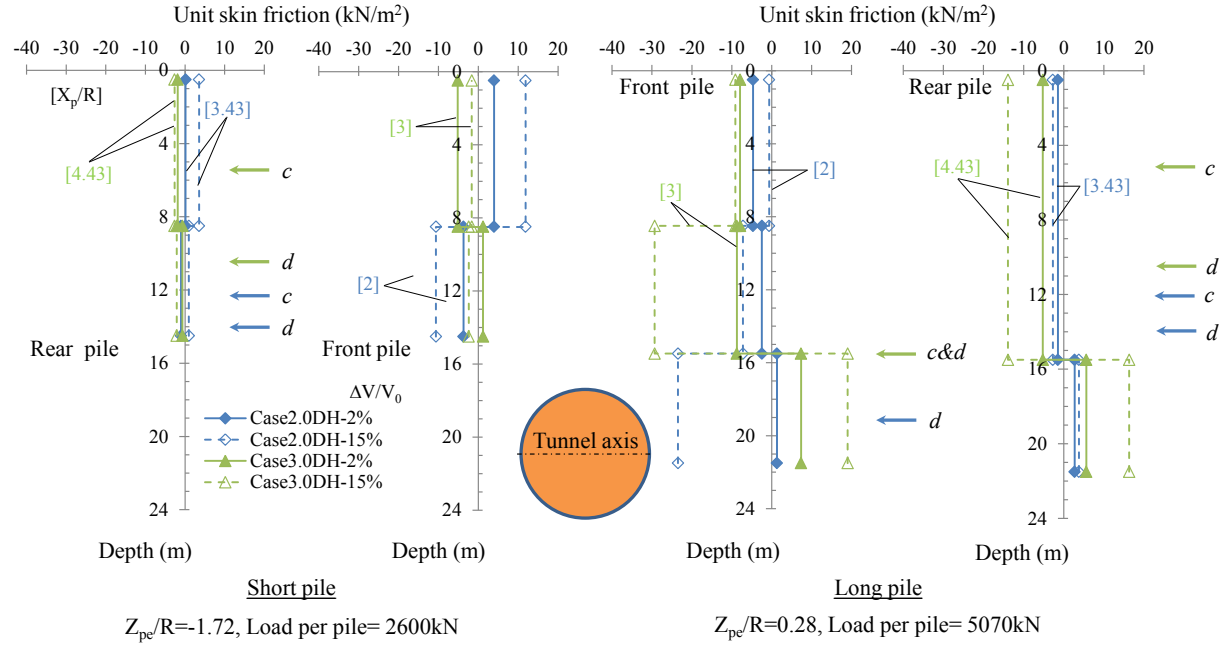

(a)

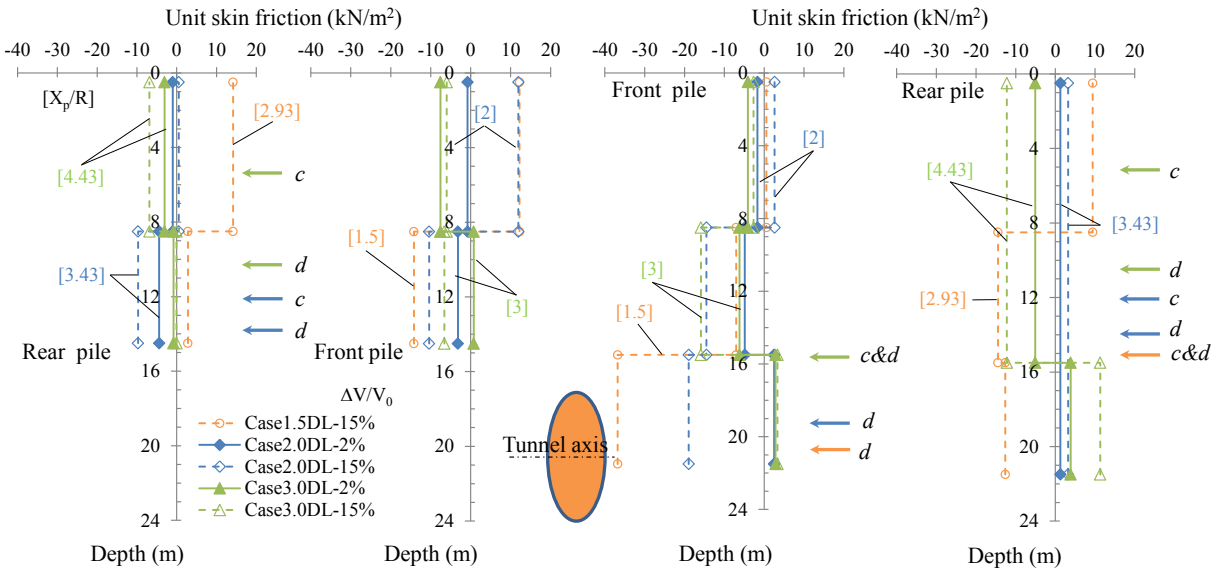

Z_{pe}/R=-1.72, Load per pile= 1900kN

Z_{pe}/R=0.28, Load per pile= 2600kN

(b)

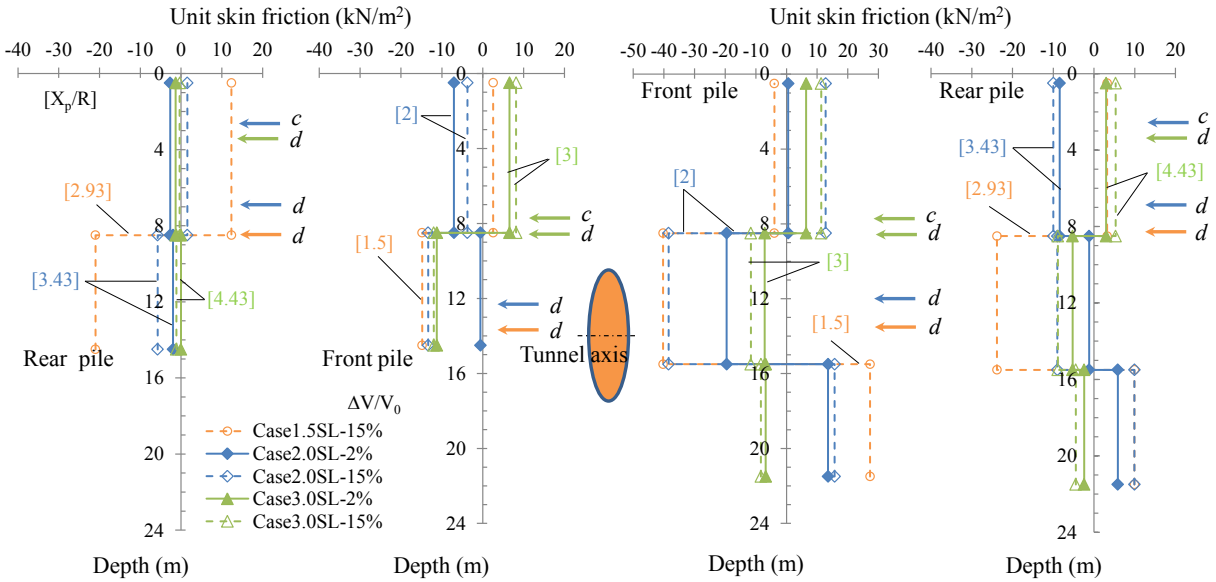

Z_{pe}/R=0.28, Load per pile= 1900kN

Z_{pe}/R=2.28, Load per pile= 2600kN

(c)

Figure 5.19 Mobilization of pile skin frictions by tunneling at ground loss ratio of 2% and 15% : (a) test series B(1); (b) test series B(2); (c) test series C

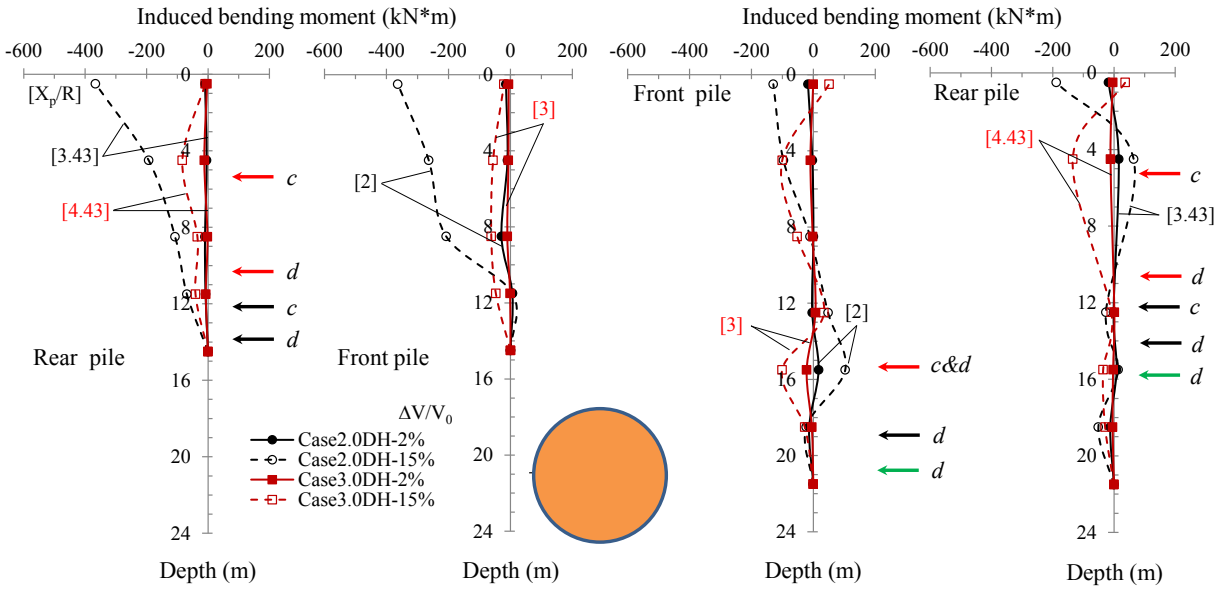

Z_{pe}/R=-1.72, Load per pile= 2600kN

Z_{pe}/R=0.28, Load per pile= 5070kN

(a)

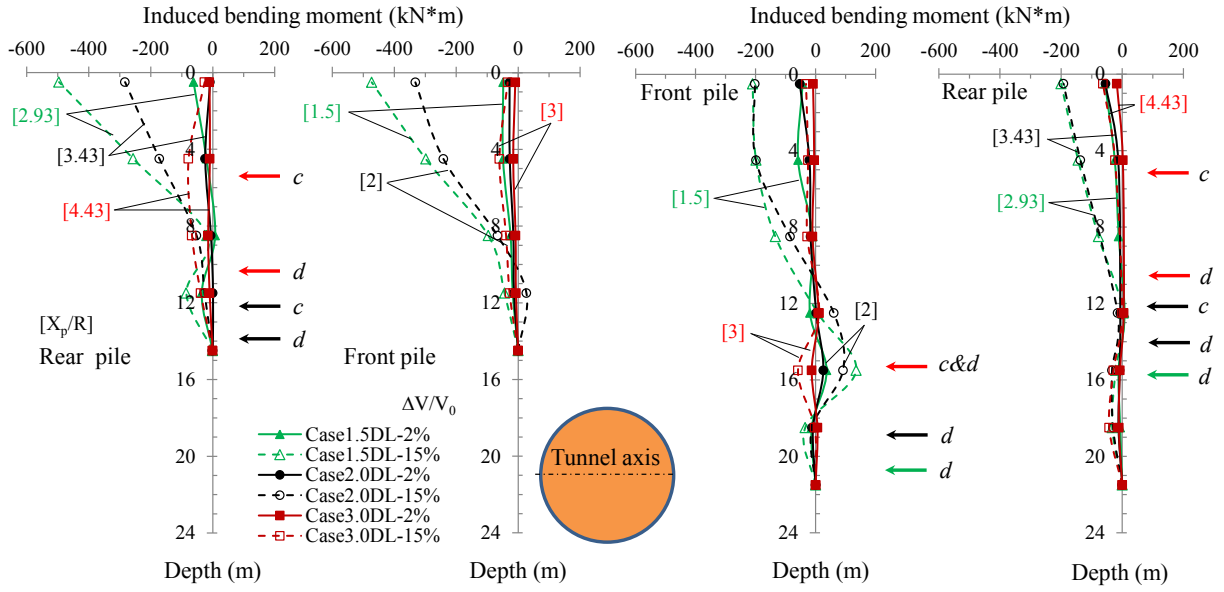

Z_{pe}/R=-1.72, Load per pile= 1900kN

Z_{pe}/R=0.28, Load per pile= 2600kN

(b)

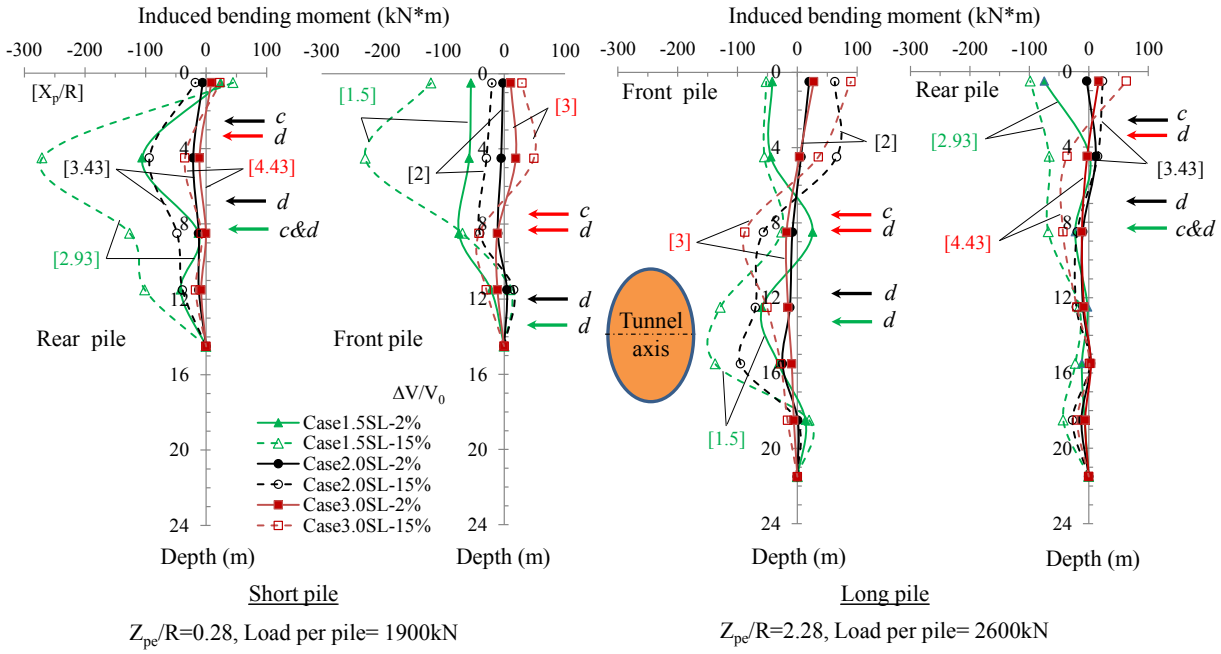

(c)

Figure 5.20 Pile bending moment profile with depth at ground loss ratio of 2% and 15%
(a) test series B(1); (b) test series B(2); (c) test series C

Chapter 6

Practical application of the study

6.1 Introduction

From the results of the previous chapter, the revised zone of influence from the **Jacobsz et al., (2004)** can be used to explain the development of axial force and bending moment along the piles. The magnitude of adverse effect for piles depends on the relative positions between pile and tunnel. If the piles are rested inside the zone of influence, the pile will suffer from the negative skin friction and the stress reduction caused by the large soil movement toward the tunnel. Therefore, the boundary of influence zone could be utilized to find the safe distance between existing pile and newly tunnel for planning of tunnel construction.

In the past, the investigations about the safe distance have been done by many researchers. **Bezuijen and Schrier (1994)** recommended the safe distance between tunnel and pile end is 2 times tunnel diameter. **Kaalberg et al. (2006)** performed the full-scale tests at Second Heinenoord tunnel to confirm the minimum distance between pile end and the tunnel which caused a reduction of stress around the pile ends during tunneling**.** The wooden piles (single and group) and concrete piles were installed prior to conducting the two directions of TBM under those piles with various distances. As a result, the piles showed large settlement than the soil surface when the piles were above the TBM passage. By the CPT tests and static ultimate bearing

tests, the pile bearing capacity had no effect by tunneling when the distance between piles and tunnel equaled to 0.25D in small ground loss ($\Delta V/V_0$< 2%). Therefore, from the overall results, the recommendation of safe distance between pile end and the tunnel is equal to 0.5D (X_p/R=2.0) at small ground loss ($\Delta V/V_0$ < 2%). The effect of ground loss for the safe distance need to be further investigated in the next step especially at large ground loss ratio. In addition, not only the bearing capacity is used for the safety criteria but also other criteria such as the vertical settlement and inclination (uneven settlement) are more important for an investigation.

6.2 The average value of pile end depth from the boundary of Zone C and D (Z_{da})

6.2.1 Proposal of equation for Z_{da} parameter

As discussed in the previous chapter, the displacements of pile cap are significantly influenced by X_p/R and Z_{pe}/R. In this study, the pile end depth from the boundary of Zone C and D, Z_d, is considered as a parameter which reflects the effect of X_p and Z_{pe}. The average value of pile end depth from the boundary of Zone C and D (Z_{da}) can be derived from the pile end depth of front pile (Z_{df}) and rear pile (Z_{dr}) as indicated in equation 6.1. (**Fig. 6.1**)

$$\frac{Z_{da}}{L} = \left(\frac{Z_{df}+Z_{dr}}{2}\right)\left(\frac{1}{L}\right) \qquad (6.1)$$

Where Z_{da} = average Z_d of the front pile (Z_{df}) and the rear pile (Z_{dr})

L = pile embedment length

Z_{df} = pile end depth from zone C and D of the front pile

Z_{dr} = pile end depth from zone C and D of the rear pile

As indicated in **Fig. 6.1**, the values of Z_{df} or Z_{dr} become negative and positive when the pile ends are rested shallower and deeper than the boundary of Zone C and D (line *c* and *d*) respectively. If the pile end position is exceeded the two times of inflection points ($2x_i$), normalized pile end depth from the boundary of Zone C and D and pile embedment depth (Z_{df}/L , Z_{dr}/L) will equal to 1. The reference line for Z_{da}/L is shown in **Fig. 6.2**.

From previous studies (**Standing (1996); Jacobsz et al., (2004); Loganathan et al., (2000)**), the distances of 2 times tunnel diameter (2D) above tunnel crown and below tunnel toe are conservative distance to avoid the effect of tunneling. Therefore, the proposed parameter (Z_{da}/L) can be applied if the pile ends positions are rested inside square area as indicated in **Fig. 6.1** – otherwise the effect from the tunnel is negligible when all of pile foundations are rested outside the square area. The validity of this proposed square area will be justified in the later section. From the past study, the piles will certainly induce large adverse effect when the piles are rested in Zone A. However, the effect is ambiguous when the pile is rested outside the Zone A and very near the tunnel.

The individual and average values of pile end depth from the boundary of Zone C and D are listed in **Table 6.1**.

6.2.2 Pile cap movement with normalized Z_{da} parameter and the limitation

In **Fig. 6.3- Fig. 6.5**, three displacement components of pile cap are plotted against Z_{da}/L (equation 6.1) and the displacements are shown in normal scale, and logarithmic scales in the figures to discuss the behavior for both small and large volume loss ratios. Negative value or small value of Z_{da}/L means the front pile of the pile group rested in the Zone B or close to the boundary between the Zone B and C (i.e. short pile group with C/D=2.5). From the figure, it can be confirmed that the condition of the front and rear piles resting in the large soil movement zone and less movement zone (the Zone D) respectively (i.e. Case1.5-DL of short pile group) caused large uneven settlement of pile group, resulting in large lateral movement and inclination at the pile cap.

There is a unique relation between the three components of pile cap movements (θ, δx, δz) and Z_{da}/L for the cases with the pile end depth deeper than the tunnel axis, regardless of pile length and tunnel cover and depth ratio. The values of displacements from three components tend to increase as the values of Z_{da}/L are reduced for both small and large ground loss ratio. In addition, this unique relation could be observed in the vertical settlement (δz) of short pile groups with the pile end depths shallower than the tunnel crown. However, the inclination (θ) and horizontal displacement (δx) showed the disconnected correlation in the range of Z_{da}/L from 0.3 to 0.4 (between X_p/R=3.0 of test B(1), B(2) and X_p/R=1.5 of test C as illustrated in **Fig. 6.6**). These behaviors indicated some limitation in Z_{da}/L parameter when the pile ends are rested at the tunnel elevation (test C series) and shallower than the tunnel (test B(1) and B(2) series).

The difference could be attributed to the difference of lateral soil displacement profile between the cases of C/D=1.5 and 2.5. The horizontal displacements near the ground surface (see **Fig. 6.8**) were not so different from x=1.5R to 4.5R for the large C/D, but for the small C/D it showed the larger value at x=1.5R to 2.0R and significantly reduced as x increased. In C/D=1.5, the soil horizontal movement tend to induce more inclination of pile than the case with C/D=2.5 as indicated by blue line in **Fig.6.8**.

In addition, the development of bending moment of short pile group between case3.0-DL was significantly smaller than case1.5-SL (See **Fig. 6.9**). Pile ends of test C also embedded in less displacement zone (Zone D) and very close to the tunnel which leaded to induced more bending moment because the pile ends behaved like a fixed end condition.

The pile cap horizontal movement and inclination depend on the combined mechanisms of induced soil horizontal movements and the pile deflection caused by bending moment as shown in **Fig. 6.7.** Pile end is moved horizontally (δx_{pe}) by the induced soil horizontal movements and pile is deflected (θ_p) by the induced bending moment along the pile. As a result, pile cap horizontal movement will equal to the following equation.

$$\delta x = \delta x_{pe} + L' tan\theta_p \qquad (6.2)$$

Where δx = horizontal movement of pile cap

δx_{pe} = horizontal movement of pile end

θ_p = angle of pile deflection

L’ = total length of pile

Nevertheless, not only induced bending moment is related to the pile cap inclination, but also the effect of differential settlements between the front and the rear pile is also affected the magnitude of pile cap inclination.

As the zoning was made based on the vertical soil displacement, there is a limitation of the applicability of Z_{da}/L as a parameter which includes the effects of both X_p/R and Z_{pe}/R. However, the effect of X_p became small when the piles end rested deeper than the line *c* and *d* of zone boundary ($Z_{da}/L > 0.5$) which can be confirmed for all three components of pile cap movement of the long pile groups in case C series. In overall results, it shows that the vertical settlement is reduced as the Z_{da}/L increases.

To find a suitable parameter for improving those disconnected trends, the parameter of relative pile end depth from the boundary of Zone C and D of front pile (Z_{df}/L) is selected to plot against the vertical settlement (δz), horizontal displacement (δx) and inclination (θ) of short pile group as shown in **Fig. 6.10-6.12**. In the figures, the values of Z_d/L of front pile become smaller than the average Z_d/L because it does not include the values of Z_d/L of the rear pile. In addition, there is a gap between test series B and C and the disconnected pattern in horizontal movement and inclination of short pile results are still present in the plot with Z_{df}/L. In addition, horizontal movement (δx) and inclination (θ) of short pile are plotted with the average pile portion in Zone B and C as illustrated in **Fig. 6.13**. The average pile portion equals to 1 if the entire pile portion is rested inside the Zone B and C and the value equals to 0 if the entire pile portion as indicated in **Fig. 6.13**. In **Fig. 6.13(c)**, the entire portion of front pile is rested inside Zone B and C and 80% of rear pile portion is rested inside zone B and C. Therefore, the average value of pile portion in Zone B and C equals to 0.9 as indicated in **Fig. 6.13(a)**. In **Fig. 6.13(a), 6.13(b)**, the disconnected trends between test series B and C still appear due to the difference of soil horizontal movement and induced bending moment as explain before. Finally, the results imply that the average value of Z_d/L between front and rear pile (Z_{da}/L) is more suitable to represent the response of piles than the individual value of Z_d/L and average pile portion in Zone B and C.

The pile cap movements are significantly reduced when the pile ends are considerably deeper than the tunnel elevation ($Z_{pe}/R = 2.28$) and the pile groups are located horizontally far from the tunnel ($X_p/R = 3.0$). Therefore, the distance of 2D from the toe of tunnel and the horizontal distance of $2x_i$ are the approximately area to apply the Z_{da}/L parameter for investigating the preliminary assessment of building safety (**Fig. 6.1**).

6.2.3 Building assessment with normalized Z_{da} parameter

Boscardin and Cording (1989) indicated the three damage definitions from the possible adverse effect (i.e. differential settlement) from the tunnel excavation by the following.

(a) **Architectural damage**: the damage does not affect the functional ability of the structure. It usually appears with the crack on the wall panel or finishes. The threshold for the wide of crack equal to 1/64 inch of plaster wall and 1/32 inch for masonry wall

(b) **Functional damage**: this type of damage is affected by the utility of building functions such as falling plaster, jammed door or window and inclined floor

(c) **Structural damage** the building may collapse due to the distortions of main support elements such as columns, beams, and shear wall.

The assessment of stability from damages structures due to ground movement from excavation or seismic motion from the earthquake have to be conducted to the decision between reinforcement or rebuilt those structures. The uneven settlement of structures which can lead to additional and unexpected stresses on members and joints becomes one of the important parameters to assess the building stability. **J. McCormick et al., (2008)** proposed the permissible residual deformation based on safety, functionality and construction tolerances. Residual deformation consists of an inclination of horizontal members and tilt of vertical members. The perceptions of the human and physical ailment are one of the important parameters to consider the allowable inclination angle (**Kaga et al., 2005; Seto et al., 2006**). The recommended values which do not intervene the living for the people are between 0.005 rad- 0.006 rad (**Yasuda and Hashimoto, 2002; Fujii et al., 2002**). In addition, **Japanese Law Publication (2000)** provides the limitation of non-functional building when the inclination is exceeded 0.006 rad. In construction tolerance, the tolerance for wood frame and reinforced concrete structures is estimated at 0.003 rad (**AIJ, 1997**) and the tolerance for steel-frame structures is approximately around a half of reinforced concrete structure (**AIJ, 1996**). For the safety aspect, when the door frame is tilted larger than the 0.005 rad, it will affect the functional evacuation system (**McCormick et al. 2008**).

The inclinations are plotted against ground loss ratio with various average relative depths from the boundary of Zone C and D (Z_{da}/L) as shown in **Fig. 6.14**. The variation of Z_{da}/L are derived from the test series B(2) and C with the same vertical loads on the pile caps. The values

of relative horizontal distance from the tunnel center to the front pile (X_p/R) are also arranged in the caption. In the figure, the construction tolerance value of inclination at 0.003 rad (**AIJ, 1997**) and the safety tolerance value at 0.005 rad (**McCormick et al. 2008**) are indicated by the broken lines. The maximum inclination of building and damage pattern are listed in **Table 6.3**. The cases with large value of Z_{da}/L (Case2.5-SL (Z_{da}/L=0.66); Case3.0-SL (Z_{da}/L=0.75) of short pile group and Case2.0-SL (Z_{da}/L=0.69); Case2.5-SL (Z_{da}/L=0.77); Case3.0-SL (Z_{da}/L=0.83) of long pile group) tended to develop the inclination less than the construction tolerance (green broken line in the **Fig. 6.14**). In **Table 6.2**, the possibly induced ground loss with quality of construction and ground conditions are summarized ("**Technical manual," (2014)**). It shows that the ground loss in usual construction could not occur larger than 4% ground loss. Therefore, in tunnel excavation, the cases with induced inclination exceed the safety tolerance (red broken line in the **Fig. 6.14**) at 4% ground loss should be avoid to excavation in those positions (Case1.5-DL (Z_{da}/L=-0.21); Case2.0-DL (Z_{da}/L=-0.04); Case1.5-SL (Z_{da}/L=0.26) of short pile group and Case1.5-DL (Z_{da}/L=0.17); Case2.0-DL (Z_{da}/L=0.29) of long pile group).

In the limitation of vertical settlements, **Rankin (1988)** proposed the tolerance of maximum vertical settlement for the building as shown in **Table 6.4**. From the table, the maximum settlement for the safety of the structure equal to 10mm and the structure may trigger the damage on the building when the maximum settlement larger than 50 mm. Therefore, the vertical settlements were plotted against the ground loss ratio with various Z_{da}/L from test series B(2) and C as shown in **Fig.6.15.** The safety tolerance (10 mm) for the vertical settlement is indicated in the figure by the green broken line and the tolerance of settlement which can trigger damage to the structure (50 mm) is also indicated by the red broken line. As a result, in **Fig. 6.15**, the case with large value of Z_{da}/L (Case2.5-SL (Z_{da}/L=0.66); Case3.0-SL (Z_{da}/L=0.75) of short pile group and Case2.0-SL (Z_{da}/L=0.69); Case2.5-SL (Z_{da}/L=0.77); Case3.0-SL (Z_{da}/L=0.83) of long pile group) tended to develop the vertical settlement less than the safety tolerance at 10 mm (green broken line). In addition, the cases with exceed the safety tolerance (red broken line in **Fig. 6.15**) which are similar to the limitation of inclination are Case1.5-DL (Z_{da}/L=-0.21); Case2.0-DL (Z_{da}/L=-0.04); Case2.5-DL (Z_{da}/L=0.13) of short pile group and Case1.5-DL (Z_{da}/L=0.17); Case2.0-DL (Z_{da}/L=0.29); Case2.5-DL (Z_{da}/L=0.41) of long pile group.

From the limitation of two criteria (inclination and vertical displacement of pile cap), Z_{da}/L parameter could be used as a preliminary assessment for prevent the damage to the adjacent pile foundations. The excavation should be avoided in the positions which provide small values

of Z_{da}/L. From **Fig.6.14** and **Fig.6.15**, the range values of Z_{da}/L that provide the less effect from tunneling are summarized in **Table 6.5**.

In addition, with the safety tolerance (red broken line) on inclination (θ) and vertical settlement (δz), the allowable ground loss ratio ($\Delta V/V_o$) for each values of Z_{da}/L could be estimated as indicated in **Table 6.6**.

Therefore, the excavation should be avoided in the relative positions which give the normalized average values of pile end depth from the boundary of Zone C and D (Z_{da}/L) less than 0.4 and small effect from tunneling when Z_{da}/L is larger than 0.65 as listed in **Table 6.5**. In the intermediate zone, tunnel could be excavated in these positions with ground loss control.

6.3 Mitigation of adverse effect to adjacent foundation

As mention in the previous section, the intermediated zone with Z_{da}/L =0.4-0.65 (**Table 6.6**) is possible to construct the tunnel if the excavation carefully controls soil movement caused by the ground loss ratio ($\Delta V/V_o$). Many researchers tried to find the effective solution to mitigate the soil movement due to the ground loss from underground construction such as development the tunnel machine, ground movement control technique, grouting technique, ground barrier technique etc.

A. Gens et al. (2006) presented the mitigation methods to ground movement at a new metro line in Barcelona by a jet grouted columns, compensation grouting, and structural jacking. Even the cover ground is considerable large, there is a chance to induce the damage to adjacent structures. Consequently, the ground control techniques are significantly important in the major of the new tunnel construction project. The installation of a structural element (i.e. diaphragm wall, pile, jet grout column) between the excavation and the nearby buildings is one of the popular methods. Jet grout column shows advantage point of high flexible for installation among the structural element methods. From the study, the jet grouting method could be enhanced by improvement of soil removal and this method performed great outcome to reduce the ground settlement especially at the elevation near the soil surface. In the sensitive area for ground movement, a structural jacking provided an effective result better than the compensation grouting due to a directly acting on the concern structures. The fundamental concept for structural grouting is to control the differential movements between the various parts of the structure. Finally, the selection of ground minimization methods depend on the characteristics of the construction site, accessibility, the relative position between tunnel and structures and ground conditions.

E. Bilotta et al., (2006) proposed the method to prevent the soil movement to a nearby structure using diaphragm wall in between tunnel and the protected structures by numerical analysis. The mitigation ground displacement is very important to the adjacent sensitive foundation such as historic buildings. An analysis was conducted by the code PLAXIS in effective stresses and undrained conditions. The various lengths of diaphragm wall were installed in the range of 1-1.5D away from the tunnel (D = tunnel diameter). With the different distance from the tunnel, the reduction of soil movements is identical. The effectively embedded depths of diaphragm wall were approximately equal to 2-2.5C for heavy wall type and 1.5-2C for light wall type (C = soil cover depth). In addition, the magnitude of soil settlement reduction of light weight wall was larger than the heavyweight wall. In both different weight cases, there was no effect of soil reduction, when the embedment depth of diaphragm wall was deeper than 3-3.5C. The stiffness and thickness of the wall also showed no difference in reduction between flexible and rigid wall. The smooth wall had more effective soil reduction than the rough one.

6.4 Conclusion

The pile depth in the less movement zone (Z_d) can be used as a parameter, which incorporate the effects of relative horizontal distance (X_p) and relative positions between pile end and tunnel center (Z_{pe}). The behavior of pile group is controlled by component of the front and rear piles. Therefore, the average of pile depth in the less movement zone (Z_{da}) between front pile (Z_{df}) and the rear pile (Z_{dr}) is introduced. This parameter will be normalized by the pile embedment depth (L).

The plot between pile cap movement and relative depth from the zone to the pile length (Z_{da}/L) showed some unique trend. The values of Z_{da}/L increased with a decrease of vertical settlement (δz) of pile cap at small to large ground loss ratio. These trends can also be applied to the inclination (θ) and lateral movement (δx) if pile ends are rested deeper than the tunnel as shown in long pile group results. However, the short pile groups with pile ends are rested inside and outside Zone B and C (between test series with C/D = 1.5 and 2.5, **Fig. 6.6**) showed the disconnected trends of lateral movement and inclination with Z_{da}/L. The results indicated the limitation of Z_{da}/L parameter in the lateral and inclination movement in the range of $0.3 < Z_{da}/L < 0.4$. It may come from the combined effects of the lateral movements and the pile deflection when the pile end is very close to the tunnel ($X_p/R \leq 2.0$).

In **Fig.6.3** and **6.4**, the magnitude of inclination and lateral movement of the cases with $X_p/R \leq 2.0$ (i.e. Case1.5-SL of short pile group) were larger than the cases with similar relative pile depth in the less movement zone (Z_{da}/L) but the position is far from the tunnel (i.e. Case3.0-DL of short pile group). In addition, it was found that when the relative depth of the zone to the pile length (Z_{da}/L) was larger, the effect from X_p became small. In other words, the pile groups with large magnitude of Z_{pe} showed small lateral movement and inclination of pile cap, even though, the front piles were close to the tunnel. Therefore, the results from long pile group showed the unique trend between Z_{da}/L and three components of pile cap movement.

The allowable ground loss ratio ($\Delta V/V_o$) with various positions from the tunnel could be estimated by applying Z_{da}/L parameter for required displacements of the foundation. The example of how to use the Z_{da}/L parameter is presented in this dissertation. Furthermore, this parameter needs to be verified for confirming its applicability make more applicable by testing with various condition such as changing the pile material, changing the soil conditions (clay or multi layers of soil). The allowable ground loss ratio ($\Delta V/V_o$) could be changed by the field conditions, but the concept will raise some awareness to the design engineer. As a result, the design engineer should prepare the suitable methods to mitigate the adverse effects if the tunnel is needed to be constructed in the position with small Z_{da}/L (< 0.4).

Table 6.1 The individual and the average value of pile end depth from the boundary of Zone C and D

Case	C/D	Short pile group			Long pile group		
		Z_{df}/L	Z_{dr}/L	Z_{da}/L	Z_{df}/L	Z_{dr}/L	Z_{da}/L
Case2.0-DH	2.5	-0.27	0.18	**-0.04**	0.14	0.45	**0.29**
Case2.5-DH		-0.15	0.41	**0.13**	0.22	0.61	**0.41**
Case3.0-DH		-0.02	0.64	**0.31**	0.31	0.77	**0.54**
Case1.5-DL		-0.38	-0.03	**-0.21**	0.06	0.28	**0.17**
Case2.0-DL		-0.27	0.18	**-0.04**	0.14	0.45	**0.29**
Case2.5-DL		-0.15	0.41	**0.13**	0.22	0.61	**0.41**
Case3.0-DL		-0.02	0.64	**0.31**	0.31	0.77	**0.54**
Case1.5-SL	1.5	0.09	0.43	**0.26**	0.39	0.62	**0.50**
Case2.0-SL		0.20	0.85	**0.53**	0.47	0.91	**0.69**
Case2.5-SL		0.32	1.00	**0.66**	0.55	1.00	**0.77**
Case3.0-SL		0.49	1.00	**0.75**	0.67	1.00	**0.83**

Table 6.2 Various ground loss values with construction practice and ground conditions ("**Technical manual," (2014)**)

Quality of construction practice and	ground conditions	Ground loss (%)
Good practice and tight control of face pressure	Firm ground	0.5
Normal practice with closed face machine	Slowly raveling ground Squeezing ground	1.0
Poor practice with closed face machine	Raveling ground	2.0
Poor practice with closed face machine	Fast raveling Poor ground	3.0
Poor practice with little face control	Running ground	> 4.0

Table 6.3 Maximum inclination and the effect (**AIJ, 1997; Kaga et al., 2005; McCormick et al., 2008**)

Maximum inclination of building (rad, °)	Damage pattern
0.003 rad (0.17°)	Negligible: Construction tolerance
0.005 rad (0.29°)	Functionality: damage to door system, rigid frame, and an overall hindrance to daily life

Table 6.4 Maximum vertical settlement and the effect (**Rankin, 1988**)

Maximum settlement of building (mm)	Damage pattern
< 10	Negligible: superficial damage does not occur
10-50	Slight: superficial damage may occur but does not significantly damage to the main structure
50-75	Moderate: superficial and structural damage are occurred and possible damage to the rigid pipeline
> 75	High: buildings are damaged in both superficial and structural component and possible damage to the pipeline system

Table 6.5 Summation of normalized average values of pile end depth from the boundary of Zone C and D (Z_{da}/L) for safety and damaged zones to the adjacent pile foundation

Description of zones	Z_{da}/L			
	Inclination		Vertical settlement	
	Short Pile group	Long Pile group	Short Pile group	Long Pile group
Negligible zone	0.66 0.75	0.69 0.77 0.83	0.66 0.75	0.69 0.77 0.83
Intermediate zone	0.13 0.31 0.53	0.41 0.50 0.54	0.26 0.31 0.53	0.41 0.50 0.54
Damaged zone	-0.21 -0.04 0.26	0.17 0.29	-0.21 -0.04 0.13	0.17 0.29

Table 6.6 Summation of allowable ground loss ration by range of Z_{da}/L

Inclination (θ)		Vertical settlement (δz)	
Z_{da}/L	$\Delta V/V_o$	Z_{da}/L	$\Delta V/V_o$
< 0	2.0-2.5%	< 0	2.5-3.0%
0-0.3	2.5-3.0%	0-0.3	3.0-4.5%
0.3-0.5	3.0-4.0%	0.3-0.5	4.5-6.5%
0.5-0.65	4.0-5.5%	0.5-0.65	8.0-10.0%
> 0.65	Negligible	> 0.65	Negligible

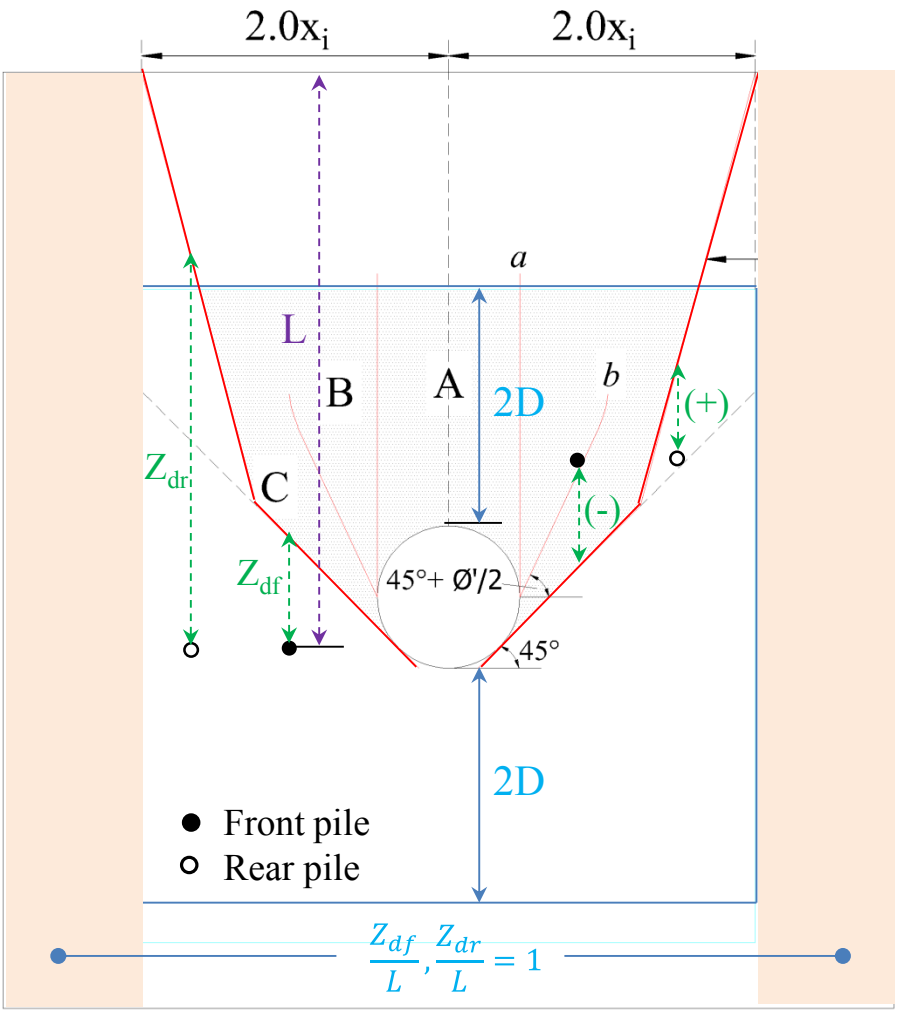

Fig.6.1 Pile end depth of the front and the rear pile from the boundary of Zone C and D

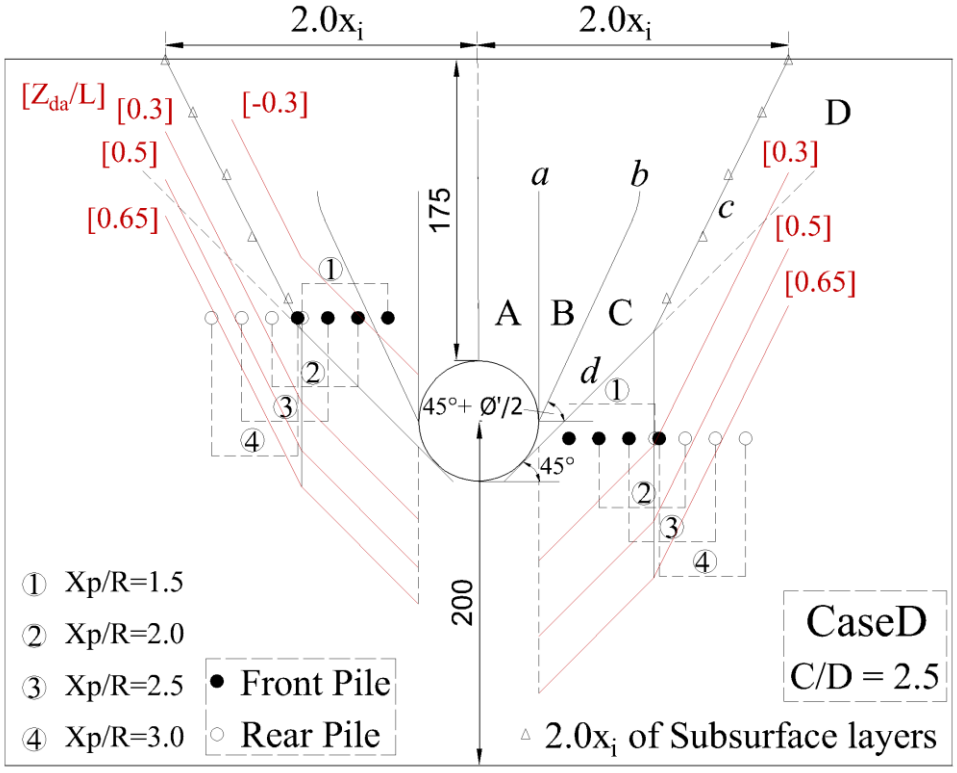

(a)

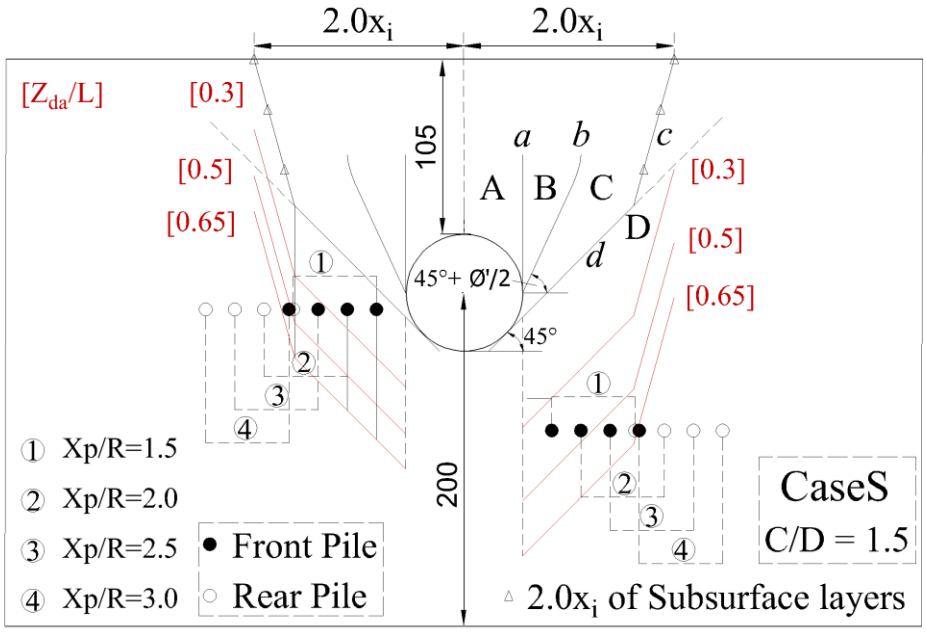

(b)

Fig.6.2 Zone of influence and reference line for value of Z_{da}/L

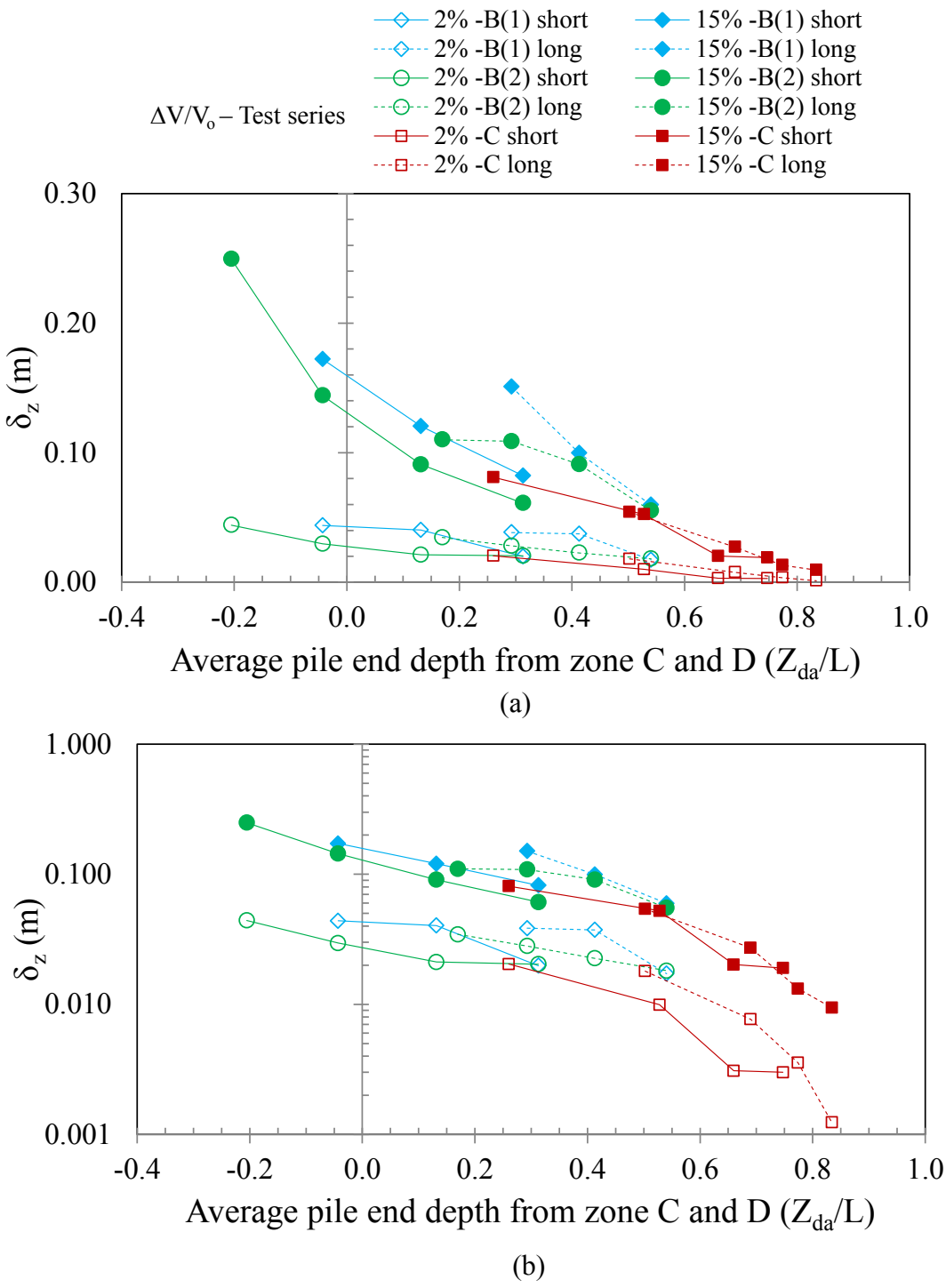

Fig.6.3 Comparison of vertical settlement of the pile cap at the ground loss ratio of 2% and 15% with average relative depth from the boundary of Zone C and D:
(a) Normal scale; (b) logarithmic scale

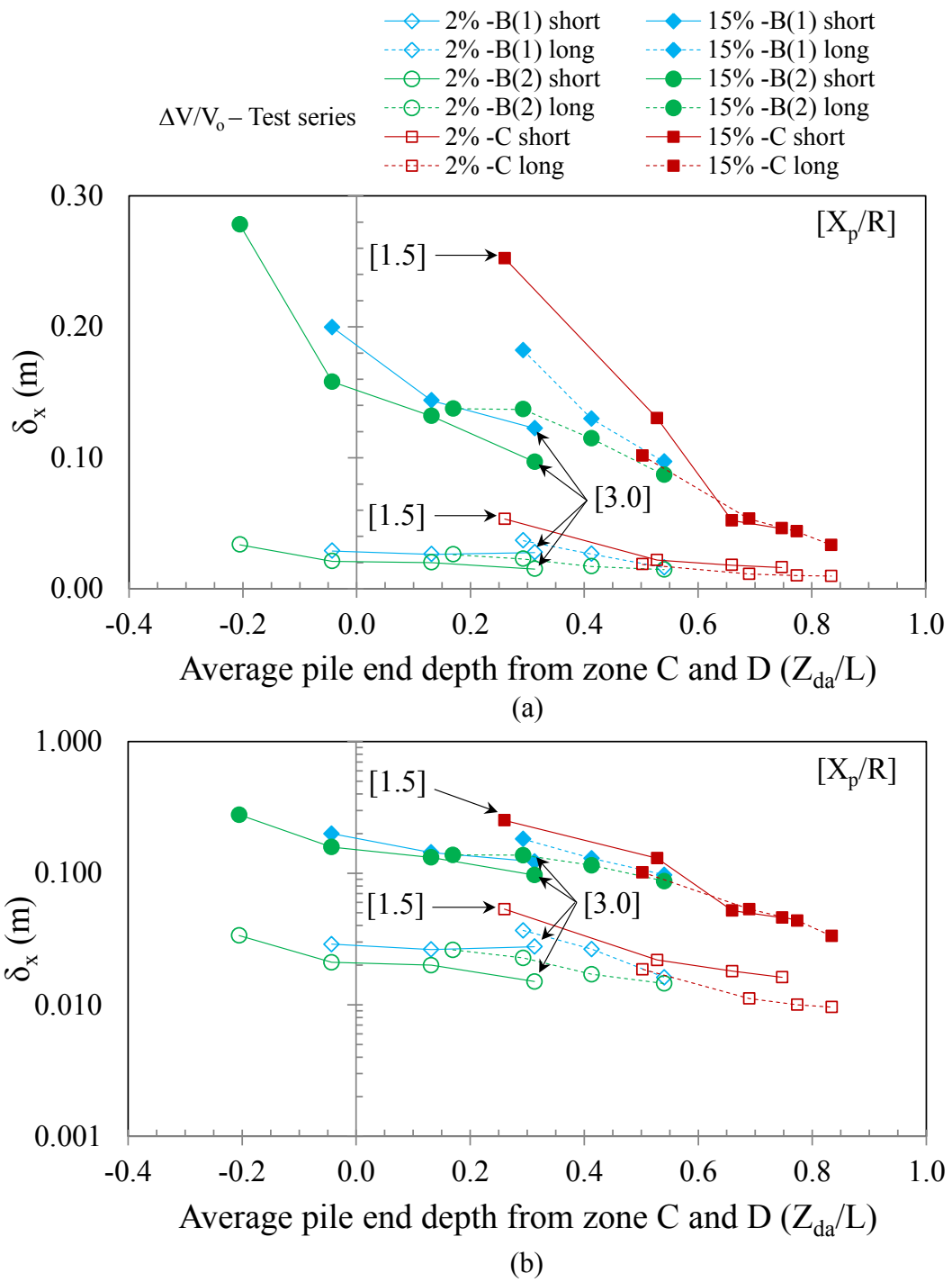

Fig.6.4 Comparison of horizontal movement of the pile cap at the ground loss ratio of 2% and 15% with average relative depth from the boundary of Zone C and D:
(a) Normal scale; (b) logarithmic scale

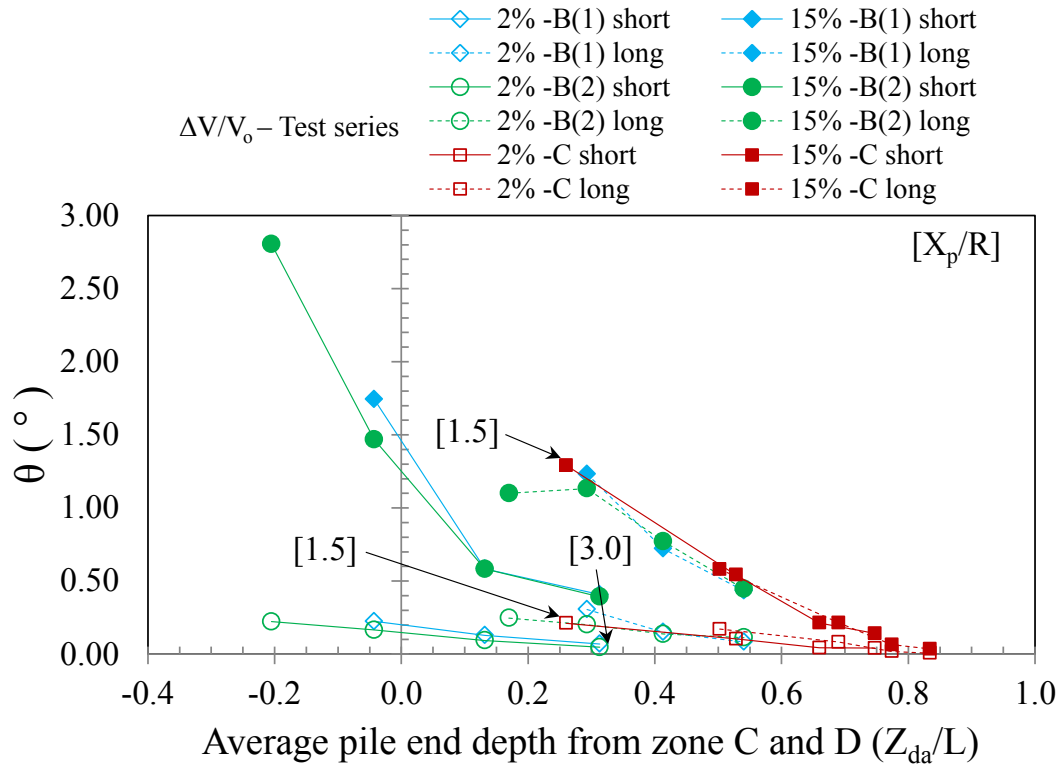

(a)

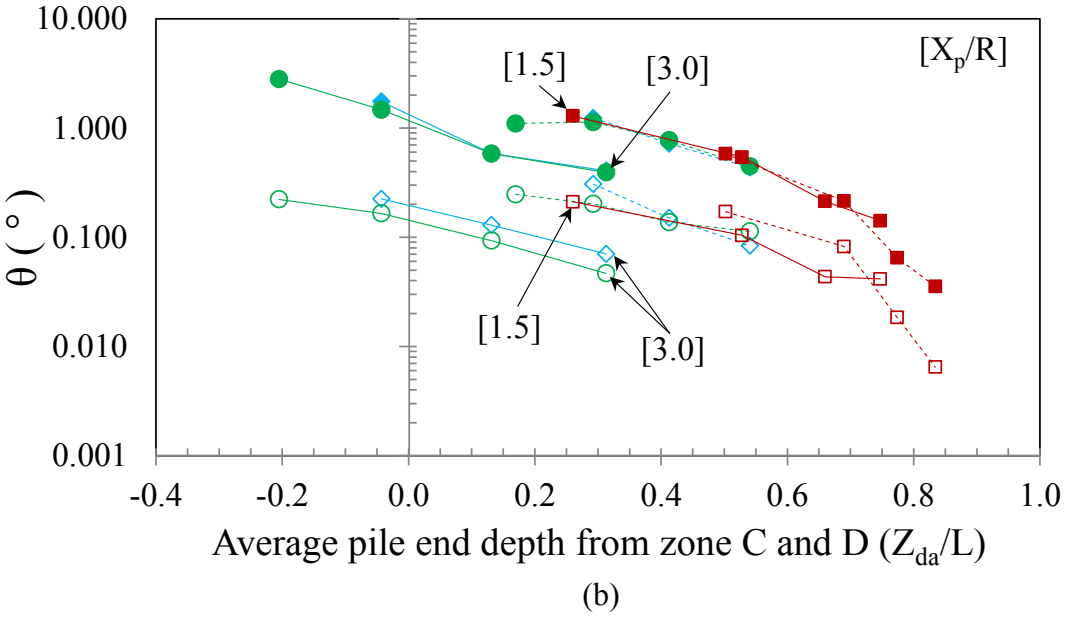

(b)

Fig.6.5 Comparison of inclination of the pile cap at the ground loss ratio of 2% and 15% with average relative depth from the boundary of Zone C and D:
(a) Normal scale; (b) logarithmic scale

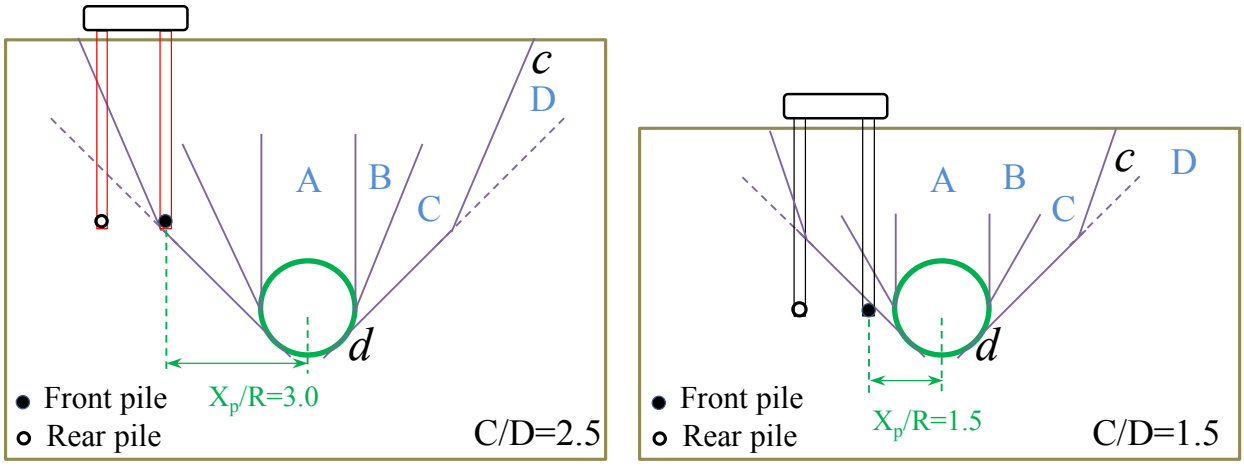

Fig. 6.6 Short pile positions with similar Z_{da}/L values: (a) Case3.0-DL; (b) Case1.5-SL

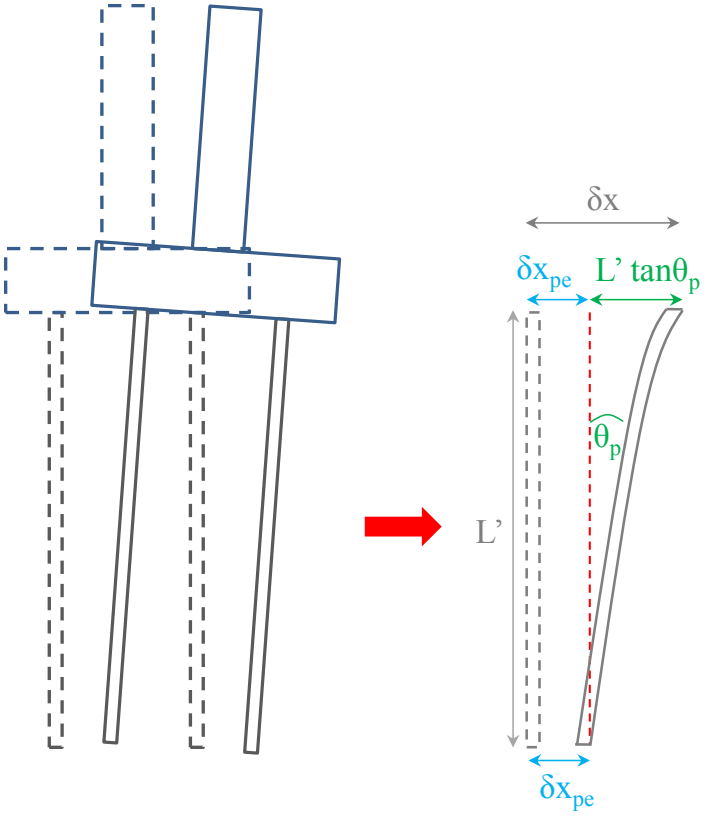

Fig. 6.7 The combined mechanism of pile horizontal movement and pile deflection for horizontal movement and inclination of pile cap

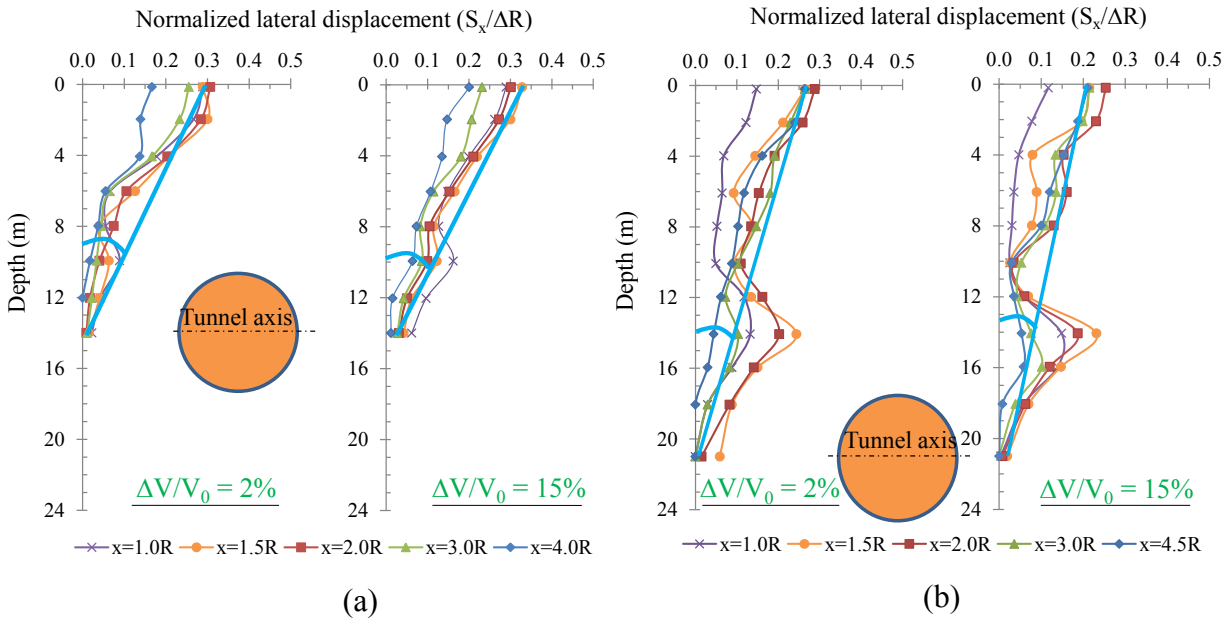

Fig. 6.8 Induced inclination of pile caused by horizontal movement of soil:
(a) C/D=1.5; (b) C/D=2.5

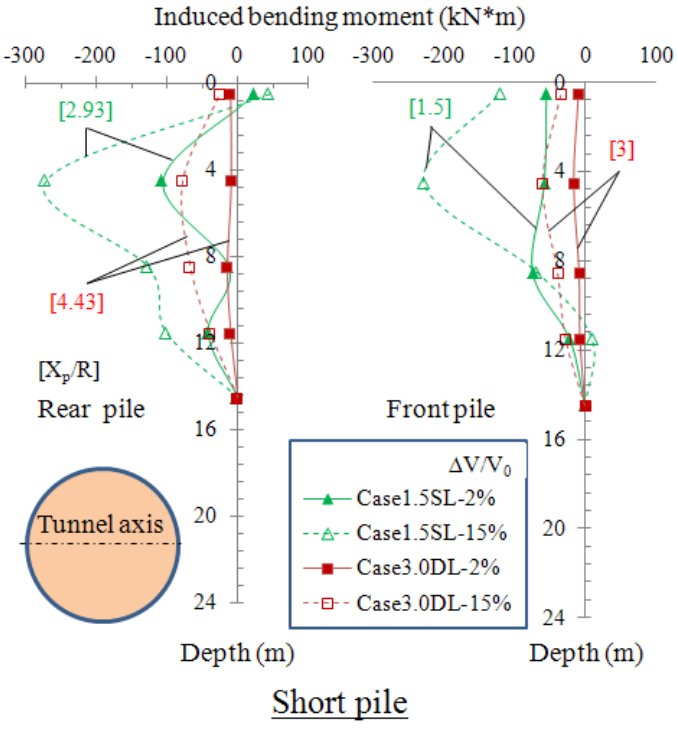

Fig. 6.9 Comparison of induced bending moment along short pile between Case1.5SL and Case3.0DL

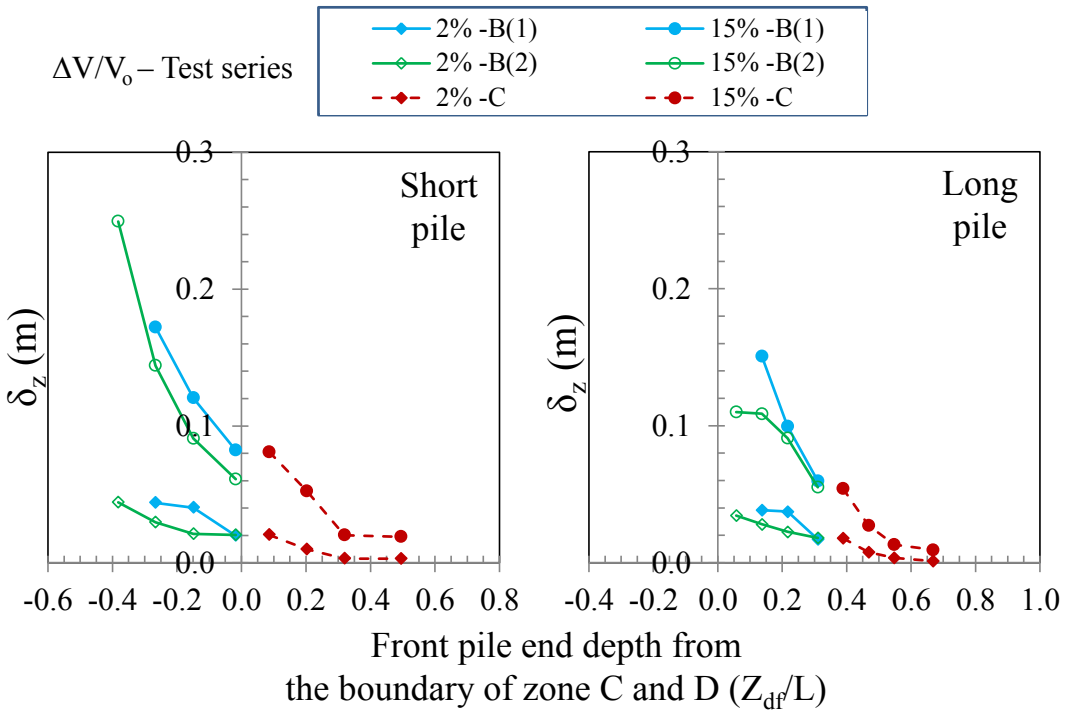

(a)

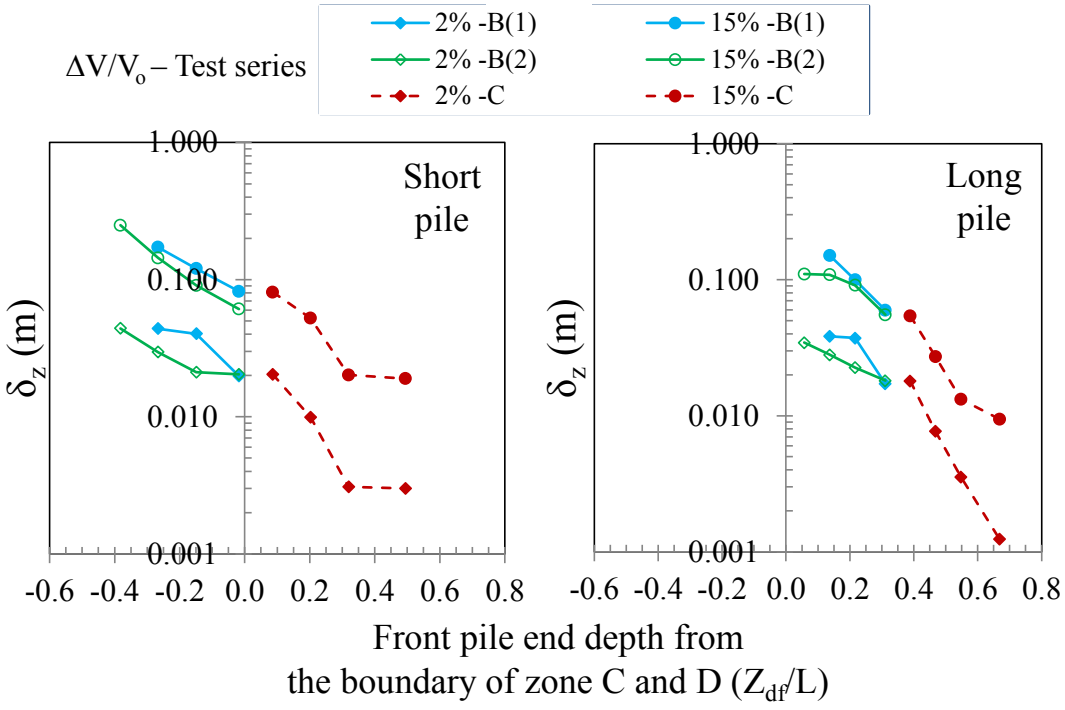

(b)

Fig.6.10 Comparison of vertical settlement of the pile cap at the ground loss ratio of 2% and 15% with relative depth of front pile from the boundary of Zone C and D: (a) Normal scale; (b) logarithmic scale

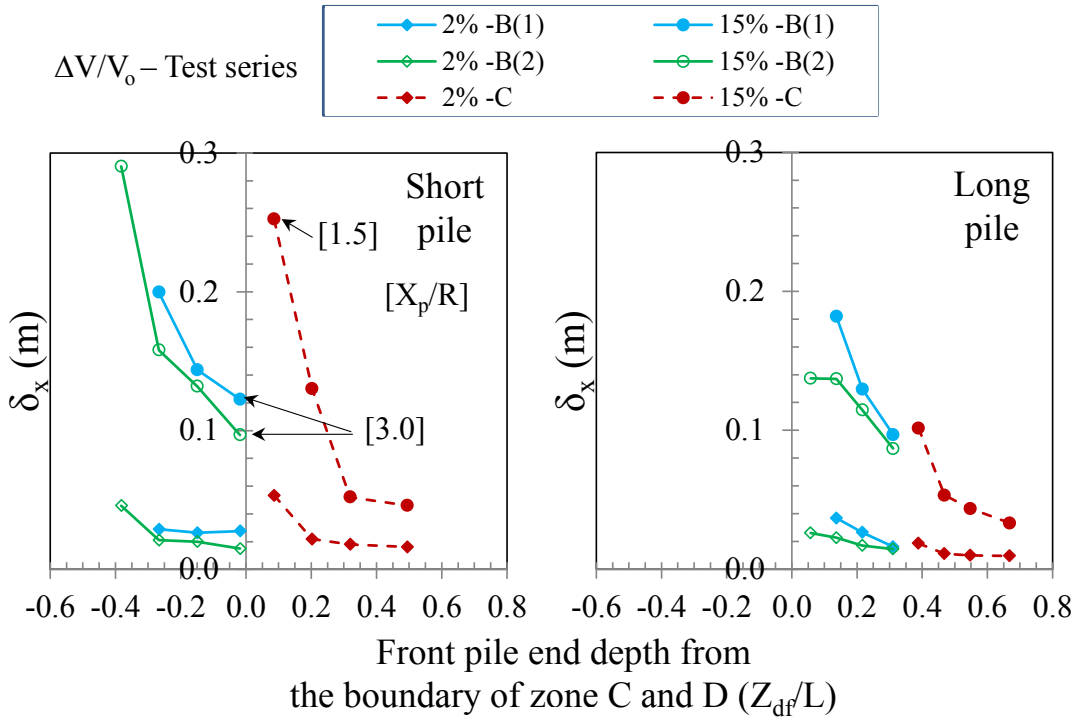

(a)

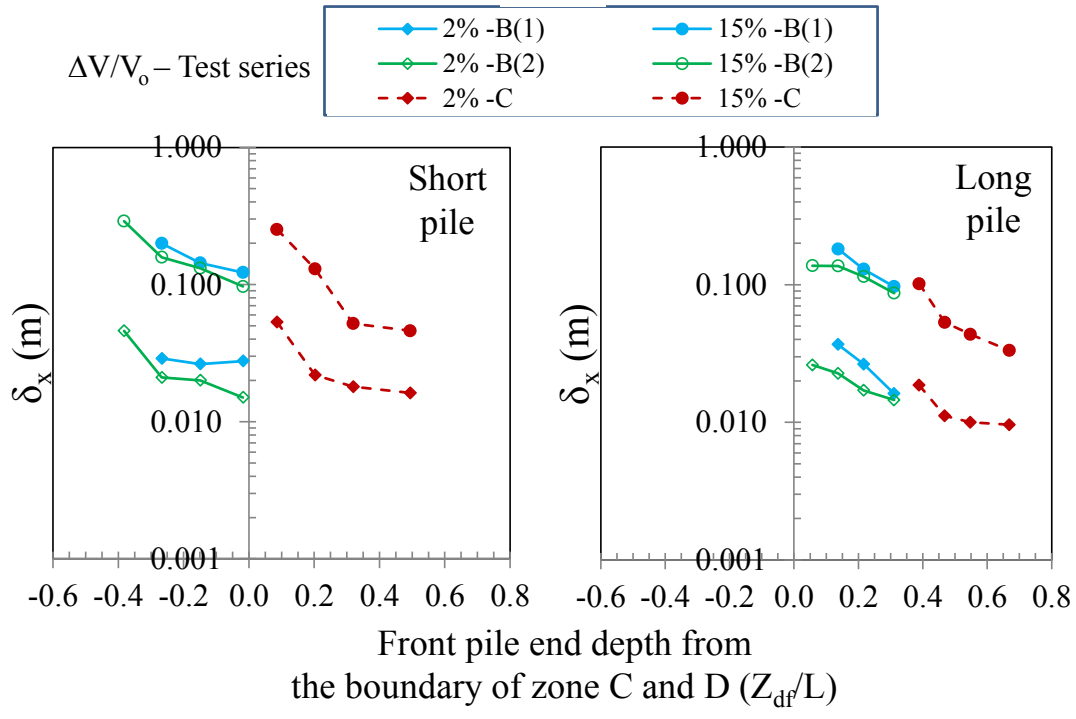

(b)

Fig.6.11 Comparison of horizontal movement of the pile cap at the ground loss ratio of 2% and 15% with relative depth of front pile from the boundary of Zone C and D:
(a) Normal scale; (b) logarithmic scale

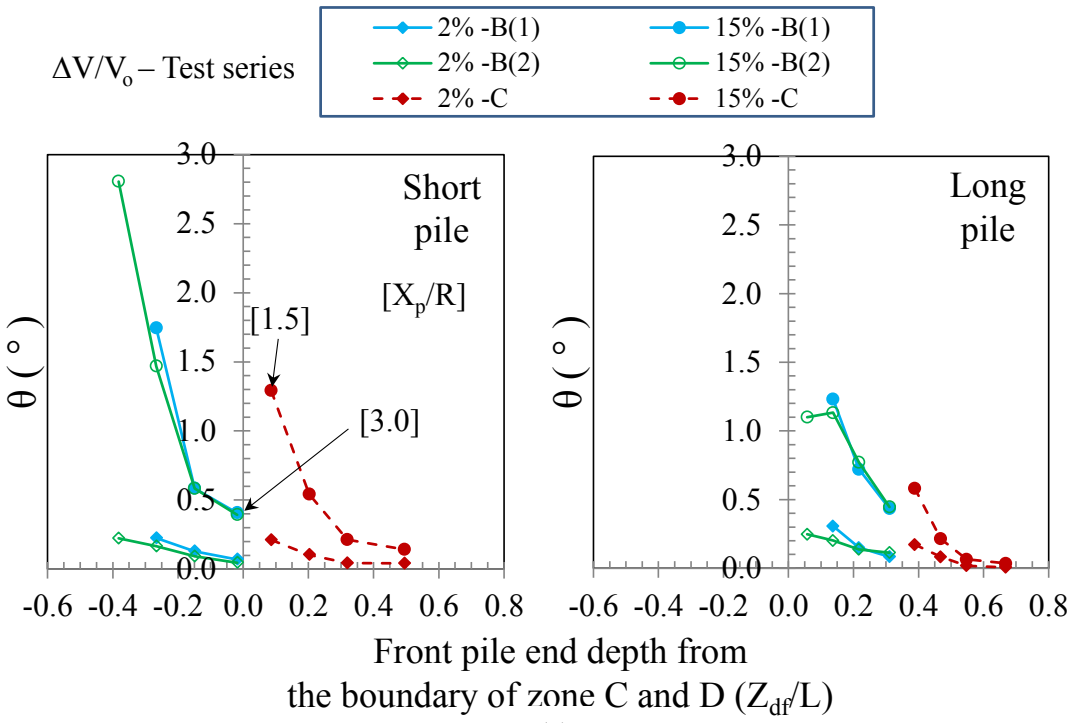

(a)

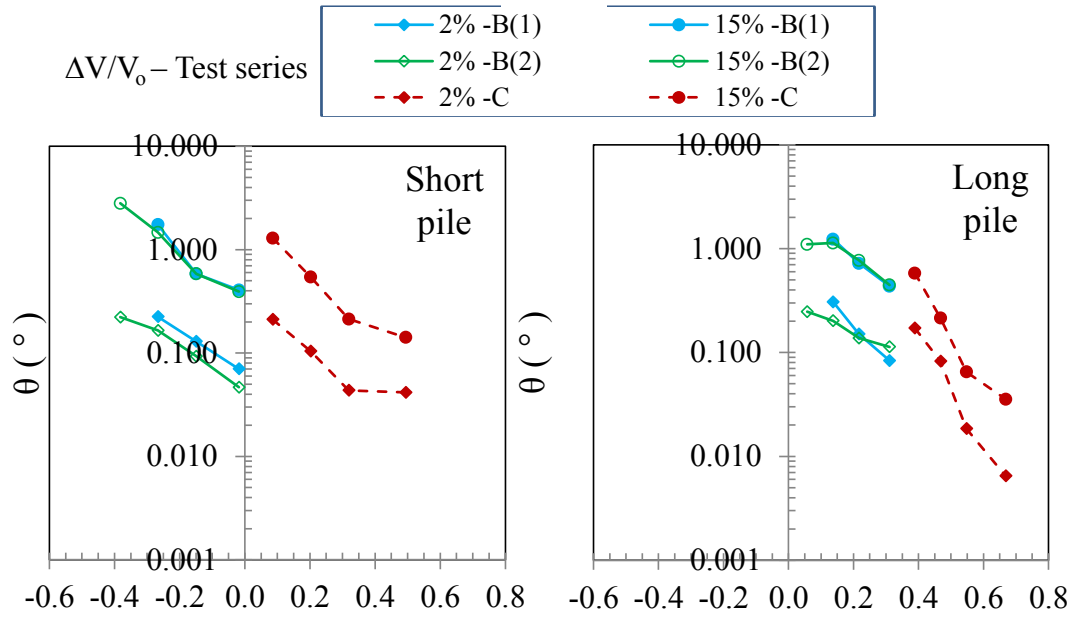

(b)

Fig.6.12 Comparison of inclination of the pile cap at the ground loss ratio of 2% and 15% with relative depth of front pile from the boundary of Zone C and D:
(a) Normal scale; (b) logarithmic scale

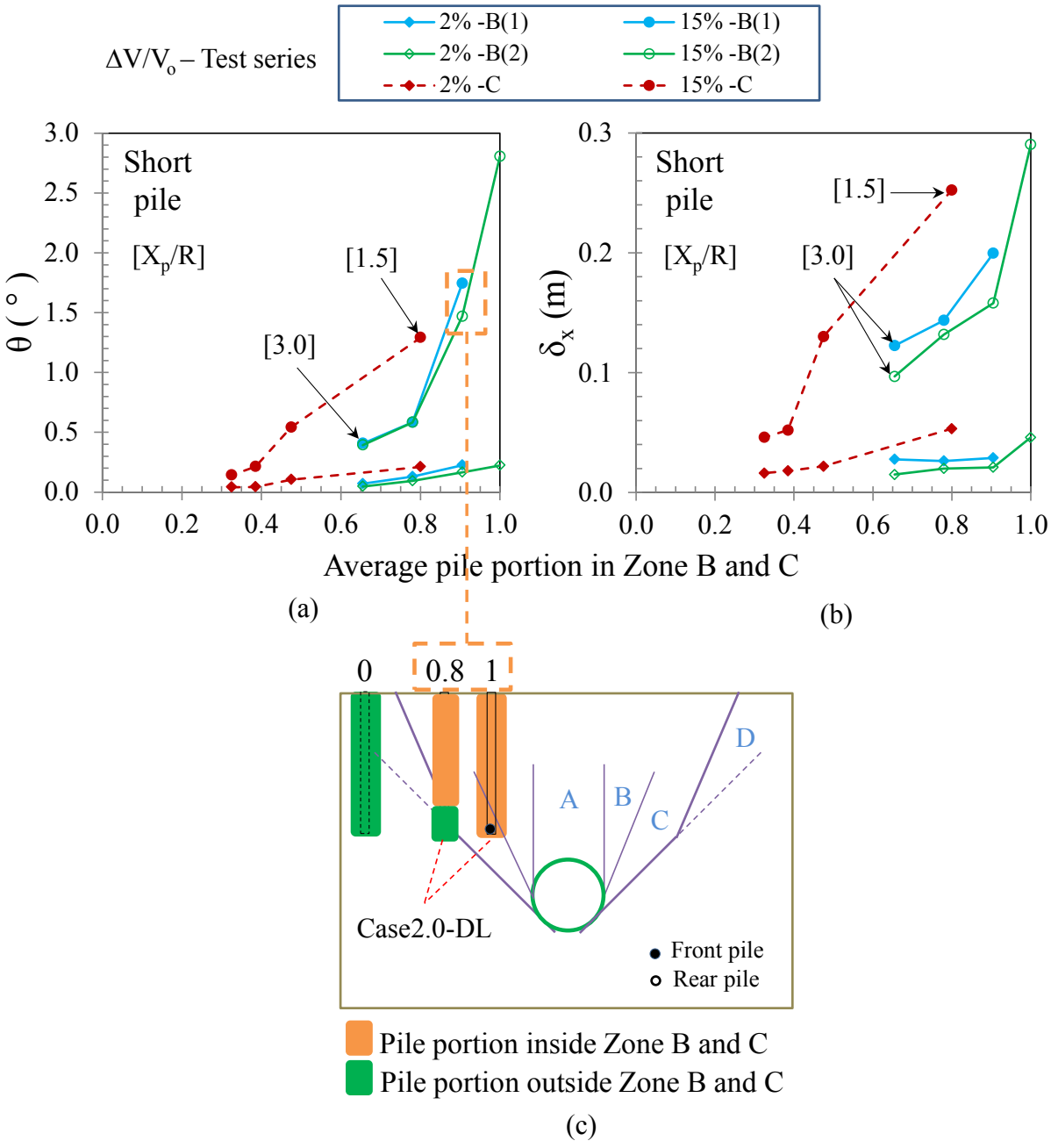

Fig.6.13 Comparison of pile cap movement with average pile portion in Zone B and C: (a) Inclination; (b) horizontal movement;
(c) schematic drawing of pile portion in Zone B and C

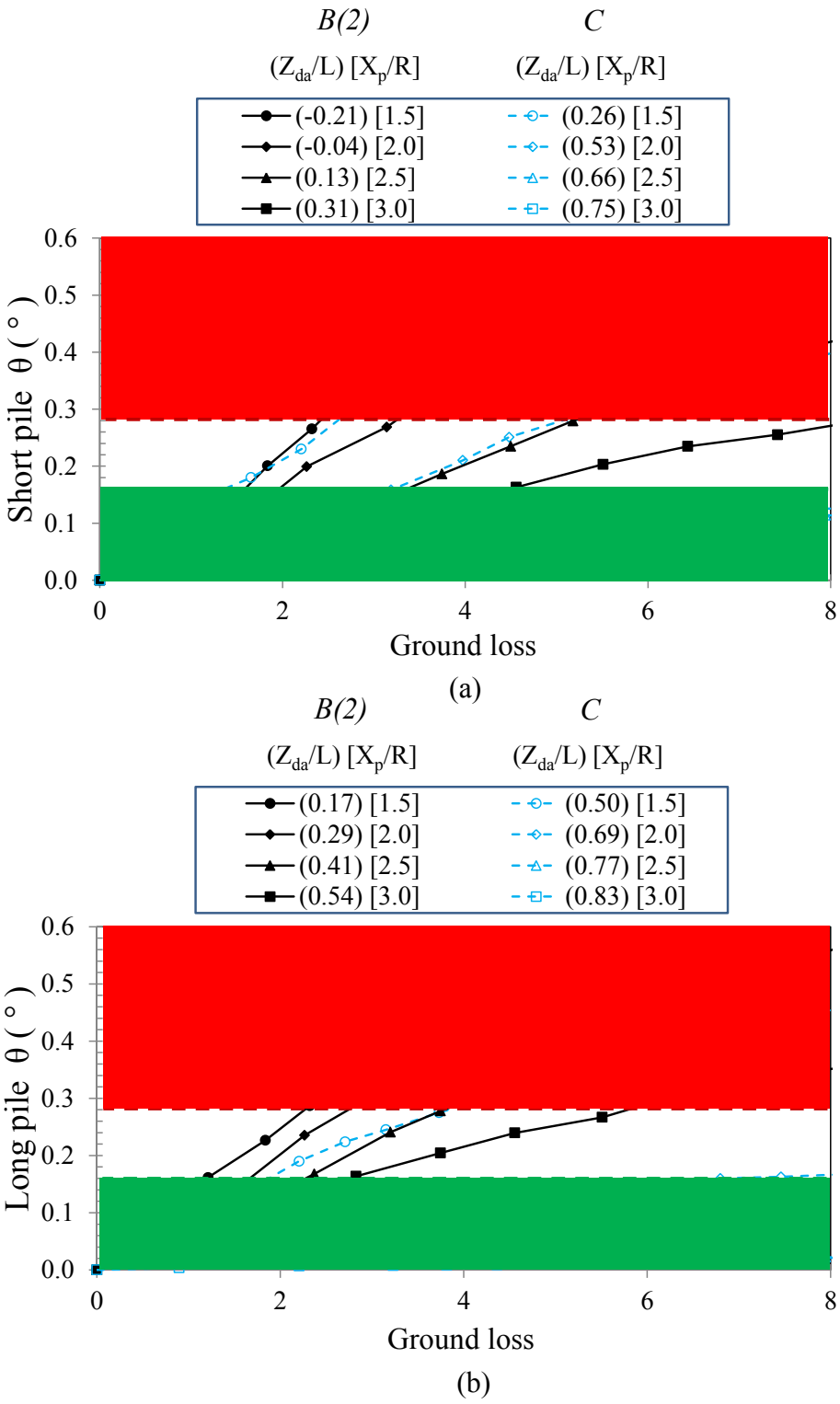

Fig.6.14 Comparison of inclination at the various ground loss ratio with average relative depths from the boundary of Zone C and D: (a) short pile; (b) long pile

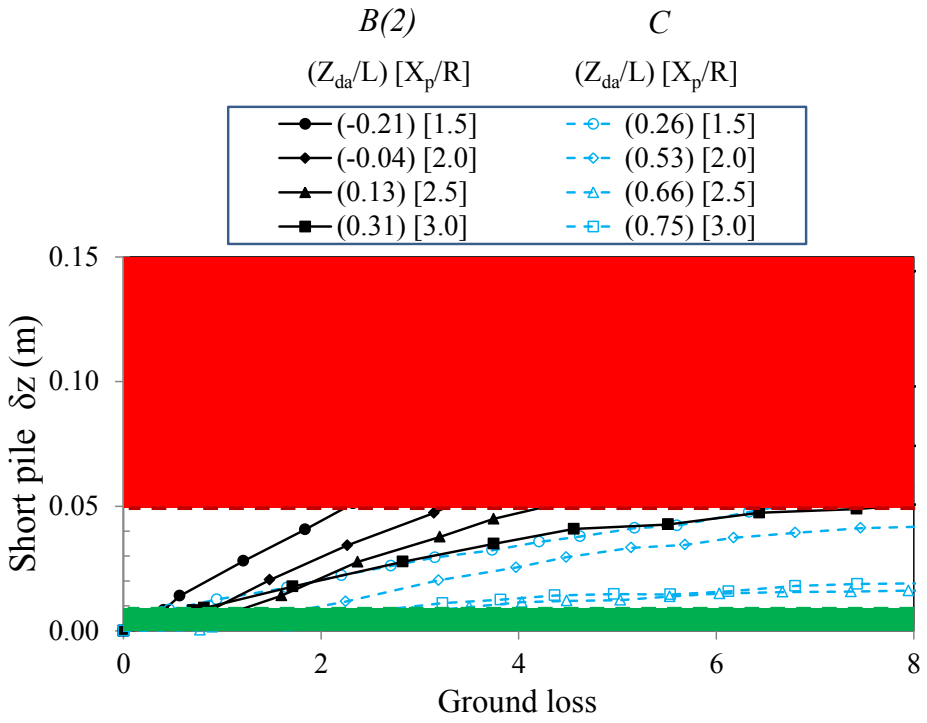

(a)

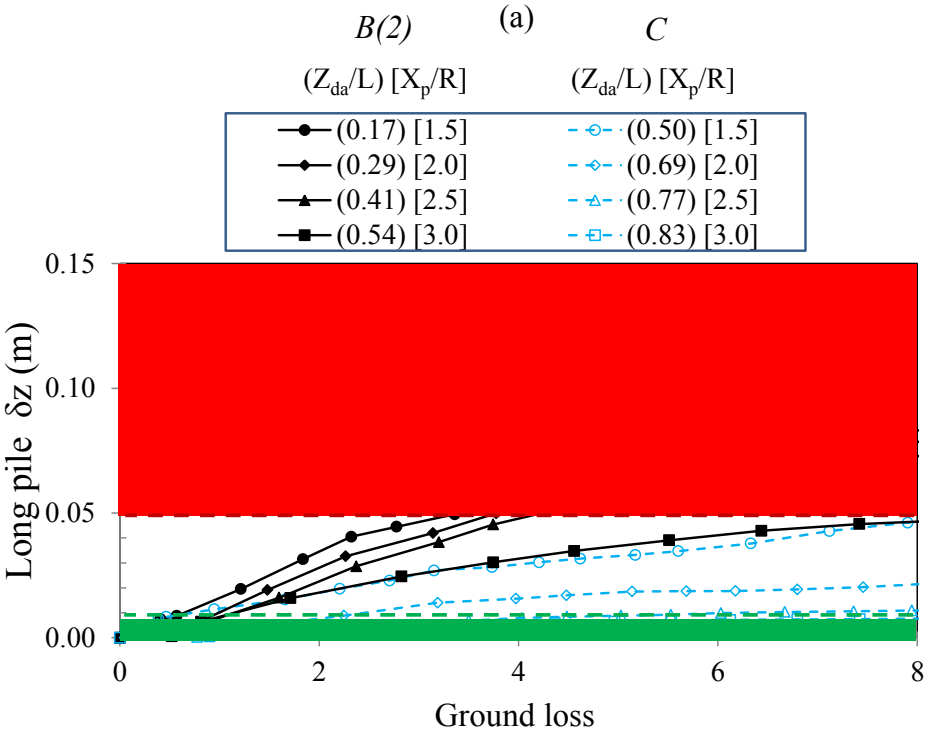

(b)

Fig.6.15 Comparison of vertical settlement at the various ground loss ratios with average relative depths from the boundary of Zone C and D: (a) short pile; (b) long pile

Chapter 7

Conclusion

The awareness of tunnel construction under congested underground condition has been focused over the last few decades ago. Tunnel excavation causes stress reduction and ground movement due to the ground loss. More recently, tunnel machine has been developed to minimize the amount of ground loss but it is difficult to control the induced ground loss from beginning to end of the excavation process. The study on the effects of these changes on the adjacent pile foundation is essential when a bored tunnel is constructed in an urban area with many pile foundations. Therefore, physical modeling using centrifuge has been proposed for study tunnel-soil-pile interaction. The centrifuge method can provide ground stress of a full-scale prototype within a small scale test. The results from centrifuge tests could be contributed to the design of new tunnel excavation or preliminary assessment of existing pile foundations.

7.1 Main conclusions

In chapter 2, the important of the soil-tunnel-pile study has been addressed to find the harmful effect of adjacent pile foundation. The development of numerical calculation and physical modeling using centrifuge have been introduced to investigate the soil-tunnel-pile behavior due to lack of recorded data on the real site construction. Numerical calculation is convenient for study the complex behavior under various conditions, but there are some

uncertainties about the proposed method. Physical model has been justified validity to investigate this complex interaction. The development of tunnel models and the limitation of each type of tunnel model were presented. In this research, the mechanical tunnel machine has been utilized to simulate tunneling process by reduction of the diameter. This tunnel machine can reduce or increase the diameter in co-axial direction from small to large ground loss ratio. The process will create clear boundary condition for evaluating the complex phenomena.

Many researchers have been carried out the essential results about mechanical of piles subjected to tunneling-induced soil movements. However, the results of the complex interaction are insufficient and need for further investigation, especially in the pile group foundation. Therefore, the development of centrifuge modeling of pile foundation was firstly proposed, the fundamental of ground movement caused by tunneling was clarified, and the mechanical response of pile group and the safety preliminary assessment were investigated.

In chapter 3, the principal of centrifuge technique and the development of centrifuge modeling of pile foundation were addressed. The limitation of air and liquid pressure types of model tunnel were explained. In this study, the tunnel machine which can provide consistent radial contraction were utilized and attached to rigid plain strain container. The grouting process could be simulated with the shape of co-axial diameter reduction. The tunnel can create large ground loss ratio which is corresponding to the failure of tunnel.

The careful model preparations such as constant pouring of air pluviation method, the installation of holding unit for measured equipment, relative positions of short and long pile groups, and tunnel machine preparation were explained. The displaced vectors of ground movement have been traced by Particle Image Velocimetry (PIV) method. The displacement vectors have been tracked within divided patches by the sequence images. The accuracy of PIV depends on the quality of images. The rows of LED light have been installed along the window screen to enhance the image quality. In addition, the wild vectors caused by swaying camera during the centrifuge have been modified by the Photoshop. The calibration techniques of all equipment were pointed out. The bearing capacity of pile model was estimated by pile end settlement due to the flexibility of pile. The pile end settlement can be defined by the pile head settlement measure by potentiometer (PTM) subtraction with pile compression.

In chapter 4, fundamental behavior of ground movement caused by tunneling with and without the presence of pile foundations was clarified. The main objectives of the chapter were

not only to investigate the shape of the settlement trough but also to prove the performance of tunnel machine by comparison with recorded data from real field. The K parameters which represent the shape of ground movement from the tests showed good agreement with an empirical relation derived from sandy soils at small ground loss ratio.

The ground movement at the tunnel center along the pile groups need to be displayed, but the test system could only measure the ground movement on the front screen. Therefore, the accuracy of PIV measurement must be verified by comparing with the results from PTM measured at the central cross section line of the model. The comparison is identical, especially for ground loss ratio less than 7-10%.

Both shape of the soil surface and subsurface settlement profile could be approximated as Gaussian distribution curve from small (2%) to large (15%) ground loss ratio ($\Delta V/V_o$). The width of the settlement trough which is equal to the distance between two inflection points tended to increase with the presence of pile group, especially when the pile group position becomes closer to the tunnel. However, the shape of the settlement trough becomes steeper at the central portion at large ground loss ratio.

In the graph between vertical settlements of the soil surface and ground loss ratio, the development of the soil surface settlement showed non-linearity. The magnitudes of soil settlement were large for the small ground loss ratio ($\Delta V/V_o < 4\%$) and these magnitudes were reduced for the large ground loss ratio. This behavior could be observed both the cases with and without the pile groups. The presence of pile groups tended to increase the vertical settlement of the soil surface, especially at large ground loss ratio. The effect was considerable for the case with a large load and the cases with small cover and depth ratio (C/D = 1.5). In addition, the effect of pile groups on the ground movement could also be observed at the location more than five times pile diameter (the distance between centers of piles to the window front screen).

In chapter 5, the effects of tunnel cover depth, pile length, lateral position of piles from the tunnel, and vertical load to the pile group on the pile response were discussed. The rate of piles settlement with the ground loss ratio also indicated the non-linear behavior as the same as soil surface settlement. The Zones of influence are defined referring **Jacobz S.W.(2004)** and a boundary (line-c) between less movement and large movement zones are determined by the liner line on $2x_i$ depth variation or approximated from the empirical equation (**Moh et al., 1996**).

The relative positions of pile ends and the zone of influence could be used to explain the behavior of pile groups, for example, the pile group experiences large lateral movement and inclination when the front and rear piles rest in or close to the Zone B and the Zone D respectively. In other words, the front piles settle larger than the rear piles, causing a large uneven settlement.

The reduction of pile end bearing loads during tunneling were observed when the pile ends rested in zone B or close to the boundary between Zone B and C because the stress reduction around the tunnel perimeter due to large ground movement. However, the increment of pile end bearing could be measured when the pile ends rested in less displacement zone (Zone D). In addition, due to large ground movements within the zone of influence, the pile portions inside the zone of influence developed negative skin friction. However, the magnitude of negative skin friction tended to reduce at the soil surface or when the pile portions rested in the Zone D. In the cases with large pile settlement, the positive skin frictions were developed, especially in the area of Zone D (less soil displacement).

Relative horizontal distance (X_p) and the relative pile depth embedded in the less displacement (Zone D) are the critical factors to control the shape and the magnitude of bending moment. If the pile end is rested in the Zone D, the pile end will behave like a fixed end and large bending moment will be developed. If the pile end is rested inside the Zone B or C, the pile will be moved along with the soil movement and the shape of bending moment profile will be different from the former cases. In addition, the vertical load effect slightly affected the increment of the bending moments and axial forces.

In chapter 6, the new parameter, the pile depth in the less movement zone (Z_d), which is adapted from the zone of influence and the behavior of various relative positions between pile group and tunnel is introduced. The parameter incorporates the effect of relatively horizontal distance (X_p) and relative position between pile end and tunnel center (Z_{pe}). The average of relative depth in the less movement zone (Z_{da}/L) showed the unique trend when this parameter is plotted against pile cap movement. The magnitudes of pile cap movements reduced as the values of Z_{da}/L increased, especially when the pile ends were rested deeper than the tunnel elevation. However, this parameter has some limitations for inclination and horizontal movements of pile cap between the cases with pile end shallower than the tunnel crown (test B(1) and B(2) series) and the cases with pile end at the tunnel elevation (Test C series) ($0.3 \leq Z_{da}/L \leq 0.5$). It may come from the difference of lateral soil movement and induced bending moment along the pile,

especially when the pile groups are near the tunnel ($X_p/R < 2.0$). Nonetheless, the Z_{da}/L parameter could be used as a preliminary assessment for safety of adjacent buildings. If the values of this parameter are small ($Z_{da}/L < 0.4$), tunnel excavation should be conducted with carefully ground loss control. In addition, the allowable ground loss ratio ($\Delta V/Vo$) with various positions from the tunnel could be estimated by applying the Z_{da}/L parameter for required displacements of the foundation.

7.2 Recommendations for further study

The test with pile ends rested in the Zone A of influence should be conducted to estimate the effects on the pile foundation. The adverse effect of the pile foundation could be more than the cases with pile end rested in Zone B according to the result from **Jacobs et al., 2004**. In this study, the harmful effects on pile foundation are considerable when the pile end is shallower than the tunnel elevation. However, to avoid the effect of tunneling, the tunnel tends to be excavated under the pile foundation with significant distance (2D, **Standing (1996); Jacobsz et al., (2004); Loganathan et al., (2000)**) between pile end and tunnel crown. It will benefit to examine when the adverse effects start to reduce as the distance reduced.

The effect of pile rigidity should be investigated by changing into rigid pile material such as the aluminum pile, brass pile etc. The acrylic material will give the axial and bending rigidity smaller than the prototype material. The same test setup with changing to rigid material may improve the applicable range of allowable ground loss.

The speed of taking picture should be improved because the interval time between images is 20 second which is too slow to capture the tunneling process precisely. The holding system of the camera should be improved to reduce the image's vibration. In this study, dry sand was used to simplify the test condition. Saturated sand or clay could be applied in the soil material. Those test results will help to improve the knowledge of pile group response and allowable ground loss.

BiBLIOGRAPHY

1) **Andrawes, K. Z. and Butterfield, R.**: The measurement of planer displacements of sand grains, *Geotechnique 23*, No. 5, pp.571-576, 1973.
2) **Architecture Institute of Japan, AIJ:** Technical Guideline on Steel Construction, On-site Construction, Architectural Institute of Japan, Japan, 1996.
3) **Architecture Institute of Japan, AIJ:** Standard Specifications and Commentary on Building Construction, Reinforced Concrete. JASS5, Japan, 1997.
4) **Attewell P.B., Farmer I.W.**: Ground deformations resulting from shield tunnelling in London Clay, *Canadian Geotechnical Journal,* Vol. 11: 380-395, 1974.
5) **Barratt D.A., Tyler R.G.**: Measurements of ground movement and lining behavior on the London Underground at Regent's Park, *Report LR 684*, Crowthorne: Transport and Road Research Laboratory, 1976.
6) **Bezuijen A. and Schrier J.V.**: The influence of a bore tunnel on pile foundations, *Proc. of Centrifuge 94*, pp. 681-686, 1994.
7) **Bilotta F., Russo G., Viggiani C.:** Numerical study of a measure for mitigating ground displacements induced by tunneling; *Geotechnical Aspects of Underground Construction in soft Ground 2006 Taylor & Francis Group,* London. pp. 357-362, 2006.
8) **Bjerrum L.**, Johannessen I.J., Eide O.: Reduction of negative skin friction on steel piles to rock, Proc. 7th ICSMFE, Mexico City, Vol. 2, pp.27-34, 1969.
9) **Bozozuk M**.: Downdrag measurement on 160-ft floating pipe test pile in marine clay, *Canadian Geotechnical Journal*, Vol.9, No.2, pp. 127-136, 1972.
10) **Caicedo, B.**: Geotechnical centrifuge applications to foundation engineering teaching, *Proc., 1st Int. Conf. on Geotechnical Engineering Education and Training*, Balkema, Rotterdam, The Netherlands, pp. 271-274, 2000.
11) **Caporaletti and Burghignoli:** Centrifuge study of tunnel movements and their interaction with structures; *Geotechnical Aspects of Underground Construction in soft Ground 2006*, Taylor & Francis Group, London. pp. 99-105, 2006.
12) **Chen L.T., Poulos H.G., Loganathan N**.: Pile response caused by tunnelling, J. Geotechnical and Geoenvironmental Engineering, ASCE, Vol. 125, No.3, pp. 207-215, 1999.

13) **Chissolucombe I,, Assis A.P., Farias M.M.:** Soil-structure interaction and its influence on displacements induced by tunnel excavations *Geotechnical Aspects of Underground Construction in soft Ground 2006*, Taylor & Francis Group, London. pp. 509-514, 2006.

14) **Clough G. W., Schmidt, B.**: Design and performance of excavations and tunnels in soft clay, *State of the art report, International Symposium on Soft Clay*, Bangkok, Thailand, 1977. In Soft clay engineering, Amsterdam: Elsevier, pp. 569-634, 1980.

15) **Clough G. W., Schmidt, B.**: Design and performance of excavations and tunnels in soft clay, Soft Clay Engineering, Elsevier, Amsterdam, 1981.

16) **Cording E.J.**: Control of ground movements around tunnels in soil, *Proceeding of 9th Pan-American Conference,* Soil Mech. Found. Engng, Valparaiso, pp. 2195-2244, 1991.

17) **Craig W. H.**: Use of a centrifuge in geotechnical engineering education. *Geotech. Test. J*., 12(4), pp. 288-291, 1989.

18) **Deane A.P., Bassett R.H**.: The Heathrow Express Trial Tunnel, *Proceedings of Institution of Civil Engineers Geotechnical Engineering*, Vol. 113, July, pp. 144-156, 1995.

19) **Dyer M**.R., Hutchinson M.T., Evans N.: Sudden Valley Sewer: A case history, *Geotechnical Aspects of Underground Construction in Soft Ground*, (Mair R and Taylor R (eds)). Balkema, Rotterdam, pp. 671-676, 1996.

20) **Fellenius B.H**.: Downdrag on piles due to negative skin friction, *Canadian Geotechnical Journal*, Vol.9, No.4, pp.323-337, 1972.

21) **Fellenius B.H.**: Negative skin friction and settlement of piles, 2nd International seminar, Pile foundations, Nanyang Technological Institute, Singapore, 1984.

22) **Fujii, M. et al.:** Damage to a repair of foundations of residential buildings in liquefied areas in Hygoken-Nanbu earthquake. *Soil and Foundation,* Vol.46, pp.9-12, 2002.

23) **Fukushima S., Tatsuoka, F.**: Strength and deformation characteristics of saturated sand at extremely low pressures, *Soils and Foundations*, Vol. 24, No.4, pp. 30-48, 1984.

24) **Gens A., Mariano A.Di, Gesto J.M.:** Ground movement control in the construction of a new metro line in Barcelona ; *Geotechnical Aspects of Underground Construction in soft Ground 2006 Taylor & Francis Group,* London. pp. 389-395, 2006.

25) **GEO-SLOPE INTERNATIONAL:** Sigma/W version-3 for Finite Element Tension Deformation Analysis. Calgary, Alberta, Canada, 1978.

26) **Glossop N.H.**: Soil deformation caused by soft ground tunnelling, *PhD thesis*, Cambridge University, 1978.

27) **Grant R.J. and Taylor R.N.**: Centrifuge modeling of ground movements due to tunneling in layered ground; *Geotechnical Aspects of Underground Construction in soft Ground 1996 Mair & Taylor Group*, Rotterdam. pp. 507-512, 1996.

28) **Hergarden H.J.A.M., Van der Poel J.T., van der Schrier J.S.:** Ground movements due to tunnelling: Influence on pile foundations, *Geotechnical Aspects of Underground Construction in Soft Ground*, (Mair R and Taylor R (eds)). Balkema, Rotterdam, pp. 519-524, 1996.

29) **Itasca:** FLAC3D User's Guide, *Itasca Consulting Group*, USA, 2002.

30) **Jacobsz S.W.**: The effects of tunnelling on piled foundations, *PhD thesis*, University of Cambridge, 2002.

31) **Jacobz S.W., Bowers K.H. and Moss N.A., Zanardo G.:** The effects of tunneling on piled structures on the CTRL, *Geotechnical Aspects of Underground Construction in soft Ground 2006,* Taylor & Francis Group, London. pp. 115-121, 2006.

32) **Jacobsz S.W., Standing J.R., Mair R.J., Soga K., Hagiwara T. and Sugiyama T.:** Tunnelling effects on driven piles, *Proc. Int. Conf. on Response of buildings to excavation induced ground movements*, London, Jardine F.M. (ed). CIRIA Special Publn 201, CIRIA, London, pp 337-348, 2003.

33) **Jacobsz S.W., Standing J.R., Mair R.J., Hagiwara T. and Sugiyama T.**: Centrifuge modelling of tunnelling near driven piles, *Soils and Foundation*s 44(1), pp. 49–56, 2004.

34) **Japanese Law Publication:** Residential Dispute Proceeding Technical Handbook, Japan, 2000.

35) **Johannessen I.J., Bjerrum L**.: Measurment of the compression of a steel pile to rock due to settlement of surrounding clay, *Proc. 6th ICSMFE*, Montreal, Vol.2, pp. 261-264, 1965.

36) **Kaalberg F.J., Lengkeek H.J., Teunissen E.A.H.**: Evaluatie van de meetresultaten van het proefpalenprojek ter plaatse van de tweede Heinenoordtunnel (in Dutch), *Adviesbureau Noord/Zuidlijn Report no. R981382*, Amsterdam, 1999.

37) **Kaalberg F.J., Teunissen E.A.H., Tol A.Fv and Bosch J.W.** : Dutch research on the impact of shield tunneling on pile foundations, *Proc. of 16th International Conference of Soil Mechanics and Foundation Engineering*, Vol. 3, Osaka, pp. 1615–1629, 2005.

38) **Kaga K., et al.:** Vestibular sensitivity and sense of inclination, Journal of Cognitive Science 7:1, pp.16-22, 2005.

39) **Katoh. Y., Miyake. M., Wada. S.**: Ground deformation around shield tunnel. *In Proceedings of the International Conference on Centrifuge Modelling (Centrifuge '98)*, Tokyo, Japan, 23-25 September 1998. Edited by T. Kimura, O. Kusakabe, and J.Takemura. Balkema, Rotterdam, the Netherlands. pp. 733-738, 1998.

40) **Kitiyodom P., Masumoto T., Kawaguchi K.:** Analyses of pile foundations subjected to ground movements induced by tunneling*, Geotechnical Aspects of Underground Construction in soft Ground 2006,* Taylor & Francis Group, London. pp. 551-557, 2006.

41) **Kwast E.A., Oosterhout G.P.C. van.**: Measurements and evaluation of the influence of two bored tunnels at reduced distance (<0.5D) in a homogenous sand layer, *Geotechnical Aspects of Underground Construction in soft Ground 2006*, Taylor & Francis Group, London. pp. 133-137, 2006.

42) **Lee C.J. and Chiang K.H.**: Responses of single piles to tunneling-induced soil movements in sandy ground, *Canadian Geotechnical Journal*, Vol. 44, No. 10, pp. 1224-1241, 2007.

43) **Lee G.T.K., Ng C.W.W.**: Effects of advancing open face tunneling on an existing loaded pile, *Journal of Geotechnical and Geoenvironmental Engineering*, ASCE, Vol. 131, No. 2, pp. 193-201, 2005.

44) **Lee G.T.K. and Ng C.W.W.**: Three-dimensional numerical simulation of tunneling effects on an existing pile, *Geotechnical Aspects of Underground Construction in soft Ground 2006*, Taylor & Francis Group, London. pp. 139-144, 2006.

45) **Lee R.G., Turner A.J., and Whitworth L.J.** : Deformations caused by tunneling beneath a piled structure, *Proc. of 13th International Conference of Soil Mechanics and Foundation Engineering*, Vol. 2, New Deli, pp. 873–878, 1994.

46) **Loganathan, N. & Poulos, H.G.:** Analytical prediction for tunneling-induced ground movements in clays. *Journal of Geotechnical and Geoenvironmental Engineering ASCE 124(9)*, pp. 846-856, 1998.

47) **Loganathan N., Poulos H.G. and Stewart D.P.**: Centrifuge model testing of tunnelling-induced ground and pile deformations, *Geotechnique*, Vol. 50, No. 3, pp. 283-294, 2000.

48) **Madabhushi, S. P. G., Take, W. A**.: Use of a mini-drum centrifuge for teaching of geotechnical engineering. *Proc., Physical Modelling in Geotechnics*: ICPMG'02, St. Johns, Canada, pp. 221-228, 2002.

49) **Mair R.**: Centrifuge modelling of tunnel construction in soft clay, *PhD. thesis*, University of Cambridge, UK, 1979.

50) **Mair R.J., Taylor R.N.:** Theme lecture: Bored tunneling in the urban environment, *Proceedings of 14th International Conference Soil Mechanics and Foundation Engineering*, Balkema, Rotterdam, The Netherlands, pp. 2352-2385, 1997.

51) **Mair R. J., Taylor R. N., Bracegirdle A.**: Subsurface settlement profiles above tunnels in clay. *Geotechnique*, Vol. 43, No. 2, pp. 315-320, 1993.

52) **Mair R.J., Taylor R.N., Burland J.B.**: Prediction of ground movements and assessment of risk of building damage due to bored tunneling, *Proceeding of International Symposium Geotechnical Aspects of Underground Construction in Soft Ground*, London, pp. 713-718, 1996.

53) **Mahmoud A. and Magued I.**: Analysis of tunneling-induced ground movements using transparent soil models*, Journal of geotechnical and geoenvironmental engineering*, pp. 525-535, 2011.

54) **Marshall, A.M., Farrell, R., Klar, A., and Mair, R.J.**: Tunnels in sands – the effect of size, depth, and volume loss on greenfield displacements, *Geotechnique* Vol. 62, No.5, pp. 385-399, 2012.

55) **Martos, F.**: Concerning an approximate equation of the subsidence trough and its time factors, *Proc. International Strata Control Congress*, Leipzig, pp. 191-205, 1985.

56) **Mayerhof, G.G.:** Penetration test and bearing capacity of cohesion less soils, Journal of Soil Mechanics and Foundation Division, ASCE, Vol.82, No. SM1, pp.1-19, 1956

57) **McCormick J., Aburano H., Ikenaga M., Nakashima M.:** Permissible residual deformation levels for building structures considering both safety and human elements, *The 14th World Conference on Earthquake Engineering*, October 12-17, 2008, Beijing, China, 2008.

58) **McCormick J., Mauka Y., Pan P., Nakashima M.:** Evaluation of Non-Structural Partition Walls and Suspended Ceiling Systems through a Shake Table Study. *Proc. of the 2008 ASCE Structures Congress*, 2008.

59) **Moh Z.-C., Hwang R.N., Ju D.H**.: Ground movements around tunnels in soft ground, *Geotechnical Aspects of Underground Construction in Soft Ground*, (Mair R and Taylor R (eds)). Balkema, Rotterdam, pp. 725-730, 1996.

60) **Naval Facilities Engineering Command (NAVFAC, 2014)** Retrieved August 2, 2014, from http://www.finesoftware.eu/help/geo5/en/table-of-ultimate-friction-factors-for-dissimilar-materials-01/

61) **O'Reilly M.P., New B.M.**: Settlements above tunnels in the United Kingdom – their magnitude and prediction, *Tunnelling'82*, London: IMM, pp. 173-181, 1982.

62) **Pang C.H., Yong K.Y., Chow Y.K., Wang J.:** The response of pile foundations subjected to shield tunneling *Geotechnical Aspects of Underground Construction in soft Ground 2006,* Taylor & Francis Group, London. pp.737-743, 2006

63) **Peck R.B.**: Deep excavations and tunnelling in soft ground, *Proc. 7th Int. Conf. Soil Mech*, Mexico, State of the art 3, pp. 225-290, 1969.

64) **Philips, E.**: De l'équilibré des solides élastiques semblables, *C.R. Acad. Sci*., Paris, 68, pp. 75-79, 1869.

65) **Potts R.B.:** Behaviour of lined and unlined tunnels in sand. *PhD Thesis*, Engineering Department, Cambridge University, 1976.

66) **Rankin W. J.**: Ground movements resulting from urban tunneling; prediction and effects, *Proc. Conference on Engineering Geology of Underground Movements*, Nottingham, London: Geological Society, pp. 79-92, 1988.

67) **Roscoe, K. H., Arthur, J. R. F and James, R. G.**: The determination of strains in soils by an X-ray method, *Civ. Engng Public Works Rev. 58*, pp. 873-876, pp. 1009-1012, 1963.

68) **Schmidt, B**.: Settlements and ground movements associated with tunneling in soils, *PhD thesis*, University of Illinois, Urbana, 1969.

69) **Schofield, A. N.**: Geotechnical centrifuge development corrects Terzaghi's error., Cambridge University Engineering Department (CUED), *lecture to the Tokyo Conference of TC2*, 23 September 1998.

70) **Selemetas D., Standing J.R., Mair R.J.**: The response of full-scale piles to tunnelling, *Geotechnical Aspects of Underground Construction in soft Ground,* Taylor & Francis Group, London. pp. 893-899, 2006.

71) **Seto M., et al.:** Sensitivity and memory of body inclination (part 1) – Ability to restore to vertical position, Equilibrium Research 55:5, 204, 1996.

72) **Standing J.R., Burland. J.G.**: Investigating variation in tunneling volume loss – a case study; *Geotechnical Aspects of Underground Construction in soft Ground,* Taylor & Francis Group, London. pp. 305-311, 2006.

73) **Standing J.R., Leung W.Y.M.T.:** Investigating stresses around tunnels and piles using photo-elasticity techniques; *Geotechnical Aspects of Underground Construction in soft Ground 2006,* Taylor & Francis Group, London, pp.171-177, 2006.

74) **Sugiyama T., Hagiwara T., Nomoto T., Nomoto M., Ano Y., Mair R.J., Bolton M.D., Soga K.**: Observations of ground movements during tunnel construction by slurry shield method at the Docklands Light Railway Lewisham extension-east London, *Soils Found. 39*, No.3, pp.99-112, 1999.

75) **Surjadinata J., Carter J.P., Hull T.S., Poulos H.G.**: Analysis of effects of tunneling on single piles, *Geotechnical Aspects of Underground Construction in soft Ground 2006*, Taylor & Francis Group, London. pp. 665-671, 2006.

76) **Take W. A.**: The influence seasonal moisture cycles on clay slopes, *PhD thesis*, University of Cambridge, 2002.

77) **Takemura J., Kondoh M., Esaki T., Kouda M. and Kusakabe O.:** Centrifuge model tests on double propped wall excavation in soft clay, *Soils and Foundation*s 39(3), pp. 75-87, 1999.

78) **Tatsuoka F., Sakamoto M., Fukushima S., Kawamura T**.: Strength and deformation characteristics of sand in plane strain compression at extremely low pressures, *Soils and Foundations*, Vol. 26, No.1, pp. 65-84, 1986.

79) **Taylor, R. N**.: Geotechnical centrifuge technology. London: *Blackie Academic and Professional*, 1995.

80) **Taylor, R. N., Grant, R. J., Robson, S. and Kuwano, J.**: An image analysis system for determining plane and 3-D displacements in soil models, *Proc. Centrifuge '98*, pp.73-78. Tokyo, 1998.

81) **Technical Manual for Design and Construction of Road Tunnels - Civil Elements (2014)** Retrieved June 2, 2014, from http://www.fhwa.dot.gov/bridge/tunnel/pubs/nhi09010/07a.cfm

82) **Terzaghi K**.: Shield tunnels of the Chicago subway, *J. Boston Soc. Civil Engrs.* 29, pp. 163-210, 1942.

83) **Tol van A.F.:** The effects of tunneling on existing structures; *Geotechnical Aspects of Underground Construction in soft Ground 2006,* Taylor & Francis Group, London. pp. 31-42, 2006.

84) **Yasuda S., Hashimoto T.**: Differential settlement caused by liquefaction in Tottori-Seibu earthquake, *Annual Meeting of Japanese Society of Civil Engineers*, pp.1029-1030, 2002.

85) **Vorster T.E.B., Klar A., Soga K., Mair R.J.**: Estimating the effects of tunneling on existing pipelines, *Journal of geotechnical and geoenvironmental engineering*, ASCE, pp.1399-1409, 2005.

86) **Walker L.K. and Darvall P.L.**: Dragdown on coated and uncoated piles, *Proc. 8th ICSMFE*, Moscow, Vol.2, pp.257-262, 1973.

87) **White D. J.**: An investigation into the behavior of pressed-in piles, *PhD thesis*, University of Cambridge, 2002.

88) **White D.J., Take W.A.**: GeoPIV: Particle Image Velocimetry (PIV) software for use in geotechnical testing, *Technical Report*, CUED/D-SOILS/TR322 Cambridge University Engineering Department, 2002.

89) **White, D. J., Take, W. A. and Bolton, M. D.**: Soil deformation measurement using particle image velocimetry (PIV) and photogrammetry, *Geotechnique 53*, No. 7, pp. 619-631, 2003.

90) **Xu K.J., Poulos H.G.:** 3-D elastic analysis of vertical pile subjected to "passive" loadings. *Computers and Geotechnics 28*, pp.349-375, 2001.

Appendix A –Values of x_i and K

Table A.1 Variation of K and x_i of subsurface by **Mair et al., (1993)**

$\frac{Z}{Z_o}$	x_i	$K = \frac{x_i}{Z_o - Z}$
0	0.175	0.500
0.05	0.191	0.509
0.10	0.208	0.519
0.15	0.224	0.531
0.20	0.240	0.544
0.25	0.256	0.558
0.30	0.273	0.575
0.35	0.289	0.594
0.40	0.305	0.617
0.45	0.321	0.643
0.50	0.338	0.675
0.55	0.354	0.714
0.60	0.370	0.763
0.65	0.386	0.825
0.70	0.403	0.908
0.75	0.419	1.025
0.80	0.435	1.200

$$K = \frac{0.175 + 0.325(1 - \frac{Z}{Z_o})}{Z_o - Z}$$

Table A.2(a) Variation of K and x_i of subsurface by **Moh et al., (1996) [C/D=1.5]**

Z (m)	Z_o (m)	$\frac{Z}{Z_o}$	D (m)	x_i (m)	$K = \frac{x_i}{Z_o - Z}$
0	14	0	7	6.09	0.435
1		0.05		5.92	0.455
2		0.10		5.73	0.477
3		0.14		5.53	0.503
4		0.19		5.33	0.533
5		0.24		5.11	0.567
6		0.29		4.87	0.609
7		0.33		4.62	0.660
8		0.38		4.34	0.724
9		0.43		4.04	0.807
10		0.48		3.69	0.923
11		0.52		3.29	1.097
12		0.57		2.80	1.399
13		0.62		2.12	2.121

$$K = \frac{(\frac{D}{2})(\frac{Z_o}{D}^{0.8})(\frac{Z_o - Z}{Z_o})^m}{Z_o - Z}$$

m = 0.4 (for sand)
m = 0.8 (for clay)

Table A.2(b) Variation of K and x_i of subsurface by **Moh et al., (1996) [C/D=2.5]**

Z (m)	**Z_o (m)**	$\frac{Z}{Z_o}$	**D (m)**	**x_i (m)**	$K = \frac{x_i}{Z_o - Z}$
0		0		8.43	0.401
1		0.05		8.27	0.413
2		0.10		8.10	0.426
3		0.14		7.92	0.440
4		0.19		7.75	0.456
5		0.24		7.56	0.473
6		0.29		7.37	0.491
7		0.33		7.17	0.512
8		0.38		6.96	0.535
9		0.43		6.74	0.562
10	21	0.48	7	6.51	0.592
11		0.52		6.26	0.626
12		0.57		6.01	0.667
13		0.62		5.73	0.716
14		0.67		5.43	0.776
15		0.71		5.11	0.851
16		0.76		4.75	0.950
17		0.81		4.34	1.086
18		0.86		3.87	1.290
19		0.90		3.29	1.645
20		0.95		2.49	2.494

$$K = \frac{(\frac{D}{2})(\frac{Z_o}{D}^{0.8})(\frac{Z_o - Z}{Z_o})^m}{Z_o - Z}$$

m = 0.4 (for sand)
m = 0.8 (for clay)

Table A.3 Variation of K and x_i of subsurface by **Dyer (1996)**

$\frac{Z}{Z_o}$	**x_i**	$K = \frac{x_i}{Z_o - Z}$
0	0.28	-
0.24	0.30	2.29
0.41	0.34	1.99
0.56	0.41	1.80
0.71	0.59	1.61
0.86	1.16	1.51

Table A.4 Variation of K and x_i of subsurface from test cases [C/D=2.5]

Case0-D				**$\Delta V/V_o$ = 2.0-2.5%**		**$\Delta V/V_o$ = 14.5-15.0%**	
Z (mm)	**Z_o (mm)**	$\frac{Z}{Z_o}$	**D (mm)**	**x_i (mm)**	$K = \frac{x_i}{Z_o - Z}$	**x_i (mm)**	$K = \frac{x_i}{Z_o - Z}$
0	210	0	70	90.3	0.430	77.7	0.370
12		0.06		87.5	0.442	76.9	0.388
30		0.14		81.9	0.455	71.1	0.395
48		0.23		78.1	0.482	66.8	0.412
66		0.31		74.6	0.518	65.4	0.454
84		0.40		71.1	0.564	61.6	0.489
102		0.49		65.5	0.606	56.5	0.523
120		0.57		63.0	0.700	53.4	0.593
138		0.66		57.0	0.792	51.1	0.709

Case2.0-DH				**$\Delta V/V_o$ = 2.0-2.5%**		**$\Delta V/V_o$ = 14.5-15.0%**	
Z (mm)	**Z_o (mm)**	$\frac{Z}{Z_o}$	**D (mm)**	**x_i (mm)**	$K = \frac{x_i}{Z_o - Z}$	**x_i (mm)**	$K = \frac{x_i}{Z_o - Z}$
0	210	0	70	107.1	0.510	89.9	0.428
12		0.06		104.1	0.526	87.5	0.442
30		0.14		97.1	0.539	83.4	0.463
48		0.23		93.1	0.575	78.7	0.486
66		0.31		87.2	0.605	75.5	0.525
84		0.40		79.3	0.629	70.0	0.556
102		0.49		72.8	0.674	63.2	0.585
120		0.57		67.2	0.747	58.0	0.645
138		0.66		61.4	0.854	54.2	0.753

Case2.5-DH				**$\Delta V/V_o$ = 2.0-2.5%**		**$\Delta V/V_o$ = 14.5-15.0%**	
Z (mm)	**Z_o (mm)**	$\frac{Z}{Z_o}$	**D (mm)**	**x_i (mm)**	$K = \frac{x_i}{Z_o - Z}$	**x_i (mm)**	$K = \frac{x_i}{Z_o - Z}$
0	210	0	70	105.9	0.505	93.1	0.440
12		0.06		101.7	0.514	86.2	0.467
30		0.14		91.7	0.510	83.9	0.466
48		0.23		84.2	0.519	76.3	0.471
66		0.31		78.2	0.543	72.2	0.501
84		0.40		74.8	0.594	69.1	0.549
102		0.49		68.4	0.633	63.6	0.589
120		0.57		62.1	0.690	57.7	0.641
138		0.66		58.2	0.808	54.2	0.752

Case3.0-DH				$\Delta V/V_o$ = 2.0-2.5%		$\Delta V/V_o$ = 14.5-15.0%	
Z (mm)	**Z_o (mm)**	$\frac{Z}{Z_o}$	**D (mm)**	**x_i (mm)**	$K = \frac{x_i}{Z_o - Z}$	**x_i (mm)**	$K = \frac{x_i}{Z_o - Z}$
0	210	0	70	100.8	0.480	77.7	0.370
12		0.06		98.7	0.498	75.0	0.379
30		0.14		91.8	0.510	72.1	0.400
48		0.23		83.1	0.525	70.2	0.432
66		0.31		81.5	0.566	65.8	0.457
84		0.40		77.5	0.615	63.4	0.503
102		0.49		68.8	0.637	57.1	0.529
120		0.57		62.6	0.696	51.9	0.577
138		0.66		55.0	0.764	47.4	0.658

Case1.5-DL				$\Delta V/V_o$ = 2.0-2.5%		$\Delta V/V_o$ = 14.5-15.0%	
Z (mm)	**Z_o (mm)**	$\frac{Z}{Z_o}$	**D (mm)**	**x_i (mm)**	$K = \frac{x_i}{Z_o - Z}$	**x_i (mm)**	$K = \frac{x_i}{Z_o - Z}$
0	210	0	70	106.9	0.509	86.1	0.410
12		0.06		101.4	0.512	83.4	0.421
30		0.14		98.3	0.546	76.1	0.423
48		0.23		90.7	0.560	70.6	0.436
66		0.31		85.1	0.591	68.1	0.473
84		0.40		81.3	0.645	65.6	0.521
102		0.49		72.8	0.674	60.5	0.560
120		0.57		64.1	0.712	53.1	0.590
138		0.66		58.3	0.810	48.5	0.673

Case2.0-DL				$\Delta V/V_o$ = 2.0-2.5%		$\Delta V/V_o$ = 14.5-15.0%	
Z (mm)	**Z_o (mm)**	$\frac{Z}{Z_o}$	**D (mm)**	**x_i (mm)**	$K = \frac{x_i}{Z_o - Z}$	**x_i (mm)**	$K = \frac{x_i}{Z_o - Z}$
0	210	0	70	103.9	0.495	84.0	0.400
12		0.06		99.8	0.504	81.9	0.414
30		0.14		95.5	0.530	73.9	0.410
48		0.23		89.1	0.550	69.0	0.426
66		0.31		84.2	0.585	66.4	0.461
84		0.40		79.3	0.630	64.6	0.512
102		0.49		72.0	0.667	59.8	0.554
120		0.57		63.6	0.707	53.8	0.598
138		0.66		58.9	0.818	48.5	0.674

Case2.5-DL				$\Delta V/V_o$ = 2.0-2.5%		$\Delta V/V_o$ = 14.5-15.0%	
Z (mm)	**Z_o (mm)**	$\frac{Z}{Z_o}$	**D (mm)**	**x_i (mm)**	$K = \frac{x_i}{Z_o - Z}$	**x_i (mm)**	$K = \frac{x_i}{Z_o - Z}$
0	210	0	70	102.4	0.488	84.2	0.401
12		0.06		101.2	0.511	83.5	0.421
30		0.14		92.2	0.512	74.9	0.416
48		0.23		83.5	0.516	69.5	0.429
66		0.31		81.2	0.564	66.7	0.463
84		0.40		79.3	0.629	64.3	0.510
102		0.49		72.6	0.672	57.3	0.530
120		0.57		64.9	0.721	51.9	0.577
138		0.66		58.4	0.811	47.6	0.661

Case3.0-DL				$\Delta V/V_o$ = 2.0-2.5%		$\Delta V/V_o$ = 14.5-15.0%	
Z (mm)	**Z_o (mm)**	$\frac{Z}{Z_o}$	**D (mm)**	**x_i (mm)**	$K = \frac{x_i}{Z_o - Z}$	**x_i (mm)**	$K = \frac{x_i}{Z_o - Z}$
0	210	0	70	94.5	0.450	75.6	0.360
12		0.06		92.7	0.468	76.7	0.368
30		0.14		87.3	0.485	71.6	0.398
48		0.23		79.5	0.491	64.9	0.401
66		0.31		76.7	0.532	64.2	0.420
84		0.40		73.3	0.582	61.9	0.471
102		0.49		67.3	0.624	57.8	0.535
120		0.57		62.7	0.697	52.0	0.566
138		0.66		56.0	0.778	47.2	0.635

Table A.5 Variation of K and x_i of subsurface from test cases [C/D=1.5]

Case0-S				$\Delta V/V_o$ = 2.0-2.5%		$\Delta V/V_o$ = 14.5-15.0%	
Z (mm)	**Z_o (mm)**	$\frac{Z}{Z_o}$	**D (mm)**	**x_i (mm)**	$K = \frac{x_i}{Z_o - Z}$	**x_i (mm)**	$K = \frac{x_i}{Z_o - Z}$
0	140	0	70	61.6	0.440	51.1	0.365
12		0.09		59.8	0.467	50.8	0.367
30		0.21		56.3	0.512	43.3	0.393
48		0.34		52.3	0.568	40.3	0.439
66		0.47		47.0	0.635	38.9	0.526
84		0.60		43.5	0.777	38.9	0.699

Case1.5-SL				$\Delta V/V_o$ = 2.0-2.5%		$\Delta V/V_o$ = 14.5-15.0%	
Z (mm)	**Z_o (mm)**	$\frac{Z}{Z_o}$	**D (mm)**	**x_i (mm)**	$K = \frac{x_i}{Z_o - Z}$	**x_i (mm)**	$K = \frac{x_i}{Z_o - Z}$
0	140	0	70	68.0	0.486	58.5	0.418
12		0.09		66.6	0.520	53.9	0.421
30		0.21		61.8	0.562	48.9	0.445
48		0.34		55.5	0.603	44.2	0.480
66		0.47		49.4	0.668	40.2	0.543
84		0.60		45.3	0.809	38.8	0.692

Case2.0-SL				$\Delta V/V_o$ = 2.0-2.5%		$\Delta V/V_o$ = 14.5-15.0%	
Z (mm)	**Z_o (mm)**	$\frac{Z}{Z_o}$	**D (mm)**	**x_i (mm)**	$K = \frac{x_i}{Z_o - Z}$	**x_i (mm)**	$K = \frac{x_i}{Z_o - Z}$
0	140	0	70	68.1	0.486	58.1	0.415
12		0.09		64.7	0.505	54.0	0.422
30		0.21		56.0	0.510	47.5	0.432
48		0.34		54.7	0.595	42.5	0.462
66		0.47		50.3	0.680	40.3	0.545
84		0.60		47.1	0.840	39.5	0.705

Case2.5-SL				$\Delta V/V_o$ = 2.0-2.5%		$\Delta V/V_o$ = 14.5-15.0%	
Z (mm)	**Z_o (mm)**	$\frac{Z}{Z_o}$	**D (mm)**	**x_i (mm)**	$K = \frac{x_i}{Z_o - Z}$	**x_i (mm)**	$K = \frac{x_i}{Z_o - Z}$
0	140	0	70	65.0	0.464	57.4	0.410
12		0.09		63.8	0.499	51.6	0.403
30		0.21		54.9	0.500	44.6	0.406
48		0.34		52.7	0.573	43.3	0.471
66		0.47		48.6	0.657	39.9	0.539
84		0.60		47.5	0.849	39.8	0.711

Case3.0-SL				$\Delta V/V_o$ = 2.0-2.5%		$\Delta V/V_o$ = 14.5-15.0%	
Z (mm)	**Z_o (mm)**	$\frac{Z}{Z_o}$	**D (mm)**	**x_i (mm)**	$K = \frac{x_i}{Z_o - Z}$	**x_i (mm)**	$K = \frac{x_i}{Z_o - Z}$
0	140	0	70	63.0	0.450	56.0	0.400
12		0.09		57.1	0.446	52.0	0.406
30		0.21		54.9	0.499	44.7	0.407
48		0.34		51.3	0.558	41.0	0.446
66		0.47		48.1	0.650	38.8	0.511
84		0.60		44.8	0.800	37.5	0.670

Appendix B – Axial force development from 2%, 5%, 10%, and 15% ground loss ratio

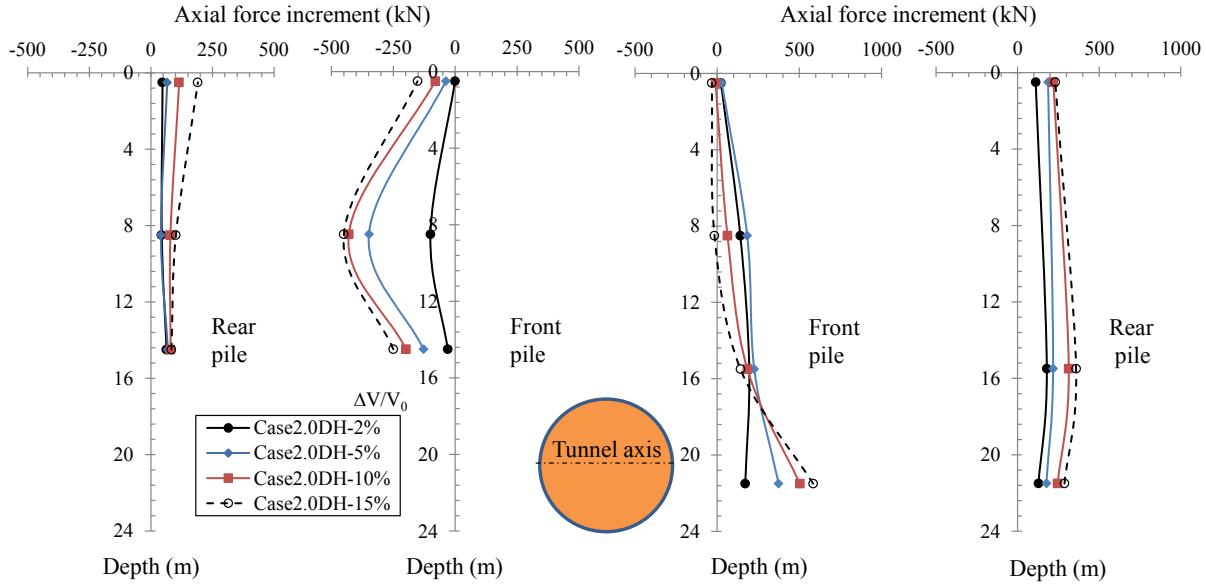

Short pile

Z_{pe}/R=-1.72, Load per pile= 2600kN

Long pile

Z_{pe}/R=0.28, Load per pile= 5070kN

(a)

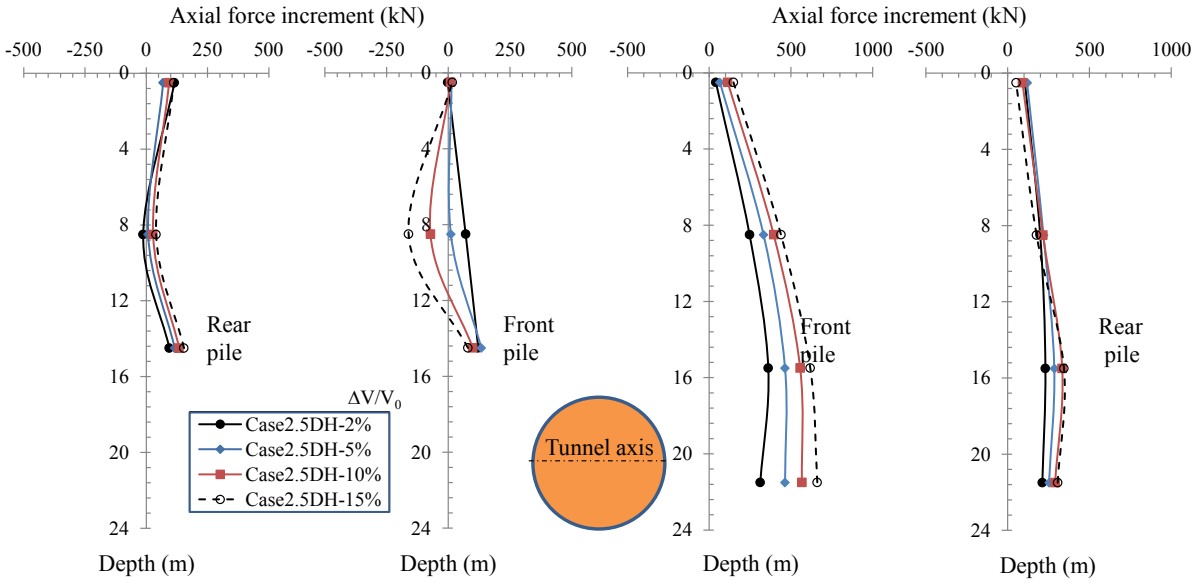

Short pile

Z_{pe}/R=-1.72, Load per pile= 2600kN

Long pile

Z_{pe}/R=0.28, Load per pile= 5070kN

(b)

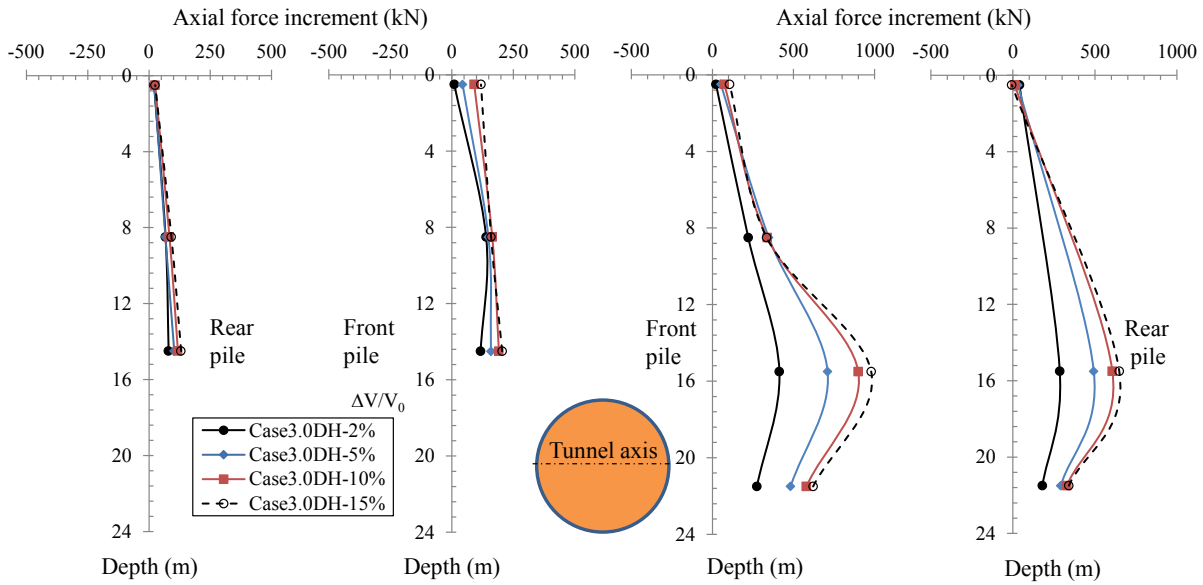

(c)

Figure B.1 Pile axial force increment profile with depth at ground loss ratio of 2%, 5%, 10%, and 15%: (a) Case2.0-DH; (b) Case2.5-DH; (c) Case3.0-DH

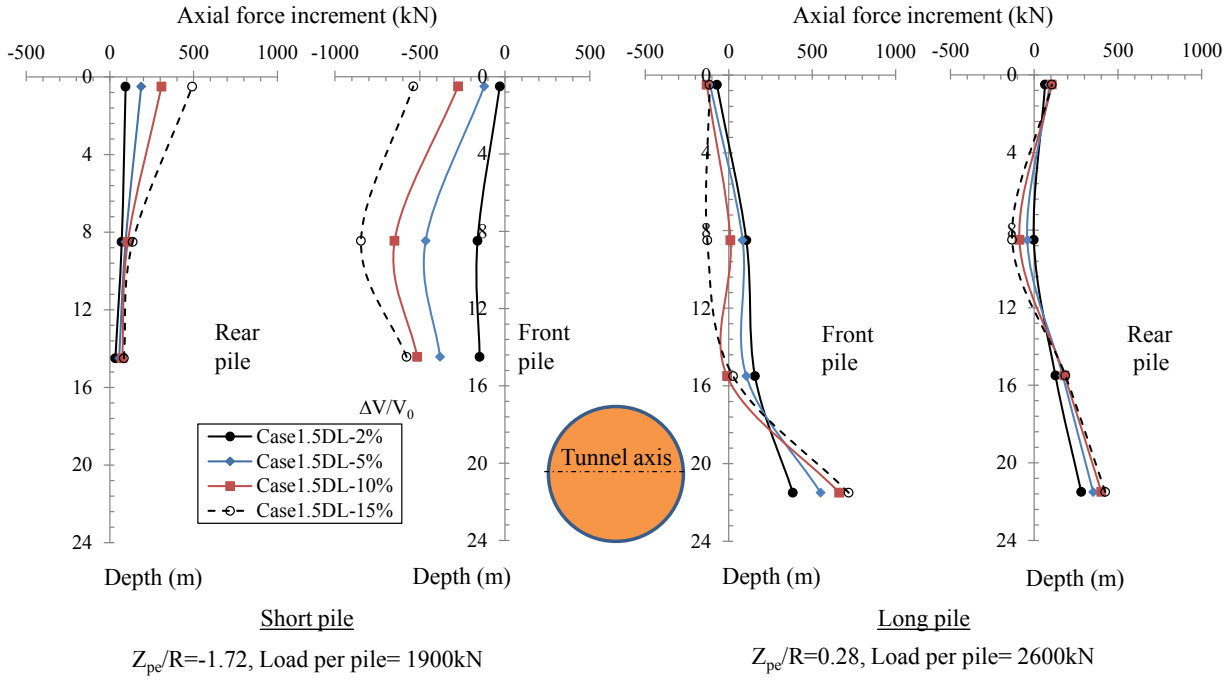

(a)

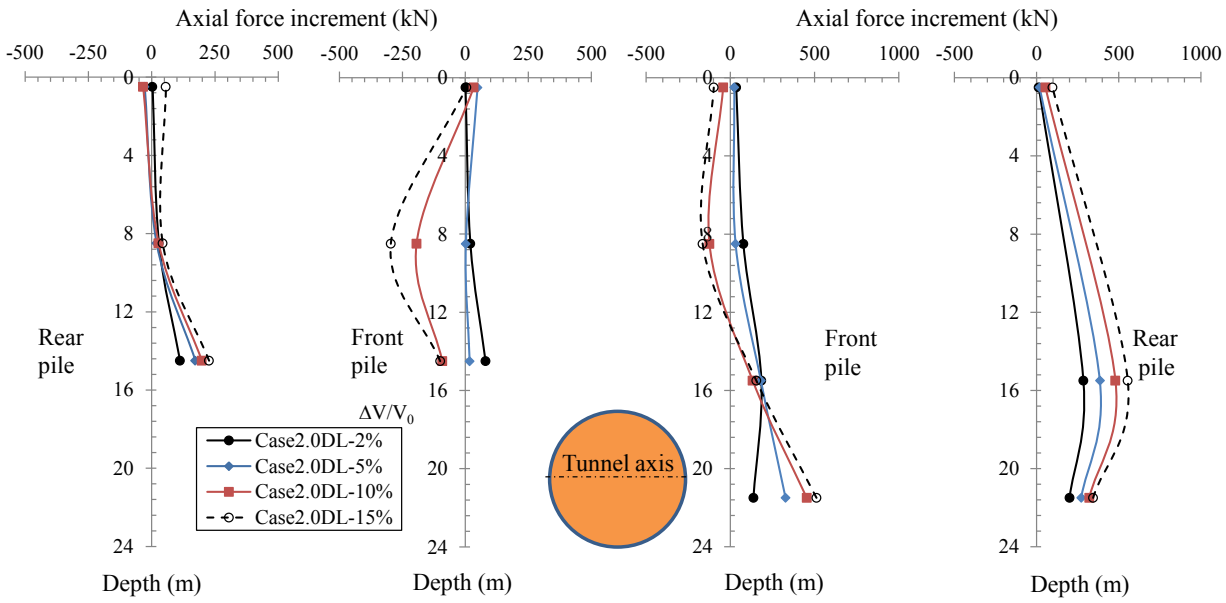

Short pile

Z_{pe}/R=-1.72, Load per pile= 1900kN

Long pile

Z_{pe}/R=0.28, Load per pile= 2600kN

(b)

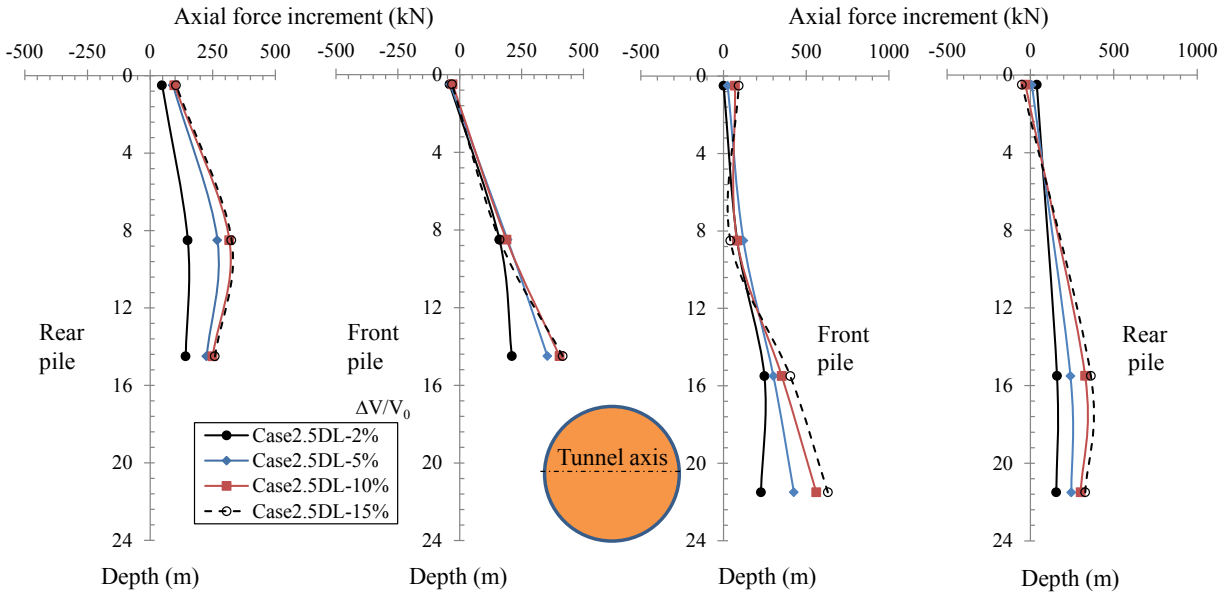

Short pile

Z_{pe}/R=-1.72, Load per pile= 1900kN

Long pile

Z_{pe}/R=0.28, Load per pile= 2600kN

(c)

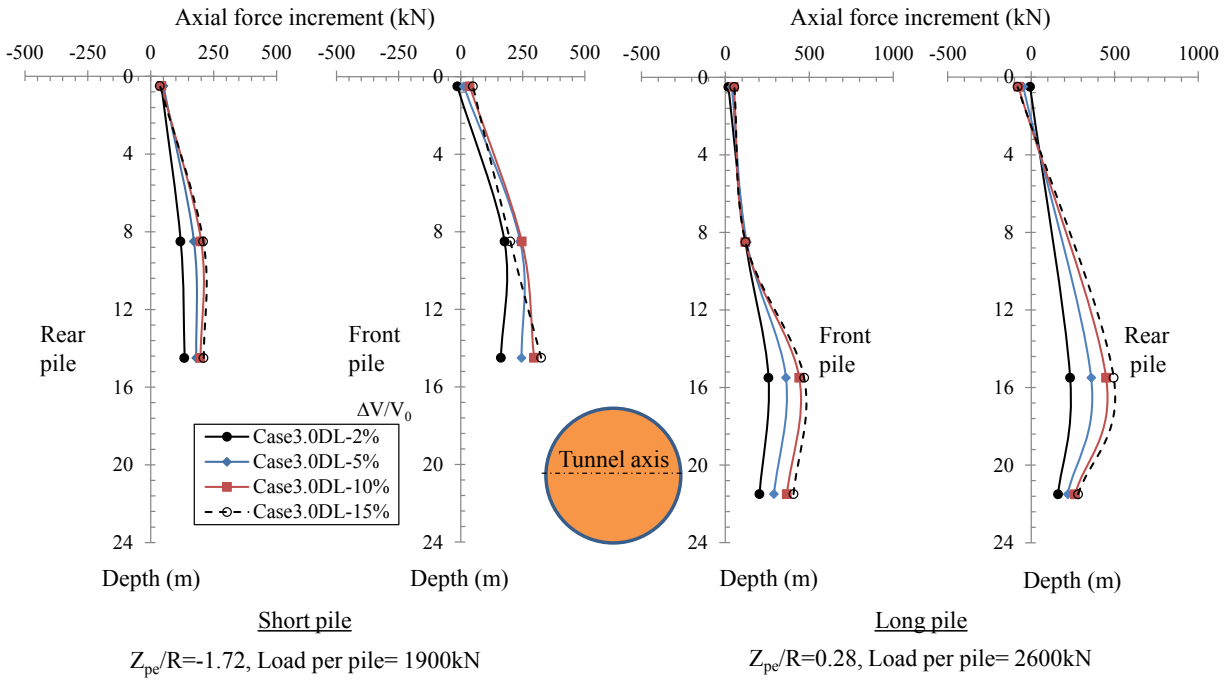

(d)

Figure B.2 Pile axial force increment profile with depth at ground loss ratio of 2%, 5%, 10%, and 15%: (a) Case1.5-DL; (b) Case2.0-DL; (c) Case2.5-DL; (d) Case3.0-DL

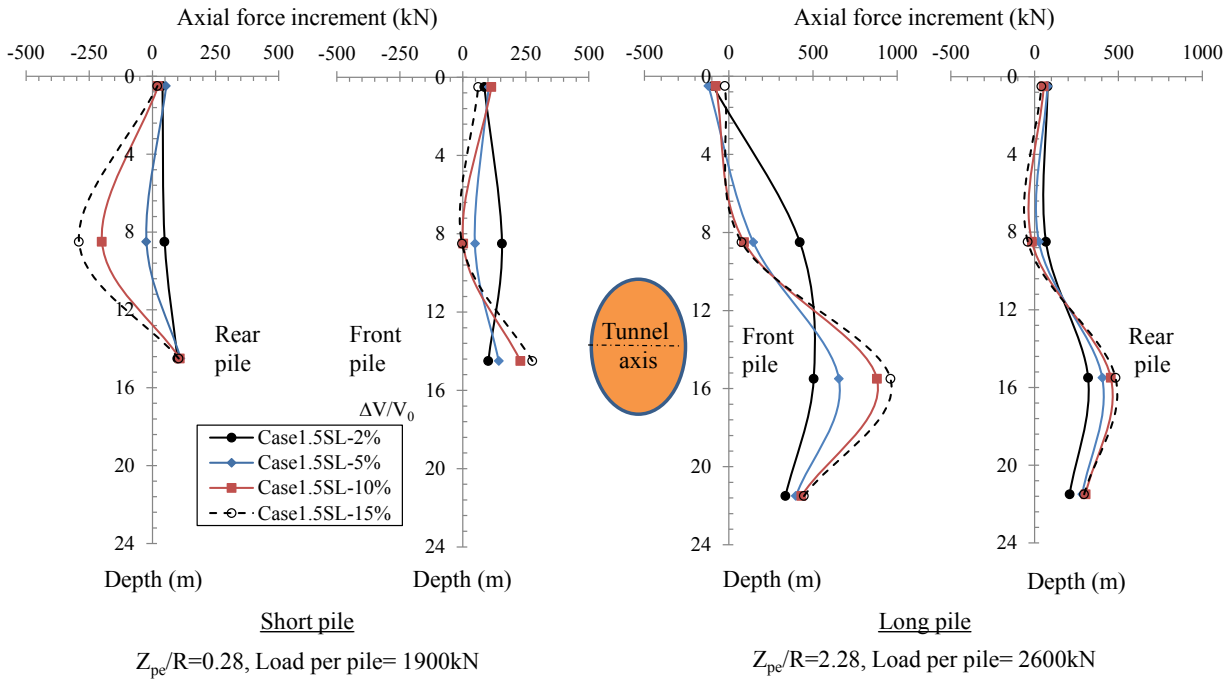

(a)

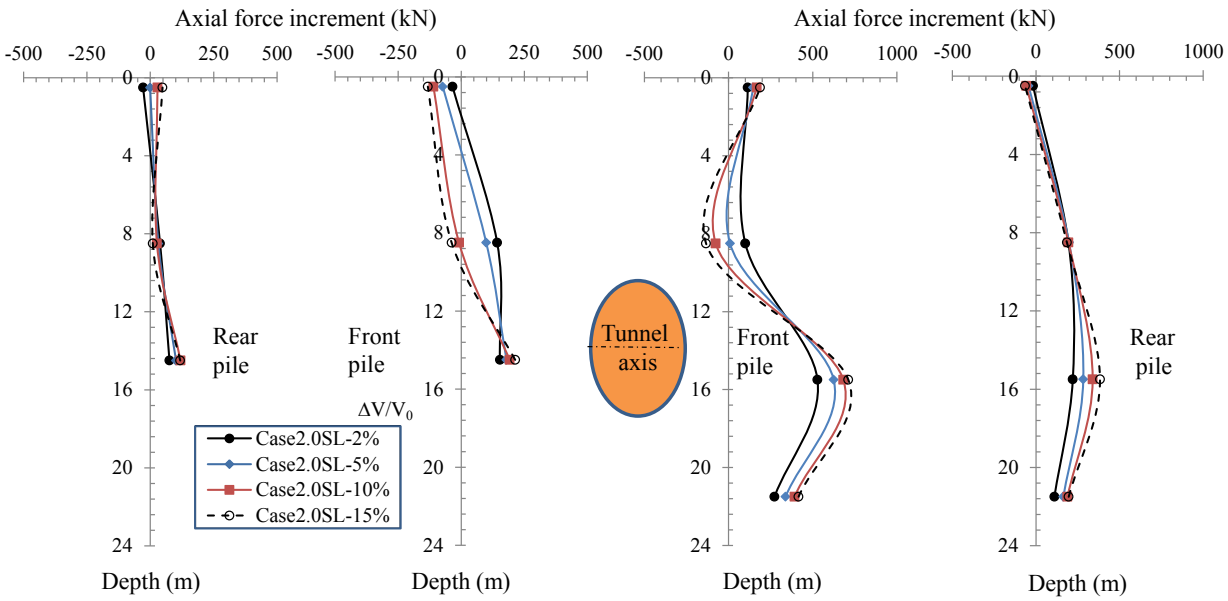

Short pile

Z_{pe}/R=0.28, Load per pile= 1900kN

Long pile

Z_{pe}/R=2.28, Load per pile= 2600kN

(b)

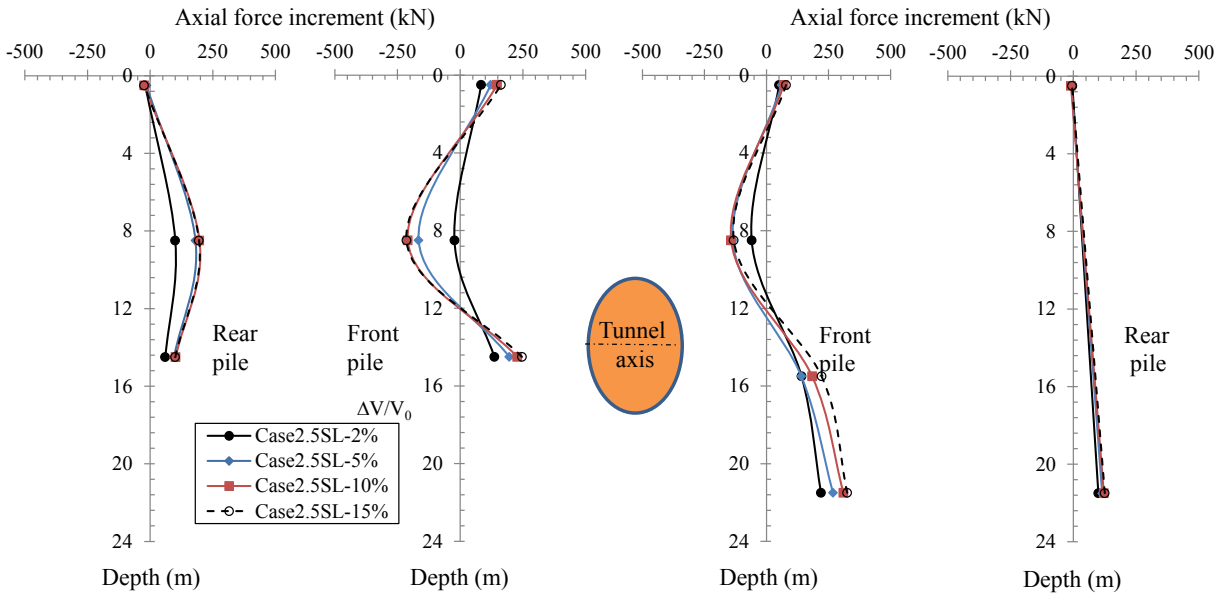

Short pile

Z_{pe}/R=0.28, Load per pile= 1900kN

Long pile

Z_{pe}/R=2.28, Load per pile= 2600kN

(c)

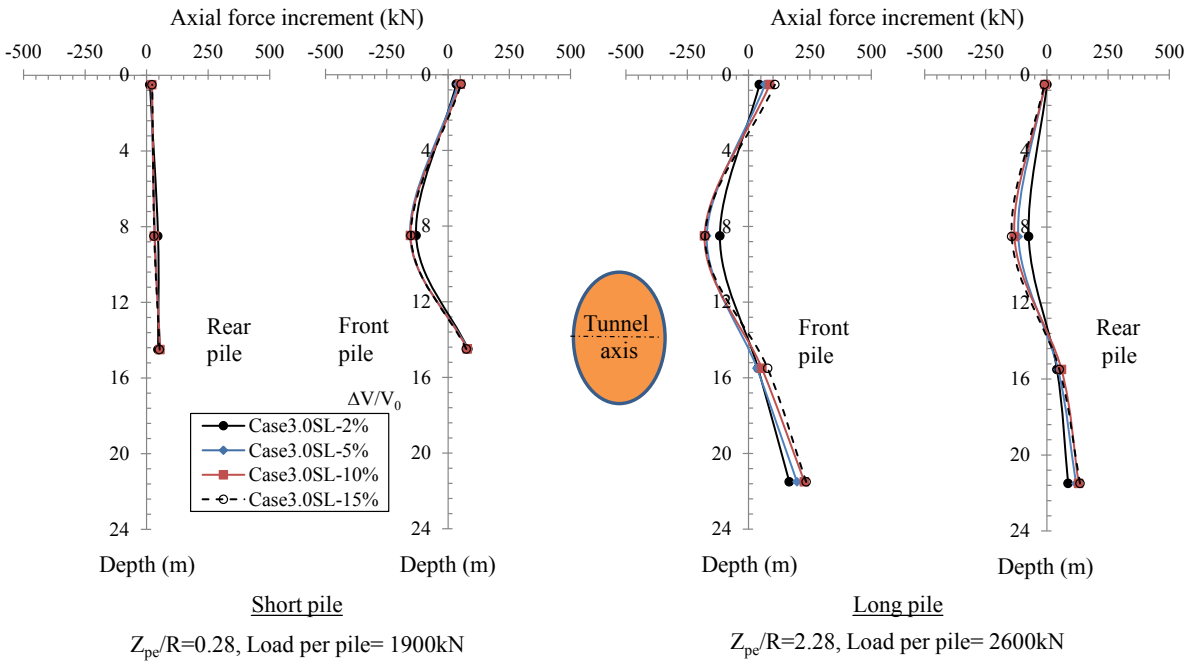

(d)

Figure B.3 Pile axial force increment profile with depth at ground loss ratio of 2%, 5%, 10%, and 15%: (a) Case1.5-SL; (b) Case2.0-SL; (c) Case2.5-SL; (d) Case3.0-SL

Appendix C – Bending moment development from 2%, 5%, 10%, and 15% ground loss ratio

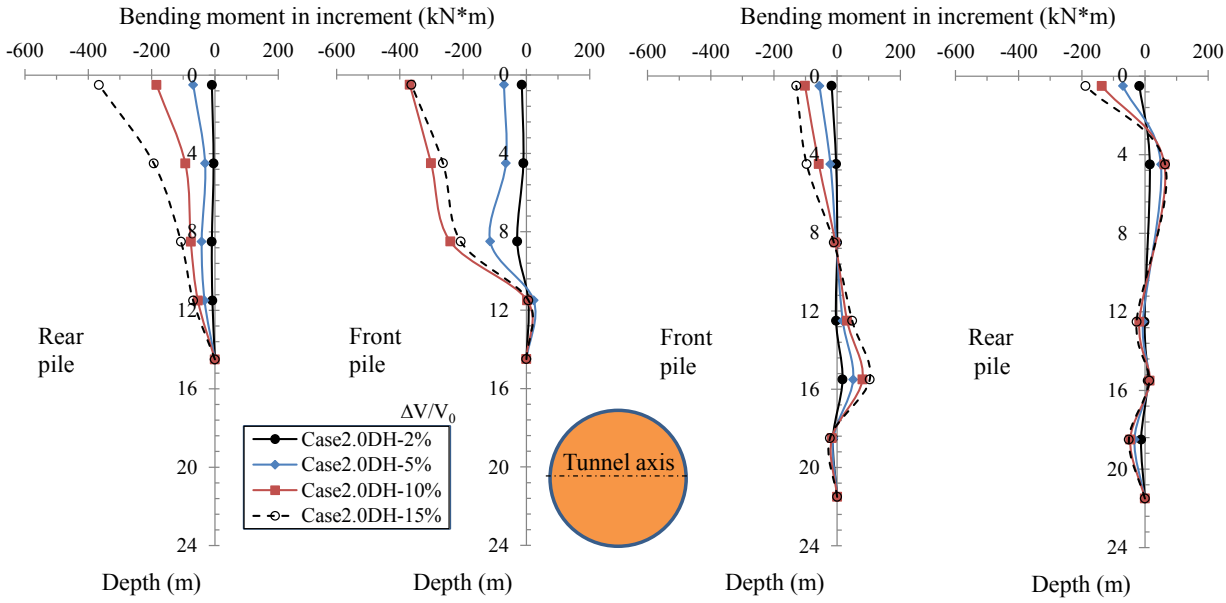

Z_{pe}/R=-1.72, Load per pile= 2600kN

Z_{pe}/R=0.28, Load per pile= 5700kN

(a)

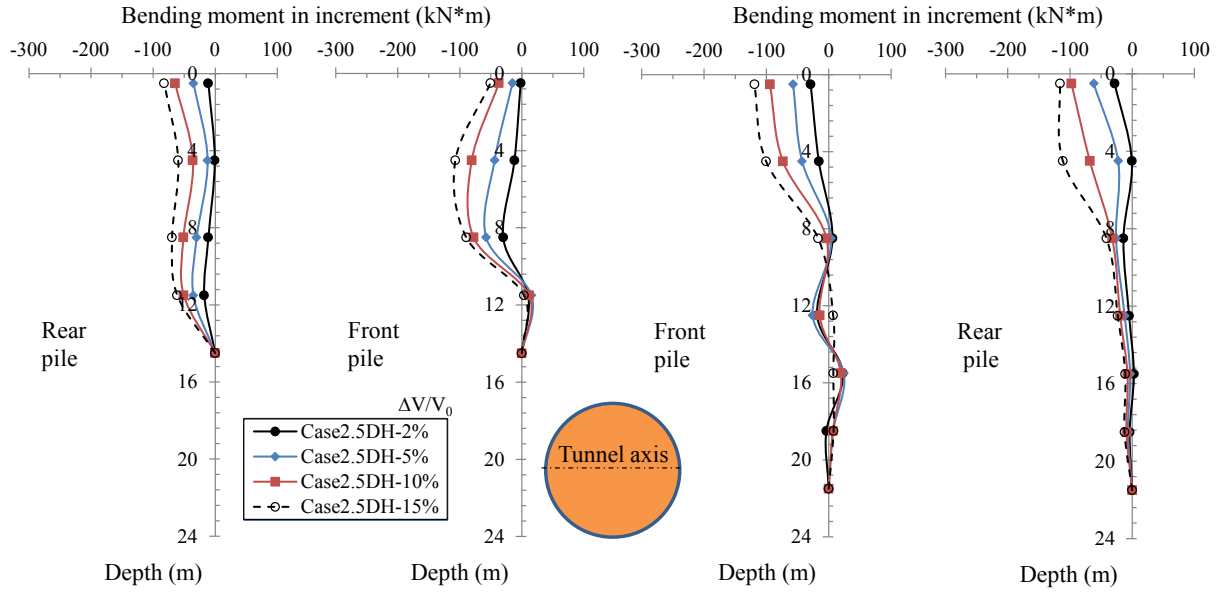

Z_{pe}/R=-1.72, Load per pile= 2600kN

Z_{pe}/R=0.28, Load per pile= 5700kN

(b)

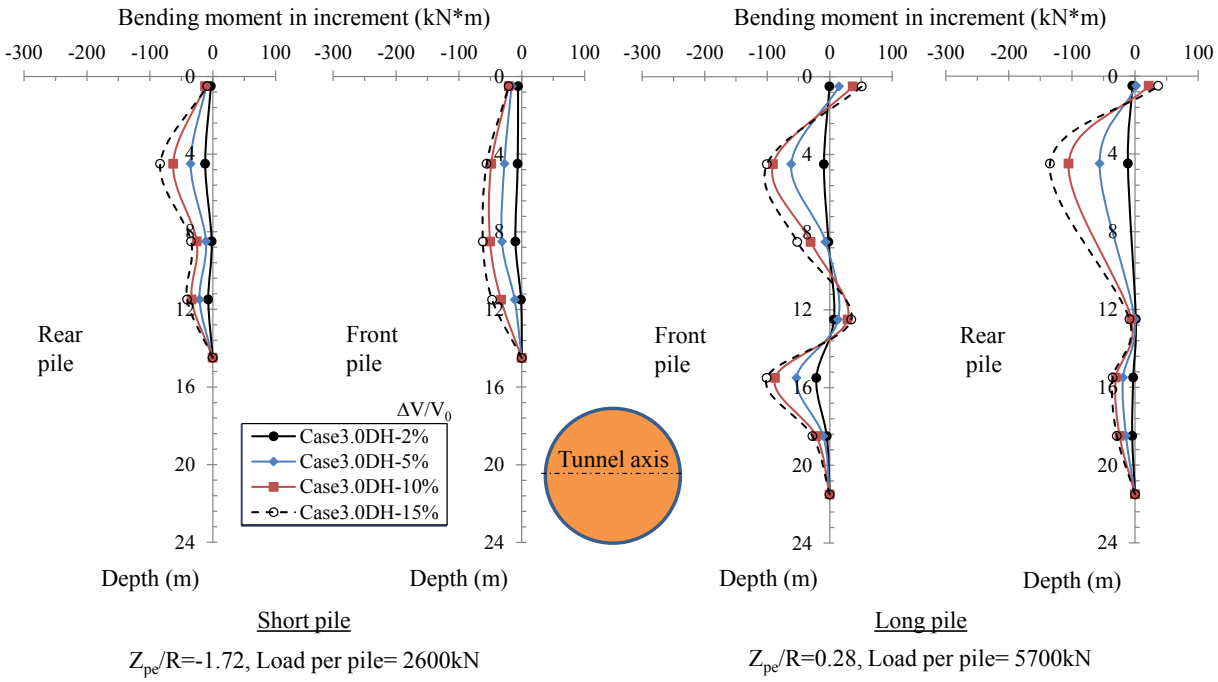

(c)

Figure C.1 Pile bending moment profile with depth at ground loss ratio of 2%, 5%, 10%, and 15%: (a) Case2.0-DH; (b) Case2.5-DH; (c) Case3.0-DH

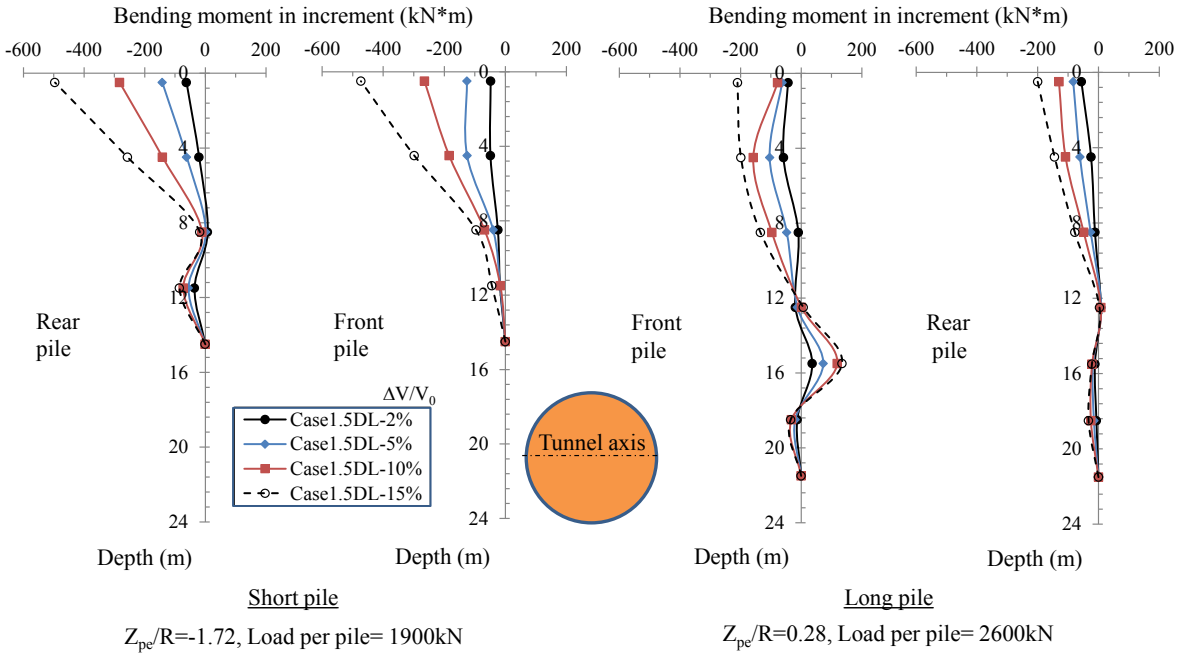

(a)

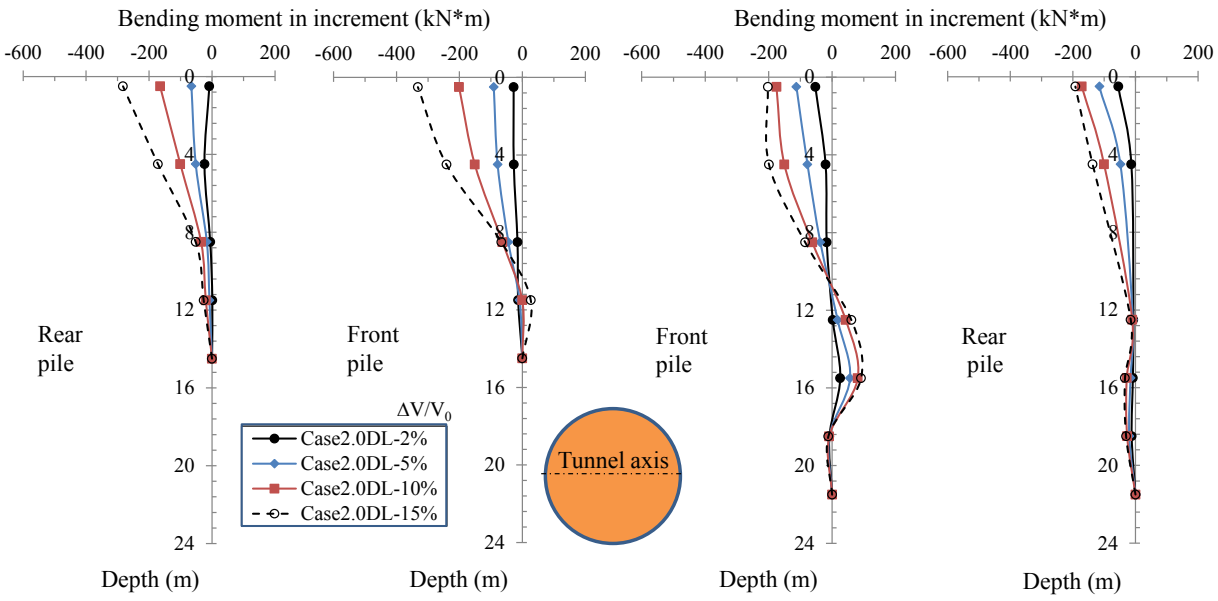

Z_{pe}/R=-1.72, Load per pile= 1900kN

Z_{pe}/R=0.28, Load per pile= 2600kN

(b)

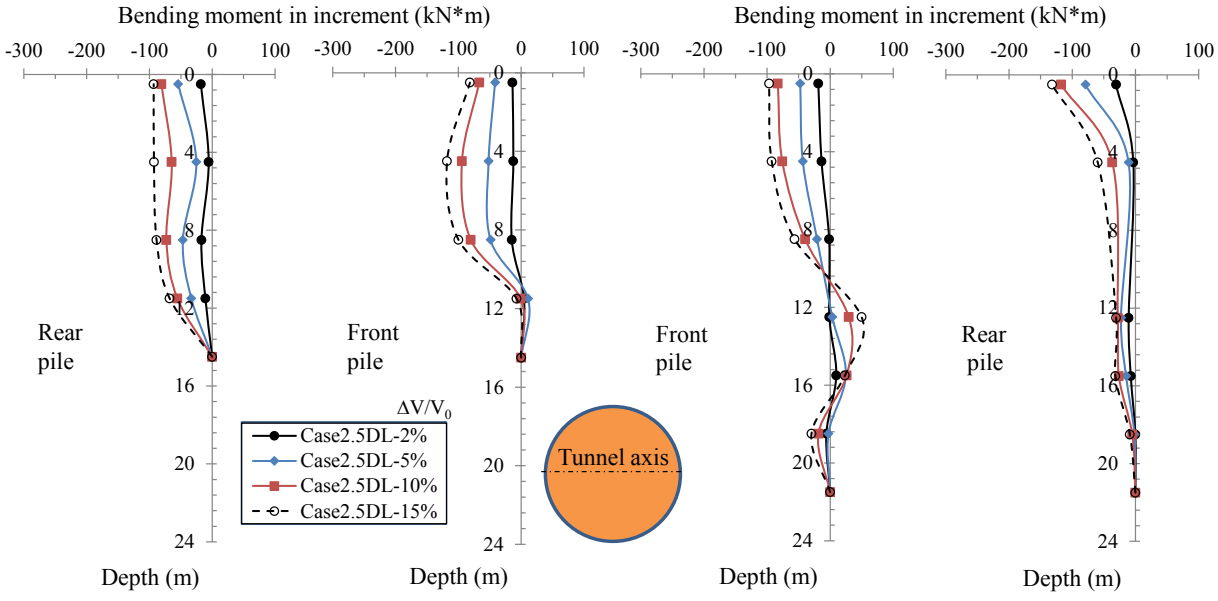

Z_{pe}/R=-1.72, Load per pile= 1900kN

Z_{pe}/R=0.28, Load per pile= 2600kN

(c)

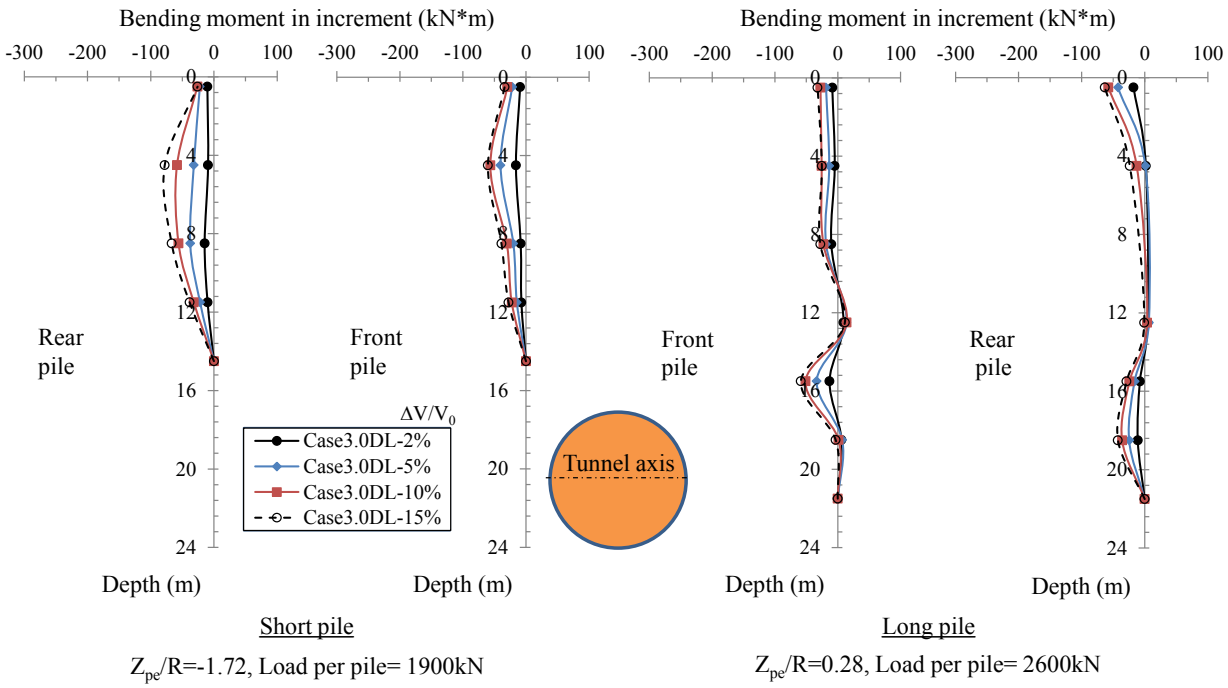

(d)

Figure C.2 Pile bending moment profile with depth at ground loss ratio of 2%, 5%, 10%, and 15%: (a) Case1.5-DL; (b) Case2.0-DL; (c) Case2.5-DL; (d) Case3.0-DL

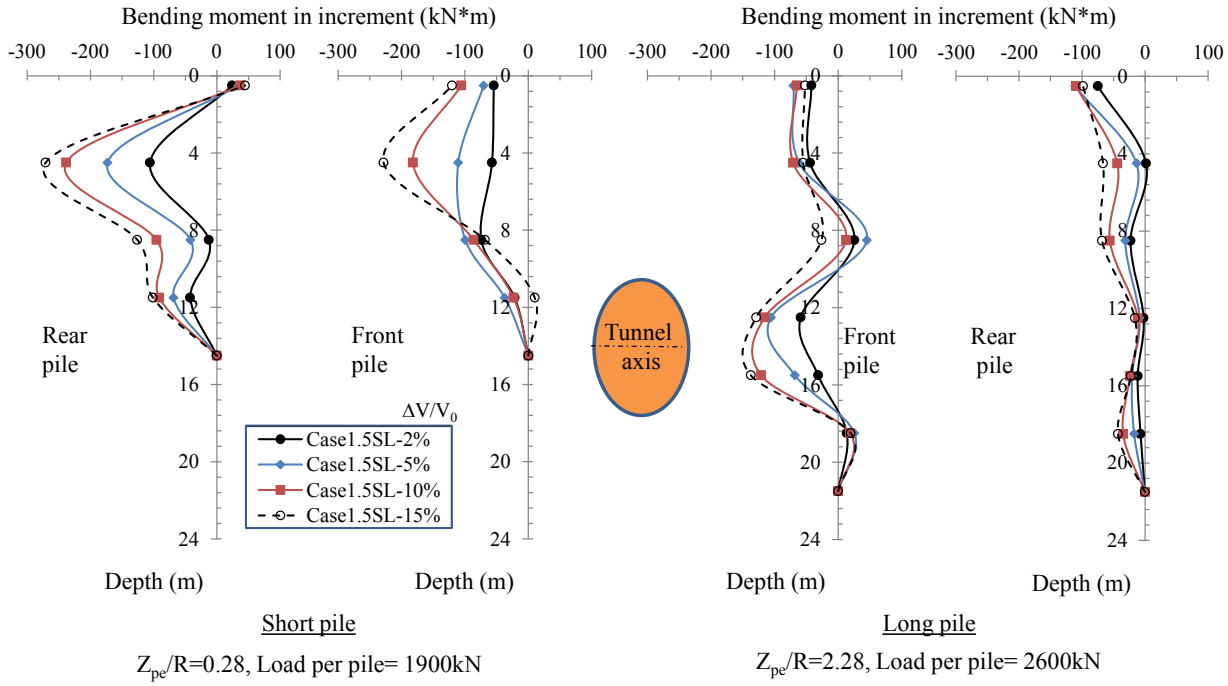

(a)

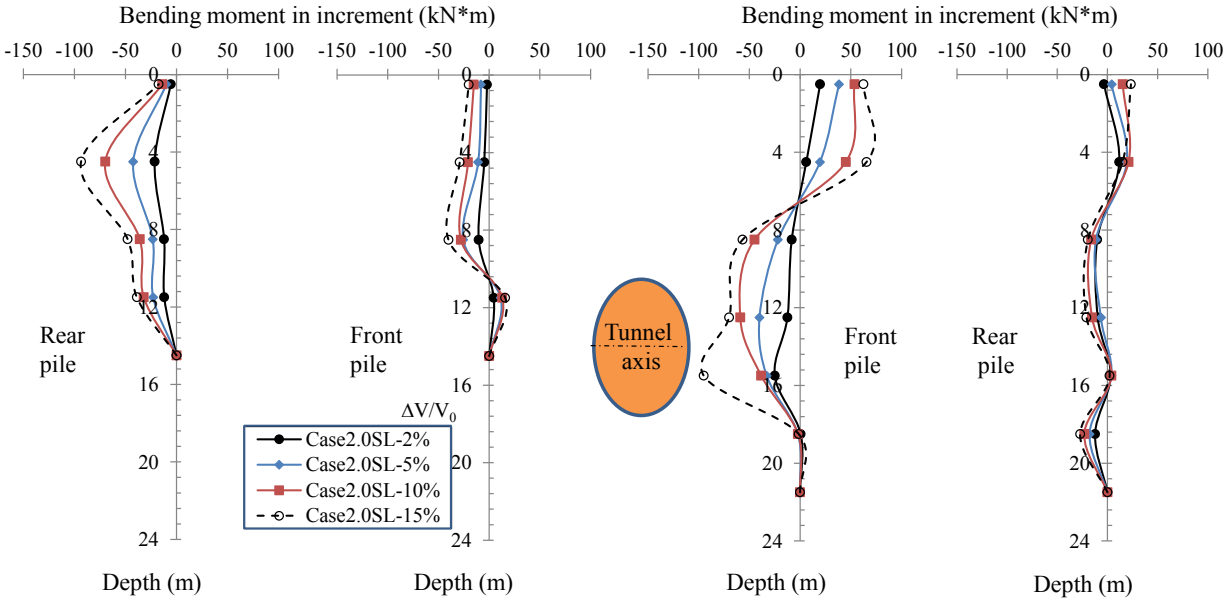

Short pile

Z_{pe}/R=0.28, Load per pile= 1900kN

Long pile

Z_{pe}/R=2.28, Load per pile= 2600kN

(b)

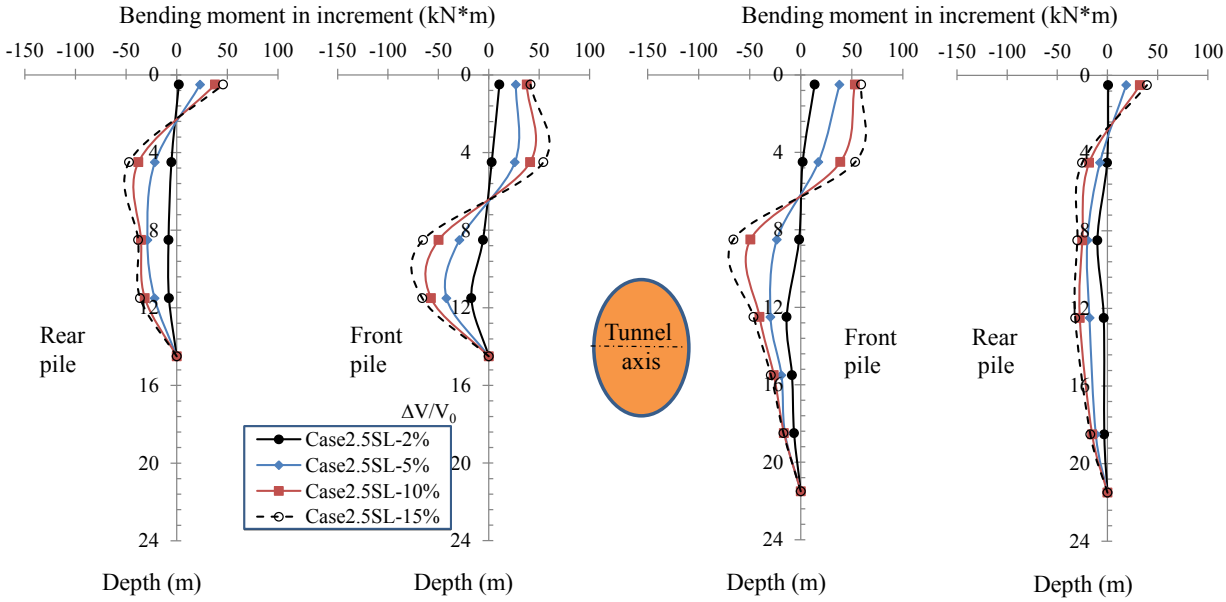

Short pile

Z_{pe}/R=0.28, Load per pile= 1900kN

Long pile

Z_{pe}/R=2.28, Load per pile= 2600kN

(c)

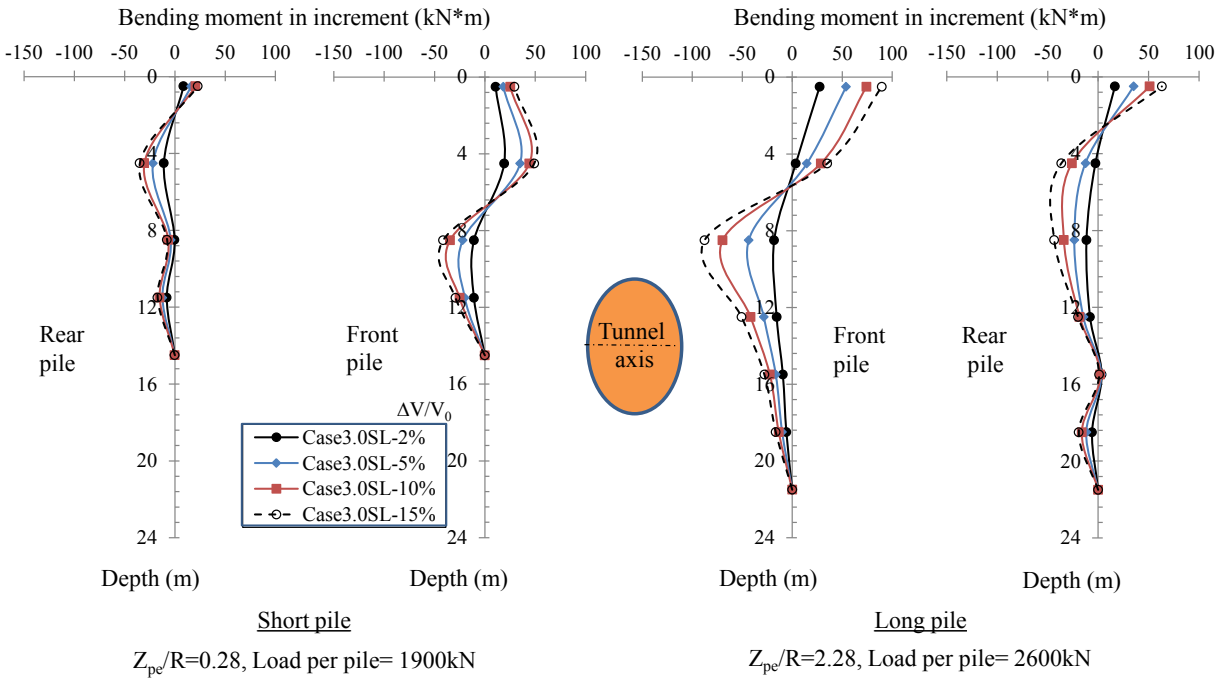

(d)

Figure C.3 Pile bending moment profile with depth at ground loss ratio of 2%, 5%, 10%, and 15%: (a) Case1.5-SL; (b) Case2.0-SL; (c) Case2.5-SL; (d) Case3.0-SL